Intelligent Control and Protection Methods for Modern Power Systems Based on WAMS

Liu, Leo

Publication date:
2013

Document Version
Publisher's PDF, also known as Version of record

Intelligent Control and Protection Methods for Modern Power Systems Based on WAMS

By

Chengxi Liu

Department of Energy Technology

AALBORG UNIVERSITY
DENMARK

A Dissertation Submitted to
the Faculty of Engineering, Science and Medicine, Aalborg University
in Partial Fulfillment for the Degree of Doctor of Philosophy

September 2013

Aalborg, Denmark

Aalborg University

Department of Energy Technology

Pontoppidanstraede 101

9220 Aalborg East, Denmark

ISBN: 987-87-92846-35-8

Printed in Denmark by Aalborg University

Statement

1. Thesis Title:

Intelligent Control and Protection Methods for Modern Power Systems Based on WAMS

2. Name of the PhD student:

Chengxi Liu

3. Names of Supervisors:

Zhe Chen & Claus Leth Bak

4. List of published and submitted paper:

1st Authored Journal Papers:

[J1] **Chengxi Liu**, Kai Sun, Zakir Hussain Rather, Zhe Chen, Claus Leth Bak, Paul Thøgersen and Per Lund, "A systematic approach for dynamic security assessment and the corresponding preventive control scheme based on decision trees," *IEEE Transaction on Power Systems*, vol. 29, no. 2, pp. 717-730, Mar. 2014.

[J2] **Chengxi Liu**, Zakir Hussain Rather, Zhe Chen and Claus Leth Bak, "An overview of decision tree applied to power systems," *International Journal of Smart Grid and Clean Energy*, vol. 2, no. 3, pp. 413-419.

[J3] **Chengxi Liu**, Zakir Hussain Rather, Zhe Chen and Claus Leth Bak, "Multi agent system based adaptive protection for dispersed generation integrated distribution systems," *International Journal of Smart Grid and Clean Energy*, vol. 2, no. 3, pp. 406-412.

[J4] **Chengxi Liu**, Zakir Hussain Rather, Weihong Huang, Kai Sun, Zhe Chen, Claus Leth Bak, Paul Thøgersen and Per Lund, "Optimization of dynamic VAR resource with consideration of wind farms to address delayed voltage recovery issues," Submitted to *IEEE Transaction on Sustainable Energy*.

Co-Authored Journal Papers:

[J5] Zakir Hussain Rather, Zhe Chen, **Chengxi Liu**, Paul Thøgersen, Per Lund and Brian Kirby, "Realistic approach for phasor measurement unit placement – Part II: a case study of

Danish power system and learnings from practical experience," Submitted to *IEEE Transaction on Power Delivery*.

1st Authored Conference Papers:

[C1] **Chengxi Liu**, Claus Leth Bak, Zhe Chen and Zhou Liu, "Adaptive voltage stability protection based on load identification using phasor measurement units," in *Proc. of IEEE International Conference on Advanced Power System Automation and Protection (APAP2011),* Beijing, China, Oct. 2011.

[C2] **Chengxi Liu**, Zhe Chen and Zhou Liu, "A communication-less overcurrent protection for distribution system with distributed generation integrated," in *Proc. of the 3rd International Symposium on Power Electronics for Distributed Generation System (PEDG2012),* Aalborg, Denmark, Jun. 2012.

[C3] **Chengxi Liu**, Quan Xu, Zhe Chen and Claus Leth Bak, "Vulnerability evaluation of power system integrated with large-scale distributed generation based on complex network theory," in *Proc. of the 47th International Universities' Power Engineering Conference (UPEC2012),* London, UK, Sep. 2012.

[C4] **Chengxi Liu**, Zakir Hussain Rather, Nathen Stearn, Zhe Chen, Claus Leth Bak and Paul Thøgersen, "Practical testing and performance analysis of phasor measurement unit using Real Time Digital Simulator (RTDS)," in *Proc. of IEEE International Energy Conference & Exhibition (EnergyCon2012)*, Florence, Italy, Sep. 2012.

[C5] **Chengxi Liu**, Zhe Chen, Claus Leth Bak, Per Lund, Peter Rønne-Hansen and Zhou Liu, "Transient stability assessment of power system with large amount of wind power penetration: the Danish case study," in *Proc. of the 10th International Power and Energy Conference (IPEC2012),* Ho Chi Minh City, Vietnam, Dec. 2012.

[C6] **Chengxi Liu**, Zakir Hussain Rather, Zhe Chen, Claus Leth Bak and Paul Thøgersen, "Importance sampling based decision trees for security assessment and the corresponding preventive control schemes: the Danish case study," in *Proc. of IEEE PES PowerTech (PowerTech2013),* Grenoble, France, Jun. 2013.

[C7] **Chengxi Liu**, Claus Leth Bak, Zhe Chen and Per Lund, "Dynamic security assessment of western Danish power system based on ensemble decision trees," in *Proc. of the 12th International Conference on Development in Power System Protection (DPSP 2014)*, Copenhagen, Denmark, Mar. 2014.

Co-Authored Conference Papers:

[C8] Zhou Liu, Zhe Chen, Haishun Sun and **Chengxi Liu**, "Control and protection cooperation strategy for voltage instability," in *Proc. of 47th International Universities' Power Engineering Conference (UPEC2012),* London, UK, 2012.

[C9] Zhou Liu, Zhe Chen, **Chengxi Liu**, Haishun Sun and Yanting Hu "Multi-agent system based wide area protection against cascading events," in *Proc. of the 10th International Power and Energy Conference (IPEC2012)*, Ho Chi Minh City, Vietnam, Dec. 2012.

[C10] Zhou Liu, Zhe Chen, Haishun Sun and **Chengxi Liu**, "Emergent load shedding strategy based on sensitivity analysis of relay operation margin against cascading events," in *Proc. of IEEE PES International Conference on Power Systems Technology (POWERCON2012),* Auckland, New Zealand, Nov. 2012.

[C11] Zakir Hussain Rather, **Chengxi Liu**, Zhe Chen, Claus Leth Bak and Paul Thøgersen, "Dynamic security assessment of Danish power system based on decision trees: today and tomorrow," in *Proc. of IEEE PES PowerTech (PowerTech2013),* Grenoble, France, Jun. 2013.

[C12] Hongzhi Liu, Zhe Chen and **Chengxi Liu**, "Enhanced dynamic voltage stability supported by VSC-HVDC for offshore wind applications using trajectory sensitivity analysis," in *Proc. of Wind Integration Workshop*, London, UK, Oct. 2013.

[C13] Zakir Hussain Rather, **Chengxi Liu**, Zhe Chen and Paul Thøgersen, "Optimal PMU placement by improved particle swarm optimization," in *Proc. of IEEE PES Innovative Smart Grid Technologies Conference (ISGT Asia),* Bangalore, India, Nov. 2013.

5. **This present report combined with the above listed scientific papers has been submitted for assessment in partial fulfillment of the PhD degree. The scientific papers are not included in this version due to copyright issues. Detailed publication information is provided above and the interested reader is referred to the original published papers. As part of the assessment, co-author statements have been made available to the assessment committee and are also available at the Faculty of Engineering and Science, Aalborg University**

Acknowledgement

I would like to thank the Department of Energy Technology, Aalborg University (ET-AAU) and the financial support provided by *Danske Strategiske Forskningscentre* under the project DSF 09-067255, "Development of a Secure, Economic and Environmentally-friendly Modern Power System" (*SEEMPS*).

I owe gratitude to many people that continuously helped me in various ways during my research. In particular I would express my sincere appreciation to:

– My supervisors, Prof. Zhe Chen and Prof. Claus Leth Bak for giving me this opportunity to work in this area, for their trust and encouragement and for all guidance, advices and comments throughout the project.

– Dr. Kai Sun from the University of Tennessee, Knoxville (UTK) for his continuous support, suggestions and comments and for all the fruitful discussions during my stay in United States.

– Project steering group members, especially Per Lund, Peter Rønne-Hansen, Tony Yip and Poul Erik Morthorst, Birgitte Bak-Jensen and John K. Pedersen for their for their valuable suggestions in the project meetings.

– Project members, Zakir Hussain Rather, Pietro Raboni, S. Mostafa F. Astaneh, Iker Diaz de Zerio Mendaza and Jiakun Fang for their cooperation and discussions.

– Other colleagues in our research group, especially Chi Su, Zhou Liu, Hongzhi Liu, Fujing Deng, Yunqian Zhang, Xiongfei Wang, Yan Liu, Jie Tian, Yanbo Wang, Rongwu Zhu, Chao Wang and Yanjun Tian for sharing valuable the information and knowledge.

– Hongzhi Liu, Ke Ma and Huai Wang for creating a good atmosphere in the office.

– Bin Wang, Fengkai Hu and Weihong Huang for their hospitality and help during my stay at UTK.

– Corina Gregersen and Karina K. Ludvigsen for their help with miscellaneous matters as well as Casper Jørgensen and Cam Pham for English-Danish translations.

Last but not least, I would like to appreciate my parents, grand-parents for all their love and support.

Abstract

Continuously growing demand for electricity, driven by deregulated power markets, has forced power systems to operate closer to their security operation limits. Meanwhile, the increasing penetration of large scale renewable energy may impact the operation of power systems by bringing more uncertainties. Under these circumstances, Wide Area Measurement System (WAMS) is widely applied in modern power systems, which is composed of a number of phasor measurement units (PMUs) that can provide high resolution real–time measurements synchronized by global positioning systems (GPS). WAMS can be used to (1) effectively assess the vulnerability of power grids; (2) provide online dynamic security assessment (DSA) with high reliability; (3) intelligently control and prevent power systems from the risk of insecurity and instability; (4) accurately identify the parameters of power system models and provide adaptive corrective control schemes.

Power system is a complex non-linear dynamic system. The key to power system vulnerability assessment is to find the vulnerable elements which could cause large-area power outages under attacks. For the aspect of structural vulnerability assessment, several vulnerability indices i.e. structural vulnerability index (SVI), contingency vulnerability index (CVI) and operational vulnerability index (OVI) are proposed to evaluate the impact of distributed generation (DG) on power system vulnerability. The assessment shows that DG units are able to shorten the electrical distance between power sources and power loads, alleviate long-distance large-capacity transmission, improve the reliability of power system after contingencies, and increase transmission efficiency. For the aspect of dynamic vulnerability assessment, critical clearing time (CCT) is computed by screening of a number of contingencies in various operating conditions. By statistical analysis, vulnerable areas in terms of transient stability are identified. Furthermore, the result of CCT computation in different typical scenarios can evaluate the impact of wind power on power system transient stability. Other influencing factors to power system transient stability are also evaluated, e.g. power output of generators in central power plants (CPP), load consumption level and the power exchange in high voltage direct current (HVDC) links. Both structural and dynamic vulnerability assessment, aiming at providing an early awareness of power system insecurity, are conducted by simulations in the DIgSILENT model of western Danish power system.

DSA is the assessment of the ability of a certain power system to withstand a defined set of contingencies and to survive in the transition to an acceptable steady-state condition. Among pattern recognition techniques, decision trees (DT) using the algorithm of classification and regression trees (CART) is applied in DSA of western Danish power system. It not only provides the results of security assessment but also reveal the principles learned by DTs for security assessment. The systematic approach adopts new methodology that trains contingency-oriented DTs on daily basis using the database generated by importance sampling method. The number of time-domain simulations necessary for importance sampling is significantly reduced, so computation burden is highly reduced, which makes the online DSA possible for even considering large scale integration of uncertain power generation from windfarms and other DG units.

Based on the result of DSA, intelligent contingency control scheme guided by paralleled DTs is able to draw the system from insecure zone to the secure zone. In this approach, two DTs work in tandem, i.e. Observation DT (ODT) and Prevention DT (PDT). Fed with real-time wide area measurements, ODT of measurable variables is employed for online DSA to identify potential security issues and PDT of controllable variables provides online decision support on preventive control strategies against those issues. Finally, optimization of preventive control is conducted to find the most economical trajectory of preventive control. The proposed approach is comprehensively verified by a number of credible contingencies in western Danish power systems with annual data of operating conditions.

In order to prevent voltage collapse, the online identification of load characteristic using PMU measurement-based approach is proposed to evaluate the proximity to voltage instability. Based on different load characteristics, adaptive corrective control schemes were implemented. The method can correctly predict and prevent the voltage collapse, and minimize the amount of load shedding.

Dansk Resumé

Den konstant stigende efterspørgsel efter elektricitet drevet af et liberaliseret elmarked, sætter større krav til at elnet fungerer nær dets sikkerhedskrav. Imellemtid skaber den stigende udbredelse af vedvarende energi i større skala usikkerhed ved driften af elnettet.

Under disse omstændigheder er Wide Area Measurement System (WAMS) almindeligt anvendt i det moderne elnet, hvilket består af et antal Phasor measurement units (PMU), som kan give højopløsning realtidsmålinger der synkroniseres med global positioning system (GPS). WAMS kan bruges til: (1) effektivt at vurdere elnets sårbarhed; (2) give et dynamisk sikkerheds vurdering (DSA) med høj pålidelighed; (3) intelligent kontrollere og forhindre strømsystemer imod risikoen for usikkerhed og ustabilitet; (4) præcist identificere af elnets model parametre og levere adaptive korrigerende kontrol strategi.

Elnet er et komplekst ikke-lineær dynamisk system. Nøglen til elnets sårbahedsvurdering er at finde de sårbare elementer, som kunne forårsage strømsvigt for store områder under udfaldet. For strukturel sårbarhedsvurdering aspekt mange sårbarhed indeks, m.a.o. structural vulnerability index (SVI), contingency vulnerability index (CVI) og operational vulnerability index (OVI) for at evaluere påvirkningen af decentral produktion (DG) på elnet sårbarhed. Evalueringen viser, at DG-enheder er i stand til at; forkorte den elektriske afstand mellem strømkilder og belastninger, lette langdistance højkapacitet transmission, forbedre pålideligheden af elsystemet efter uventet begivenhed og samt øge overførings virkningsgrad. For en dynamisk sårbarhedsvurdering, critical clearing time (CCT) beregnes på baggrund af screening af en række uventet begivenheder under forskellige driftsbetingelser. Ved en statistisk analyse, sårbar områd i form af transient stabilitet er indentificeret. Desuden kan resultatet af CCT beregningen i forskellige scenarier evaluere effekten af vindkraft på elsystemet transient stabilitet. Andre indvirke faktorer som påvirker elsystemet's transient stabilitet tages også med i betragtningen, f.eks. udgangseffekten på generatorer i central power plants (CPP), strømforbruget og at strømudvekslingen i højspænding jævnstrøm anlæg (HVDC). Både strukturelle og dynamiske sårbarhedsvurderinger stræber efter at give en tidlig bevidsthed om elsystemet usstabilitet er udført ved simuleringer i DIgSILENT model af det vestlige danske elnet.

DSA er vurdering af et bestemt elsystems evner til at modstå et sæt uforudsete forhold og kunne klare i overgangen til en acceptabel stabil tilstand. Blandt mønstergenkendelsesteknikker, decision trees (DT), ved hjælp af algoritmen af classification and regression trees (CART) er anvendt i DSA for det vestlige danske elsystem. Det handler ikke kun om at frembringe resultater af sikkerhedsvurderingen, men også afdække de principper lært af DTs for sikkerhedsvurderingen. Den systematiske tilgang adopterer en ny metode, der optræner uforusetlig orienteret DT på daglig basis som anvendt databasen der genereret af betydning sampling methoden. Antallet af tidsdomæne simuleringer som er nødvendige for betydning sampling er reduceres betydeligt, så beregnings kompleksiteten er stærkt reduceret, hvilket gør online DSA muligt for intergrere betænkelig større skala af uvis elproduktion fra vindmølleparker og andre DG enheder.

Baseret på resultaterne fra DSA, er det intelligent uforudsete kontrolsystem styret af parallelkoblede DT i stand til at trække systemet fra usikre zone til den sikre zone. Ved denne tilgang arbejder to DT i tandem, dvs. Observation DT (ODT) og prevention DT (PDT). Fodret med realtid bred områd målinger, ODT af målbare variable er anvendt til online DSA for at identificere potentielle sikkerhedsproblemer og PDT af kontrollerbare variabler giver realtime beslutningsstøtte om forebyggende kontrol strategier mod disse problemstilling. Endelig er optimering af præventiv kontrol anvendt for at finde den mest økonomiske bane for forebyggende kontrol. Den foreslåede fremgangsmåde er grundigt kontrolleret af en række troværdige målinger af uventet begivenhed i vestdanske elsystemer med årlige data for driftsbetingelser.

Med det formål at forhindre spændingssammenbrud, online identifikation af belastning karakteristisk anvendes PMU målingen tilgang og det foreslås at evaluere i nærhed af spændingsustabiliteten. Baseret på forskellige belastningskarakteristikaene blev adaptive korrigerende kontrol ordninger gennemført. Fremgangsmåden kan præcist forudsige og forhindre spændingssammenbrud, og minimere mængden af frakobling af belastning.

Table of Contents

Abbreviations

A_*x*_*y*	Voltage angle of bus *x* minus that of bus *y*.
AGC	Automatic generation control.
AVR	Automatic voltage regulator.
CART	Classification and regression tree.
CCT	Critical clearing time.
CFS	Critical fault screening.
CHP	Combined heat and power plant.
CPP	Central power plant.
CT	Classification tree.
CVI	Contingency vulnerability index.
DFIG	Doubly-fed induction generator.
DG	Distributed generation.
DK1	Western Danish power system.
DK2	Eastern Danish power system.
DOE	Department of energy in US.
DPL	DIgSILENT Programming language.
DSA	Dynamic security assessment.
DSO	Distribution system operator.
DT	Decision tree.
EI	Efficiency index.
EMS	Energy management system.
EMT	Electromagnetic transient.
ENTSO-E	European network of transmission system operators for electricity.
FDR	Frequency disturbance recorder.
FNET	Frequency monitoring network.
FRC	Full-rated converter.
FSIG	Fixed speed induction generator.

GPS	Global positioning system.
G_CPP*x*	MW-output of central power plant *x*.
HVDC	High-voltage direct current.
LCC-HVDC	Line-commuted converter based high-voltage direct current.
VSC-HVDC	Voltage-sourced converter based high-voltage direct current.
ICT	Information and communication techniques.
IED	Intelligent electronic device.
IS	Importance sampling.
LS	Learning set.
LSE	Least square estimation.
LVRT	Low voltage ride through.
NS	Normal sampling.
OC	Operating condition.
ODT	Observation decision tree.
OEL	Over excitation limit.
OHL	Overhead line.
OLTC	On-load tap-changer.
OOB	Out-of-bag.
OVI	Operational vulnerability index.
PCC	Point of common coupling.
PDC	Phasor data concentrator.
PDT	Prevention decision tree.
PMU	Phasor measurement unit.
POC	Point of connection.
PV	Photovoltaic.
P_*x*_*y*	MW-power flow from bus *x* to bus *y*.
Q_*x*_*y*	MVar-power flow from bus *x* to bus *y*.
RF	Random forest.
RMS	Root mean square.
RT	Regression tree.
RTDS	Real-time digital simulator.

SCADA	Supervisory control and data acquisition.
SPDC	Super phasor data concentrator.
SPS	System protection scheme.
SVC	Static var compensator.
SVI	Structural vulnerability index.
TEF	Transient energy function.
TS	Test set.
TSO	Transmission system operator.
T-D	Time-domain.
UFLS	Under-frequency load shedding
UGC	Underground cable.
UVLS	Under-voltage load shedding.
WACS	Wide area control system.
WAMPAC	Wide area monitoring, protection and control.
WAMS	Wide area measurement system.
WAPS	Wide area protection system.

PART I

BACKGROUND, OBJECTIVES AND STATE-OF-THE-ART

Chapter 1

Introduction

1.1 Background and Motivations

New challenges to power systems have been induced by the rapid increasing penetration of renewable energy resources and the changes of electricity generation style, such as photovoltaic (PV) system, wind farms and other distributed generation (DG) units, including combined heat and power (CHP) plants. In 2012, a total of about 45GW of new power capacity was constructed in the European Union (EU), in which solar PV systems accounted for 16.8GW (37%), wind power accounted for 11.9GW (26%), followed by other types of generation. The renewable share of new power installations was 70% in 2012 [1]. The energy policies in many EU countries have set ambitious targets for the promotion of renewable energy. The European Wind Energy Association (EWEA) has planned to meet 23% European electricity with wind by 2030 [2].

Denmark stands in the leading position in developing wind power technologies. The total installed capacity of wind power in Denmark had reached 4348MW by July 2013, including offshore wind farms with capacity of 908MW [1], [3]. 10.27TWh electricity had been generated from wind turbines in 2012, which supplied 30.0% of annual electricity consumption [4]. Denmark also has experienced a vast growth in the dispersed generation since 1980s. About 50% of the electricity production capacity is dispersed generation in Danish power system, mainly from CHP units and onshore wind turbines. 75% of the total wind capacity is installed in western Denmark [5].

The large scale wind farms and DG units would play significant roles as power source in modern power systems, which make the control and protection of power systems more complicated. According to recommendations in final reports on the blackouts in US and EU [6]-[8], the modern power systems should not only rely on local and independent control mechanisms, but also on wide-area and coordinated control schemes, should not only be protected by conventional protections based on localized information as the first defense line, but also by system-level protection schemes (SPS) as the second and the third defense lines.

High-resolution real-time wide-area measurements with synchronized time stamps are necessary for gathering not only local signals but also global signals with high accuracy and low time delay. With the development of measurement and communication technologies, wide area measurement systems (WAMS) have been widely applied in power systems worldwide in the last two decades, based on which, advanced emergency control and protection approaches have been being developed to handle the system faults and disturbances, improve the system stability, reduce the risk of cascading failures and blackouts, and realize power system quick restoration.

Danish power system is endeavoring to sit in the front row and many activities based on WAMS have been implemented not only on laboratory scale but also as pilot projects on system scale, such as calculating short-circuit power of HVDC stations, monitoring low-frequency oscillations, early warning of instability and oscillations, logging the system events [9]. However, most of the applications are still in the "monitoring" stage, in which WAMS only serves as a redundant measurement system to provide the backup security schemes. There is an urgent need to provide online wide area control and protect schemes based on WAMS for Danish power system.

1.2 Research Objectives

This PhD project is the Working Package 4 (WP4) of the *SEEMPS* project — "Development of a Secure, Economic and Environmentally-friendly Modern Power System". The aim of this working package is to develop adaptive and intelligent control and protection schemes based on WAMS to prevent instability, cascading failures and blackouts in power systems. Western Danish power system is the studied system throughout this project.

Four milestones of this project are listed below, and each milestone has been achieved by the author's publications as cited behind:

- WP4.1 Study the dynamic and transient characteristics of the power system with large wind power and distributed generation [C3], [C5];
- WP4.2 Develop the multi-agent protection [C2], [J3] and intelligent contingency control system based on WAMS [J1], [C6], [J2];
- WP4.3 Explore overall power system quick recovery strategies based on wide area state estimation [C1], [J4];
- WP4.4 Evaluate and verify the developed protection system and contingency control strategies [C4], [C7].

In this project, WAMS/PMU is proposed to (1) effectively assess the vulnerability of the power grid; (2) reliably provide the online dynamic security assessment (DSA) and predict the system security in case of disturbances; (3) intelligently control and protect power systems from the risk of insecurity and instability; (4) accurately identify the parameters of power system models. These are the main topics of this thesis.

There are mainly two aspects of power system vulnerability assessment: structural vulnerability assessment and dynamic vulnerability assessment. For the aspect of structural vulnerability assessment, vulnerability indices are necessary to evaluate the impact of dispersed generation on power grid vulnerability. For the aspect of dynamic vulnerability assessment, a number of credible contingencies in various operating conditions (OC) should be screened to identify the vulnerable areas and evaluate the impact of wind power and other factors on system security and stability. Both structural vulnerability assessment and dynamic vulnerability assessment aim at providing an early awareness of power system insecurity.

There are a number of methodologies for power system DSA. Among the methodologies based on pattern recognition algorithms, decision tree (DT) using the algorithm of classification and regression trees (CART) will be applied in the online DSA of western Danish power systems. The adopted methodology should be able to not only provide the security assessment for current OC but also reveal the principles learned by DTs. Fed with the online measurements from WAMS, the system security can be reliably predicted in case of credible contingencies in western Danish power system, such as single 3-phase short-circuit in the transmission lines or busbars or loss of single generation unit.

Based on the online data from WAMS, a preventive control scheme for western Danish power system is necessary to draw the system from insecure region to the secure region. Then, the most economical control trajectory is significant for operators to implement the preventive control with the lowest cost.

In order to prevent voltage collapse, online identification of load characteristics based on PMU measurement is useful to evaluate the proximity to voltage instability. Then based on different load characteristics, adaptive corrective control schemes will be implemented. The method should be capable of correctly predicting and preventing the voltage collapse with minimized load shedding.

In order to emphasize the main topics of this project, the above main objectives of the PhD project will be presented in detail in the following chapters in the main part of the thesis. Other objectives, e.g. protection based on multi-agent concept and

practical test of PMU devices, will be covered in the attached published papers of the PhD candidate behind the main part of the thesis.

1.3 Scopes and Limitations

The scopes and limitations of this research are as follows:

- During the simulation in DIgSILENT/PowerFactory, as for load flow calculation, AC load flow only with balanced, positive sequence is considered; unbalanced load flow is not considered. As for time-domain simulation, Root Mean Square (RMS) values (Electromechanical Transients) only with balanced, positive sequence components are considered, RMS values with unbalanced components and EMT values (Electromagnetic Transients) are not considered.
- The original model of western Danish power system developed in DIgSILENT PowerFactory is provided by Danish TSO—Energinet.dk. Later, some of the important elements are replaced by more detailed models using typical data, e.g. offshore wind farms, LCC-HVDC links.
- For wide-area control and protection schemes, the issues of bit error rate and communication delay of WAMS are not considered in the scope of this research.
- During short-term time-domain simulations (within 10sec) for DSA, the wind speed of each wind turbine is assumed to be invariant.

1.4 Thesis Outline

This PhD dissertation contains eleven chapters and will be organized as five parts as follows:

- **Part I – Background, Objectives and State-of-the-art**

Chapter 1—Introduction: Provides the background, motivations and objectives of this project. Also the technical contributions and the limitations of the project are discussed.

Chapter 2—State-of-the-art: Presents a comprehensive overview of phasor measurement unit (PMU) techniques, reviews the current applications of PMU all over the world, especially in Denmark, and analyzes the limitations of PMU. In addition, a literature survey of PMU applications in wide area monitoring, protection

and control (WAMPAC) is provided in terms of the classifications of power system stability issues.

- **Part II – Vulnerability Assessment of Power Systems**

Chapter 3—Introduction of Danish Power System: Discusses the Danish power system, focusing on the characteristics of current Danish power system and the challenges of future Danish power system.

Chapter 4—Structural Vulnerability Assessment: Introduces some principles of complex network theory and proposes several vulnerability indices to assess the structural vulnerability of western Danish power system, especially explores the impact of DG units on the structural vulnerability of the power grid.

Chapter 5—Dynamic Vulnerability Assessment: Describes the detailed models of onshore and offshore wind farms in DIgSILENT/PowerFactory, assesses the dynamic vulnerability of western Danish power system based on critical clearing time (CCT) screening in different positions, for various scenarios. Besides, the impacts of the main influencing factors on the dynamic vulnerability of power systems are investigated.

- **Part III – Dynamic Security Assessment and Corresponding Preventive Control Scheme**

Chapter 6—Introduction of Decision Tree Algorithms: Introduces the fundamental knowledge of decision tree algorithms and provides an overview on a variety of decision tree applications in the field of power systems.

Chapter 7—Preventive Control Scheme Based on Decision Trees: Proposes a decision tree based systematic approach for the online dynamic security assessment and the corresponding preventive control scheme. With the help of WAMS, a novel approach employs two decision trees to work in tandem for the preventive control of western Danish power systems. Then, the optimal control trajectory is searched out taking into account the cost of generation rescheduling and the penalty on the violation of international power exchange.

Chapter 8—Online Dynamic Security Assessment Based on Random Forest: Surveys the methodologies of dynamic security assessment and introduces the principles of random forest (RF) algorithm. A methodology that uses RF for online DSA is proposed, which can not only assess the security states of current operating conditions with high accuracy, but also indicate the adaptability of the created RF model.

Chapter 9—Case Study of Online DSA and Corresponding Preventive Control in Danish Power System: Verifies the proposed online dynamic security assessment and corresponding preventive control scheme by the case study of western Danish power system.

- **Part IV – Other Applications of PMU**

Chapter 10—Identification of Load Characteristic and the Corresponding Adaptive Corrective Scheme: Analyzes the relationship between load characteristic and the voltage collapse point and then develops an adaptive corrective scheme based on the identification of load characteristics using PMU measurements.

- **Part V – Conclusions and Perspectives**

Chapter 11—Conclusions and Future Work: Presents the main conclusions of the thesis, followed by the discussion of perspective work in the future.

References

[1] J. Waldau, F. M. Ferrario, M. Banja *et al.*, "Renewable Energy Snapshot 2013," *Joint Research Center of European Commission*.

[2] United in tough times, *The European Wind Energy Association Annual Report 2012*.

[3] Oversigtstabel Vindkraft. (Jul. 2013). Stamdataregister for vindmøller, [Online]. Available: http://www.ens.dk/info/tal-kort/statistik-noegletal/oversigt-energisektoren/stamdataregister-vindmoller, assessed on 31-Aug-2013.

[4] *IEA Wind Annual Report 2012*, International Energy Agency, [Online]. Available: http://www.iea.org/publications/freepublications/publication/IEA_Annual_Report_publicversion.pdf, assessed on 29-Aug-2013.

[5] P. Lund, "The Danish cell project – Part 1: background and general approach," in *Proc. of IEEE PES General Meeting*, Tampa, USA, Jun. 2007.

[6] U.S.-Canada Power System Outage Task Force, *Final Report on the August 14, 2003 Blackout in the United States and Canada: Causes and Recommendations*, Apr. 2004.

[7] UCTE Investigation Committee, *Final Report of the Investigation Committee on the 28 September 2003 Blackout in Italy*, Apr. 2004.

[8] Elkraft System, *Power failure in Eastern Denmark and Southern Sweden on 23 September 2003 Final Report on the Course of Events*, Nov. 2003.

[9] *Tilstandsovervågning af elnettet med PMU_WAMS*, [Online]. Available: http://www.energinet.dk/DA/Soeg/Sider/Publikationsvisning.aspx?Filter1Value=2262&Filter1Field=Id, assessed on 27-Aug-2013.

Chapter 2

State-of-the-art

2.1 Wide Area Measurement System

In the past few decades, power systems have been deregulated, restructured and decentralized in order to increase their efficiency, to reduce the operational cost and to set free the consumers from their limitations of choosing electricity providers [1]. Additionally, renewable energy techniques are being rapidly developed worldwide and integrated to the power grids with a tremendous pace which bring more challenges in the operation, control and protection of power systems [2]-[4]. As one of the prospective solutions to these challenges, wide area measurement system (WAMS) becomes more and more prevalent for modern power systems. WAMS are synergistic combination of distributed measuring instruments, time-synchronization devices, automation equipments, monitoring equipments and communication employed to construct a system-wide strategy in order to better estimate, monitor, control and protect the power system intelligently and adaptively [5], [6]. Phasor measurement units (PMUs), are the distributed measuring devices commercially available and widely applied to power systems, which play an important role in WAMS

In this chapter, the main techniques of PMU are firstly introduced followed by the state-of-the-art of PMU installation and application worldwide, especially in Denmark. Based on the author's experience in the practical test of PMU devices, the potentials and limitations of PMU are presented [7]. Finally, a literature survey of PMU applications is provided in terms of the classification of power system stability issues.

2.1.1 Phasor Measurement Units Techniques

PMU is a device which measures the electrical variables of an electrical power grid using a common time source for the synchronization of those measured variables [8]. Currently, PMUs can be dedicated devices, or PMU function can also be incorporated into intelligent electronic devices (IEDs), such as digital protective relays, digital fault recorders, digital disturbance recorders and so on through the firmware upgrade [9].

The first PMU prototype was invented by A. G. Phake and J. S. Thorp *et al.* in Virginia Tech. in 1988, which was then applied to Bonneville Power Administration

(BPA) and American Electric Power (AEP), both belonging to the western system coordinating council (WECC) [10], [11]. These PMUs were tested and used by utilities for several years before the first commercial unit, Macrodyne 1690, introduced in 1991 [12]. The initial motivation of bringing PMU to BPA was due to the fact that the WECC faced the critical lack of dynamic information throughout 1980s, so WECC was the first field test-bed for WAMS implementation [13]-[15].

In 1995, the US Department of Energy (DOE) and the Electric Power Research Institute (EPRI) launched the WAMS project. The aim of this project was to reinforce the western system dynamic information network (WesDINet). Dynamic information provided by WesDINet has been very important and useful for understanding the blackouts. This dynamic information could also be used for the purpose of avoiding future disturbances. Furthermore, during the deregulation and restructuring process, information resources provided by this WAMS were utilized to maintain the system reliability [16].

Since 2000, more and more WAMSs have been developed over the world. More PMU models have become available with a wide range of options. Many novel applications have been developed for the analysis of recorded data as well as the real time display and alarming [17].

In 2002, US DOE initiated the Eastern Interconnection Phasor Project (EIPP), building on over a decade of experience in WECC. In 2007, North American Electric Reliability Corporation (NERC) formally joined DOE in this effort, and expanded it to include all interconnections within North America. Hence, at this time, the EIPP was renamed as the North American SynchroPhasor Initiative (NASPI) [18], [19].

Simultaneously, a more convenient frequency monitoring network (FNET) system based on frequency disturbance recorders (FDRs) installed at ordinary 120V outlets was developed to measure the power system frequency and voltage. Currently, the system is operated by the Center for Ultra-wide-area Resilient Electric Energy Transmission Networks (CURENT) located at University of Tennessee, Knoxville, USA [20]-[24].

A PMU can measure 50/60 Hz AC waveforms (voltage and current) typically at a rate of 48 or 96 samples per cycle. The analog AC waveform is digitized by Analog to Digital (A/D) converter for each phase. A phase-lock oscillator along with a Global Positioning System (GPS) reference source provides the needed high-speed synchronized sampling with 1 μs accuracy. The time tagged phasors can then be transmitted to a phasor data concentrator (PDC) or directly to the super phasor data concentrator (SPDC) in the control center with the rate up to 60 samples per second

[25], [26]. Fig. 2.1 shows the PMU module and the structure of WAMS [5], [18]. A list of WAMS related standards as of July 2012 is summarized in Table 2.1 [27], [28].

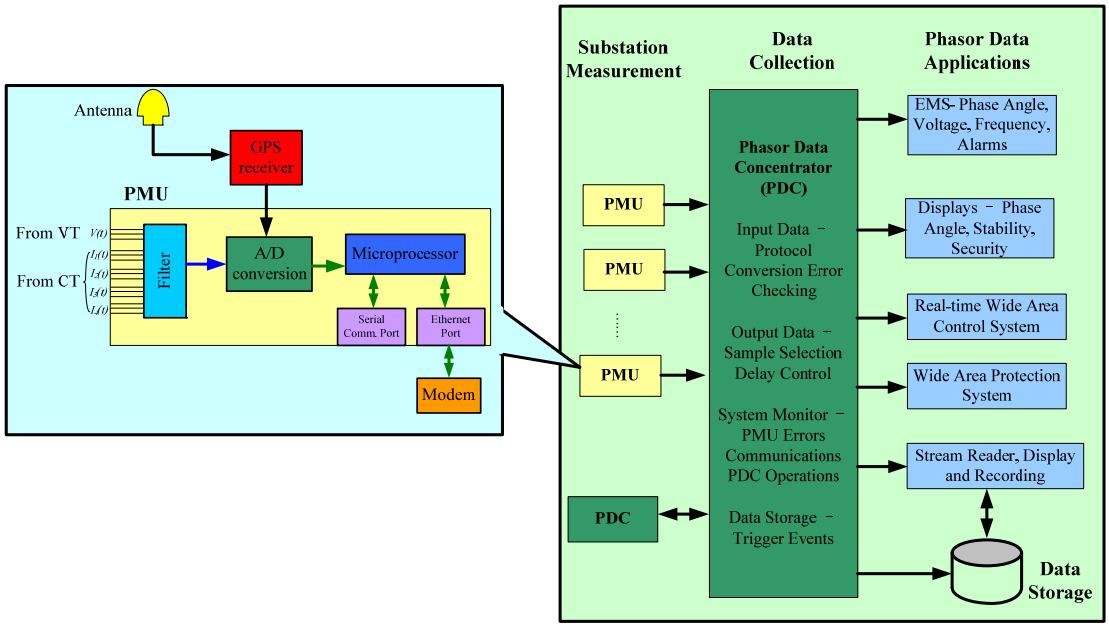

Fig. 2.1 PMU module and wide area measurement system (WAMS).

TABLE 2.1 LIST OF WAMS RELATED STANDARDS AS OF 2012

Standard No.	Name	Statues
IEEE 37.111-1999	COMTRADE	Approved [29]
IEEE 37.118-2005	Standard for synchrophasors for power systems	Approved [30]
IEEE 37.232-2007	Recommended practice for naming time sequence data files	Approved [31]
IEEE 37.239-2010	COMFEDE	Approved [32]
IEEE PC37.238-2011	Standard profile for use of 1588, precision time protocols in power system applications	Approved [33]
NERC CIP 2-9, Version #5	Cyber security standards transition guidance	Approved [34]
IEC 61850 (90-5), 2012	PMU logical node	Approved [35]
IEEE 37.118.1-2011	Synchrophasor measurement	Approved [36]
IEEE 37.118.2-2011	Synchrophasor communications	Approved [37]
IEC 61850	Substation automation	Approved
IEC 61970	Common information model	Approved
IEEE 1815-2010	DNP standard for electric power system communications	Approved [38]
IETF RFC6272	Internet Protocol Standards for Smart Grid	Approved [39]
IEC 60255-24, Ed. 2	IEC version of COMTRADE	In approval process
PC C37.244	Guide for Phasor Data Concentrator Requirements for Power System Protection, Control and Monitoring	In approval process
PC C37.242	Guide for Phasor Data Concentrator Requirements for Power System Protection, Control and Monitoring	In approval process
PC 37.240	Standard for cyber security requirement for substation automation, protection and control systems	Under development

2.1.2 State-of-the-art of PMU applications

During the last two decades, the installation of PMUs has increased considerably all over the world, because the need for the better estimation of the overall power systems' state is recognized to be a significant factor to improve its resilience in face of catastrophic failures. However, in most countries, PMUs only take the responsibility of power systems monitoring, while the wide-area close-loop control and protection of power system are still in their infancy stage, albeit some of the advanced technologies have already been in the field-test stages. Table 2.2 gives a brief survey on the focuses of PMU applications around the world, i.e. North America, Continental Europe, Russia, Nordic countries and China [40]-[47].

TABLE 2.2 APPLICATIONS OF PMU ALL OVER THE WORLD

Countries/Regions	Applications
North America	● Analysis of system oscillation modes (low frequency oscillations), generator performance and model validation, HVDC model validation, phase-angle alarm; ● Dynamic data monitoring and analysis (angle, frequency, power flows); ● Restoration: synchronization check, and black start; ● Situational awareness for reducing blackouts, increasing power transfers monitoring, quick situation assessment, integrity protection scheme; ● Disturbance analysis, dynamic analysis, postmortem analysis, data visualization using geographical maps; ● State estimation; ● Trending display of frequency, phase angle monitoring; ● Evaluation of voltage and transient stability.
Continental Europe	● Voltage phase angle difference monitoring; ● Line thermal monitoring (medium value between two substations); ● Voltage stability monitoring (online P–V curves); ● Online monitoring of system damping (online modal analysis with online parameter estimation).
Russia	● System performance monitoring and analysis; ● Reference dynamic model (RDM) validation; ● Validation test after the disturbance of imbalance of active power; ● Low-frequency (i.e. 0.02-0.2Hz) oscillation monitoring and damping; ● Steady-state assessment and dynamic performance investigation for emergency control.
Nordic Countries	● Calculation of short-circuit power by HVDC lines by monitoring the margin to collapse; ● Monitoring low-frequency oscillations in the grid by early warning of instability and oscillation in the grid; ● Verification of power system simulation models by state estimation; ● Logging the system events by optimization of the operation using the electronic registration; ● Backup security scheme by redundant measuring systems.
China	● Dynamic analysis of the available transmission capability; ● Wide-area data recording and playback; ● Online frequency oscillation analysis; ● Close-loop low-frequency identification and damping control system; ● State estimation; ● Security assessment; ● Adaptive protection and emergency control.

TABLE 2.3 DETAILS OF PMU INSTALLATION IN WESTERN DANISH POWER SYSTEM AS OF 2012.

No.	Bus (Voltage Channel)	Bay (Current Channel)	Status
1	Vester Hassing 400 kV	Nordjyllandsværket	In operation
2	Vester Hassing 400 kV	ZL1 (shunt reactor)	In operation
3	Tjele 400 kV	Askjær	In operation
4	Fraugde 400 kV	Pole 1	In operation
5	Kassø 400 kV	Revsing	In operation
6	Kassø 400 kV	Flensburg	In operation
7	Ensted 220 kV	Flensburg	In operation
8	Trige 220 kV	Anholt windfarm	Planned
9	Anholt windfarm 220 kV	Trige	Planned
10	Tjele 400 kV	KT52 transfo. (Tjele 400/150kV)	Planned
11	Tjele 400 kV	Pole 4	Planned
12	Revsing 400 kV	Tjele	Planned

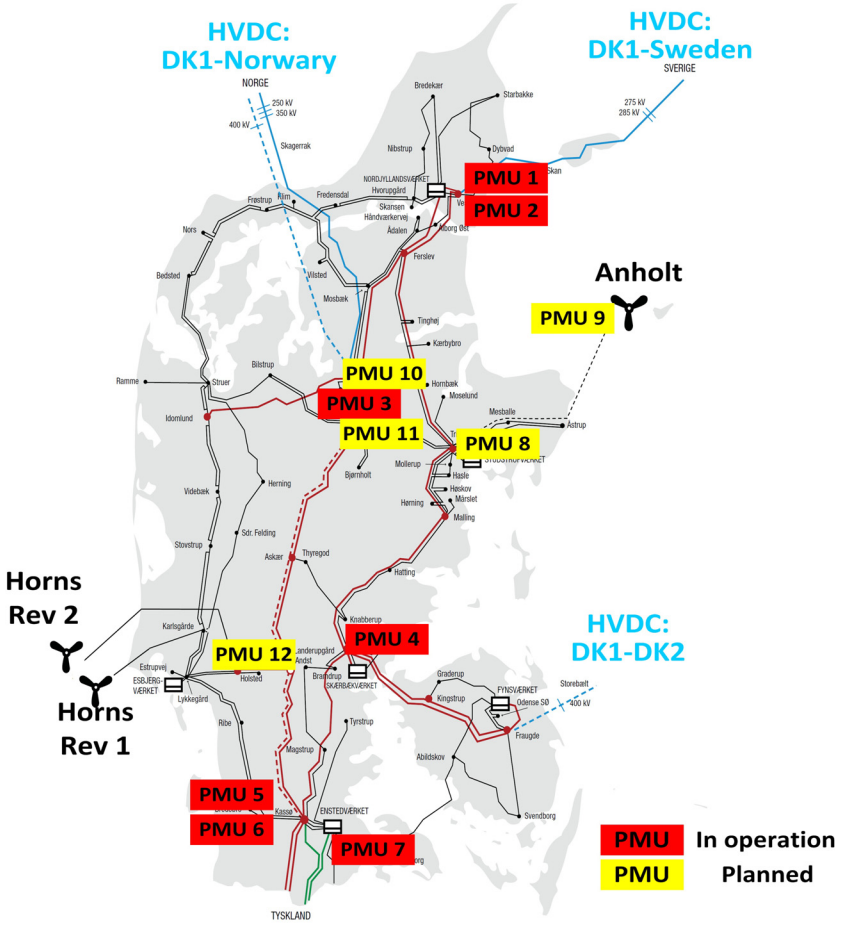

Fig. 2.2 PMU placement in western Danish power system as of 2012.

Danish power system is also making endeavor to sit in the front row and many activities have implemented not only on the laboratory scale but also as pilot project on the system scale [48], [49]. As shown in Fig. 2.2, by the year of 2012, 7 PMUs have been deployed for daily operation monitoring in western Danish power system, and 5 more PMUs will be implemented in the following years. According to system

plan, there will be more PMUs installed for higher observability in Danish power grid in the future. Table 2.3 lists the details of PMU placement in western Danish power system as of 2012.

2.1.3 Limitations of Phasor Measurement Units

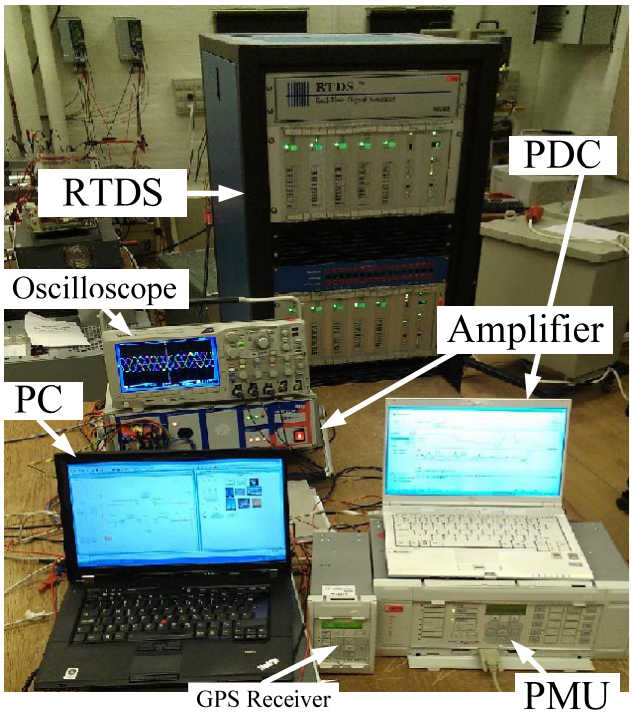

Fig. 2.3 Hardware setup of the RTDS based PMU testing platform.

In the author's previous publication [C4], the laboratory test and performance analysis of MiCOM PMU P847-B from Alstom Grid is carried out using Real Time Digital Simulator (RTDS). The hardware setup of RTDS based PMU testing platform is shown in Fig. 2.3. Based on the steady state testing and dynamic testing of Alstom PMU, some limitations of PMUs can be summarized as follows:

- Although the rate of reporting frames of PMU is much higher than that of Remote Terminal Unit (RTU) in SCADA systems, the rate of phasor frames is still limited to once per cycle of system frequency (50/60Hz). Therefore, some phenomenon with very short time constant or very fast dynamics, such as switching transient and traveling waves, can not be reported by PMU data.
- Since PMUs only provide the measurements of fundamental frequency of positive sequence component of voltage and current curves as well as the negative sequence and zero sequence component, the usage is restricted in the applications of harmonic analysis and the related issues in power systems.
- Even though PMUs give options in the configuration of its filtering windows, (5, 7 or 13 cycles for Alstom P847-B) during transient conditions after large

disturbances, waveforms of voltage and current would change significantly within one cycle. The calculated frequency and phasor are not standardized, which restricted the PMU in the primary protection of power systems.

- PMUs have the best steady state performance, lowest total vector error (TVE) only in the nominal frequency (50/60Hz), so in the emergency condition with large frequency deviation, the PMU data is not highly accurate unless they are carefully compensated.
- The current transformers and voltage transformers also bring some error to degrade the performance of measurements, so a carefully configuration of PMU is necessary before the commission in order to align the measured phasor with the real phasor for different operating conditions.

2.2 Phasor Measurement Units Applications

With the development of information communication technology (ICT), PMU and its associated WAMS technologies have become more and more matured in recent years, but their practical value is decided by the applications of the collected data. Many PMU applications have been developing quickly recently, such as power system state estimation [50], real-time congestion management [51], validation of system models [52], post-disturbance analysis [53], thermal monitoring [54] etc., however, the most fruitful and promising applications stay in the wide area monitoring, control and protection system (WAMPAC).

2.2.1 Wide Area Monitoring, Protection and Control System

Up to now, there is not a clear discrimination between wide area control and wide area protection. Different definitions of wide area control and wide are protection could be found in different sources. Hence, a suite of different systematic applications aimed at handling various wide area requirements can also be summarized by the concept of WAMPAC [27], [45], [55], [56]. However, a definition of wide area control system described below is employed in this thesis. Wide Area Control System (WACS) is defined as a systematic approach which is based on the analysis of wide area stability and security issues; after the recognition of an operating state prone to instability or insecurity, WACS influences the behavior of power system to follow a certain continuous trajectory to avoid instability and keep the power system within secure/stable boundaries. Usually, the response-based feedback control loop is employed to implement WACS, as illustrated in Fig. 2.4.

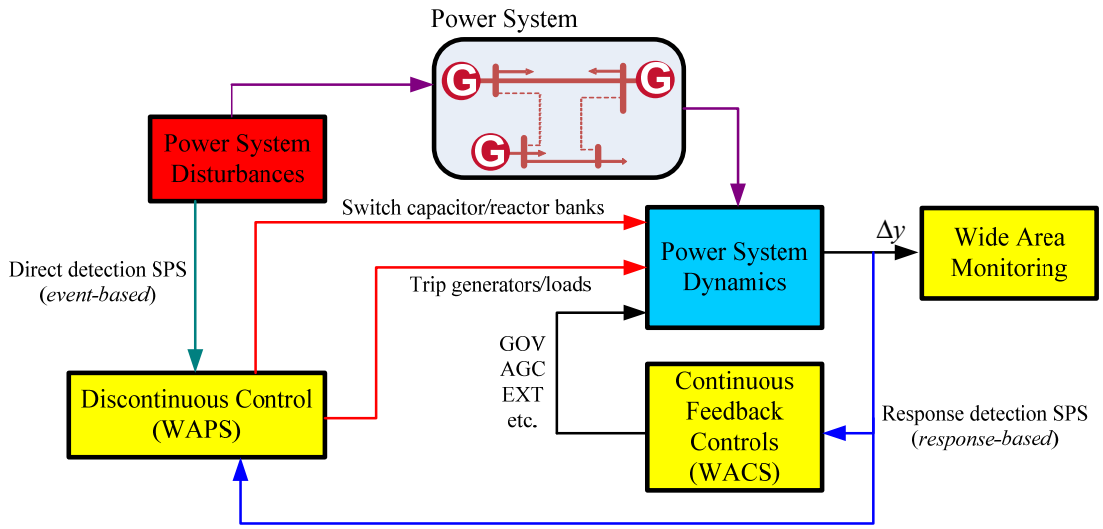

Fig. 2.4 Wide area monitoring, protection and control system [14].

The overall power system stability problem can be classified into several sub-categories, based on considerations regarding the physical natures, severity of disturbances, time spans etc.. In 2004, Kundur *et al.* provided the authoritative classification of power system stability problems, as shown in Fig. 2.5 [57]. A lot of discussion and research have been made in many publications and reports on building WAMPAC system for avoiding a specific stability problem, such as, frequency stability, voltage stability, transient stability and small signal stability.

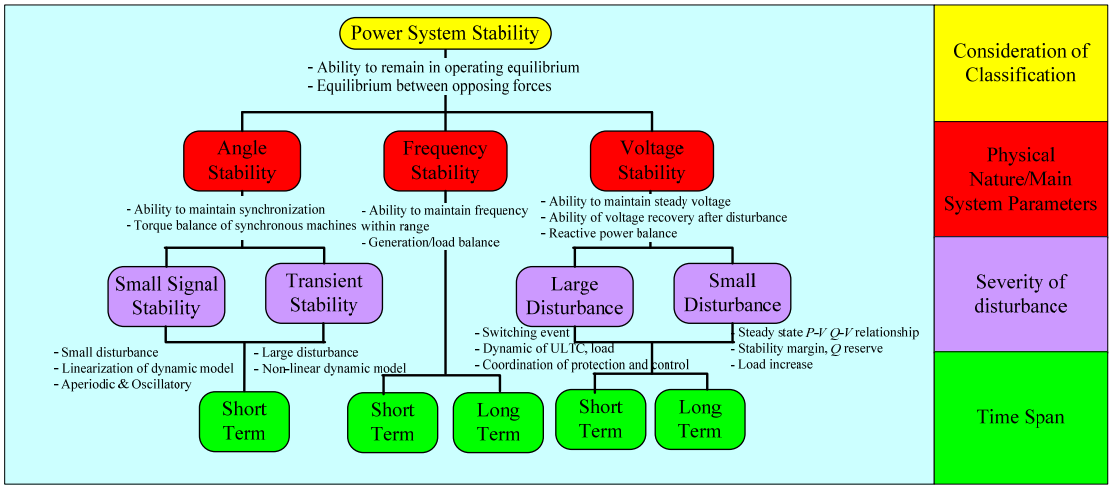

Fig. 2.5 Classification of the power system stability problems into sub-categories [57].

2.2.2 WAMPAC Applications in Frequency Stability

Keeping frequency within the nominal operating range (ideally at nominal constant frequency, 50Hz or 60Hz) is a significant aspect for the proper operation of a power

system. In Denmark, the primary regulation must be supplied at a frequency deviation of up to ±200mHz relative to the reference frequency of 50Hz with a permitted dead-band of only ±20mHz [58]. Ancillary services, such as primary reserves, secondary reserves (load frequency control) and tertiary reserves (manual reserves) are delivered to Danish power grid to maintain the frequency in different time-scale. The maximum acceptable frequency deviation for continuous operation of generators and other apparatus must be within 49.5Hz to 50.5Hz [59]. When the boundary is reached, unit protection may disconnect the power plants, which may make the situation even worse, because frequency may further decrease and it may result in the total collapse of the whole system. Therefore, some other emergency control schemes can be employed to prevent the blackouts, such as:

- HVDC power transfer control;
- Load shedding;
- Controlled disconnection with neighboring systems to prevent the spread of frequency outrange;
- Controlled islanding of local system into separate areas with balanced generation and load.

For current common practice, most of these emergency frequency control actions are executed manually by the operators of power grids expect Automatic Under-Frequency Load Shedding (AUFLS). They are triggered momentarily or after a time delay if the frequency drops below a predefined level and/or over a predefined rate of change [60]. The current AUFLS schemes in western Denmark (DK1) and eastern Denmark (DK2) are shown in Table 2.4 [61].

TABLE 2.4 AUTOMATIC UNDER-FREQUENCY LOAD SHEDDING SCHEME IN DENMARK

Power Grid	Configuration	Total
DK1	10% of consumption, f<48.5Hz momentary, f<48.7Hz 20sec. 10% of consumption, f<48.3Hz momentary, f<48.5Hz 20sec. 10% of consumption, f<48.1Hz momentary, f<48.3Hz 20sec. 10% of consumption, f<47.9Hz momentary, f<48.1Hz 20sec. 10% of consumption, f<47.7Hz momentary, f<47.9Hz 20sec.	Total 50%
DK2	15% of consumption, f<48.7Hz momentary, f<48.9Hz 20sec. 25% of consumption, f<47.7Hz momentary, f<47.9Hz 20sec.	Total 40%

Nevertheless, the effectiveness of AUFLSs is strongly dependent on the tuning and configuration based on the pre-study of the system, there is no on-line coordination between them. In addition, since AUFLSs are not capable of adapting to the current operating condition, and in Denmark, large amount of dispersed generation varies quite often, the disconnection of distribution feeders may deteriorate the frequency instability. The weakness of abovementioned emergency frequency control scheme

can be overcome by WAMPAC system, as described in [62]-[66]. Some of them have already been commissioned for operation.

Hydro-Quebec's defense plan commissioned an adaptive AUFLS system in 2000, called Remote Load Shedding System (RLSS) [62]. RLSS can calculate the power to be shed dependent on the severity of events in 735kV transmission network and send commands to Programmable Load Shedding Systems (PLSS) which is a device that executes the received load shedding commands in emergency scenarios and works as a back up for conventional local under-frequency load shedding (UFLS) relays. In [63], neural network algorithm is used to estimate the dynamic response of the power system for the UFLS. This information is then used to calculate an optimal amount of load to be shed. In [64], predictive control is applied in UFLS, which takes into account both frequency and voltage sensitivity/dependency of loads. Immediately after a disturbance, the load behavior and parameters are observed and then used in the predictive control of load shedding. In [65], a hierarchical scheme is proposed based on WAMS for the coordinated control of conventional synchronous generators, wind farms and FACTS to greatly improve the short-term frequency regulation capacity of power system with a large penetration of wind energy. In [66], a novel self-healing scheme for load curtailment in power system under critical contingencies is proposed considering both frequency and voltage response from WAMS.

2.2.3 WAMPAC Applications in Voltage Stability

Voltage stability refers to the ability of power systems to maintain steady voltage at all buses in the system after being subjected to a disturbance from a given initial operating condition [67]. Whilst, voltage collapse usually takes on the form of a dramatic drop of transmission system voltage, which is basically caused by an unavailability of reactive power support in some nodes of the network, where the voltage uncontrollably falls [68], [69]. Lack of reactive power may essentially have two origins. (1) Gradual increase of power demand where the reactive power cannot be met in some buses or (2) Sudden change of a network topology redirecting the power flows in such a way that the reactive power cannot be delivered to some buses.

More advanced local approaches for detection and evaluation of voltage instability have been presented in [70]-[74]. The external grid in the supervised node is represented by Thevenin equivalent circuit and the load is modeled by impedance. The point of equal impedances between Thevenin equivalent circuit and load impedence is then representing a boundary between stable and unstable conditions.

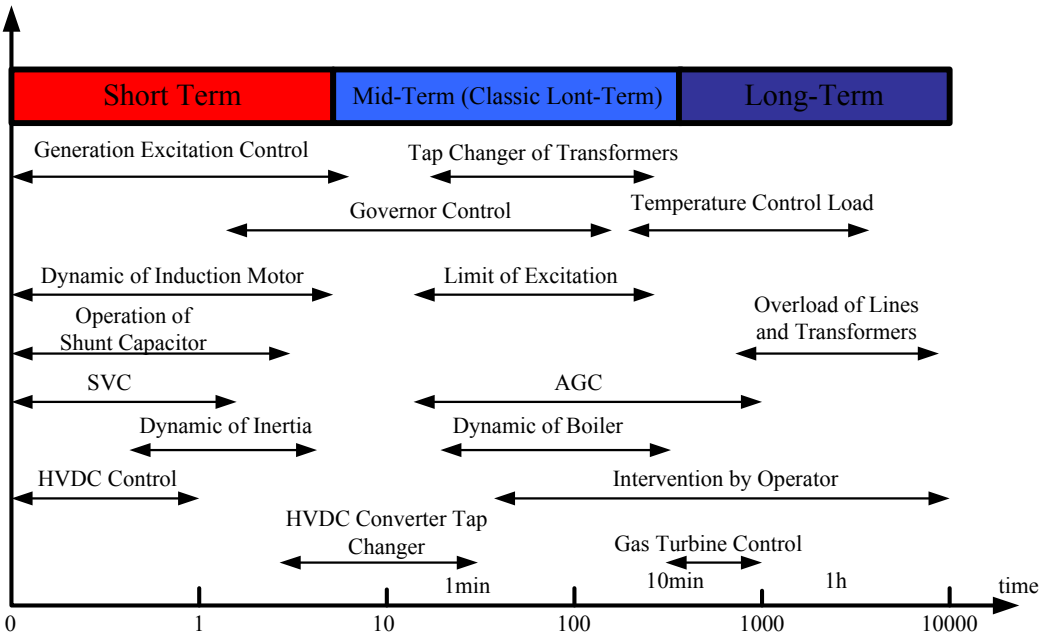

Fig. 2.6 Time frame of voltage power stability problem [68].

However, the analyses of real voltage collapses have shown their wide area nature and that they can be sorted basically into two categories according to the speed of their evolution——short-term voltage instability as well as mid-term and long-term voltage instability [67]-[69]. Short-term voltage instability is in the range of seconds (usually 1~3 sec) and the main role in the incidents is played by the dynamics of induction motors as a load, mainly from air conditioning system. The time scale of the mid-term and long-term voltage instability ranges from tens of seconds up to several minutes, even to several hours. It mainly involves impact of a topology change or gradual load increase, i.e. slow dynamics, as shown in Fig. 2.6 [68]. Therefore the major part of the research activities in this area has focused on the steady state aspects of voltage stability, i.e. finding the maximum load ability point of the *P*-*V* curve. This provides a basis for a number of indices from WAMS, expressing the proximity to the voltage collapse [75]-[78].

The preliminary research of wide area control system against long-term voltage stability is based on SCADA system in southern Sweden [79]. Karlsson *et al.* implement the logical decision-making process and order specific automatic actions based on global data from distributed SCADA system to maintain the system voltage. Later, they propose a coordinated WAMPAC system against voltage collapse based on model-predictive control and heuristic tree search [80]. The simulation based on Nordic-32 test system shows that the coordinated scheme reduces the amount of required load shedding by 35% compared to the local scheme.

For short-term voltage stability issue, an idea of preventive analysis is proposed based on the regular on-line *N-1* contingency analysis and applied immediately after the insecure operating condition is detected. In the voltage instability case, it means calculations of a minimal load shedding necessary to stabilize the power system subjected to any contingency from the selected range. Thus, an optimization problem can be formulated, where the objective function to be minimized is the amount of load shedding [81]. A step forward is Quasi Steady-State (QSS) approximation in [82]. This method consists of voltage stability evaluation based on the time-domain simulation with a simplified description of power system dynamics.

In [83], a novel concept for monitoring voltage instability with the characteristics of voltage-sensitive loads as well as the reactive-power reserves of generators taken into account is presented. Based on the local measurements from PMU as well as system-wide information on reactive-power reserves, the algorithm is adopted to determine the onset point of voltage collapse, suggests deploying control actions, such as load shedding, in case the stability margin is small and the reactive-power reserves are almost exhausted.

Corsi *et al.* propose wide area voltage control based on a hierarchical structure [84]. Two additional higher levels – Secondary Voltage Regulation (SVR) and Tertiary Voltage Regulation (TVR) are adopted to enrich the primary voltage regulation (PVR). National TVR shall coordinate with SVRs which control the voltage of pilot buses assigned to each area. The implementation of SVRs is reported to be already finished in the Italian power system [85], [86].

In [14], Taylor *et al.* propose a wide area stability and voltage control system and implement it in Bonneville Power Administration (BPA). From the simulation result based on the archived data, it is concluded that the fuzzy-rule based WACS could have prevented the cascading failure in Aug. 10th, 1996 and the blackout event in Jun. 14th 2004.

In [87], [88], Glavic *et al.* deal with the early detection of impending voltage instability from the system states provided by PMUs. It performs efficient sensitivity trajectory analysis to identify when a combination of load powers has passed through a maximum. The proposed method is tested on Nordic-32 system.

When power system is integrated with nonlinear model (e.g. over excitation limit) and dynamic model (e.g. dynamic load), it is difficult to exactly evaluate the voltage stability margin based on measurements from PMUs. Some advanced algorithms are adopted to assess the voltage stability margin considering complex power system models. In [89], artificial neural network is used to monitor voltage stability margin in

real time. In [90], the linear relationship between reactive power reserves and voltage stability margin is fitted out, which also realizes the early awareness of voltage instability based on PMUs.

2.2.4 WAMPAC Applications in Transient Stability

Transient stability involves a severe disturbance (typically 3-phase bolted short circuit) followed by trips of lines and transformers to clear the short circuit. After the disturbance, the response of power systems can be equivalent to the dynamics of a physical system, for example, ball-on-concave-surface (BOCS) mechanical system [91]. For transient instability cases, the power excited by the disturbance is then absorbed by rotors of generators, increasing their kinetic energy which results in the sudden acceleration of the rotors above the acceptable revolution, and eventually loss of synchronization.

Therefore, the countermeasures taken against this scenario aim to either dissipate the undelivered power, (e.g. braking resistor, FACTS devices, HVDC control etc.) or reduce the mechanical power which accelerates the generators. (e.g. fast-valving, disconnection of generators, controlled islanding etc.)

An application of traditional measure of transient angle instability – equal area criterion (EAC) (expressing a balance between the accelerating and decelerating energy), on emergency control is presented in [92]. The angles of the generators in the system are predicted approximately 200ms ahead. According to it, the generators are ranked and grouped into two categories. For the generators in the critical category, one-machine-infinite-bus (OMIB) equivalent is modeled and extended equal area criterion (EEAC) is applied to assess their stability. Pre-assigned corrective action is executed if an unstable generator is identified. In principle the similar algorithm is used for both off-line and on-line use [93], where the dynamic EEAC is employed for screening of the most severe contingencies that are then analyzed in detail. Simple rules derived from the classical relations of OMIB equivalent are proposed in [94]. The simulation results of Tokyo Interconnected Network show that the prediction of the loss of synchronism is 0.7s earlier, thus providing longer time for countermeasures.

In [95], simulation results show how the blackout of power system in Taiwan on July 29th, 1999 could have been avoided employing WAMS system against transient instability. The proposed algorithm aims to the protection of (extra high voltage) EHV tie lines connecting the generation area in the south with the load area in the north. The line power flow limit was used to modify the EAC for stability of the generators in the south.

In [96], an algorithm is suggested, which does not require knowledge of the system and uses only the on-line PMU measurements of generator's rotor angles and power mismatches to predict the transient angular stability of generators. It implies that it is not necessary for tuning procedure when this method is applied on another power system. Simulation tests on the 179-bus WSCC system have been carried out.

In [97], Kamwa *et al.* propose a PMU placement method for efficient assessment of the dynamic performance of Hydro-Quebec system to maximize the information content of the captured signals. Later, in [98], they proposed the fuzzy logic based wide-area severity index (WASI) for classification learning in order to predict the transient stability of power systems by post-disturbance measurement from PMU. The proposed algorithm has been successfully tested on Hydro-Quebec power system.

Many advanced machine learning algorithms based on PMU data, such as artificial neural network [99], decision trees [100], support vector machines [101], and reinforce learning method [102], are used to assess and protect against power system transient instability. Most of them consider *N-1* contingencies. In [103], a real time stabilizing control approach for responding to *N-k* contingencies, with larger *k*, is developed utilizing WAMS. The controls can follow an optimal principle in driving the rotor angles to an acceptable equilibrium point, at the minimum cost, by predicting the state response trajectories.

In [104], two systematic protection schemes for controlled islanding of Uruguayan electrical power system are proposed. Compared with the current utilities' practical scheme, the necessary load shedding can be reduced by 18% if only local PMU measurements are used, and reduced by 30% if system-wide PMU measurements are used.

2.2.5 WAMPAC Applications in Small Signal Stability

Some power systems lack a "natural" damping of oscillations, which would be instable when subjected to any minor disturbance or sometimes even under normal operating conditions if there is no countermeasures to increase the damping [105], [106]. In [107], it is stated that the extension of the transmission capacity by adding new lines does not necessarily improve the damping significantly.

A traditional way of damping the oscillation is to use Power System Stabilizer (PSS), which controls the output voltage of the generator. The coordinated tuning of PSSs is a complex task, since they should be robust—work in the wide range of operating conditions and provide the best possible performance [108].

Research of Hydro-Quebec system by Kamwa *et al.* has done significant work in the field of damping of inter-area oscillations. In [109], two-loop PSSs are proposed. The speed sensitive local loop operating the usual way is extended with a global loop using PMU measurements from two suitably selected areas. Five control sites comprising of four generators and one synchronous condenser have been chosen for the implementation of the proposed method. The simulations results show that a significant improvement in the damping of inter-area oscillations has been achieved [110].

In [111], a damping control system based on WAMS for multiple HVDC links is proposed to enhance the damping of inter-area modes and to minimize the interactions between different control loops. According to the test on China Southern Power Grid (CSG), the damping ratio of inter-area oscillation can be enhanced to more than 10%, and the power transfer capability in CSG can be increased by more than 100MW during summer peak load.

Various techniques aiming at the identification of oscillation modes from PMU measurements have been reported. For example, for the estimation of inter-area oscillation modes in Nordel grid, the PMU measurements from distribution network have been utilized [112]. However, the distribution network is probably not the best choice since the measurements contain quite a lot of noise and extraction of information about the two typical Nordel oscillation modes was difficult. The monitoring of frequency on the transmission level, triggered by disturbances, shows more promising results [113]. Continental Europe system is multiple times larger than Nordel system, so the recorded oscillations measured from transmission network have much lower frequency and the measurement noise is more easily filtered out.

2.3 Summary

In this chapter, the phasor measurement units (PMU) techniques are introduced followed by the state-of-the-art of PMU installation and implementation worldwide, especially in Denmark. Based on the author's experience in the practical test of PMU devices, the potentials and limitations of PMU are presented. Furthermore, a literature survey of PMU applications in the monitoring, control and protection of power systems is presented.

Although much progress of WAMS has been achieved in the past two decades or so, there is still a big gap between current research status and industrial applications in the proposed theories, algorithms, methodologies etc.. Many problems still need to be

solved. For most power systems, the reliability of system-wide approaches is still waiting for the validation, test and improvement of the close-loop applications in industry.

Part of the content in this chapter has also been reported in the author's previous publication in [C4].

References

[1] R. D. Christie, B. F. Wollenberg and I. Wangensteen, "Transmission management in deregulated environment," *Proc. of the IEEE*, vol. 88, no. 2, pp. 170-195, Feb. 2000.

[2] F. Blaabjerg, R. Teodorescu, M. Liserre *et al.*, "Overview of control and grid synchronization for distributed power generation systems," *IEEE Trans. Ind. Electron.*, vol. 53, no. 5, pp. 1398-1409, Oct. 2006.

[3] F. Blaabjerg, Z. Chen and S. B. Kjaer, "Power electronics as efficient interface in dispersed power generation systems," *IEEE Trans. Power Electron.*, vol. 19, no. 5, pp. 1184-1194, Sep. 2004.

[4] Z. Chen, J. M. Guerrero and F. Blaabjerg, "A review of state of the art of power electronics for wind turbines," *IEEE Trans. Power Electron.*, vol. 24, no. 8, pp. 1859-1875, Aug. 2009.

[5] K. E. Martin and J. R. Carroll, "Phasing in the technology," *IEEE Power and Energy Magazine*, vol. 6, no. 5, pp. 24-33, Sep.-Oct. 2008.

[6] S. Horowitz, D. Novosel, V. Madani *et al.*, "System-wide protection," *IEEE Power and Energy Magazine*, vol. 6, no. 5, pp. 34-42, Sep.-Oct. 2008.

[7] C. Liu, Z. H. Rather, N. Stearn *et al.*, "Practical testing and performance analysis of Phasor Measurement Unit using real time digital simulator (RTDS)," in *Proc. of Energy Conference and Exhibition (ENERGYCON)*, Florence, Italy, Jun. 2012.

[8] A. G. Phadke, "Synchronized phasor measurements," in *Proc. of IEEE/PES Transmi. and Distrib. Conference and Exhibition: Asia Pacific*, Oct. 2002.

[9] R. O. Burnett, M. M. Butts and P. S. Sterlina, "Power system applications for phasor measurement units," *IEEE Comput. Appl. Power*, vol. 7, no. 1, pp. 8-13, Jan. 1994.

[10] J. S. Thorp, A. G. Phadke, and K. J. Karimi, "Real time voltage-phasor measurements for static state estimation," *IEEE Trans. Power App. Sys.*, vol. PAS-104, no. 11, pp. 3098-3106, Nov. 1985.

[11] A. G. Phadke, J. S. Thorp, and K. J. Karimi, "State estimation with phasor measurements," *IEEE Trans. Power Syst*., vol. 1, no. 1, pp. 233-241, Feb. 1986.

[12] A. G. Phadke, "Synchronized phasor measurements-a historical overview," in *Proc. of IEEE/PES Transmi. and Distrib. Conference and Exhibition: Asia Pacific*, Oct. 2002.

[13] J. F. Hauer and C. W. Taylor, "Information, reliability and control in the new power system," in *Proc. of American Control Conference*, Philadelphia, PA, Jun. 1998.

[14] C. W. Taylor, D. C. Erickson, K. E. Martin *et al.*, "WACS-wide area stability and voltage control system: R&D and online demonstration" *Proc. of the IEEE*, vol. 93, no. 5, pp. 892-906, May 2005.

[15] J. Y. Cai, Z. Huang, J. Hauer *et al.*, "Current status and experience of WAMS implementation in North America," in *Proc. of IEEE/PES Transmi. and Distrib. Conference and Exhibition: Asia Pacific*, Dalian, China, 2005.

[16] W. A. Mittelstade, P. E. Krause, P. N. Overholt *et al.*, "The DOE wide area measurement system (WAMS) project – demonstration of dynamic information technology for the future power system," EPRI report, no. CONF-960434-1, Jul. 1996.

[17] A. G. Phadke and J. S. Thorp, *Synchronized Phasor Measurements and Their Applications*. New York: Springer, 2008.

[18] J. E. Dagle, "The north American synchrophasor initiative," in *Proc. of IEEE PES General Meeting*, Galgory, AB, Canada, Jul. 2009.

[19] NASPI Home Page: https://www.naspi.org/, assessed on 24-Aug-2013.

[20] Z. Zhong, C. Xu, B. J. Billian *et al.*, "Power system frequency monitoring network (FNET) implementation," *IEEE Trans. Power Syst.*, vol. 20, no. 4, pp. 1914-1921, Nov. 2005.

[21] Y. Zhang, P. Marham, Y. Xia *et al.*, "Wide-area frequency monitoring network (FNET) architecture and applications," *IEEE Trans. Power Syst.*, vol. 1, no. 2, pp. 159-167, Sep. 2010.

[22] W. Li, J. Tang, and Y. Liu, "Online detection of start time and location for hypocenter in North America power grid," *IEEE Trans. Smart Grid*, vol. 1, no. 3, pp. 253-260, Dec. 2010.

[23] R. M. Gardner and Y. Liu, "Generation-load mismatch detection and analysis," *IEEE Trans. Smart Grid*, vol. 3, no. 1, pp. 105-112, Mar. 2012.

[24] Y. Liu, Z. Yuan, P. N. Markham *et al.*, "Application of power system frequency for digital audio authentication," *IEEE Trans. Power Del.*, vol. 27, no. 4, pp. 1820-1828, Oct. 2012.

[25] A. G. Phadke, "Synchronized phasor measurements in power systems," *IEEE Comput. Appl. Power*, vol. 6, no. 2, pp. 10-15, Apr. 1993.

[26] A. G. Phadke, B. Pickett, M. Adamiak *et al.*, "Synchronized sampling and phasor measurements for relaying and control," *IEEE Trans. Power Del.*, vol. 9, no. 1, pp. 442-452, Jan. 1994.

[27] M. Kezunovic and T. Popovic, "Wide area monitoring, protection and control system (WAMPAC) standards for cyber security requirements," EPRI report, version 2.0, Oct. 2012.

[28] K. E. Martin, G. Benmouyal, M. G. Adamiak *et al.*, "IEEE standard for synchrophasors for power systems," *IEEE Trans. Power Del.*, vol. 13, no. 1, pp. 73-77, Jan. 1998.

[29] *Common format for transient data exchange (COMTRADE) for power systems*, IEEE Standard 37.111-1999., Mar. 1999.

[30] *IEEE Standard for Synchrophasors for Power Systems*, IEEE Standard C37.118-2005., Mar. 2005

[31] *IEEE Recommended Practice for Naming Time Sequence Data Files*, IEEE Standard 37.232-2007, Aug. 2007.

[32] *IEEE Standard Common Format for Event Data Exchange (COMFEDE) for Power Systems*, IEEE Standard 37.239-2010, Nov. 2010.

[33] *IEEE Standard Profile for Use of IEEE 1588 Precision Time Protocol in Power System Applications*, IEEE Standard C37.238-2011, 2011.

[34] *North American Electric Reliability Corporation for Approval of Critical Infrastructure Protection Reliability Standards Version 5*, NERC Standard CIP 2-9, Version #5

[35] *Communication Networks and Systems for Power Utility Automation – Part 90-5: Use of IEC 61850 to Transient Synchrophasor Information According to IEEE C37.118*, IEC Standard 61850 (90-5), 2012.

[36] *IEEE Standard for Synchrophasors Measurements for Power Systems*, IEEE Standard C37.118.1-2001., Dec. 2001

[37] *IEEE Standard for Synchrophasors Data Transfer for Power Systems*, IEEE Standard C37.118.2-2001., Dec. 2001

[38] *Internet Protocols for the Smart Grid*, IETF. RFC 6272, Jun. 2001.

[39] *IEC TC57 Security Standards for the Power System's Information Infrastructure – Beyond Simple Encryption, Xanthus Consulting International,* Jun. 2007.

[40] A. G. Phadke and R. M. Moraes, "The wide world of wide-area measurement," *IEEE Power and Energy Magazine*, vol. 6, no. 5, pp. 52-65, Sep.-Oct. 2008.

[41] M. Chenine, Z. Kun, and L. Nordstrom, "Survey on priorities and communication requirements for PMU-based applications in the Nordic region," in *Proc. of IEEE PES PowerTech*, Bucharest, Romania, Jul. 2009.

[42] X. Zhao, J. Østergaard, M. Togeby *et al.*, "Evaluating frequency quality of Nordic system using PMU data," in *Proc. of PES General Meeting*, Pittsburgh, PA, USA, Jul. 2008.

[43] Q. Yang, T. Bi, and J. Wu, "WAMS Implementation in China and the challenges for bulk power system protection," in *Proc. of PES General Meeting*, Tampa, FL, USA, Jun. 2007.

[44] X. Xie, Y. Xin, J Xiao *et al.*, "WAMS applications in Chinese power systems," *IEEE Power and Energy Magazine*, vol. 4, no. 1, pp. 54-63, Sep.-Oct. 2006.

[45] V. Terzija, G. Valverde, D. Cai *et al.*, "Wide-area monitoring, protection and control of future electric power networks," *Proc. of the IEEE*, vol. 99, no. 1, pp. 80-93, Jan. 2011.

[46] S. Chakrabarti, E. Kyriakides, T. Bi *et al.*, "Measurements get together," *IEEE Power and Energy Magazine*, vol. 7, no. 1, pp. 41-49, Jan.-Feb. 2009.

[47] T. Rauhala, K. Saarinen, M. Latvala *et al.*, "Applications of phasor measurement units and wide-area measurement system in Finland," in *Proc. of IEEE PowerTech*, Trondheim, Norway, Jun. 2011.

[48] J. Rasmussen and P. Jørgensen, "Synchronized phasor measurements of a power system event in eastern Denmark," *IEEE Trans. Power Syst.*, vol. 21, no. 1, pp. 278-284, Feb. 2006.

[49] R. G. Valle, G. Yang, K. E. Martin *et al.*, "DTU PMU laboratory development – testing and validation," in *Proc. of IEEE ISGT Europe*, Gothenburg, Sweden, Oct. 2010.

[50] M. Zhao and A. Abur, "Multi area state estimation using synchronized phasor measurement," *IEEE Trans. Power Syst.*, vol. 20, no. 2, pp. 611-617, May 2005.

[51] A. Leirbukt, K. Uhlen, M. T. Palsson *et al.*, "Voltage and control for enhanced utilization of power grids," in *Proc. of IEEE PES Power System Conference and Exposition*, New York, USA, Oct. 2004.

[52] J. F. Hauer, W. A. Mittelstadt, K. E. Martin *et al.*, "Use of the WECC WAMS in wide-area probing tests for validation of system performance and modelling," *IEEE Trans. Power Syst.*, vol. 24, no. 1, pp. 250-257, Feb. 2009.

[53] S. Skok, I. Ivankovic and Z. Cerina, "Applications based on PMU technology for improved power system utilization," in *Proc. of PES General Meeting*, Tempa, FL, USA, Jun. 2007.

[54] Y. V. Makarov, P. Du, T. B. Nguyen, *et al.*, "PMU-based wide-area security assessment: concept, method, and implementation," *IEEE Trans. Smart Grid*, vol. 3, no. 3, pp. 1325-1332, Sep. 2012.

[55] J. Thorp, A. Abur, M. Begovic *et al.*, "Gaining a wide perspective," *IEEE Power and Energy Magazine*, vol. 6, no. 5, pp. 43-51, Sep.-Oct. 2008.

[56] D. Karlsson, M. Hemmingsson and S. Lindahl, "Wide area system monitoring and control – terminology, phenomena, and solution implementation strategies," *IEEE Power and Energy Magazine*, vol. 2, no. 5, pp. 68-76, Sep.-Oct. 2004.

[57] P. Kundur, J. Paserba, V. Ajjarapu *et al.*, "Definition and classification of power system stability IEEE/CIGRE joint task force on stability terms and definitions," *IEEE Trans. Power Syst.*, vol. 19, no. 3, pp. 1387-1401, May 2004.

[58] *Ancillary services to be delivered in Denmark Tender conditions,* Energinet.dk, Oct. 3rd, 2012.

[59] *Wind turbine connected to grids with voltages above 100kV, Technical regulation for the properties and the regulation of wind turbines,* Grid code from Energinet.dk, Dec. 2004.

[60] B. Delfino, S. Massucco, A. Morini *et al.*, "Implementation and comparison of different under frequency load-shedding schemes," in *Proc. of IEEE PES Summer Meeting*, Vancouver, CA, Jul. 2001.

[61] *Automatic Under-Frequency Load Shedding (AUFLS) Technical Report Appendix A: A Collation of International Policies for Under Frequency Load Shedding*, Transpower System Operator, Aug. 2010.

[62] G. Trudel, S. Bernard and G. Scott, "Hydro-Quebec's defense plan against extreme contingencies," *IEEE Trans. Power Syst.*, vol. 14, no. 3, pp. 958-965, Aug. 1999.

[63] M. A. Mitchell, J. A. Pecas Lopes, J. N. Fidalgo *et al.*, "Using a neural network to predict the dynamic frequency response of a power system to an under-frequency load shedding scenario," in *Proc. of IEEE PES Summer Meeting*, Seattle, WA, USA, Jul. 2000.

[64] M. Larsson and C. Rehtanz, "Predictive frequency stability control based on wide-area phasor measurements," in *Proc. of IEEE PES Summer Meeting*, Chicago, USA, Jul. 2002.

[65] K. Seethalekshmi, S. N. Singh and S. C. Srivastava, "A synchrophasor assisted frequency and voltage stability based load shedding scheme for self-healing of power system," *IEEE Trans. Smart Grid*, vol. 2, no. 2, pp. 221-230, Jun. 2011.

[66] A. E. Leon, J. M. Mauricio, A. Gomez-Exposito *et al.*, "Hierarchical wide-area control of power systems including wind farms and FACTS for short-term frequency regulation," *IEEE Trans. Power Syst.*, vol. 27, no. 4, pp. 2084-2092, Nov. 2012.

[67] P. Kundur, *Power System Stability and Control*, New York: McGraw-Hill, 1994, pp. 959-1024.

[68] C. W. Taylor, *Power System Voltage Stability*, New York: McGraw-Hill, 1994.

[69] Th. Van Cutsem and C. Vournas, *Voltage Stability of Electric Power Systems*, Norwell, MA, USA: Kluwer Academic Publisher, 1998, pp. 959-1024.

[70] K. Vu, M. M. Begovic, D. Novosel *et al.*, "Use of local measurements to estimate voltage-stability margin," *IEEE Trans. Power Syst.*, vol. 14, no. 3, Aug. 1999.

[71] F. Gubina and B. Strmcnik, "Voltage collapse proximity index determination using voltage phasors approach," *IEEE Trans. Power Syst.*, vol. 10, no. 2, May 1995.

[72] S. Corsi and G. N. Taranto, "A real-Time voltage instability identification algorithm based on local phasor measurements," *IEEE Trans. Power Syst.*, vol. 23, pp. 1271-1279, 2008.

[73] I. Smon, G. Verbic, and F. Gubina, "Local voltage-stability index using Tellegen's theorem," *IEEE Trans. Power Syst.*, vol. 21, no. 3, pp. 1267-1275, Aug. 2006.

[74] S. M. Abdelkader and D. J. Morrow, "Online tracking of Thevenin equivalent parameters using PMU measurements," *IEEE Trans. Power Syst.*, vol. 27, no. 2, pp. 975-983, May 2012.

[75] H. D. Chiang and R. Jean-Jumeau, "Towards a practical performance index for predicting voltage collapse in electric power systems," *IEEE Trans. Power Syst.*, vol. 10, no. 2, May 1995.

[76] C. Belhadj, R. Mohamedi, S. Lefebvre *et al.*, "Voltage stability modelling and real-time monitoring using expert system for operation assistance," *IEEE Trans. Power Syst.*, vol. 11, no. 2, May 1996.

[77] L. Wang and A. A. Girgis, "On-line detection of power system small disturbance voltage instability," *IEEE Trans. Power Syst.,* vol. 11, no. 3, Aug. 1996.

[78] A. Berizzi, P. Bresesti, P. Marannino *et al.*, "System-area operating margin assessment and security enhancement against voltage collapse," *IEEE Trans. Power Syst.*, vol. 11, no. 3, Aug. 1996.

[79] A. Ingelsson, P. O. Lindström, D. Karlsson *et al.*, "Wide-area protection against voltage collapse," *IEEE Computer Applications in Power*, vol. 10, issue 4, pp. 30-35, Oct. 1997.

[80] M. Larsson and D. Karlsson, "Coordinated system protection scheme against voltage collapse using heuristic search and predictive control," *IEEE Trans. Power Syst.*, vol. 18, no. 3, pp. 1001-1006, Aug. 2003.

[81] E. De Tuglie, M. Dicorato, M. La Scala *et al.*, "A corrective control for angle and voltage stability enhancement on the transient time-scale," *IEEE Trans. Power Syst.*, vol. 15, no. 4, Nov. 2000.

[82] L. Xie, Y. Chen and H. Liao, "Distributed online monitoring of quasi-static voltage collapse in multi-area power systems," *IEEE Trans. Power Syst.*, vol. 27, no. 4, pp. 2271-2279, Nov. 2012

[83] B. Milosevic, and M. Begovic, "Voltage-stability protection and control using a wide-area network of phasor measurements," *IEEE Trans. Power Syst.*, vol. 18, no. 1, pp. 121-127, 2003.

[84] S. Corsi, "Wide area voltage protection," *IET Gener., Transm. Distrib.*, vol. 4, no. 10, pp. 1164-1179, 2010.

[85] S. Corsi, M. Pozzi, C. Sabelli *et al.*, "The coordinated automatic voltage control of the Italian transmission grid – Part I: reasons of the choice and overview of the consolidated hierarchical system," *IEEE Trans. Power Syst.*, vol. 19, no. 4, pp. 1723-1732, Nov. 2004.

[86] S. Corsi, M. Pozzi, M. Sforna *et al.*, "The coordinated automatic voltage control of the Italian transmission grid – Part II: control apparatus and field performance of the consolidated hierarchical system," *IEEE Trans. Power Syst.*, vol. 19, no. 4, pp. 1733-1741, Nov. 2004.

[87] M. Glavic and Th. Van Cutsem, "Wide-area detection of voltage instability from synchronized phasor measurements. Part I: principle," *IEEE Trans. Power Syst.*, vol. 24, no. 3, pp. 1408-1416, Aug. 2009.

[88] M. Glavic and Th. Van Cutsem, "Wide-area detection of voltage instability from synchronized phasor measurements. Part II: simulation results," *IEEE Trans. Power Syst.*, vol. 24, no. 3, pp. 1417-1425, Aug. 2009.

[89] D. Q. Zhou, U. D. Annakkage and A. D. Rajapakse, "Online monitoring of voltage stability margin using an artificial neural network," *IEEE Trans. Power Syst.*, vol. 25, no. 3, pp. 1566-1574, Aug. 2010.

[90] B. Leonardi and V. Ajjarapu, "An approach for real time voltage stability margin control via reactive power reserve sensitivities," *IEEE Trans. Power Syst.*, vol. 28, no. 2, pp. 615-625, May 2013.

[91] K. Sun, S. T. Lee, and P. Zhang, "An adaptive power system equivalent for real-time estimation of stability margin using phase-plane trajectories," *IEEE Trans. Power Syst.*, vol. 26, no. 2, pp. 915-923, May 2011.

[92] D. Ernst and M. Pavella, "Closed-loop transient stability emergency control," in *Proc. of IEEE PES Winter Meeting*, Singapore, Jan. 2000.

[93] P. Kundur, G. K. Morison and L. Wang, "Techniques for on-line transient stability assessment and control," in *Proc. of IEEE PES Winter Meeting*, Singapore, Jan. 2000.

[94] T. Minakawa, "The required technological breakthrough in developing universal emergency control systems in terms with transient and dynamic stability," in *Proc. of IEEE PES Winter Meeting*, Singapore, Jan. 2000.

[95] Y. J. Wang, C. W. Liu, L. D. Sue *et al.*, "A remedial control scheme protects against transient instabilities based on phasor measurement units (PMUs) – a case study," in *Proc. of IEEE PES Summer Meeting*, Seattle, WA, USA, Jul. 2000.

[96] G. G. Karady, A. A. Daoud and M. A. Mohamed, "On-line transient stability enhancement using multi-agent technique," in *Proc. of IEEE PES Winter Meeting*, New York, NY, USA, Jan. 2002.

[97] I. Kamwa and R. Grondin, "PMU configuration for system dynamic performance measurement in large multiarea power systems," *IEEE Trans. Power Syst.*, vol. 17, no. 2, pp. 385-394, May 2002.

[98] I. Kamwa, S. R. Samantaray and G. Joos, "Development of rule-based classifiers for rapid stability assessment of wide-area post disturbance records," *IEEE Trans. Power Syst.*, vol. 24, no. 1, pp. 258-270, Feb. 2009.

[99] F. Hashiesh, H. E. Mostafa, A. R. Khatib *et al.*, "An intelligent wide area synchrophasor based system for predicting and mitigating transient instabilities," *IEEE Trans. Smart Grid*, vol. 3, no. 2, pp. 645-652, Jun. 2012.

[100] K. Sun, S. Likhate, V. Vittal *et al.*, "An online dynamic security assessment scheme using phasor measurements and decision trees," *IEEE Trans. Power Syst.*, vol. 22, no. 4, pp. 1935-1943, Nov. 2007.

[101] F. R. Gomez, A. D. Rajapakse, U. D. Annakkage *et al.*, "Support vector machine-based algorithm for post-fault transient stability status prediction using synchronized measurements," *IEEE Trans. Power Syst.*, vol. 26, no. 3, pp. 1474-1483, Aug. 2011.

[102] R. Hadidi and B. Jeyasurya, "Reinforcement learning based real-time wide area stabilizing control agents to enhance power system stability," *IEEE Trans. Smart Grid*, vol. 4, no. 1, pp. 489-497, Mar. 2013.

[103] G. C. Zweigle and V. Venkatasubramanian, "Wide-area optimal control of electric poewr systems with application to transient stability for higher order contingencies," *IEEE Trans. Power Syst.*, vol. 24, no. 1, pp. 258-270, Feb. 2009.

[104] R. Franco, C. Sena, G. N. Taranto *et al.*, "Using synchrophasors for controlled islanding – a prospective application for the Uruguayan power system," *IEEE Trans. Power Syst.*, vol. 28, no. 2, pp. 2016-2024, May 2013.

[105] G. Rogers, *Power System Oscillations*, Dordrecht, Netherlands: Kluwer Academic Publishers Group, 2000.

[106] A. R. Messina, *Inter-area Oscillation in Power Systems – A Nonlinear and Nonstationary Perspective*, New York: Springer, 2009.

[107] K. S. Shim, H. K. Nam, S. G. Song *et al.*, "Application results of the eigen-sensitivity theory of augmented matrix to small signal stability analysis of large power systems," in *Proc. of IEEE PES Summer Meeting*, Seattle, WA, USA, Jul. 2000.

[108] I. Kamwa, S. R. Samantaray and G. Joos, "Compliance analysis of PMU algorithms and devices for wide-area stabilizing control of large power systems," *IEEE Trans. Power Syst.*, vol. 28, no. 2, pp. 1766-1778, May 2013.

[109] I. Kamwa, "Using MIMO system identification for modal analysis and global stabilization of large power systems," in *Proc. of IEEE PES Summer Meeting*, Seattle, WA, USA, Jul. 2000.

[110] J. Wang, C. Fu and Y. Zhang, "Design of WAMS-based multiple HVDC damping control system," *IEEE Trans. Smart Grid*, vol. 2, no. 2, pp. 363-374, Jun. 2011.

[111] I. Kamwa, R. Grondin and Y. Hebert, "Wide-area measurement based stabilizing control of large power systems – a decentralized/hierarchical approach," *IEEE Trans. Power Syst.*, vol. 16, no. 1, pp. 136-153, Feb. 2001.

[112] M. Hemmingsson, O. Samuelsson, K. O. H. Pedersen *et al.*, "Estimation of electro-mechanical mode parameters using frequency measurements," in *Proc. of IEEE PES Winter Meeting*, Columbus, OH, USA, Jan.-Feb. 2001.

[113] H. Breulmann, E. Grebe, M. Loesing *et al.*, "Analysis and damping of inter-area oscillations in the UCTE/CENTREL power system," *CIGRE, 38-113*, Session 2000.

PART II

VULNERABILITY ASSESSMENT OF POWER SYSTEMS

Chapter 3

Introduction of Danish Power System

3.1 Characteristics of Current Danish Power System

Danish power grid comprises two non-synchronous systems, i.e. western Danish power system (DK1) and eastern Danish power system (DK2). Western Danish power system in Jylland Peninsula and Fyn Island which is synchronous with the European Network of Transmission System Operators for Electricity (ENTSO-E) RG Continental Europe via Germany, while eastern Danish power system in Zealand Island which is synchronous to Nordic system via Sweden. Besides, another small island situated in Baltic Sea, i.e. Bornholm Island, is operated by a distribution system operator (DSO), Østkraft, at 60kV and connected to Swedish power system at 132kV [1], [2]. DK1 and DK2 are interconnected by Great Belt High Voltage Direct Current (HVDC) link. Key figures of Danish power system as of 2011 are given in Table 3.1 [3], [4]. As can be seen, the ratio between installed wind power and consumption in DK1 is about twice higher than that in DK2. The geographical map of western and eastern Danish transmission systems in 2010 is shown in Appendix A [5].

TABLE 3.1 KEY FIGURES OF WESTERN AND EASTERN DANISH POWER SYSTEMS AS OF 2011

Production and Load	DK1	DK2
Minimum Load (MW)	1400	900
Maximum Load (MW)	3700	2700
Capacity of Primary Power Stations (MW)	3400	3800
Capacity of CHP Plants (MW)	1643	640
Capacity of Wind Turbines (MW)	2840	960

Denmark has abundant wind power resource. Onshore wind resources are highest in the western part of the country, and on the eastern islands with coastlines facing south or west. Additionally, the country has very large offshore wind resources, and large areas of sea territory with a shallow water depth of 5~15m, where sitting of offshore wind farms is most feasible. These offshore sites offer even higher wind speed, in the range of average 8.5~9.0m/s at 50m height [6].

Western Danish power system is operated at 400kV and 150kV at transmission level and 60/20/10/0.4kV at distribution level. The geographical map of western Danish transmission system in 2010 is shown in Fig. 3.1 [7], 6 central power plants

(CPPs) with 8 large synchronous generators are connected to the transmission system. A large number of onshore wind turbines and several offshore wind farms are integrated into the distribution system and transmission system respectively.

Fig. 3.1 Geographical map of western Danish transmission system in 2010 [7].

3.1.1 High Penetration of Wind Power

Past two decades has witnessed a massive expansion of wind power generation in Denmark. The European Wind Energy Association (EWEA) has set ambitious target in developing the wind power generation [8]. Accordingly, Denmark, which currently produces about 30% of electricity from wind, plans to realize a 50% wind share of electricity production by 2025, especially, offshore wind farms [9]. As shown in Fig. 3.2, by the end of 2011, the amount of wind generation capacity in Denmark approached 3927MW and the annual share of wind generation was 28.2%. The latest report comes out that the amount of wind power generation in Denmark increased to

4162MW and annual share of wind generation increased to 30.0%, in the year of 2012 [10].

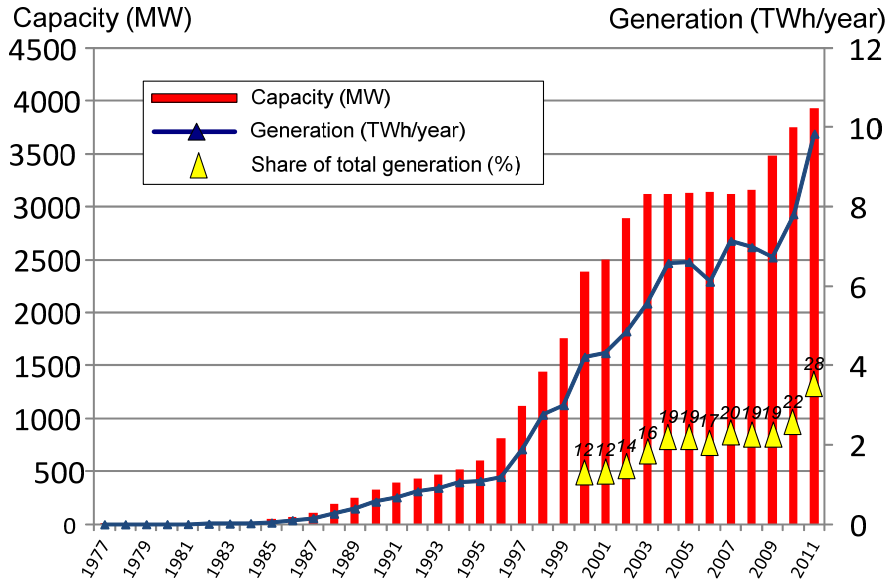

Fig. 3.2 Installed wind capacity, annual wind generation and capacity factors in Denmark from 1977 to 2011.

Two offshore wind farms Horns Rev 1 and Horns Rev 2 with capacities of 160MW and 209MW were commissioned in 2002 and 2009 respectively, while onshore wind farms with 2232MW capacity in total still composes major part of wind generation, which is distributed all over western Denmark. Anholt offshore wind farm with the capacity of 400MW is expected to be fully commissioned by the end of 2013. Table 3.2 shows the capacity of generations and load in western Danish power system [11].

TABLE 3.2 SOME KEY FIGURES OF WESTERN DANISH POWER SYSTEMS IN 2011

Production, Consumption and Power Exchange	Power (MW)
Capacity of Production, Total	7732
Capacity of Central Power Plant	3147
Capacity of Local CHP Capacity	2017
Capacity of Onshore Wind Turbines	2232
Capacity of Offshore Wind Farms	369
Capacity of Other DGs	326
Minimum Load	1306
Maximum Load	3664
Exchange Capacity Ex. (+)/ Im. (-)	3730/-3230
Maximum Capacity to ENTSO-E Ex. (+)/ Im. (-)	1500/-950
Maximum Capacity to Sweden Ex. (+)/ Im. (-)	740/-680
Maximum Capacity to Norway Ex. (+)/ Im. (-)	1000/-1000
Maximum Capacity to Eastern Denmark Ex. (+)/ Im. (-)	590/-600

As a result, primarily Energinet.dk has to face the large technical challenges in managing and operating Danish power system with a significant penetration of wind

power. The following factors are some of the reasons that Danish power system is able to be operated in scenarios with such large amount of wind power.

The interconnection of western Danish power system to external grid is so strong to overcome the wind power intermittences. In addition, the temporary fluctuation of wind energy can be compensated under the help of external grids. To the north, the western Danish power system is connected to Norway and Sweden via HVDC links. The capabilities of 3 HVDC links to Norway are 275MW, 275MW and 500MW, and the capabilities of 2 HVDC links to Sweden are 380MW and 360MW respectively. To the south, it is connected to the ENTSO-E synchronous area via two 400kV and two 220kV AC transmission lines to Germany. To the east, the HVDC link—"Great Belt" with capacity of 600MW was commissioned in July 2010 interconnecting western Danish power system and eastern Danish power system. The abundance of hydro power generation in Norwegian and Swedish power systems can cooperate with the wind power generation in Denmark and Germany. Hence, the 400kV transmission system often acts as the power transmission corridor, which is subject to significant amount of active power transport.

The reactive power generation and voltage control is mainly provided by large CPPs. Besides, two synchronous compensators at 150kV substations close at the connection points of HVDC links to Norway and Sweden, with capacity of 160MVA and 100MVA respectively are installed mainly for the secure operation of Line Commutated Converter (LCC-HVDC). Currently, the voltage regulation is maintained by the CPPs, while in the future, some large offshore power plants subjected to the new grid code will play part of the role in keeping voltage security and maintaining the power system stability.

Another factor is the set-up and development of Nordic electricity market. Currently, the Nordic electricity market consists of three markets for operation: (1) the physical day-ahead (Elspot) trade; (2) the hour-ahead (Elbas) trade and (3) the real-time market. Striving for competition among all generation companies and consumption companies provides another control mechanism to balance the power supply and demand [12].

3.1.2 Integration of Dispersed Generation

Another major characteristic of Danish power system is the integration of large amount of Dispersed Generation (DG). Various types of renewable energy (RE) are being integrated into distribution systems, because the decentralized characteristics of these nature resources. Currently more than 40% of today's installed capacity is from DG units, which are mostly connected to grid at the distribution level. Fig 3.3

showcases the evolvement of the Danish power system in the last 20 years, which has been developed from a conventional power system mainly based on centralized generation to a modernized power system with a large number of DG units [13]. Various types of DG are connected and expected to be connected to western Danish power system, some examples are:

- Onshore wind turbines, ranging from 11kW to 2MW;
- Gas-turbine CHP units, ranging from 7kW to 99MW;
- Steam-turbine CHP units, ranging from 2MW to 19MW;
- Coal-fired units, ranging from 18MW to 44MW;
- Waste-fired units, ranging from 90kW to 26MW;
- Future vehicle-to-grid (V2G) Electrical Vehicle converters.

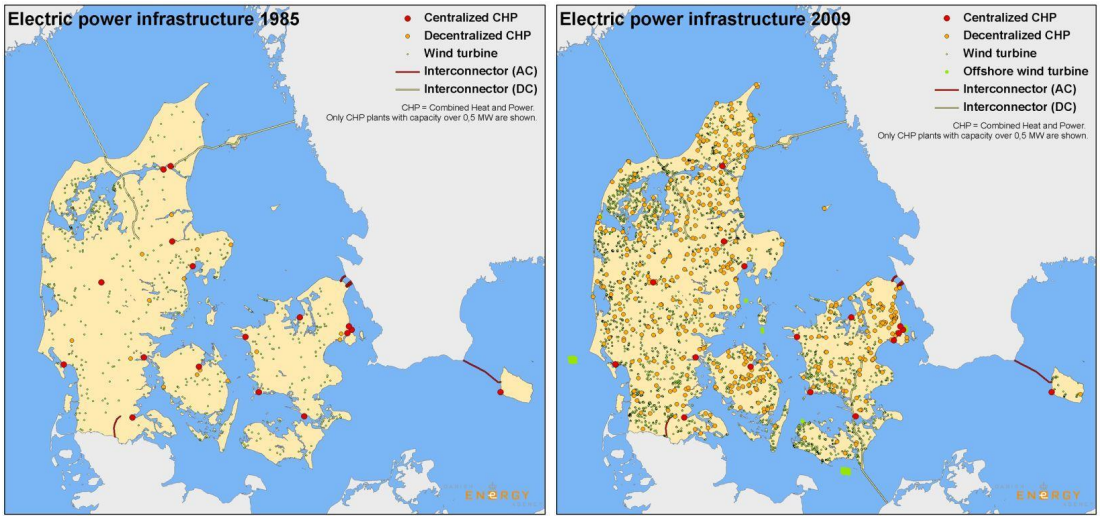

Fig. 3.3 Comparison of electrical power infrastructure in Danish grid in 1985 and 2009 [13].

3.2 Challenges of Future Danish Power System

In February 2011, Danish government announced "Energy Strategy 2050" with the aim to be fully independent of fossil fuel by 2050 [14]. Accordingly, several major transformations have been experiencing in Danish power system, such as the integration of wind energy, the phasing out of central power plants, the reinforcement of international connections, as well as the undergrounding of transmission grid.

3.2.1 Integration of Wind Energy

Wind energy is being integrated into Danish power system at tremendous pace with promising plan to experience 100% fossil fuel free society by 2050. Danish government plans to realize a large share of electricity production with wind turbines,

especially, offshore wind farms. It can be observed from the geographical map of future Danish power system in 2030, shown in Fig. 3.4, several large offshore wind farms, e.g. Ringkøbing, Jamerbugten, Læsø Syd, are expected to be integrated to transmission system. According to the system plan, offshore wind farms are being added consistently to western Danish power system to achieve 3800MW offshore wind power in future [7]. The intermittent nature of wind not only increases the challenge of power balance in the system, but also threatens power system dynamic security, such as lack of inertia and voltage flicker.

Fig. 3.4 Geographical map of future Danish transmission system in 2030 [7].

3.2.2 Phasing Out of Central Power Plants

In order to keep the a reasonable installed capacity in the grid, the number of large central power plants (CPPs) which are currently responsible for primary control actions as well as reactive power and voltage control actions has to be reduced.

According to the system plan issued by Danish TSO, i.e. Energinet.dk, the number of large synchronous generators will reduce from eight to five in the next few years [7]. Currently, Danish transmission system operator (TSO) has declared three must-run central power plants (CPPs) in western and eastern Danish power system primarily to support ancillary services to ensure secure and stable operation, however in future, Danish TSO is planning to reduce these must run power plants even further. Due to the fluctuation of wind power and the different dynamic and transient characteristics between wind farms and conventional power plants, the operation, control and protection of Danish power system with a large amount of wind power need to be developed. The security and stability for power system operation should be maintained which is expected to be the potential challenges.

3.2.3 Reinforcement of International Connections

Currently, western Danish power system is connected to Norway and Sweden through classical LCC based HVDC links. A new voltage sources converter (VSC) based HVDC link of 700MW capacity to Norway is under construction and is expected to be commissioned soon. Albeit, VSC-HVDC interconnections could be used for dynamic support from technical point of view, however, due to current market regulations, these VSC-HVDC interconnections are not providing dynamic support to western Danish power grid. Besides, these regulations of Nordic market do not allow the change of power flow direction within each transaction hour, though reduction in power flow in predetermined direction is allowed on quarter hourly basis [15]. Another HVDC link—Cobra, interconnecting Denmark and Holland, with planned capacity of 600MW~700MW, are expected to be commissioned in 2018, which will help to balance the wind patterns and contribute to the integration of environmentally-friendly wind power into power systems for both countries. Besides, the cross border AC transmission lines to Germany has already been strengthened to (Export) 1780/ (Import) -1500MW.

3.2.4 Under-grounding of Transmission Grid

An adequate and robust electricity transmission grid is a precondition for realizing the objectives on the fully renewable energy dependent future power system. As a result, Danish government issued a plan in 2008 that they will completely change Danish electrical power transmission system [16]. It was decided that the entire grid with voltage below or equal to 150kV has to be under-grounded. All the existing overhead lines (OHL) are planed to be substituted by underground cables (UGC). Besides, all new 400kV connections are built by under-grounded cables [17]. The

transformation of under-grounding the power grid is expected to bring challenges to power system operation, control and protection [18], [19].

3.3 Summary

This chapter describes the transmission power system in Denmark, which is the studied system throughout the thesis. Both the characteristics of current Danish power system and the challenges of future Danish power system are discussed.

The main content of this chapter has also been reported in the author's previous publications in [C3], [C5] and [C11].

References

[1] J. R. Pillai and B. Bak-Jensen, "Vehicle-to-Grid for islanded power system operation in Bornholm," in *Proc. of IEEE PES General Meeting*, Minnesota, Jul. 2010.

[2] J. R. Pillai and B. Bak-Jensen, "Vehicle-to-Grid Systems for frequency regulation in an islanded Danish distribution network," in *Proc. of IEEE Vehicle Power and Propulsion Conference*, Lille, Sep. 2010.

[3] Z. H. Rather, Z. Chen and P. Thøgersen, "Impact of wind energy integration on reactive power reserve and its smart solution: a Danish power system case study," in *Proc. of IEEE Int. Conf. on Pow. Syst. Tech. (POWERCON)*, Auckland, New Zealand, Nov. 2012.

[4] Z. H. Rather, Z Chen and P. Thøgersen, "Challenges of Danish power system and their possible solutions," in *Proc. of IEEE Int. Conf. on Pow. Syst. Tech. (POWERCON)*, Auckland, New Zealand, Nov. 2012.

[5] *Dansk elforsyning 2009, statistik,* pp. 9. danskenergi, 2009.

[6] *Wind resource atlas for Denmark*, 1999, [Online]. Avalable: http://www.windatlas.dk/world/DenmarkWRA.html , assessed on 01-Aug-2013.

[7] *System plan of Danish power system in 2010*. Energinet.dk, 2010, [Online]. Avalable: http://www.energinet.dk/SiteCollectionDocuments/Danske%20dokumenter/Om%20os/Systemplan%202010.pdf , assessed on 01-Aug-2013.

[8] Z. H. Rather, C. Liu and Z. Chen *et al*., "Dynamic security assessment of Danish power system based on decision trees: today and tomorrow," in *Proc. of IEEE PES PowerTech*, Grenoble, France, Jun. 2013.

[9] *Denmark Energy Agreement*, March 2012, [Online]. Available: http://www.ens.dk/en-US/ , assessed on 01-Aug-2013.

[10] *Statistic data of wind farms in Denmark*, [Online]. Available: http://www.ens.dk/da-DK/Info/TalOgKort/Statistik_og_noegletal/Oversigt_over_energisektoren/Stamdataregister_vindmoeller/Sider/forside.aspx , assessed on 01-Aug-2013.

[11] *Hourly Danish power system data in 2011*, [Online]. Available: http://www.energinet.dk/EN/El/Engrosmarked/Udtraek-af-markedsdata/Sider/default.aspx , assessed on 01-Aug-2013.

[12] T. Ackerman, *Wind Power in Power Systems.* West Sussex, UK: John Wiley & Sons, Ltd, 2005, pp. 199-232.

[13] *Danish Energy Agency*, "Danish power infrastructure in 1985 and in 2009," [Online]. Available: http://www.ens.dk/en/info/facts-figures/energy-info-maps/download-premade-maps , assessed on 01-Aug-2013.

[14] *Summary of energy strategy 2050 – from coal, oil and gas to green energy*, the Danish Government, 2011.

[15] V. Akhmatov, C. Rasmussen, P. E. Eriksen *et al.*, "Technical aspects of status and expected future tends for wind power in Denmark," *Wind Energy*, vol. 10, no. 1, pp. 31-49, Sep. 2006.

[16] *ELINFRASTRUKTURUDVALGET,* Technical report on the future expansion and undergrounding of the electricity transmission grid, 2008.

[17] *Kabelhandlingsplan 132-150kV*, Energinet.dk, 2009 (in Danish).

[18] Unnur Stella Gudmundsdóttir, "*Modelling of long High Voltage AC cables in transmission systems*," PhD Dissertation, Aalborg University, 2010.

[19] Filipe Miguel Faria da Silva, "*Analysis and simulation of electromagnetic transients in HVAC cable transmission grids*," PhD Dissertation, Aalborg University, 2011.

Chapter 4

Structural Vulnerability Assessment

4.1 Introduction

The networks of power systems, often called power grids, have been regarded as one of the most important infrastructures whose security should be paid more and more concern. However, in recent years, several large blackouts occurred in US and EU, which have resulted in direct loss up to billions of dollars [1]-[3]. These blackouts expose the potential problems of current analysis methods for power systems. So far, most work of power system analysis has focused on only one aspect of such blackouts, such as voltage stability analysis, transient stability analysis and frequency stability analysis. Although, these approaches have made impressive advances in the understanding of each aspect, it does not provide a framework for understanding the overall phenomena. Therefore, it is reasonable to go beyond these traditional deterministic bottom-up descriptions, instead to be in favor of statistical top-down approaches. The structural vulnerability is defined as the ability of a network continuing to provide key services during random failures or intentional attacks. Further technology, i.e. complex network theory, provides a feasible way to study the structural vulnerability of power grids, which has drawn the link between the topological structure and the vulnerability of networks in the statistical point of view [4].

The first systematic study about complex network theory appeared in late 1990s, aiming at studying the properties of large networks that behave as complex systems [5]-[8]. Complex network theory has received considerable attention recently since the investigation of the small-world networks [5] and the scale-free networks [7], as their characteristics have been discovered in many real networks including the power grids. Recently, with the considerable progress of its applications in many other fields, complex network theory also attracts more and more interest in assessing the structural vulnerability of power grids [9]-[14]. For example, the concept of global efficiency was widely used to assess the vulnerability or locate critical components for networked infrastructures [16]-[18]. Furthermore, the cascading failure model was also directly applied to power grids analysis [19]-[21]. These above studies have been providing a new direction for the analysis of power grids.

Although the complex network theory has made so much progress, few researchers have used it to explore the impact of large-scale dispersed generation (DG) to transmission system [22]. In case of Danish power system, a significant proportion of today's installed capacity is dispersed generation (about 40% of total capacity), such as wind turbines and combined heat and power (CHP) units, which are mostly connected to the distribution system, as shown in Fig. 4.1 [23]. In the future, more and more onshore wind farms are expected to be connected to the distribution system with voltage below 100kV, i.e. 60/20/10/0.4kV. Compared with conventional power grid which is only supplied by centralized power plant (CPP), DG units mainly supply part of the local load, while contributing much less to remote loads.

In Section 4.2, some principles of complex network theory are introduced and three vulnerability indices i.e. *SVI*, *CVI* and *OVI* are proposed to assess the structural vulnerability of power grids and to explore the impact of DG units on power grids. The result of structural vulnerability of western Danish power grid is presented in terms of aforementioned indices are presented in Section 4.3, followed by concluding comments in Section 4.4.

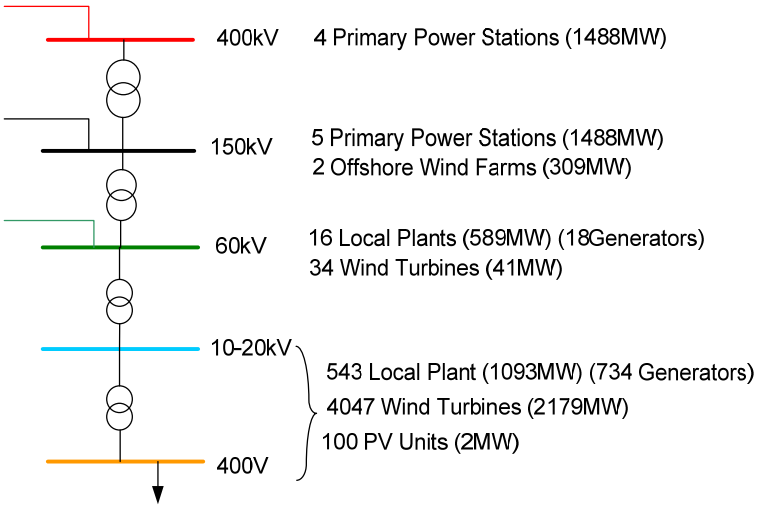

Fig. 4.1. Production capacities at each voltage level in western Danish power system [23].

4.2 Vulnerability Assessment Indices

4.2.1 Complex Network Theory

As mentioned in Section 4.1, complex network theory has gained wide acceptance and has been successfully applied in the analysis of power systems. In the complex network theory, each bus of the power system which is connected with a power source or a power sink, can be modeled as a vertex (or node), and each transmission line and

transformer can be modeled as an edge (or line). Power flow is transmitted between the terminal buses of the edges in the forward or the reverse directions [24].

Therefore, the power grid can be abstracted as a directed and weighted graph, as expressed in (4.1),

$$\mathbf{Y} = \{\mathbf{B}, \mathbf{L}, \mathbf{W}\} \tag{4.1}$$

where $\boldsymbol{B}$ ($\dim\{\boldsymbol{B}\}=N_B$) is the set of vertices (or nodes) and $\boldsymbol{L}$ ($\dim\{\boldsymbol{L}\}=N_L$) is the set of edges (or lines) with an associated set of weight $\boldsymbol{W}$. Each vertex B_i is identified by i, and each edge L_{ij} represents a connection going from vertex i to vertex j with associated weight w_{ij} [25].

Efficiency Index (*EI*), as defined in (4.2), has been widely applied to evaluate the transmission efficiency of a power grid [26].

$$EI = \frac{1}{n_g n_l} \sum_{i \in \mathbf{V}_g, j \in \mathbf{V}_l} \frac{1}{d_{ij}} \tag{4.2}$$

where n_g and n_l represent the number of the generator and the number of load respectively, $\boldsymbol{V}_g$ and $\boldsymbol{V}_l$ are the set of generators and the set of loads respectively, the geodesic distance d_{ij} ($i \in V_g, j \in V_l$) represents the least number of transmission lines or transformers in the shortest transmission path between a specific generator G_i and a specific load L_j. The statistical distribution of geodesic distance is usually adopted to measure the connectivity of a network. The lower number of d_{ij} means the lower distance or closer connectivity between sources and loads, which implies the higher efficiency of the power grid.

4.2.2 Equivalent Impedance between Generation and Load

In the fundamental theory of circuitry, Node-Current Equation is used to compute the voltage of the nodes and the current of branches in a network, as defined in (4.3).

$$\mathbf{ZI} = \mathbf{V} \tag{4.3}$$

where $\mathbf{Z}$ is the node impedance matrix, which can be written in the extended form as given in (4.4).

$$\begin{bmatrix} z_{11} & z_{12} & \cdots & z_{1n} \\ z_{21} & z_{22} & \cdots & z_{2n} \\ \vdots & \vdots & \ddots & \vdots \\ z_{n1} & z_{n2} & \cdots & z_{nn} \end{bmatrix} \begin{bmatrix} I_1 \\ I_2 \\ \vdots \\ I_n \end{bmatrix} = \begin{bmatrix} V_1 \\ V_2 \\ \vdots \\ V_n \end{bmatrix} \tag{4.4}$$

Equivalent impedance Z_{eqij} between generation bus i and load bus j can represent the difficulty in transmitting a unit current from bus i and bus j, as shown in Fig. 4.2.

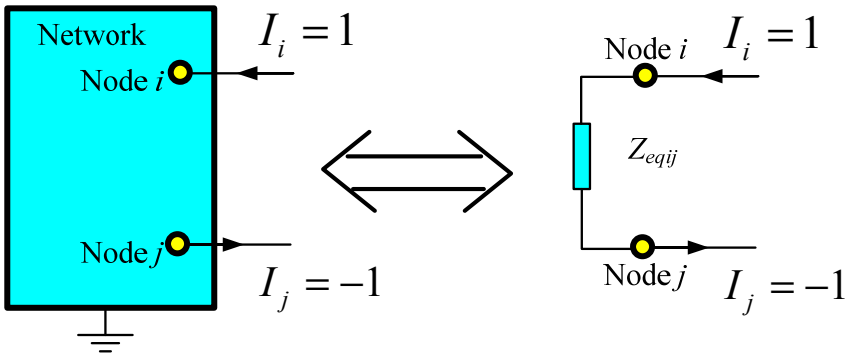

Fig. 4.2 Equivalent impedance in the equivalent electrical circuit.

Assuming a unit current is injected into bus i and withdrawn from bus j, while no other current is injected or withdrawn at other buses, as expressed in (4.5) and (4.6).

$$I_i = 1, \text{ and } I_j = -1 \tag{4.5}$$

$$\begin{bmatrix} & \vdots & & \vdots & \\ \cdots & z_{ii} & \cdots & z_{ij} & \cdots \\ & \vdots & \ddots & \vdots & \\ \cdots & z_{ji} & \cdots & z_{jj} & \cdots \\ & \vdots & & \vdots & \end{bmatrix} \begin{bmatrix} 0 \\ 1 \\ 0 \\ -1 \\ 0 \end{bmatrix} = \begin{bmatrix} \vdots \\ V_i \\ \vdots \\ V_j \\ \vdots \end{bmatrix} \tag{4.6}$$

So equivalent impedance Z_{eqij} can be calculated by the equation in (4.7),

$$Z_{ijeq} = V_{ij} / 1 = V_i - V_j = (z_{ii} - z_{ij}) - (z_{ij} - z_{jj}) = z_{ii} - 2z_{ij} + z_{jj} \tag{4.7}$$

where z_{ij} is the ith, jth element in the impedance matrix.

4.2.3 Structural Vulnerability Index (SVI)

As mentioned in Section 4.2.1, Efficiency Index (*EI*) in (4.2) adopts geodesic distance d_{ij} assuming that the electric power is only transmitted through the path with the least number of transmission elements, so d_{ij} does not represent any electrical characteristic of power grids. However, this assumption may be far away from the reality in power systems, in which the power flow from a specific generation at bus i to a specific load at bus j is distributed over all transmission lines or transformers as determined by the topology and the electrical performance of power grids.

Besides, the capacity of generator and the load in (4.2) are not considered, which should act as the weight of the transmission relationship between generation i and load j.

From the structural vulnerability point of view, the main factors of the power system vulnerability should be based on the inherent characteristics, such as the topological relationship, the impedance of transmission lines and transformers as well

as the capacity of generators and loads. The variation of power system operating conditions has little effect on the structural characteristics of power systems. Hence, this chapter proposes a novel structural vulnerability index (*SVI*) to evaluate the structural vulnerability of power systems with large amount of DG, as defined in (4.8).

$$SVI = \frac{1}{n_g n_l} \sum_{i \in V_g, j \in V_l} \frac{P_{gi}}{P_{lj} \exp(Z_{ijeq})} \tag{4.8}$$

where P_{gi} is the capacity of generation at node i, P_{lj} is the maximum load at node j, and Z_{ijeq} is the electric distance (equivalent impedance) between node i and node j.

Furthermore, compared with conventional power systems, the power system integrated with large amount of DG has relatively more generation capacity at the low voltage level. The DG units mainly supply the local load demand, contributing much less for remote loads. This characteristic has been taken in to account for *SVI* in (4.8), where $P_{gi}/exp(Z_{eqij})$ approximately represents the transmission efficiency between generation bus i and load bus j, with generation capacity P_{gi} serving as the weighting factor. The transmission efficiency from the generation bus i to the load bus j is expressed as exponentially decrease with the increase of the equivalent impedance between them (Z_{eqij}). In the case that DG unit and load are connected to the same node at the transmission level, $Z_{eqij} = 0$ and $1/exp(Z_{eqij}) = 1$, which means that DG has the highest priority to satisfy the local load demand.

So *SVI* in (4.8) is more effective and more accurate than *EI* in (4.2) for evaluating transmission efficiency of power systems before and after integrated with DG units. The higher *SVI* means the higher the transmission efficiency. The evaluation of efficiency was widely adopted as an index to assess the structural vulnerability and to locate critical components of networked infrastructures.

4.2.4 Contingency Vulnerability Index (CVI)

Contingencies in the power system are most possibly faults followed by trips of transmission lines or transformers by protection devices. When contingencies take place in the power grid, the tripping of transmission lines or transformers possibly results in the severe deterioration in the transmission performance. The reason is that the deletion of the components increase the electrical distance between sources and loads. So, it is likely that *SVI* will be lower after the removal of transmission lines or transformers.

Contingency Vulnerability Index (*CVI*) is used to evaluate the level of severity of a contingency as defined by (4.9), which is the reduction percentage of *SVI* related to

the network structure variation. Further, the decrease in the percentage of *SVI* in *N-1* contingency can also be used to identify vulnerable components of power grids.

$$CVI = \frac{SVI_0 - SVI^{/}}{SVI_0} \times 100\% \tag{4.9}$$

The higher *CVI* represents the contingency is more critical or the power system is more vulnerable after removal of this component. Therefore, operators from TSO should pay more attention on the contingencies in these identified transmission lines or transformers.

4.2.5 Operational Vulnerability Index (OVI)

Previous indices mainly focus on the structural characteristics of power grid, so the operating conditions (power flow) in the power grid are not considered, while Operational Vulnerability Index (*OVI*) is a proposed index based on operating conditions to evaluate the impact of DG integration on the operational vulnerability of power systems, as defined in (4.10). One of the significant impacts of DG integration on power grid is that it helps to reduce the long-distance large-capacity power transmission, thus to increase the power transmission efficiency.

$$OVI = \frac{\sum_l z_l \times p_l}{\sum_l z_l} \tag{4.10}$$

In (4.10), p_l represents the active power in the transmission line or transformers l, and the impedance z_l is the weight of line l. The less value of *OVI* implies the less amount of the long-distance large-capacity transmission for active power and high transmission efficiency in the network.

4.3 Structural Vulnerability Assessment of Danish Power System

A 93-bus network that representing western Danish power system integrated with large amount of DG units is used to evaluate the effect of the DG integration to power system vulnerability, as shown in Fig. 4.3. The network has 124 components (edges) composed of 112 lines and 12 transformers. Almost every node in the distribution system underneath the transmission level is integrated with DG units, such as onshore wind farms, CHP plants, etc. Besides, 12 CPPs are connected to the transmission system. The test system is simulated by DIgSILENT/PowerFactory, in which the balanced positive sequence AC load flow is calculated by adjusting the power outputs from DG units and centralized power generation units.

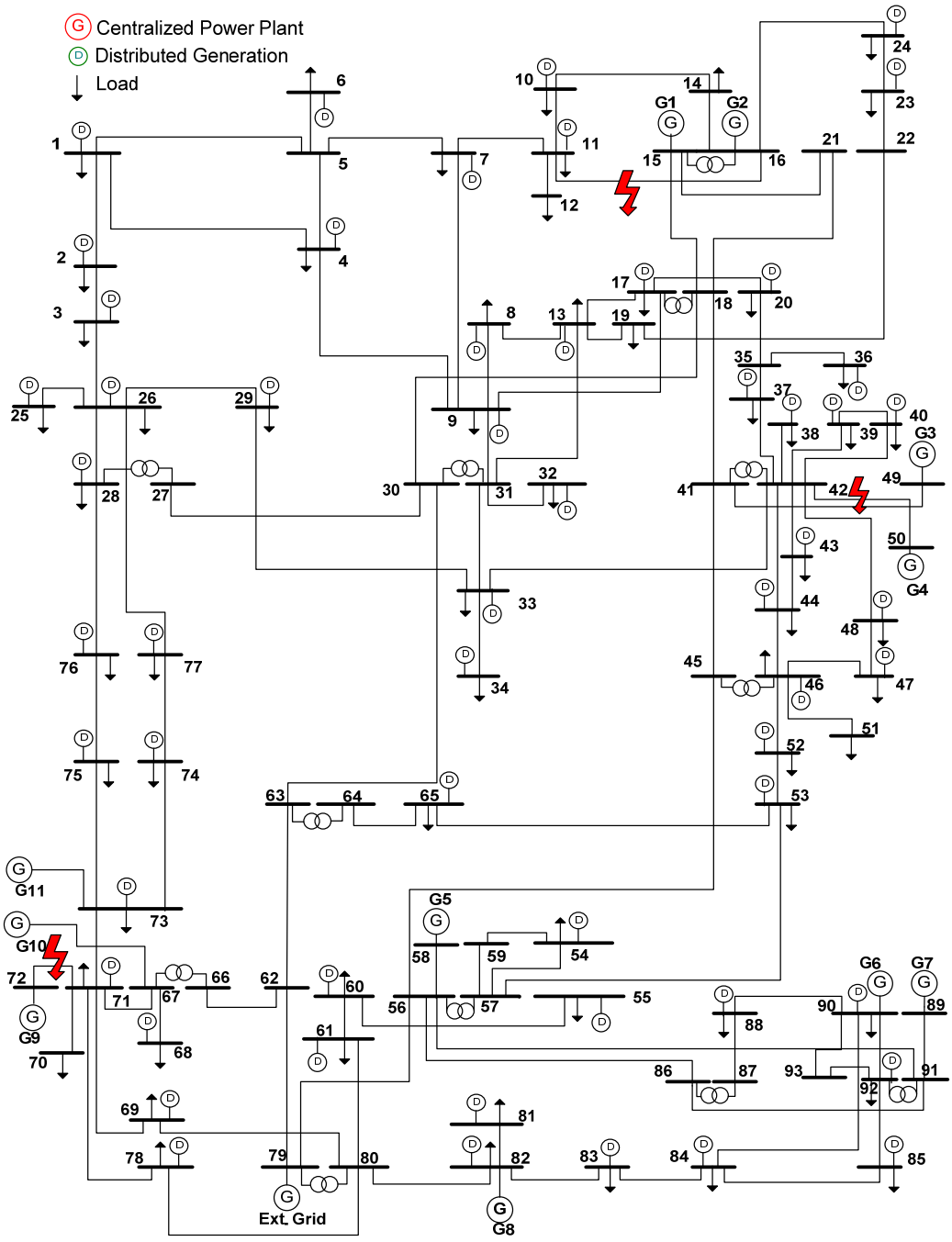

Fig. 4.3. Test power system.

4.3.1 Vulnerability Assessment Considering Network Structure

In order to evaluate the impact of DG penetration on the structural vulnerability of power systems, the share of DG output is gradually increased to replace the generation from CPPs. The load consumption in every load bus is the maximum load, remaining invariant before and after DG integration.

As shown in Fig. 4.4, with the increase of DG penetration level from 0% to 100%, the *SVI* linearly increases from 0.006 to 0.021, which means that the transmission efficiency improves with the increase of DG penetration level.

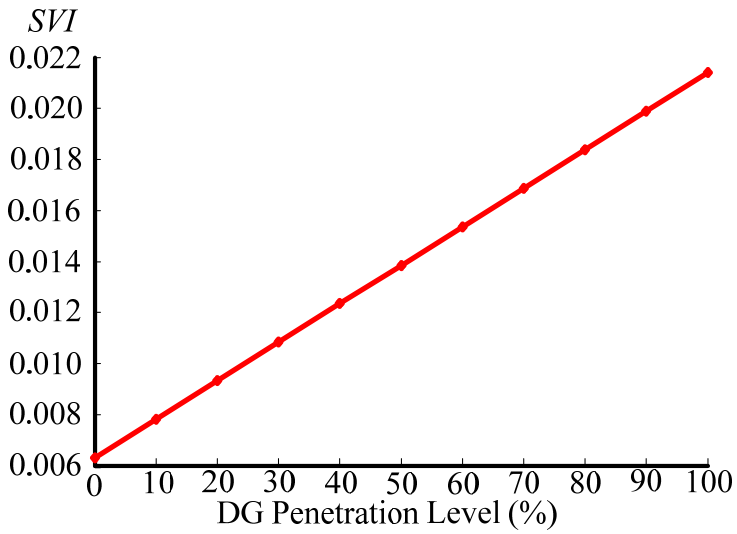

Fig. 4.4. *SVI* with respect to DG penetration level.

4.3.2 Vulnerability Assessment Considering Contingencies

In order to evaluate the impact of DG on the ability of power system to resists the *N-1* contingency, *SVI* is calculated before and after the removal of one component (transmission line or transformer). As shown in Fig. 4.5, the x-axis shows the reference number of components corresponding to every transformer and line in accordance with Fig. 4.3. It is obvious that *SVI* integrated with 100% DG is much higher than that without DG before and after *N-1* contingency. Besides, the decrease of *SVI* after *N-1* contingency with DG is generally lower than that of the case without DG integration, which indicates the power grid is stronger with DG integration regarding *N-1* contingency than that without DG. This result also testifies that the integration of DG units helps to improve the structural vulnerability of the power grid after contingencies.

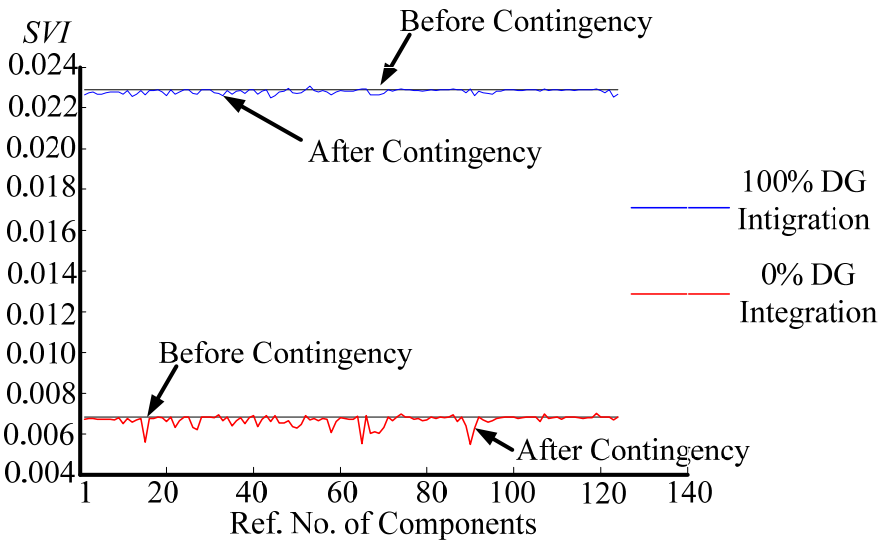

Fig. 4.5. *SVI* before and after *N-1* contingencies.

As mentioned in Section 4.2.4, *CVI* is adopted to evaluate the severity of *N-1* contingency. From another point of view, *CVI* helps to identify the vulnerable components of a power grid. As shown in Fig. 4.6, without DG integration, Line 71-72, Line 42-50 and Line 16-11 are the 3 most vulnerable components in the power grid, which have been marked in the test power system in Fig. 4.3. The blue line in Fig. 4.6 shows that the severity of the contingencies in these 3 lines is evidently reduced because of DG integration, which means that the power system is more resistant to contingencies with DG integration.

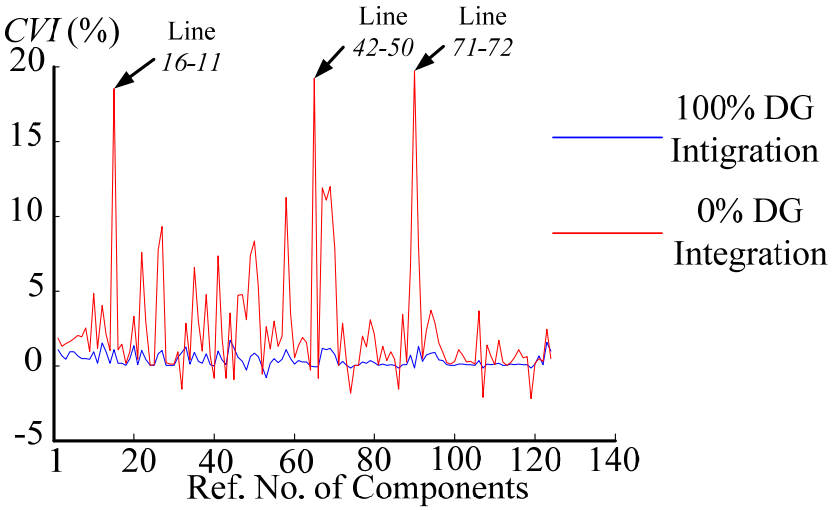

Fig. 4.6. *CVI* with and without DG integration.

Fig. 4.7 shows the descending order of *CVI* in accordance with Fig. 4.6. It is important to note here that, with DG integration, most of components have much lower *CVI*, but some components have higher *CVI*, which means the power grid is more vulnerable after contingency takes place at only a few points after DG

integration. The maximum values and mean values of *CVI* with and without DG integration are shown in Table 4.1.

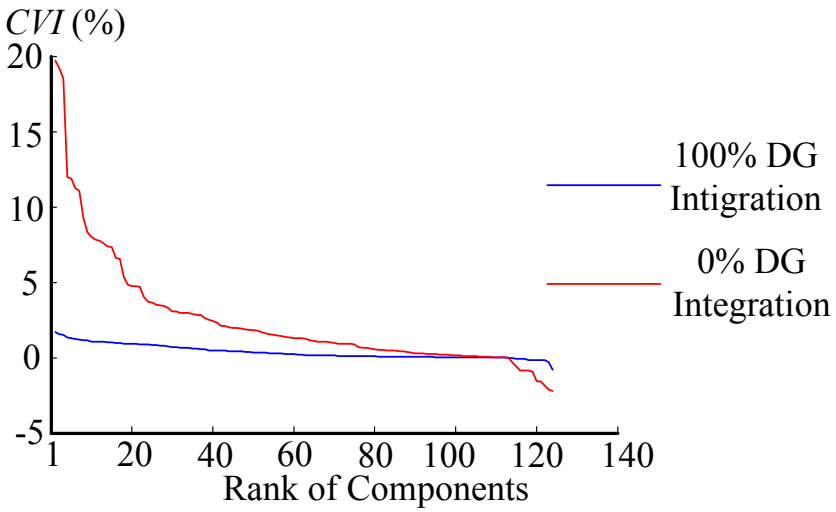

Fig. 4.7 Descending sort of *CVI*.

TABLE 4.1 STATISTICAL DATA OF *CVI*

DG Integration level	Maximum *CVI*	Average of *CVI*
0% DG Integration	19.71%	2.49%
100% DG Integration	1.72%	0.38%

Fig. 4.8 shows the descending order of *CVI* for the *N-1* contingencies in 10 most critical components. It can be seen that, with DG integration, the vulnerable conponents in the power grid have been changed.

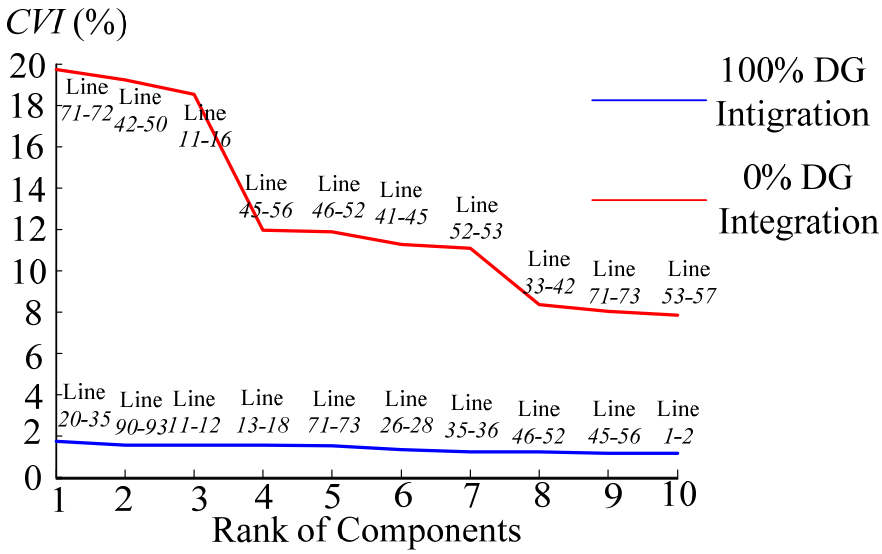

Fig. 4.8 10 most vulnerable components.

4.3.3 Vulnerability Assessment Considering Power Grid Operation

As mentioned in Section 4.2.5, one of the most significant impacts of DG integration on power grid operation is to reduce the long-distance large-capacity power transmission. *OVI* is another proposed index to evaluate the power transmission efficiency, meaning that the weighted average value of active power in all the lines and transformers with their impedance as weighting factors. The lower *OVI* implies that the less transmission distance of active power, lower power loss and higher efficiency of the network. In order to evaluate the impact of DG integration to power flow pattern, the overall load is invariant, and generation output from CPP is substituted by the increase of the DG penetration level. Fig. 4.9 shows the value of *OVI* with respect to different DG penetration levels. With the increase penetration level of DG from 0% to 100%, the *OVI* decreases from 126.66MW to 41.17MW.

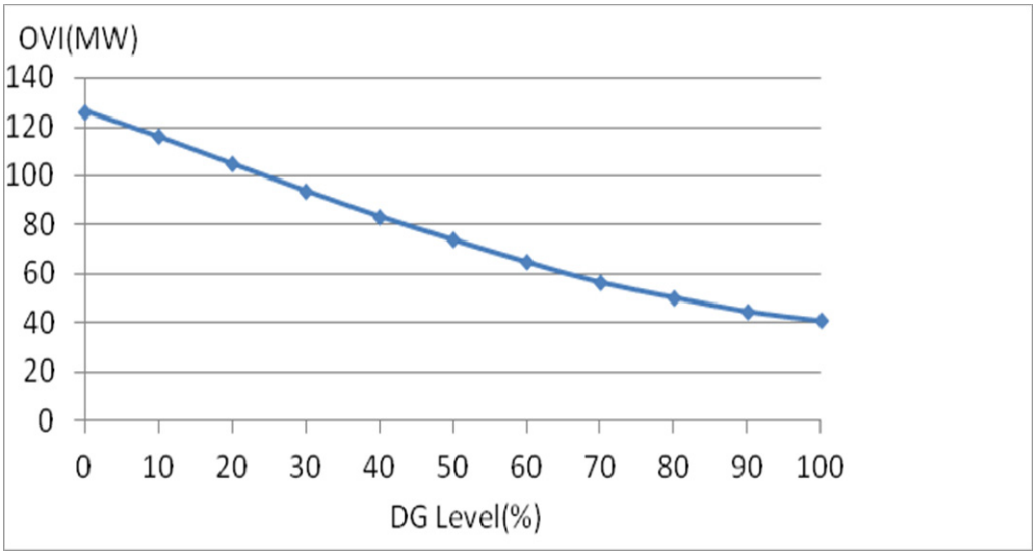

Fig. 4.9 *OVI* with respect to DG penetration level.

4.4 Summary

This chapter proposed three vulnerability indices, i.e. structural vulnerability index (*SVI*), contingency vulnerability index (*CVI*) and operational vulnerability index (*OVI*). *SVI* is the index to evaluate the topological vulnerability of the whole power grid structure. *CVI* is the index to identify the vulnerable components in a power grid. *OVI* is the index related to the operating conditions of a power system which is based on power flow pattern.

In conclusion, DG units are able to improve the reliability of the power system, shorten the electrical distance between the sources and loads, alleviate the long-distance large-capacity transmission, and increase the efficiency.

The structural vulnerability assessment based on complex network theory is also able to provide a reference to optimize the network topology, and to guide the future planning of DG integration. Besides, in the case of power system emergency conditions, these vulnerability indices based on structural characteristics are able to help in preventing cascading failures and blackouts.

The main content of this chapter has also been reported in the author's previous publication in [C3].

References

[1] D. N. Kosterev, C. W. Taylor and W. A. Mittelstadt, "Model validation for the August 10, 1996 WSCC system outage," *IEEE Trans. Power Syst.*, vol. 14, no. 3, pp. 967-979, Aug. 1999.

[2] US-Canada Power System Outage Task Force, "Final report on the August 14, 2003 blackout in the United States and Canada: Causes and Recommendations," Apr. 2004.

[3] D. Q. Gan, J. Y. Hu, and Z. X. Han, "Thinking of several international power outages in 2003," [J] (Chinese). *Automation of Electric Power Systems*, vol. 28, no. 3, pp. 1-4, 2004.

[4] I. Dobson, "Initial review of methods for cascading failure analysis in electric power transmission systems," in *Proc. of IEEE PES General Meeting*, Pittsburgh, PA, USA, Jul. 2008.

[5] D. J. Watts and S. H. Strogatz, "Collective dynamics of 'small-world's networks," *Nature*, vol. 393, no. 6684, pp. 440-442, Jun. 1998.

[6] S. H. Strogatz, "Exploring complex networks," *Nature*, vol. 410, no. 6825, pp. 268-276, Mar. 2001.

[7] A. L. Barabasi and R. Albert, "Emergence of scaling in random networks," *Science*, vol. 286, no. 5439, pp. 509-512, Oct. 1999.

[8] R. Albert, H. Jeong and A. L. Barabasi, "Error and attack tolerance of complex network," *Nature*, vol. 406, no. 6794, pp. 378-382, Jul. 2000.

[9] P. Hines, E. Cotilla-Sanchez and S. Blumsack, "Do topological models provide good information about electricity infrastructure vulnerability?" *Chaos*, vol. 20, no. 3, pp. 033122, Sep. 2010.

[10] U. Brandes and D. Fleischer, "Centrality measures based on current flow," in *Proc, of the 22nd Symposium on Theoretical Aspects of Computer Science*, Stuttgart, Germany, Feb., 2004.

[11] G. Chen, Z. Y. Dong, D. J. Hill *et al.*, "An improved model for structural vulnerability analysis of power networks," *Physica*, vol. 388, no. 19, pp. 4259-4266, Oct. 2009.

[12] E. Bompard, D. Wu and F. Xue, "The concept of betweeness in the analysis of power grid vulnerability," in *Proc. of 2010 Complexity in Engineering*, Rome, Italy, Feb. 2010.

[13] S. Arianos, E. Bompard, A. Carbone *et al.*, "Power grid vulnerability: a complex network approach," *Chaos*, vol. 19, no. 3, pp. 013119, Sep. 2009.

[14] V. Latora and M. Marchiori, "Vulnerability and protection of infrastructure networks," *Phys. Rev.*, vol. 71, no. 1, pp. 015103, Jan. 2005.

[15] E. Bompard, R. Napoli and F. Xue, "Extended topological approach for the assessment of structural vulnerability in transmission networks," *IET Gener. Transm. Dis.*, vol. 4, no. 6, pp. 716-724, Jan. 2010.

[16] V. Latora and M. Machiori, "How the science of complex networks can help developing strategies agains terrorism," *Chaos, Solitons and Fractals*, vol. 20, no. 1, pp. 69-75, 2004.

[17] S. Arianos, E. Bompard, A. Carbone *et al.*, "Power grid vulnerability: a complex network approach," *Chaos*, vol. 19, no. 1, pp. 013119, Feb. 2009.

[18] P. Crutitti, V. Latora and M. Marchiori, "Locating critical lines in high-voltage electrical power grids," *Fluct. Noise Lett.*, vol. 5, no. 2, pp. 201-208, Jun. 2005.

[19] R. Kinney, P. Crucitti, R. Albert *et al.*, "Modeling cascading failures in the North American power grid," *Eur. Phys. J. B*, vol. 46, pp. 101-107, Jun. 2005.

[20] B. C. Lesieutre, S. Roy, V. Donde *et al.*, "Power system extreme event screening using graph partitioning" in *Proc. of 38th North American Power Symposium*, Carbondale, IL, USA, Sep. 2006.

[21] J. Li, "Identification of cascading generator over excitation tripping events," M. S. Thesis, Iowa States University, 2007.

[22] Y. B. Mao, F. Liu and S. W. Mei, "On the topological characteristics of power grids with distributed generation," in *Proc. of the 29th Chinese Control Conference*, Beijing, 2010.

[23] P. B. Eriksen, T. Ackermann, H. Abildgaard *et al.*, "System operation with high wind penetration," *IEEE Power and Energy Magazine*, vol. 3, no. 6, pp. 65-74, Nov.-Dec. 2005.

[24] S. Mei, X. Zhang and M. Cao, *Power Grid Complexity*. Beijing: Tsinghua University Press and Heidelberg: Springer, 2011, pp. 208-228.

[25] R. Albert, I. Albert and G. L. Nakarado, "Structure vulnerability of the North American power grid," *Phys. Rev.*, vol. 69, no. 2, pp. 025103, Feb. 2004.

[26] D. Ming and P. Han, "Small-world topological model based vulnerability assessment algorithm for large scale power grid," [J] (Chinese). *Automation of Electric Power System*, vol. 30, no. 8, pp. 7-10, 2006.

Chapter 5

Dynamic Vulnerability Assessment

5.1 Introduction

In the recent years, the electrical generation from wind has received extensive attention and has been developing rapidly worldwide, due to the exhaustion of fossil fuel sources and the policy of greenhouse gas mitigation from power generation. However, many issues are raised when power system is integrated with large amount of wind power, in terms of power system operation, control and protection, etc. The issue of transient stability is becoming more and more important, since the wind power penetration is increasing rapidly, but the financial and regulatory conditions have forced electric utility to build power systems with less redundancy and operate them closer to security limits [1]. Hence, there are more and more challenges in the control and protection to maintain the security and stability of power system with large wind power penetration.

Transient stability of a power system is the ability to maintain synchronous operation when power system is subjected to a large severe disturbance, such as a 3-phase short circuit at the bus of an important generation plant, the loss of an important tie-line, or the loss of an important load, etc. [2], [3]. Typically, the time span to evaluate transient stability is short, within 10s. Critical clearing time (CCT) is widely used as an important index of transient stability which is defined as the maximum duration that a disturbance may sustain without losing the power system's capability of recovering to a normal operating condition [2].

A considerable number of studies have been conducted on the impact of wind generation on power system transient stability. In [4], the author compared the effect of variable speed wind generator and that of conventional synchronous generator to voltage and transient stability and concluded that the modern wind power plants equipped with power electronic devices and low voltage ride through (LVRT) ability do not reduce the stability margin. In [5], the author analyzed transient and dynamic stability in a simple 3-machine network and concluded that the fixed speed induction generator (FSIG) based wind farms contributed to the system damping significantly but are vulnerable to network faults due to voltage stability issue. Doubly fed induction generator (DFIG) based wind farms can provide a superior transient

performance in terms of voltage recovery ability following the fault. In [6], [7], specific scenarios have been examined in eastern Danish power system, but they only considered the traditional FSIG-based wind generators.

In this chapter, the detailed models of onshore and offshore wind farms are developed to evaluate the transient stability of western Danish power system. The CCT is calculated in terms of iterative time-domain simulation. From the results of CCT in different scenarios, the impacts of wind power and other influencing factors on power system transient stability are analyzed.

In Section 5.2, detailed unit-specific models of onshore and offshore wind farms in DIgSILENT/PowerFactory are described. In Section 5.3, the dynamic vulnerability assessment of Danish power system is carried out by screening of CCT for faults in different positions, for four typical scenarios, and for different influencing factors. Finally, concluding remarks is given in Section 5.4.

5.2 Modeling of Wind Farms

5.2.1 Type A: Fixed Speed Induction Generators (FSIG) Based Wind Turbines

Currently, most onshore wind turbines in Danish power system are equipped with FSIGs. These FSIGs based wind turbines can not control reactive power, so they are magnetized from the electricity grid and equipped with capacitor banks to compensate the reactive power. Fig. 5.1(a) and Fig. 5.1(b) show the control diagram of wind turbine model based on FSIG, which is represented by asynchronous generator model in DIgSILENT. Beside the generator model, wind turbine system contains aerodynamic model, shaft model, protection as well as emergency stop.

The parameters of the wind turbines and FSIGs are selected to match the typical onshore wind farms, shown in Table 5.1, while the active and reactive power outputs as well as the inertia of each wind farm are different, according to the detailed data of installed wind farms in Denmark [8].

Generally, power systems with high wind penetration are usually subjected to voltage instability issue during and after the fault, because of the high reactive power absorption from the grid. Fig. 5.2 shows the model of FSIG. When there is a fault disturbance in power grid, the sharp voltage drop at the point of connection (POC) results in the imbalance between mechanical torque and electromagnetic torque. FSIG accelerates, so the absolute value of slip rate s increases. Meanwhile, the reduction of equivalent resistance R_r/s forces FSIG to absorb considerable reactive current passing

through the leakage reactance X_r, which exacerbates the voltage decrease. According to the Danish recommendation KR-111 before 2004, the protection relay should trip the wind farm when the voltage of POC U_s is below 0.7pu for more than 0.5sec [9]. While for wind turbines commissioned after 2004, the new Danish grid code TF 3.2.6 started to require the low voltage ride-through (LVRT) capability for a specific voltage profile at the point of common coupling (PCC) [10].

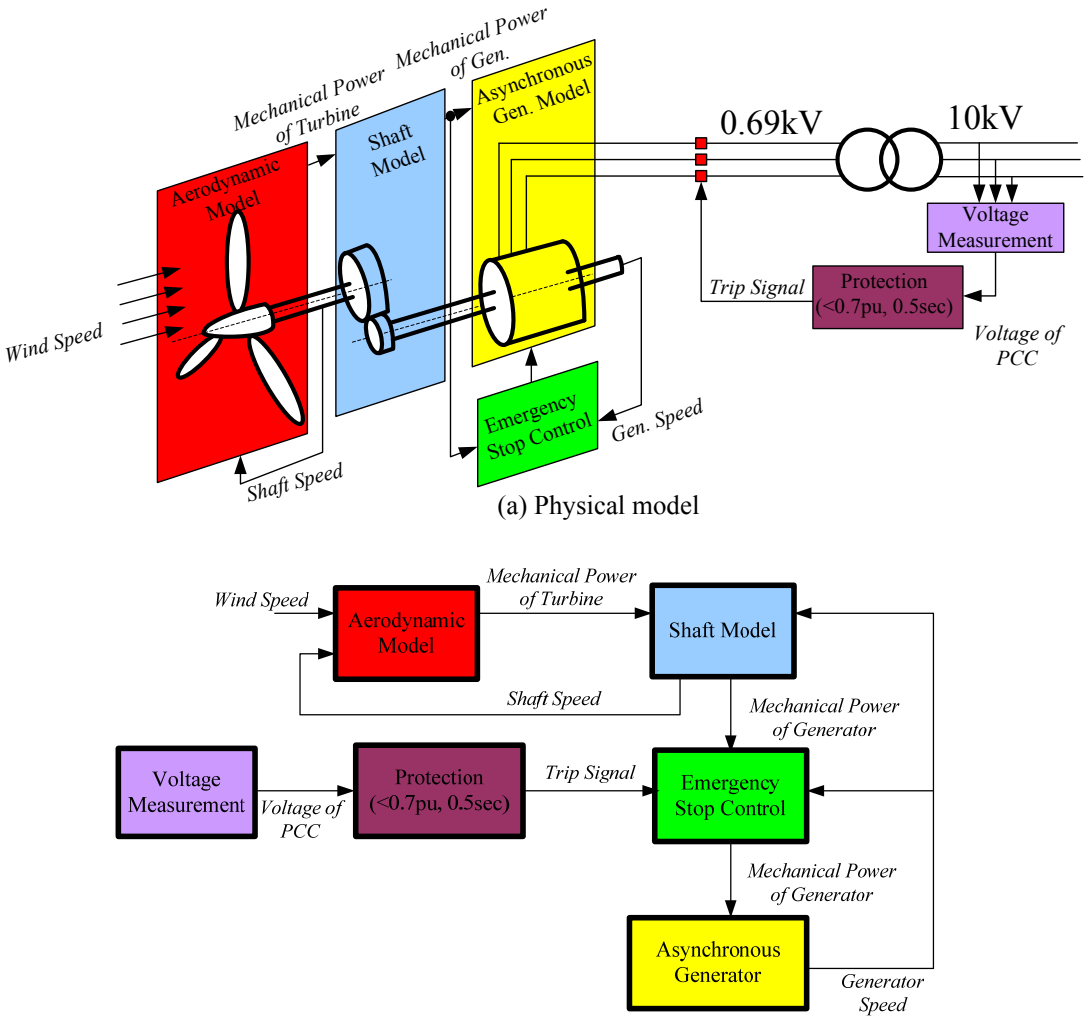

Fig. 5.1 Model of onshore wind farm with FSIG.

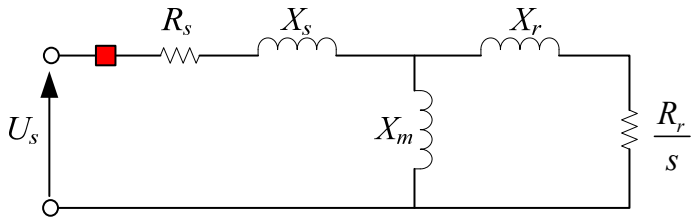

Fig. 5.2 Fixed speed induction generator (FSIG) model.

TABLE 5.1 TYPICAL DATA OF ONSHORE WIND FARM BASED ON FSIG

DATA OF FSIG AND WIND TURBINE	VALUE
Stator resistance *Rs* (pu)	0.00744
Stator reactance *Xs* (pu)	0.09266
Mag. reactance *Xm* (pu)	4.0252
Rotor resistance *Rr* (pu)	0.00667
Rotor reactance *Xr* (pu)	0.01168
Pole pairs	2
Turbine radius (m)	24
Rated mechanical power (MW)	0.765
Gear ratio	67.57

5.2.2 Type C: Doubly-Fed Induction Generator (DFIG) Based Wind Farms

Horn Rev 1 is the first large scale wind farm in the world. A total number of 80 Vestas V80-2.0MW units with DFIG, capable of producing 160MW, were installed in 2002.

The wind farm has been represented by aggregated model of 80×2MW DFIGs in DIgSILENT. Fig. 5.3(a) and Fig 5.3(b) show the control diagram of DFIG wind farm, including the models of pitch control, aerodynamic, 2-mass shaft, MPPT control, speed control, over-frequency active power reduction control, power control, current control and protections (crowbar for over-current in rotor, tripping if over-speed and tripping if over voltage or under voltage).

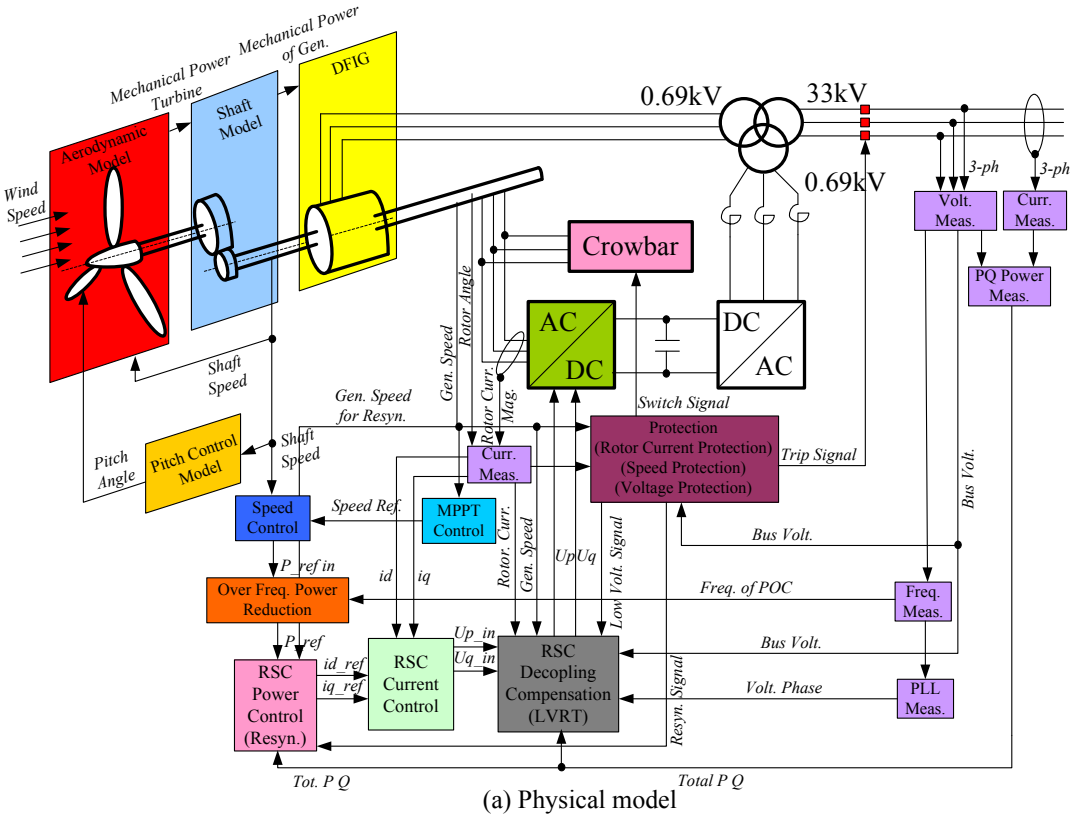

(a) Physical model

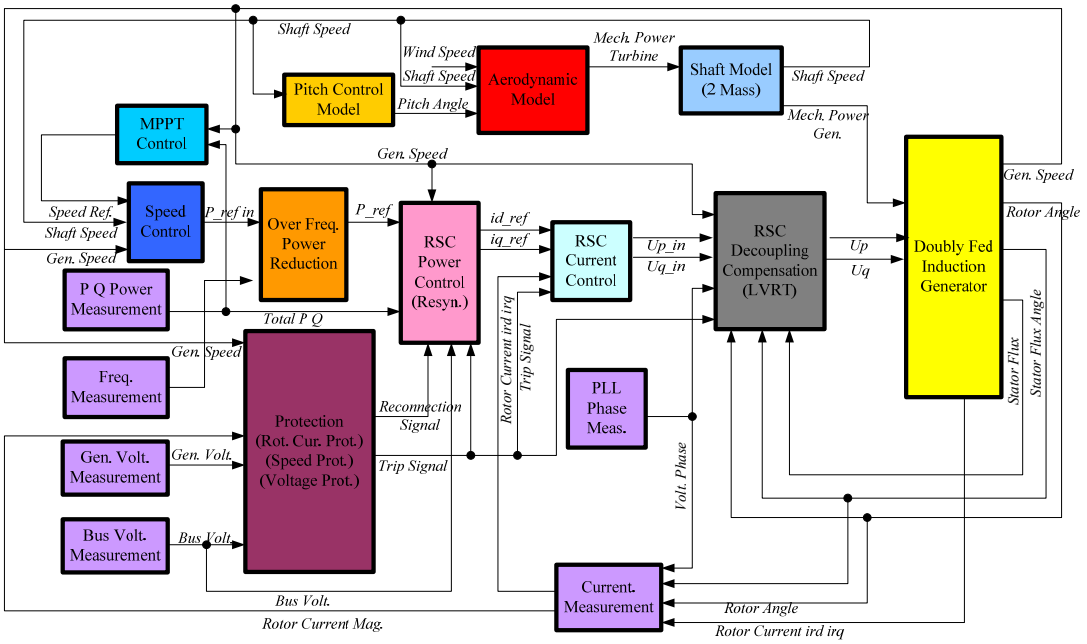

(b) DIgSILENT DSL model

Fig. 5.3 Model of offshore wind farm Horns Rev 1 based on DFIG.

The wind farm integration complies with the new Danish grid code that wind power plant must be able to withstand voltage drop to 20% of the nominal voltage in the point of connection (POC) over a period of minimum 0.5sec without disconnection. Besides, the wind power plant must have a control function capable of controlling the reactive power in Area B, as specified in Fig. 5.4 [11].

The large offshore wind farms, such as Horn Rev 1, can be required to support the frequency and voltage in the substation of PCC in the transmission system. However, during and after voltage dips, the controllability of voltage is limited due to the current rating of power converters of the wind turbines.

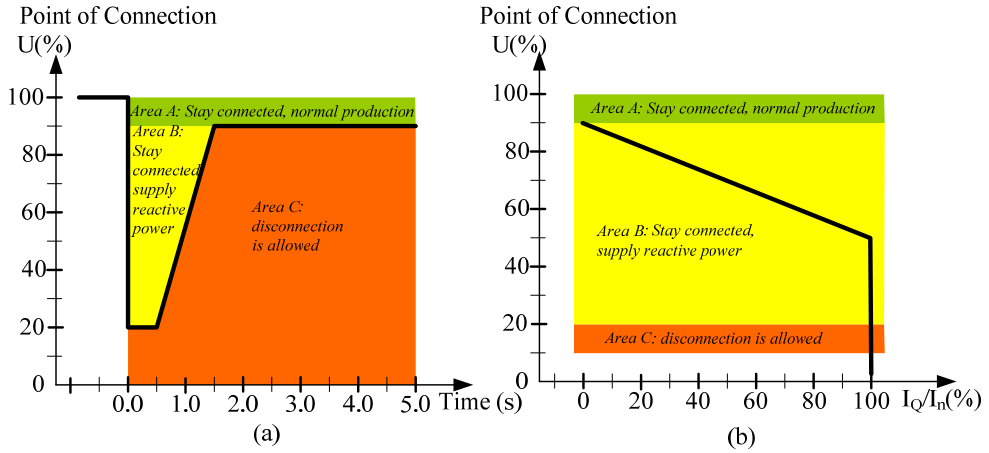

Fig. 5.4 Requirements of (a) LVRT and (b) reactive power supply for wind power plants larger than 1.5MW.

5.2.3 Type D: Variable Speed with Full-Rated Converter (FRC) Based Wind Farms

Horns Rev 2 is the wind farm with full-rated converter consisting of 91 Siemens Wind Power SWP 2.3-93 wind turbines with total generation capacity of 209MW.

The detailed model of Horns Rev 2 is represented by aggregated model of 93×2.3MW asynchronous generators and the models of generator side converter and grid side converter. The control diagram is shown in Fig. 5.5(a) and Fig 5.5(b), containing three main parts: generator model, generator side converter model and grid side converter model. The chopper is connected when the DC bus voltage is above 1.2pu, while the protection and LVRT control module ensure the integration of Horns Rev 2 in accordance with current Danish grid code as well.

The key parameters of offshore wind farms for Horns Rev 1 and Horns Rev 2 are shown in Table 5.2 [12].

TABLE 5.2 PARAMETERS OF OFFSHORE WIND FARMS IN HORNS REV 1 AND HORNS REV 2

PARAMETERS OF WIND FARM	HORNS REV 1	HORNS REV 2
Turbine name	V80-2.0 MW	SWT-2.3-93
Manufacture	Vestas	Siemens
Rated power (MW)	2	2.3
Number of turbines	80	91
Total capacity (MW)	160	209.3
Turbine diameter (m)	80	93
Cut-in wind speed (m/s)	4	4
Rated wind speed (m/s)	16	13-14
Cut-out wind speed (m/s)	25	25
Power Density(m^2/kW)	2.51	2.95
Generator type	4 pole DFIG	Asynchronous Gen
Output Voltage (V)	690	690

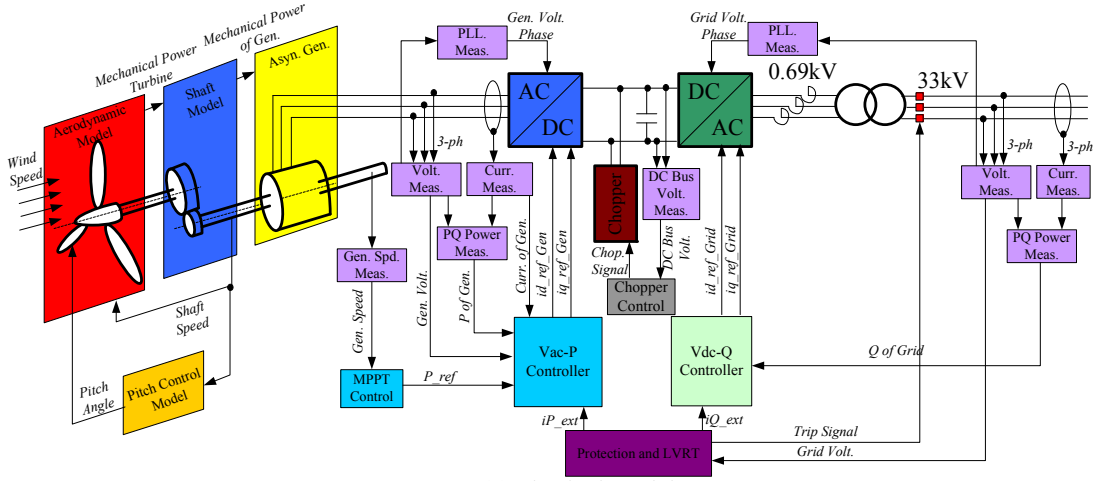

(a) Physical model

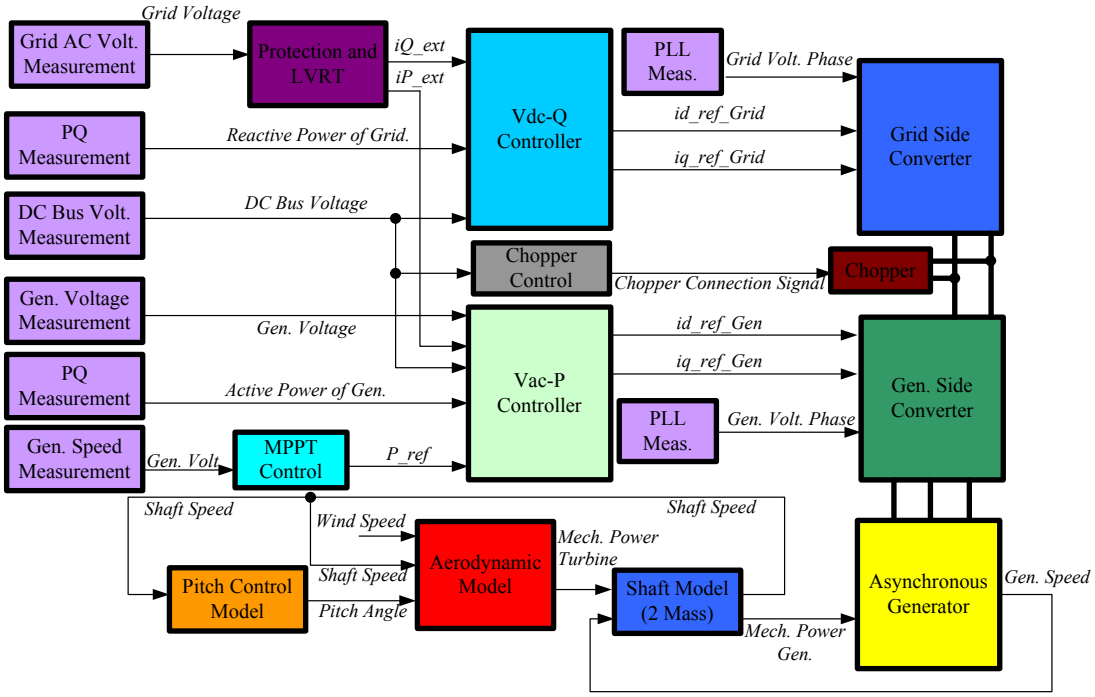

(b) DIgSILENT DSL model

Fig. 5.5 Model of offshore wind farm Horns Rev 2 based on FRC.

5.3 Dynamic Vulnerability Assessment of Danish Power System

5.3.1 Dynamic Vulnerability Assessment Based on Critical Clearing Time

CCT is an important index for transient stability, which is usually calculated by repeated time-domain simulations, more specifically, adjusting the fault duration time in time-domain simulations to find out the maximum duration of a short circuit that can maintain the synchronization of generators in the transmission power system.

Critical fault screening (CFS) is to create short-circuits in every critical position in order to search out the vulnerable areas in terms of CCT. DIgSILENT Programming Language (DPL) is used for CFS in western Danish power system. For each transmission line, a 3-phase short circuit event is created at both terminals of transmission lines, since the most critical disturbance of *N-1* contingency is the fault close to the buses. A switch event trips the faulted transmission line after the time duration of short-circuit. Bisection method is adopted to accelerate the process to find out CCT, which repeated searches the midpoint of fault duration between an adjacent stable case and unstable case. The accuracy of CCT is 0.001sec.

The CCT is dependent on many factors, such as generators' output level, the fault location and fault type, voltage and power flows before the disturbance. Therefore,

some scales are applied to tune the power production and power consumption to create different operating conditions (OCs). The basic OC is defined in Table 5.3, where the scales are defined as the percentage of the actual power with respect to their capacity. For example, 75% load level means the load consumption in the basic OC is 75% of the peak value in every load bus; 50% CPP generation means the generation output of every CPP in the basic OC is 50% of its capacity; and +75% HVDC to Sweden means the HVDC links to Sweden in the basic OC are exporting 75% power with respected to the maximum capacity of this HVDC link. The surplus power is compensated by power exchange via 400kV and 220 kV OHLs to Germany.

TABLE 5.3 SCALES OF THE BASIC OPERATING CONDITION (BASED ON POWER SYSTEM MODEL OF 2010)

SCALE	CAPACITY(MW)	PERCENTAGE (%)	POWER(MW)
Load level	3664	75	2748
CPP generation	3147	50	1573.5
CHP generation	2017	50	1008.5
Other dispersed generation	326	50	163
Wind power generation (offshore)	369	80	295.2
Wind power generation (onshore)	2232	50	1116
HVDC to Sweden	740	+75(Export)	+555
HVDC to Eastern Denmark	600	+100(Export)	+600
HVDC to Norway	1000	-50(Import)	-500

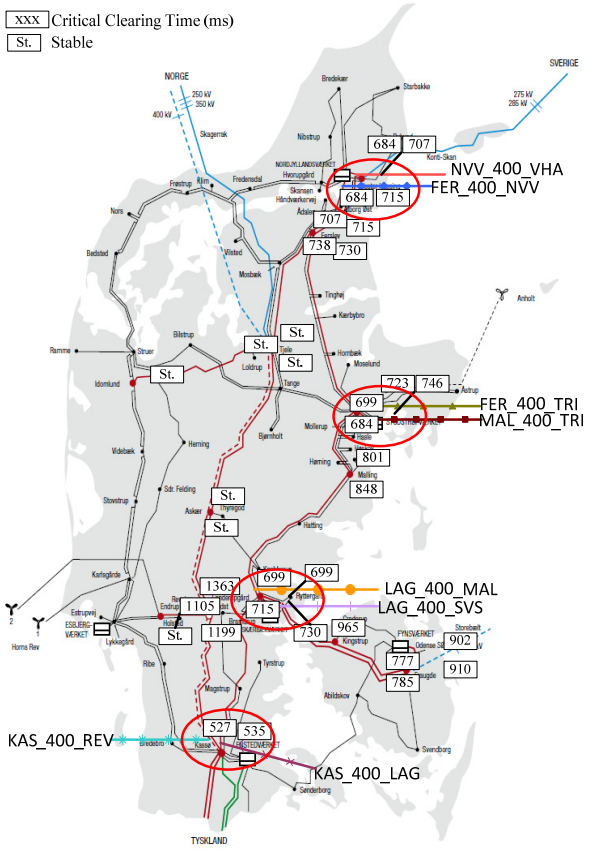

Fig. 5.6 Result of critical fault screening in western Danish power grid.

Through critical fault screening, CCTs of faults at all the terminals of 400kV transmission lines of western Danish power system in the basic OC is calculated out, as shown in Fig. 5.6. Four vulnerable areas in terms of transient stability can be identified and highlighted by red circles, in which the CCTs are generally below 700ms. Because these short-circuit locations are close to CPPs or central hub substations, the disturbances in these locations are easily to result in the out-of-step of the nearest generator. So it is reasonable to select 8 critical short-circuit locations to evaluate the impact of power flow pattern on transient stability, highlighted in Fig. 5.6.

5.3.2 Four Typical Operating Conditions

Fig. 5.7 shows the hourly wind power generation and total consumption of western Danish power system in the 2011 [13]. The jagged red line denotes that the load in working days is higher than that in holidays, but wind generation is changing irregularly. It can be noted that the wind power generation even exceeded the total load consumption in some short-term periods of 2011.

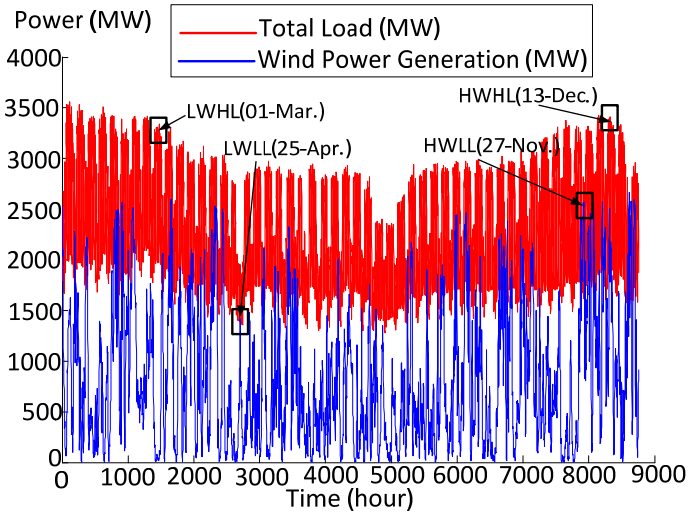

Fig. 5.7 Hourly wind power generation and load of western Danish power system in 2011.

In order to evaluate the impact of wind generation and load level on transient stability, 4 typical OCs are selected, high wind low load (HWLL), high wind high load (HWHL), low wind low load (LWLL) and low wind high load (LWHL).

Wind power generation, load and exchange power with external grid in these 4 typical OCs are shown as Fig. 5.8, where the percentages have the same respective basic values with Table 5.3. CCTs of the 4 typical OCs are calculated for the faults located in the 8 most critical positions, as shown in Table 5.4. CCTs are searched in the range between 0.1sec and 1.0sec. If the CCT of one contingency is below 0.1sec, the system can be deemed as transient instable for that *N-1* contingency.

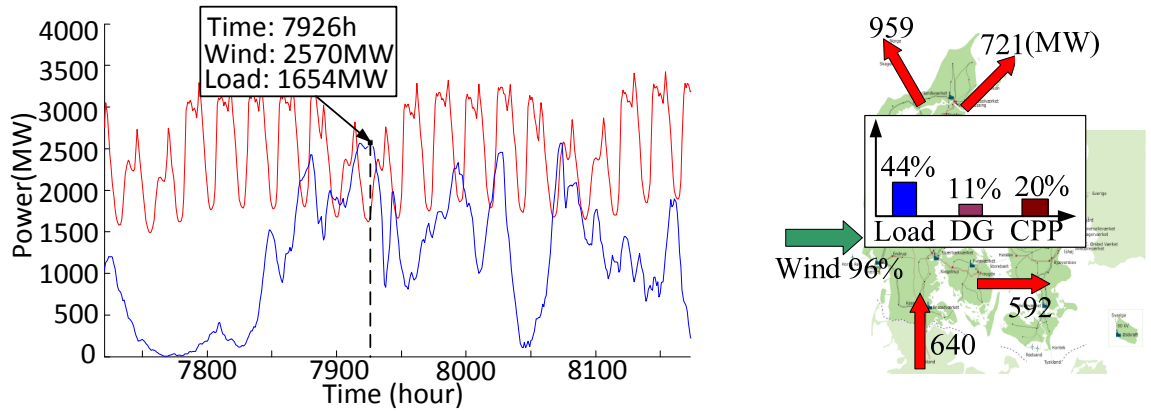

(a) High Wind Low Load (HWLL) (3AM, Nov. 27th, 2011)

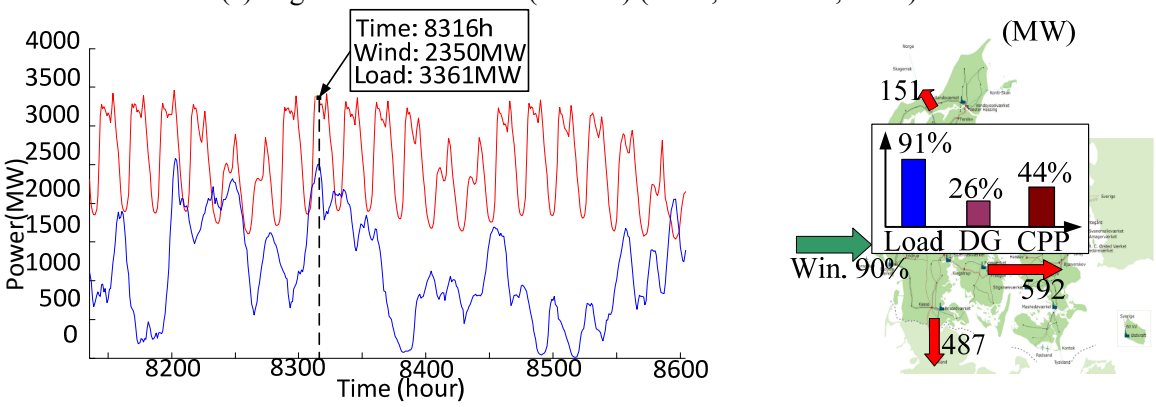

(b) High Wind High Load (HWHL) (9AM, Dec. 13th, 2011)

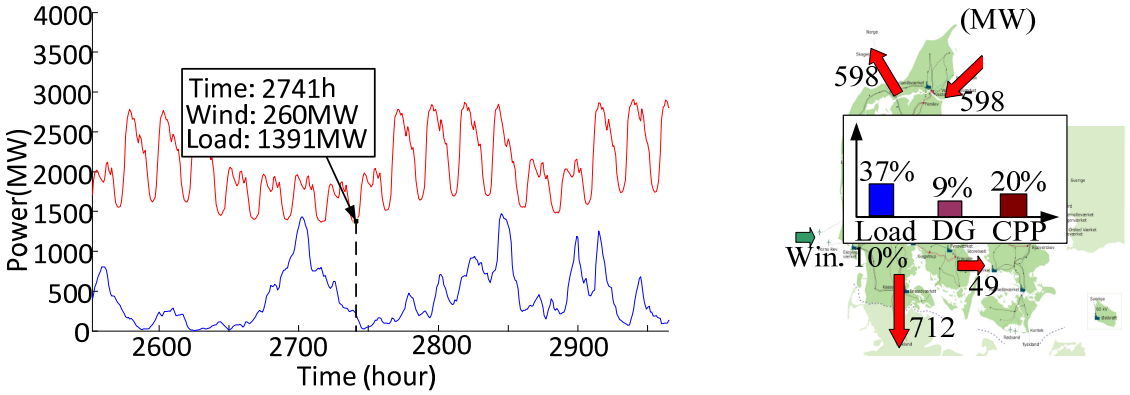

(c) Low Wind Low Load (LWLL) (2AM, Apr. 25th, 2011)

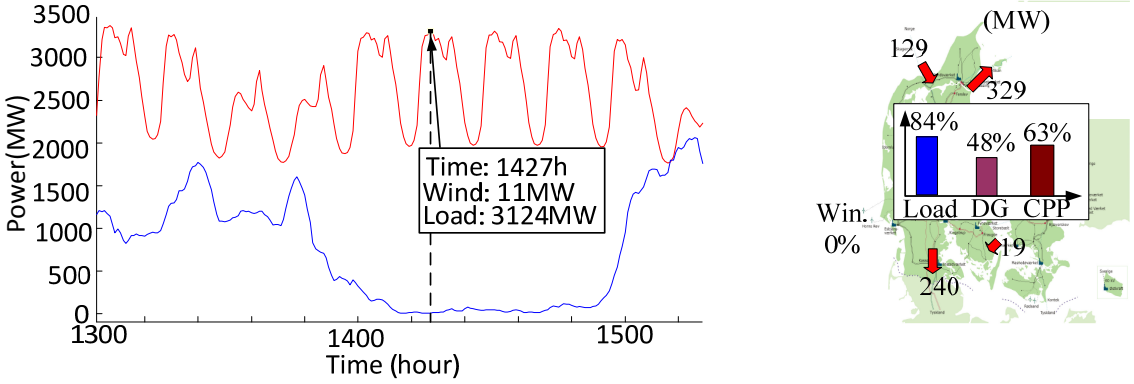

(d) Low Wind High Load (HWHL) (8AM, Mar. 1st, 2011)

Fig. 5.8 Wind power generation, load and power exchange in 4 typical OCs.

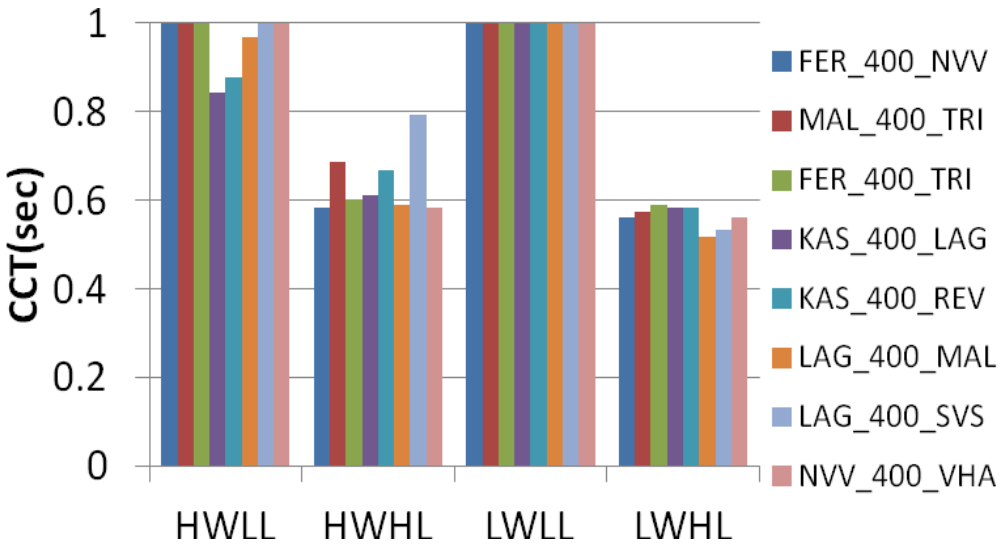

Fig. 5.9 Critical clearing time of 4 typical operating conditions.

TABLE 5.4 MOST CRITICAL *N-1* CONTINGENCIES IN TERMS OF TRANSIENT STABILITY

SHORT CIRCUIT BUS	TRIPPING OF LINE
NVV	NVV_400_VHA
NVV	FER_400_NVV
TRI	FER_400_TRI
TRI	MAL_400_TRI
LAG	LAG_400_MAL
LAG	LAG_400_SVS
KAS	KAS_400_REV
KAS	KAS_400_LAG

Results of CCTs in these 4 scenarios are shown in Fig. 5.9. One can get the conclusions that the most influential factor is the generation level of CPPs, since the higher load of CPPs implies the less reserve in these CPPs in emergency condition. Besides, if the power system is in low load scenarios, the transient stability is better because the loads of CPP are usually lower. Generally, when the wind power generation is high, the transient stability is better because wind power generation can replace part of power generation from CPPs and unburden the load of CPPs.

5.3.3 Influencing Factors of Dynamic Security

As mentioned earlier, the transient stability is highly dependent on the power flow pattern before the disturbance, and the power flow pattern can be decided by many influencing factors, such as the generation of CPPs, load consumption, wind generation as well as the power exchange with external grids. In order to evaluate the impact of these main factors on transient stability individually, the following configurations are necessary:

a) A fundamental scenario should be given, as shown in Table 5.5, where the basic values (i.e. capacities) of these percentages are the same with Table 5.3. Then the main influencing factors are changed individually in order to analyze their respective impact.

b) When considering the impacts of wind power generation and load consumption, we should not change the generation output of CPPs and power balance is kept by one external grid (i.e. ENTSO-E synchronous grid) as a Slack Bus. Since the generation output of CPPs is the most effective impact, the generation of CPP should be kept invariant while evaluating the respective impact of other impacts.

TABLE 5.5 SCALES OF FUNDAMENTAL OPERATING CONDITION (BASED ON 2010 MODEL)

SCALE	CAPACITY(MW)	PERCENTAGE (%)	POWER(MW)
Load level	3664	50	1832
CPP generation	3147	80	2517.6
CHP generation	2017	50	1008.5
Other dispersed generation	326	50	163
Wind power generation (offshore)	369	50	184.5
Wind power generation (onshore)	2232	50	1116
HVDC to Sweden	740	0	0
HVDC to Eastern Denmark	600	0	0
HVDC to Norway	1000	0	0

The impact of generation output of CPPs on transient stability is shown as Fig. 5.10. CCTs of 8 most critical short-circuit events decrease with the increase of generation output of CPPs from 30% to 100%. That is because the heavier load of CPPs, the less reserve of generators when they are subjected to disturbances. The load of CPP is the most dominant impact on transient stability, as CCTs drop evidently from 0.95sec to 0.1sec.

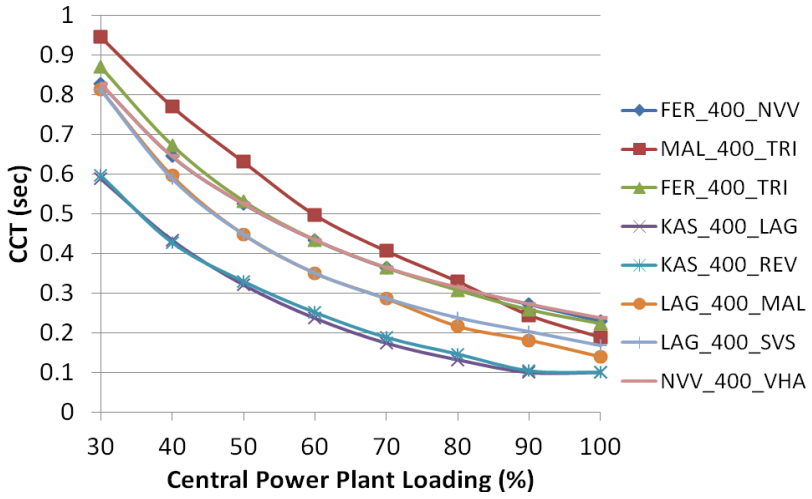

Fig. 5.10 Critical clearing time w. r. t. the generation of central power plants.

The transient stability is also dependent on the load. With the increase of the load level in all load of western Denmark, the power import from HVAC connection of the ENTSO-E grid increases in order to keep the power balance. When the load varies from 30% to 130% (expected peak load in 2030), CCTs increase from minimum 0.1sec to maximum 0.47sec regularly, as shown in Fig. 5.11. It is because more power consumption in the load contributes to the decelerating area of generators.

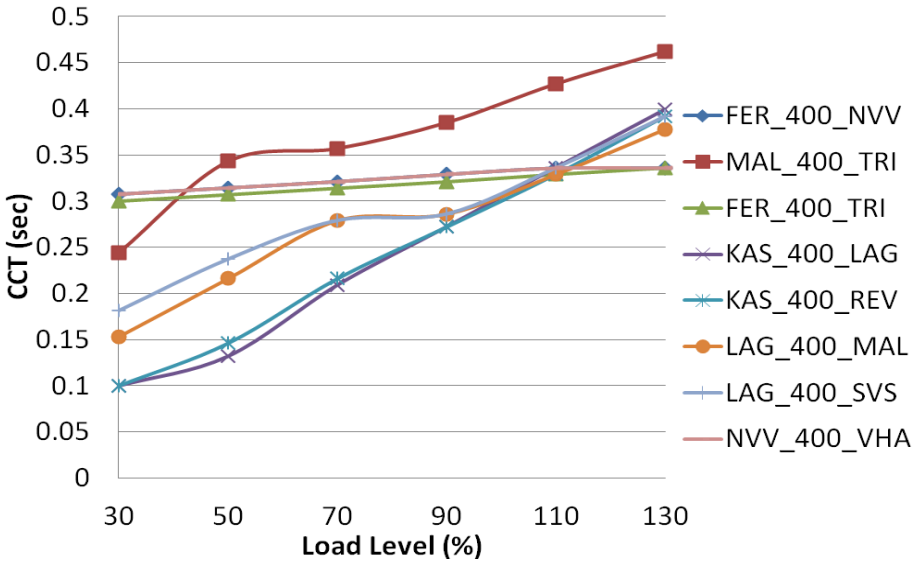

Fig. 5.11 Critical clearing time w. r. t. the load level.

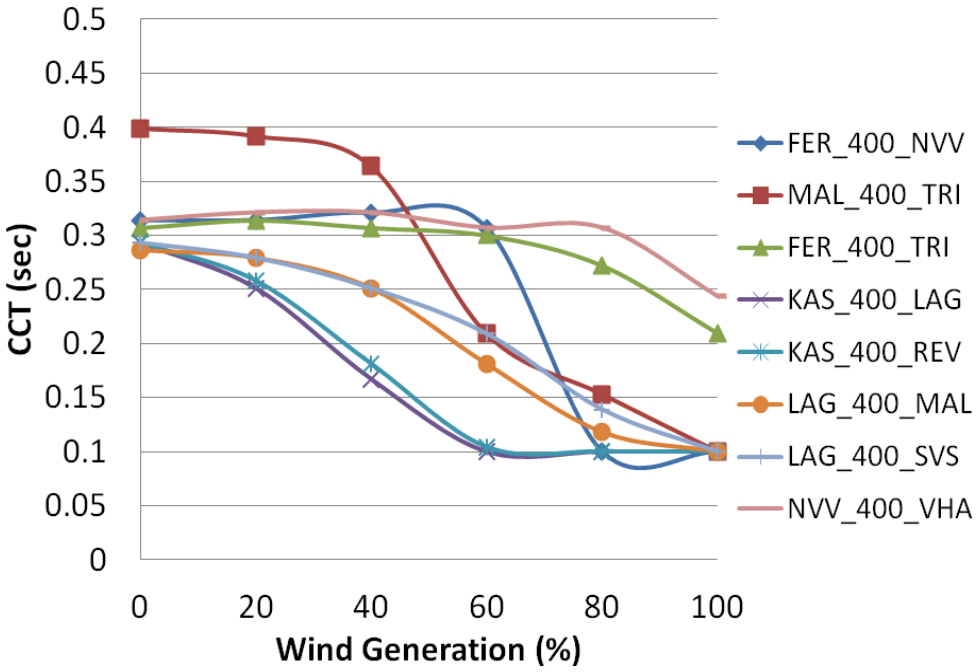

Fig. 5.12 Critical clearing time w. r. t. the wind generation level.

Since the detailed model of onshore and offshore wind farms have been built, the impact of wind power generation on transient stability can be accurately evaluated. As shown in Fig. 5.12, when the generation outputs from CPPs are invariant, the increase of wind power generation deteriorates the transient stability. It can be concluded that the wind power penetration can not exceed 60% when the HVDC with Nordic countries are disconnected.

HVDC links with emergency control usually improves the transient stability. Nevertheless, with the same control mechanism, the power exchange before the disturbance has different effect, mainly dependent on the fault position in the power grid. As shown in Fig. 5.13, when the short circuit points take place in the north part of Denmark (i.e. FER_400_NVV, FER_400_TRI and NVV_400_VHA), close to connection points of HVDC, the transient stability should be better if these HVDC links transfer more power before the disturbance, either import or export. However, when the short circuit points take place in the other part of Denmark, the transient stability improves with the increase of HVDC power output, from import 60% to export 60%, intuitively because the power output or power consumption can contribute to the decelerating area of generators [14], [15].

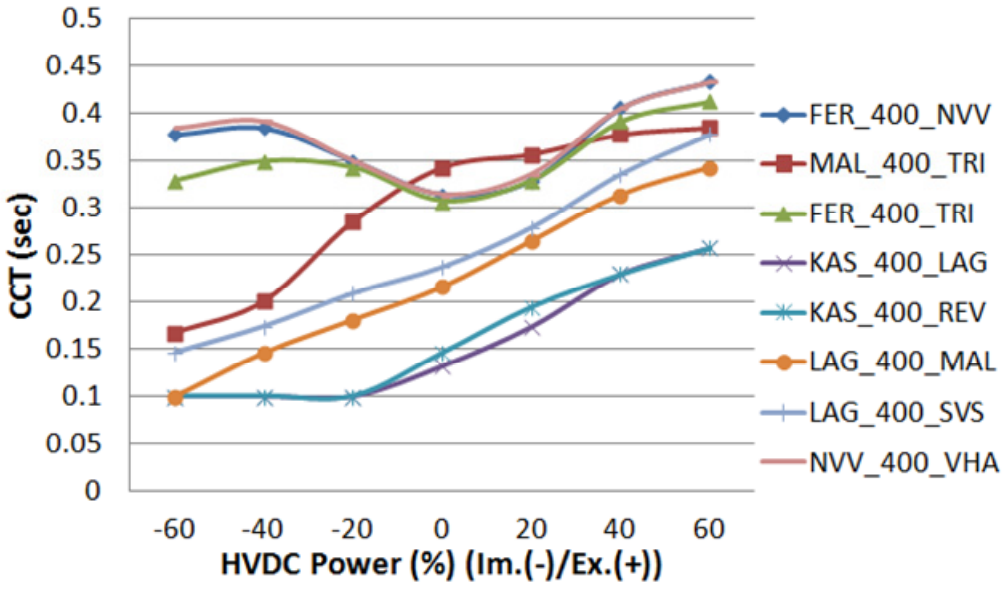

Fig. 5.13 Critical clearing time w. r. t. the power exchange of HVDC.

5.4 Summary

This chapter firstly described the modeling of Danish wind farms in DIgSILENT, both onshore and offshore wind farms with different types (FSIG, DFIG & FRC). Then, critical fault screening is conducted all across western Danish power system to

search out the vulnerable areas in terms of transient stability, and 8 most critical *N-1* contingencies are selected as the disturbances for examining the transient stability. Furthermore, 4 typical OCs in the year of 2011 are selected to evaluate the impact of wind generation level and load on transient stability. Finally, the dynamic security is assessed by calculating critical clearing time in a variety of power flow patterns. The influencing factors of transient stability are analyzed individually, such as the output of central power plants, load level, wind generation level and power exchange in HVDC links.

In conclusion, the transient stability is highly dependent on the power flow pattern before the disturbance. The output of CPPs is the most dominant factor of transient stability. The higher load of CPPs means the less reserve and worse transient stability. Besides, under the same load of CPPs, the less load consumption and the more wind generation (especially FSIG-based) are generally harmful to transient stability. The impact of the transmission power in HVDC links on transient stability is highly dependent on the position of the disturbances.

The main content of this chapter has also been reported in the author's previous publication in [C5].

References

[1] P. Kundur, *Power System Stability and Control.* London, U.K.: Mc-Graw-Hill, 1994.

[2] M. A. Pai, *Transient Stability of Power System.* Massachusetts, USA: Kluwer Academic Publishers, 2000.

[3] J. Machowski, J. W. Bialek and J. R. Bumby, *Power System Dynamics: Stability and Control. (2nd Edition)*. West Sussex, U. K.: John Wiley & Sons, Inc., 2008.

[4] E. Muljadi, C. P. Butterfield and B. Parsons, "Effect of variable-speed wind turbine generator on stability of weak grid," *IEEE Trans. Power Syst.*, vol. 22, no. 1, pp. 29-36, Mar. 2007.

[5] O. Anaya-Lara, F. M. Hughes, N. Jenkins *et al.*, "Influence of wind farms on power system dynamics and stability," *Wind Engineering,* vol. 30, no. 2, pp. 107-127, 2006.

[6] V. Akhmatov, "System stability of large wind power networks: a Danish study case," *Int. Journal of Electrical Power and Energy Systems*, vol. 28, no. 1, pp. 48-57, Oct. 2005.

[7] C. Jauch, P. Sørensen, I. Norheim *et al.*, "Simulation of the impact of wind power on the transient fault behavior of the Nordic power system," *Int. Journal of Electrical Power and Energy Systems*, vol. 77, no. 2, pp. 135-144, Mar. 2007.

[8] Statistic data of wind farms in Denmark, [Online]. Available: http://www.ens.dk/da-DK/Info/TalOgKort/Statistik_og_noegletal/Oversigt_over_energisektoren/Stamdataregister_vindmoeller/Sider/forside.aspx, assessed on 05-Aug-2013.

[9] *Connection of wind turbines to low and medium voltage networks*, The Committee Report KR-111-E, 2nd Ed., DEFU. Copenhagen, Denmark, pp. 73, Oct. 1998, [Online]. Available: http://www.defu.dk

[10] *Wind turbines connected to grids with voltages below 100 kV—Technical regulations for the properties and the control of wind turbines*, Energinet.dk, Technical Regulations TF 3.2.6. Fredericia, Denmark, pp. 41, Nov. 2004.

[11] *Technical regulation 3.2.5 for wind power plants with power output greater than 11kW.* Energinet.dk, 2010.

[12] Siemens Power Generation, "Technical Specification", [Online]. Available: http://www.ens.dk/da-DK/Info/TalOgKort/Statistik_og_noegletal/Oversigt_over_energisektoren/Stamdataregister_vindmoeller/Sider/forside.aspx, assessed on 05-Aug-2013.

[13] Hourly Danish power system data in 2011, [Online]. Available: http://www.energinet.dk/EN/El/Engrosmarked/Udtraek-af-markedsdata/Sider/default.aspx, assessed on 05-Aug-2013.

[14] M. H. Haque, "Equal-area criterion: an extension for multimachine power systems" *IEE Proceedings on Generation, Transmission and Distribution*, vol. 141, no. 3, pp. 191-197, May. 1994.

[15] O. G. C. Dahl, "Stability of the General 2-Machine System," *Transactions on American Institute of Electrical Engineers*, vol. 54, no. 2, pp. 185-188, Feb. 1935.

PART III

DYNAMIC SECURITY ASSESSMENT AND CORRESPONDING PREVENTIVE CONTROL SCHEME

Chapter 6

Introduction of Decision Tree Algorithms

6.1 Introduction

With the development of information and communication techniques (ICT), conventional power systems are being modernized with improved efficiency, reliability, economy and sustainability of generation and distribution of electricity. The huge volume of data in power systems motivates the adoption of data mining techniques in the emerging field of power system data analytics. As the mainstream of data mining algorithms applied to power systems, decision tree (DT), also named as classification and regression tree (CART), has gained increasing interests because of its high performance in terms of computation efficiency, uncertainty manageability, and interpretability. Currently, power system data are not only being gathered by architectural monitoring systems, e.g. WAMS, SCADA/EMS, FNET systems for online operation, control and protection, but also by a large number of distributed devices, e.g. smart-meters, fault recorders etc. for offline analysis and management. In addition, data from simulation, carried out by power system analysts are also playing an important role in the planning and operation of power systems. Therefore, modern power systems are enriched with huge quantity of online data, historical data, simulated data etc., ready for extraction, processing, analysis and exploration.

Data mining techniques, involving methods of artificial intelligence, machine learning, statistics and database management, are computation processes of discovering the useful information of data patterns from large data sets. Compared with many other data mining techniques, especially those with “white box” nature, such as support vector machine (SVM) and artificial neural network (ANN), DT algorithms have gained increasing interests because it not only provides the insight information of data sets with low computation burden, but also reveals the principles for further interpretation. Besides, under the background that there are more and more uncertain factors in power systems, DT algorithms are capable of managing these uncertainties by statistical methods to increase reliability.

In this chapter, the fundamental knowledge of DT algorithms is introduced, followed by an overview on a variety of DT applications to power systems for better interfacing power systems with data analytics.

6.2 Principles of Decision Trees

Decision tree is a decision support tool which uses a binary structured tree graph or model to reveal the hidden relationship between inputs and outputs, and to predict the possible consequences of the output. The data mining algorithm used in DTs is classification and regression tree (CART), which was first developed by Breiman *et al.* in the 1980s [1]. It has been widely accepted and applied in many fields, e.g. signal processing, financial analysis, chemical constituent identification, medical diagnostics etc., and was firstly introduced into the field of power systems by Wehenkel *et al.* in 1989 [2]-[5].

Fig. 6.1 shows the principle of data mining algorithms applied to power systems. Sufficient amount of data are collected from power systems, used as the learning database, including input variables as predictors and output variables as targets. Data mining engine plays a significant role to find out important patterns that are hidden in the learning database followed by the evaluation and interpretation of the created model. Thereafter, online data are obtained from the system and used as the input to predict the classification or the target values of the output. Finally, actions of control or protection are suggested or automatically taken if necessary.

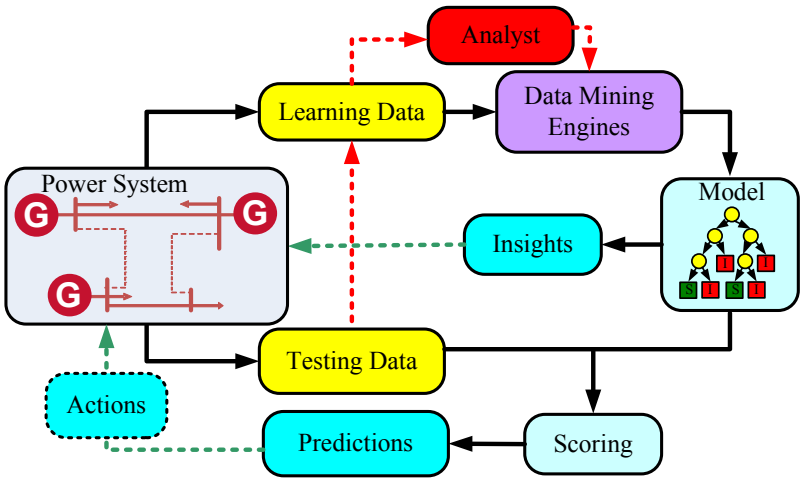

Fig. 6.1 Principle of data mining algorithms applied to power systems.

As illustrated in Fig. 6.2, given a set of attributes (i.e. *A,B,C,…*) as input predictors of case *n*, the target value (i.e. Discrete or Continuous) of the case can be predicted by dropping the case downward along a path of "if-then" questions from the root node to

a terminal node of a DT. The vector of predictors can be composed of both numerical variables (e.g. *A*) and categorical variables (e.g. *B*). Variables are called numerical variables if the predictors are real numbers, while called categorical variables if they take values in a finite set (e.g. **S**) which may not have any natural ordering. The DT is classification tree (CT) if the target is a discrete class, while it is regression tree (RT) if the target is a continuous value. Only CT is applied in the research of PART III, so it is also the focus of this chapter.

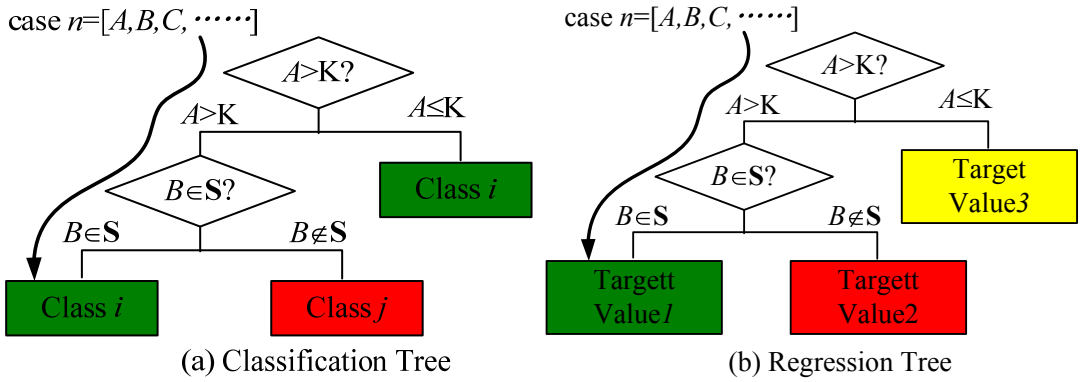

Fig. 6.2 A simple (a) classification tree and (b) regression tree.

6.2.1 Splitting Rules

A database composed of a number of cases is necessary for training the DTs. Each case in the database consists of a vector of predictors and a target, the predictors usually serve as the input attributes, and the target is the output. The cases in the database are divided into a learning set (LS) and a test set (TS). The LS is used to grow a series of DTs with increasing sizes, while the TS is used to evaluate their accuracies to decide the optimal one. As demonstrated by a 2-class problem in a 2-D space in Fig. 6.3, the training process of the DT is to iteratively split the dataset into two subsets. The fundamental idea to select each splitting rule is such that to make the cases in each of the divided subset as pure as possible.

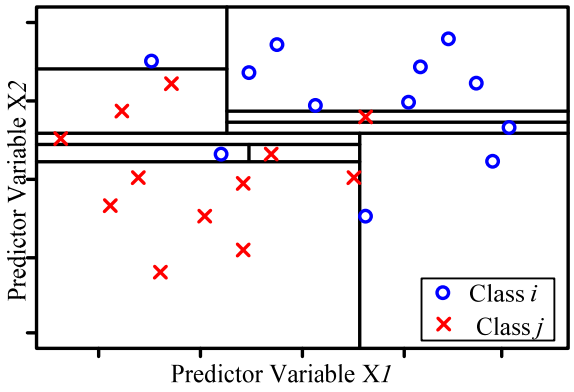

Fig. 6.3 Optimal splitting rules in 2-D space.

More generally, for a J class problem in the LS, let N_j be the number of cases of class j ($j = 1,..., J$). In a node t, the total number of cases in LS which $x_n \in t$ is denoted as $N(t)$, and the number of class j cases in node t is denoted as $N_j(t)$. The proportion of class j cases in LS falling into node t is $N_j(t)/N_j$. Therefore, for a given set of prior probabilities $\pi(j)$ that class j will be presented in the new dataset, the joint probability that a case will both be class j and fall into node t can be defined by (6.1).

$$p(j,t) = \pi(j)N_j(t)/N_j \tag{6.1}$$

Hence, the probability that any case falls in to node t is defined by (6.2).

$$p(t) = \sum_j p(j,t) \tag{6.2}$$

According to Bayesian theorem, the conditional probability that a case is class j given that it falls into node t is given by (6.3),

$$p(j \mid t) = p(j,t)/p(t) \tag{6.3}$$

which satisfies the equation in (6.4).

$$\sum_j p(j \mid t) = 1 \tag{6.4}$$

Many impurity indices are adopted to find optimal splits of a DT, such as the GINI index and the Entropy index, as defined in (6.5) and (6.6),

$$I_{GINI}(t) = \sum_{i \neq j} p(i \mid t)p(j \mid t) \tag{6.5}$$

$$I_{Entropy}(t) = -\sum_j p(j \mid t)\log p(j \mid t) \tag{6.6}$$

If a split δ of node t is predicted to send a proportion p_L of the data cases to left descendant node t_L and proportion p_R to right descendant node t_R, the decrease of impurity is defined by $\Delta I(\delta,t)$, as given in (6.7). The optimal selection of splitting rules for each node can be calculated by repeated attempts to maximize the decrease of impurity index $\Delta I(\delta, t)$ which is equivalent to select those splits that minimize the overall impurity of the whole tree $I(T)$, as defined in (6.8), in which T_t are terminal nodes of the DT.

$$\max .\Delta I(\delta,t) = \max .\left\{\left[I(t) - p_L(t)I(t_L) - p_R(t)I(t_R)\right]p(t)\right\} \tag{6.7}$$

$$I(T) = \sum_{t \in T_t} I(t) = \sum_{t \in T_t} i(t)p(t) \tag{6.8}$$

Initially, the stop-splitting rule was either that the improvement of splitting is below a threshold β or the number of cases in the terminal node is less than a given number N_{Tt}, as defined in (6.9) and (6.10).

$$\max_{t \in T_t} .\Delta I(\delta,t) \leq \beta \tag{6.9}$$

$$N(t) \le N_{Tt} \tag{6.10}$$

6.2.2 Accuracy Evaluation

The accuracy of DTs can be evaluated by internal test or external test. Internal test means using the TS selected from the same database to evaluate the accuracy, while external test is to test the accuracy of the created DT by using the cases of another independent dataset. There are 3 methods of internal test to estimate the accuracy of a DT. The first, overoptimistic, is the resubstitution estimates, which is computed using the same data as LS used to train the DT. The second is the test sample estimates. The cases in the database are randomly divided into a LS and TS. The LS is used to train the DT, while the TS is used to evaluate the accuracy of the created DT. The third, called as cross-validation, is parsimonious with data and preferred for databases with small sizes. The case in the database L are randomly divided to V subsets of equal size (i.e. $L_1, L_2, \ldots, L_V$). For every ith iteration ($i = 1,2,\ldots,V$), L-L_i is used as the LS, and L_i is used as the TS. The accuracy of DT is the average estimates of all V iterations.

Define the function $X(S)$ to be 1 if the statement S inside the parentheses is true, otherwise zero, as defined by (6.11).

$$\mathrm{X}(S) = \begin{cases} 0 & \text{statement } S \text{ is true} \\ 1 & \text{statement } S \text{ is false} \end{cases} \tag{6.11}$$

The accuracy of DT can be evaluated by resubstitution estimate, test sample estimate, and cross-validation estimate, as defined by (6.12) ~ (6.14), respectively.

$$R(d) = \frac{1}{N}\sum_{n=1}^{N} X\left(d(x_n) \neq j_n\right) \tag{6.12}$$

$$R^{TS}(d) = \frac{1}{N_{TS}} \sum_{(x_n, j_n)\in TS} X\left(d(x_n) \neq j_n\right) \tag{6.13}$$

$$R^{CV}(d^{(V)}) = \frac{1}{N_V} \sum_{(x_n, j_n)\in L_V} X\left(d^{(V)}(x_n) \neq j_n\right) \tag{6.14}$$

where N_{TS} is the number of cases in the TS, and N_V=N/V is the number of cases in L_V. Among these three estimation methods, the second one, i.e. test sample estimate, is the most popular and acceptable one, which is also been adopted in this research.

Misclassification cost is used to find the optimal DT, which is defined by the proportion of misclassified cases with cost as its weighing factor, defined in (6.15),

$$C(d) = \frac{1}{N}\sum_{i,j}\left[c(i \mid j)\cdot X\left(d_j(x_n) \neq j_n\right)\right] \tag{6.15}$$

where N is the number of test cases, $c(i|j)$ is the cost of misclassifying a class j case as a class i case.

6.2.3 Pruning of Decision Tree to the Right Size

As mentioned before, the key criterion of a successful DT is the high accuracy, in other word, low misclassification rate/cost for the cases in TS. Too large a tree will have a high misclassification rate/cost than the right sized one. The reason is that the over-fitting of LS is likely to result in the high misclassification rate/cost of the cases in the TS. On the other hand, too small a tree will not use some of the classification information available in the LS, again resulting in a higher misclassification rate/cost than the one with the right size.

As shown in Fig 6.4, the pruning process of a tree T consists of deleting a branch T_b from T, that is, cutting of all T_b except for its root node t. The pruned substree is denoted as $T_k = T_{max} - T_b$ and $T_k \prec T_{\max}$, where k is the number of nodes in the pruned tree.

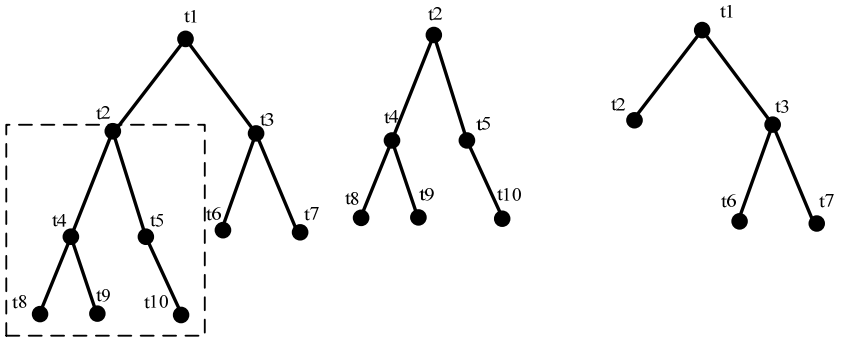

(a) unpruned tree T_{max} (b) pruned brance T_b (c) pruned subtree T_k=T_{max}-T_b

Fig. 6.4 The process of pruning a DT.

There are two criteria to select the optimal DT. The first one is to use the accuracy estimates to select the optimal sub-stree T_{opt} with the right size for all a series of pruned sub-trees by the rule defined in (6.16).

$$R(T_{opt}) = \min_{k\in[1,\max]} .R^{ts}(T_k) \tag{6.16}$$

The second one considers statistical error. The standard error estimate for $R^{TS}(T_k)$ is denoted by $\Delta R^{TS}(T_k)$ calculated by (6.17).

$$\Delta R^{TS}(T_k) = \sqrt{\frac{R^{TS}(T_k)\left[1-R^{TS}(T_k)\right]}{N^{TS}}} \tag{6.17}$$

Two DTs whose misclassification rate is smaller than the standard error estimate of either one have almost the same performance, and the optimal DT is selected as the smaller sized one within the range of $R(T_{opt})\pm\Delta R^{TS}(d)$, defined in (6.18).

$$R(T_{opt}) = \min_{k\in[1,\max]} .\left[R^{ts}(T_k)\right] \pm \Delta R^{TS}(T_k) \tag{6.18}$$

6.2.4 Prior Probabilities

In some studies, the cases in the dataset are very unbalanced with classes, so prior probabilities are a useful set of parameters to assist in constructing a more reliable DT. Prior probabilities can be adjusted to effectively control the splitting rules over the tradeoff between the class purity and tree accuracy. Combined with (6.1) and (6.2), the probability that any case falls in to node t can be defined by (6.19),

$$p(t) = \sum_j \left[\pi(j) N_j(t) / N_j \right] \tag{6.19}$$

where π_j, N_j, n_j $(j = 1,...,J)$ are the prior probabilities, number of cases in LS, and number of cases contained in node t for class i.

From (6.1) and (6.3), the conditional probability that a case is class j given that it falls into node t can be given by (6.20),

$$p(j \mid t) = \left(\pi(j) N_j(t) / N_j \right) \Big/ p(t) \tag{6.20}$$

so the probabilities $p_L(t)$, $p_R(t)$ that the cases in node t going to left descendent node t_L and right descendent node t_R are defined as (6.21) and (6.22) respectively.

$$p_L(t) = p_t^{left} / p_t^{parent} \tag{6.21}$$

$$p_R(t) = p_t^{right} / p_t^{parent} \tag{6.22}$$

Therefore, by adjusting prior probabilities π_j $(j = 1,...,J)$, one can find the overlapping region between classes for each split, as shown in yellow region in Fig. 6.5. Accordingly, the regions in red and blue are identified for different classes, with probabilities of exceptions lower than π_b and π_r, respectively.

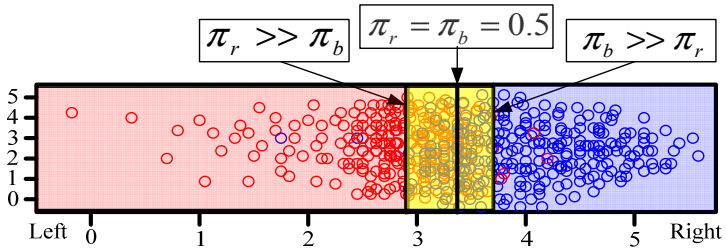

Fig. 6.5 Thresholds of DTs with respect to prior probability adjustment.

6.3 Applications of Decision Tree to Power Systems

6.3.1 Security Assessment

Among the many other applications of DT in power systems, security assessment is the most needed and versatile [2]. With the help of DT, the information regarding

scenarios of power system (e.g. operating conditions, contingencies, topologies, voltage and power etc.) can be expressed by a DT model to assess and predict the security of scenarios from a vector of input attributes.

DT is first introduced by Wehenkel *et al.* to assess the transient stability of a simple electric power system [3]. Later, transient stability assessment by DT methodology is carried out for a real power system, i.e. *EDF* system in France, with enhanced reliability for seen and unseen cases [4]. In [5], a new methodology are proposed to reduce the probability of missed alarms by adjusting the prior probabilities and misclassification costs of unstable cases, and also to reduce the probability of false alarms by incremental tree development scheme. To evaluate the overall transient stability assessment for a large scale power system, multi-contingency trees are first presented in a more compact and easier fashion compared with single-contingency trees.

In [6], DT is first used by Hatziargyriou *et al.* to assess the security of a median island power system (*Lemnos Island* system in Greece) with high penetration of renewable energy, taking the wind speed and solar radiation as candidate attributes. In [7], a DT based method of optimal dispatch of primary reserve services considering security margins as constraints is tested on *Crete Island* system in Greece.

DT is first adopted for online dynamic security assessment (DSA) for a large scale power system (*Entergy* system in USA) in a practical approach considering by Sun *et al.* [8]. This scheme builds and periodically updates DTs offline to decide critical attributes as security indicators. Then DTs provide online DSA and operation guidelines based on limited number of PMU measurements from WAMS. The security of current scenario is voted by a whole path of DTs instead of just by terminal nodes to improve the robustness of DTs. In [9], DT was used especially for voltage security assessment for *AEP* system in USA based on the information of the past and forecast 24-h ahead operating conditions. Hourly updated DTs by including newly predicted system conditions, and multiple optimal DTs, corrective DTs are proposed for robustness improvement. In [10], a real-time security assessment tool was proposed to evaluate four post-contingency security issues of *SRP* system in USA, i.e. voltage magnitude, thermal limit, voltage security and transient stability issues.

DT can also be combined with other algorithms for power system security assessment, e.g. fuzzy logic [11] and mathematical morphology [12]. In [11], Kamwa *et al.* propose a fuzzy rule-based DT for rapid stability assessment. The voltage and rotor angle curves are proceed in both time and frequency domains to extract the area-wise and system-wise features for DT training. The created DTs can accurately

predict the security of *Hydro-Quebec* system for decision making as early as 1sec or 2sec after fault clearing.

6.3.2 Preventive and Corrective Control

Continuously growing demand for electricity has forced modern power systems to operate closer to secure operating limits. Also, the increasing penetration of large scale renewable energy may impact power grids by bringing more uncertainties to grid operations. DT is a suitable tool to provide emergency control of power system in terms of its high efficiency, interpretability and uncertainty manageability.

In [13], DT is used to determine the reserves of *Crete Island* system in Greece. Then online preventive control is suggested with optimization on the cost of load shedding and the cost of spinning reserves. In [14], the application of DT for online steady state security assessment of *Hellenic* system in Greece is presented. DTs extract the relevant information regarding to line loading and voltage level and express it in terms of controllable values in the system, i.e. generator bus voltage, active power generation and transformer taps. Preventive and corrective control strategies are suggested with respect to these controllable values.

In [15], Guang *et al.* propose ISGA (integral square generator angle) index to judge the severity of contingencies for transient stability assessment. DT is trained by a large number of time-domain simulations of contingencies to give guidelines of ISGA, so as to trigger one-shot event-based corrective controls to stabilize the transient events at any time intervals of 1sec after the disturbance. In [16], one-shot response-based control is developed by Rovnyak *et al.* in response to the loss of synchronism detection.

In [17] and [18], DTs are used for preventive control (i.e. generation rescheduling) and for corrective control (i.e. load shedding) by determining the dynamic security regions. Then the preventive control and corrective control are optimized in terms of the fuel cost and the amount of load to be shed, respectively. In [19], a new methodology that using two DTs in tandem is proposed for *Energinet.dk*, which manages the Danish power system with large scale of renewables and distributed generations. One DT about measurable variables is employed for DSA to identify potential security issues, and the other DT about controllable variables provides online decision support on preventive control strategies against those issues.

In addition, DT can also be used for controlled islanding [20], [21], load shedding [22], power system quick restoration [23] and so on.

6.3.3 Protection

Some early explorations use the DTs to trigger the protection in real time, using a short window of post-fault curves (rotor angle, speed and acceleration [24] and *R-Rdot* relay [25], [26]) in the process to train a DT model, which can predict whether system insecurity/instability or even system collapse is going to occur before it really happens. Some uncertainty factors in the network composed of fault duration, fault location, system operating conditions and network topology are considered to test the robustness of the created DTs, but the reliability still can not meet the standard of industrial application. In [27], the sensitivity of prediction accuracy is demonstrated for online transient stability assessment. It is found that the prediction accuracy is increasing when the power system is getting closer to system collapse.

In [28], a methodology is proposed to reduce the likelihood of hidden failures and potential cascading failures by adjusting the security/dependability of adaptive protections. Aided by WAMS, the scheme identifies the prevailing system conditions. When the system is in "safe" state, a bias of protection settings toward "dependability" is desired; when the system is in "stressed" state, the protection settings are altered in favor of "security".

6.3.4 Forecasting, Estimation and Identification

DTs usually combine with unsupervised learning techniques to forecast the load consumption, to estimate the variables, and to identify the parameters in power systems.

In [29], Figueiredo *et al.* deals with the load forecast issue of *EDP* (Portuguese Distribution Company). Firstly, unsupervised learning (clustering) is proposed to obtain partitions of historical data into a set of consumer classes, then supervised learning (DT) is adopted to describe each class by rule-based classifications and create a DT model to assign consumer to the existing classes. The objective is to find the relevant knowledge about how and when consumers use electricity.

In [30], DT is used to estimate the line flows and bus voltage following an outage event in an efficient manner. The approach has been successfully tested by Taiwan system in China. In [31], a methodology is proposed for southern Spanish generation company to estimate the daily load patterns and their associated probability of non-connected unit. DT is used to recognize the load pattern so as to approximately predict when its generating units are connected to alleviate the network constraints.

Regression tree (RT) can also combine with other algorithms. In [32], a new method based on a hybrid technology of optimal regression tree and an artificial neural network is proposed to discover the rules in short-term load forecasting. RT

contributes to the clustering of input data, while ANN is used to predict the 1-step-ahead load. The conventional CART regards the midpoint of two learning data as a split value. Therefore, CART misclassifies the data close to the splitting values. Therefore, Mori *et al.* combines fuzzy logic with RT to predict the short-term load, in which two fuzzy membership functions were assigned to express the left and right nodes so as to increase the accuracy of prediction [33].

6.3.5 Fault Diagnosis

DT is one of the strong tools in power system fault diagnosis because of its ability to process and analyze the time-series signal. In [34], DT is used in fault diagnosis of power distribution lines, both discrete attributes (operating states) and continuous attributes (voltage and current) are included in the predictors in order to deal with the variance of fault resistance and the noise of measurement.

In [35], a decision tree-based method is proposed to detect High Impedance Fault in distribution feeders using attributes of fundamental and harmonic RMS values of current and voltage so as to reduce sampling rate of protection relays.

6.3.6 Extended Algorithms Based on Decision Tree and Software

DT is built based on a database, either from simulated data or from historical data, which is definitely significant for the quality and practicality of the DT model. There is a tradeoff between the information content in the database and the computation cost of creating a large database, so many new methods are proposed to maximize database information content and minimize computation burden. In [36], Lartin super-cube sampling is first used for efficiently identifying the security boundary region. In [37], bisection methods together with importance sampling are used to efficiently prepare the hourly database for online DSA.

As mentioned before, the algorithm of CART has advantages in terms of computation efficiency, uncertainty manageability, interpretability, as well as the ability to handle missing values [38], but it also has weakness, for instance, piece-wise sharp decision boundaries, affected by data interaction, missing the effect of weak attributes. Therefore, some extended algorithms based on DTs, such as Fuzzy DT [39], ANN DT [40], [41] Random Forest [42]-[45], Tree Net [46], [47] etc. are invented to strengthen the original CART algorithm.

There are two categories of software that provides DT based algorithms. The first type is commercialized software, e.g. Salford Predictive Modeler [48], SSPS [49], Elefant [50], Lush [51]. The other is open-source software, e.g. RapidMiner [52],

Shogun [53], Orange [54], Spider [55], Plearn [56], PyML [57], Weka [58] as well as MATLAB/Statistic toolbox.

6.4 Summary

The chapter highlights the importance of vast amount of already available data from power systems and its potential applications. Firstly, it introduces the principle knowledge of decision tree algorithm, followed by the latest state-of-the-art of decision tree algorithms applied to power systems. Moreover, advantages and weakness of decision tree algorithms are discussed. Finally, many choices of software to implement DT based algorithms are suggested.

The main content of this chapter has also been reported in the author's previous publications in [J2] and [J1].

References

[1] L. Breiman, J. Friedman, R. A. Olshen *et al.*, *Classification and Regression Trees.* Belmont, CA, Wadsworth, 1984.

[2] L. Wehenkel, "Machine learning approaches to power-system security assessment," *IEEE Intelligent Systems and Their Applications*, vol. 12, no. 5, pp. 60-72, Sep. 1997.

[3] L. Wehenkel, Th. Van Cutsem and M. Pavella, "An artificial intelligence framework for on-line transient stability assessment of electric power systems," *IEEE Trans. Power Syst.*, vol. 4, pp. 789-800, May 1989.

[4] L. Wehenkel and M. Pavella, "Decision trees and transient stability of electric power stability of electric power systems," *Automatica*, vol.27, no.1, pp. 115-134, 1991.

[5] L. Wehenkel, M. Pavella, E. Euxibie *et al.*, "Decision tree based transient stability method a case study," *IEEE Trans. Power Syst.,* vol. 9, no. 1, pp. 459-469, Feb. 1994.

[6] N. Hatziargyriou, S. Papathanassiou and M. Papadopoulos, "Decision trees for fast security assessment of autonomous power systems with a large penetration from renewables," *IEEE Trans. Energy Convers.*, vol. 10, no. 2, pp. 315-325, Jun. 1995.

[7] K. A. Papadogiannis and N. D. Hatziargyriou, "Optimal allocation of primary reserve services in energy market," *IEEE Trans. Power Syst.*, vol. 19, no. 1, pp. 652-659, Feb. 2004.

[8] K. Sun, S. Likhate, V. Vittal *et al.*, "An online dynamic security assessment scheme using phasor measurements and decision trees," *IEEE Trans. Power Syst.*, vol. 22, no. 4, pp. 1935-1943, Nov. 2007.

[9] R. Diao, K. Sun, V. Vittal *et al.*, "Decision tree-based online voltage security assessment using PMU measurements," *IEEE Trans. Power Syst.*, vol. 24, no. 2, pp. 832-839, May 2009.

[10] R. Diao, V. Vittal and N. Logic, "Design of a real-teime security assessment tool for situational awareness enhancement in modern power systems," *IEEE Trans. Power Syst.*, vol. 25, no. 2, pp. 957-965, May 2010.

[11] I. Kamwa, S. R. Samantaray, G. Joos, "Development of rule-based classifiers for rapid stability assessment of wide-area post disturbance records," *IEEE Trans. Power Syst.*, vol. 24, no. 1, pp. 258-270, Feb. 2009.

[12] H. Khoshkhoo and S. M. Shahrtash,"On-line dynamic voltage instability prdiction based on decision tree supported by a wide-area measurement system," *IET Gener. Transm. Distrb.*, vol. 6, no. 11, pp. 1143-1152, Nov. 2012.

[13] E. S. Karapidakis and N. D. Hatziargyriou, "Online preventive dynamic security of isolated power systems using decision trees," *IEEE Trans. Power Syst.*, vol. 17, no. 2, pp. 297-304, May 2002.

[14] H. D. Hatziargyriou, G. C. Contaxis and N. C. Sideris, "A decision tree method for on-line steady state security assessment," *IEEE Trans. Power Syst.*, vol. 9, no. 2, pp. 1052-1061, May 1994.

[15] L. Guang and S. M. Rovnyak, "Integral square generator angle index for stability ranking and control," *IEEE Trans. Power Syst*., vol. 20, no. 2, pp. 926-934, May 2005.

[16] Q. Gao and S. M. Rovnyak, "Decision trees using synchronized phasor measurements for wide-area response-based control," *IEEE Trans. Power Syst*., vol. 26, no. 2, pp. 855-861, May 2011.

[17] I. Genc, R. Diao, V. Vittal *et al.*, "Decision tree-based preventive and corrective control applications for dynamic security enhancement in power systems," *IEEE Trans. Power Syst*., vol. 25, no. 3, pp. 1611-1619, Aug. 2010.

[18] I. Genc, R. Diao and V. Vittal, "Computation of transient stability related security regions and generation rescheduling based on decision trees," in *Proc. of PES General Meeting*., Minneapolis, MN, USA, Jul. 2010.

[19] C. Liu, K. Sun, Z. H. Rather, Z. Chen, C. L. Bak, P. Thøgersen and P. Lund, "A systematic approach for dynamic security assessment and the corresponding preventive control scheme based on decision trees," accepted by *IEEE Trans. Power Syst*., 2013.

[20] N. Senroy, G. T. Heydt and V. Vittal, "Decision tree controlled islanding," *IEEE Trans. Power Syst*., vol. 21, no. 4, pp. 1790-2293, Nov. 2006.

[21] R. Diao, V. Vittal, K. Sun *et al.*, "Decision tree assisted controlled islanding for preventing cascading events," in *Proc. of IEEE PES Power Systems Conference and Exposition*, Seattle, USA, Mar. 2009.

[22] E. M. Voumvoulakis, A. E. Gavoyiannis, N. D. hatziargyriou *et al.*, "Decision trees for dynamic security assessment and load shedding scheme," in *Proc. of PES General Meeting*, Montreal, QC, Canada, Jun. 2006.

[23] Y. Hou, C. C. Liu, K. Sun *et al.*, "Computation of milestones for decision support during system restoration," *IEEE Trans. Power Syst*., vol. 26, no. 3, pp. 1399-1409, Aug. 2011.

[24] S. Rovnyak, S. Kretsinger, J. Thorp *et al*., "Decision trees for real-time transient stability prediction," *IEEE Trans. Power Syst.*, vol. 9, no. 3, pp. 1417-1426, Aug. 1994.

[25] S. Rovnyak, C. W. Taylor and Y. Sheng, "Decision trees using apparent resistance to detect impending loss of synchronism," *IEEE Trans. Power Del.*, vol. 15, no. 4, pp. 1157-1162, Oct. 2000.

[26] K. Mei and S. M. Rovnyak, "Response-based decision trees to trigger one-shot stabilizing control," *IEEE Trans. Power Syst.*, vol. 19, no. 1, pp. 531-537, Feb. 2004.

[27] T. Guo and J. V. Milanovic, "On-line prediction of transient stability using decision tree method – sensitivity of accuracy of prediction to different uncertainties," in *Proc. of PES PowerTech*, Grenoble, France, Jun. 2013.

[28] E. E. Bernabeu, J. S. Thorp and V. Centeno, "Methodology for a security/dependability adaptive protection scheme based on data mining," *IEEE Trans. Power Del.*, vol. 27, no. 1, pp. 104-111, Jan. 2012.

[29] V. Figueiredo, F. Rodrigues, Z. Vale *et al.*, "An electric energy consumer characterization framework based on data mining techniques," *IEEE Trans. Power Syst.*, vol. 20, no. 2, pp. 596-602, May 2005.

[30] Y. C. Chien and H. Y. Yuafi, "Estimation of line flows and bus voltages using decision trees," *IEEE Trans. Power Syst.*, vol. 9, no. 3, pp. 1569-1574, Aug. 1994.

[31] A. Ugedo, E. Lobato, J. Peco *et al.*, "Decision trees applied to the management of voltage constraints in the Spanish market," *IEEE Trans. Power Syst.*, vol. 20, no. 2, pp. 963-972, May 2005.

[32] H. Mori and N. Kosemura, "Optimal regression tree based rule discovery for short-term load forecasting," *Proc. of IEEE PES Winter Meeting*, Columbus, OH, USA, Jan. 2001.

[33] H. Mori, N. Kosemura, K. Ishiguro *et al.*, "Short-term load forecasting with fuzzy regression tree in power systems," *Proc. of IEEE Systems, Man, and Cybernetics Meeting*, Tucson, AZ, USA, Oct. 2001.

[34] M. Togami, N. Abe, T. Kitahashi *et al.*, "On the application of a machine learning technique to fault diagnosis of power distribution lines," *IEEE Trans. Power Del.*, vol. 10, no. 4, pp. 1927-1936, Oct. 1995.

[35] S. Yong and S. M. Rovnyak, "Decision tree-based methodology for high impedance fault detection," *IEEE Trans. Power Del.*, vol. 19, no. 2, pp. 533-536, Apr. 2004.

[36] V. Karishnan, J. D. McCalley, S. Henry *et al.*, "Efficient databases generation for decision tree based power system security assessment," *IEEE Trans. Power Syst.*, vol. 26, no. 4, pp. 2319-2327, Nov. 2011.

[37] C. Liu, Z. H. Rather, Z. Chen, C. L. Bak *et al.*, "Importance sampling based decision trees for security assessment and the corresponding preventive control schemes: the Danish case study," *Proc. of PES PowerTech*, Grenoble, France, Jun. 2013.

[38] M. He, V. Vittal and J. Zhang, "Online dynamic security assessment with missing PMU measurement: a data mining approach," *IEEE Trans. Power Syst.*, vol. 28, no. 2, pp. 1969-1977, May 2013.

[39] S. R. Samantary, "Decision tree-initialized fuzzy rule-based approach for power quality event classification," *IET Gener. Transm. Distrb.*, vol. 4, no. 4, pp. 530-537, Apr. 2010.

[40] Y. T. Hong, C. Y. Wen and H. L. Ching, "Power system distributed online fault section estimation using decision tree based neural nets approach," *IEEE Trans. Power Del.*, vol. 10, no. 1, pp. 540-546, Jan. 1995.

[41] L. Wehenkel, I. Houben, and M. Pavella, "Automatic learning approaches for online transient stability preventive control of the Hydro-Québec system—part II: a toolbox combining decision trees with neural nets and nearest neighbour classifiers optimized by genetic algorithms," in *Proc. of the 2nd IFAC Symp. Control of Power Plants and Power Systems*, pp. 237-242, 1995.

[42] L. Breiman, "Random forest," *Mach. Learn.* vol. 45, pp. 5-32, 2001.

[43] S. R. Samantary, I. Kamwa and G. Joos, "Ensemble decision trees for phasor measurement unit-based wide-are security assessment in the operations time frame," *IET Gener. Transm. Distrb.*, vol. 4, no. 12, pp. 1334-1348, Dec. 2010.

[44] I. Kamwa, S. R. Samantary and G. Joos, "Catastrophe predictors from ensemble decision-tree learning of wide-area severity indices," *IEEE Trans. Smart Grid*, vol. 1, no. 2, pp. 144-158, Sep. 2010.

[45] I. Kamwa, S. R. Samantary and G. Joos, "On the accuracy versus transparency trade-off of data-mining models for fast-response PMU-based catastrophe predictors," *IEEE Trans. Smart Grid*, vol. 3, no. 1, pp. 152-161, Mar. 2012.

[46] J. H. Friedman, "Stochastic gradient boosting," *Comput. Stat. and Data An.*, vol. 38, no. 4, pp. 367-378, 2002.

[47] J. H. Friedman, "Greedy Function Approximiation: A Gradient Boosting Machine," *The Annals of Statistis*, vol. 29, no. 5, pp. 1189-1232, Apr. 2001.

[48] SPM - Salford Predictive Modeler, [Online]. Available: http://www.salford-systems.com/en/products/spm, assessed on 07-Jul-2013.

[49] IBM, "IBM SSPS Modeler 14.2 Modeling Nodes," 2011.

[50] I. Mierswa, M. Wurst, R. Klinkenberg *et al.*, "Rapid prototyping for complex data mining tasks," in *Proc. of the 12th ACM SIGKDD International Conference on Knowledge Discovery and Data Mining*, 2006.

[51] L. Bottou and Y. L. Cun, *Lush Reference Manual*, 2002.

[52] K. Gawande, C. Webers, A. Smola *et al.*, *ELEFANT User Manual. Technical Report*, NICTA, 2007.

[53] S. Sonnenburg, G. Raetscch, C. Schaefer *et al.*, "Large scale multiple kernel learning," *Journal of Machine Learning Research,* vol. 7, pp. 1531-1565, Mar. 2002.

[54] J. Demsar, B. Zupan and G. Leban, "Orange: from experimental machine learning to interactive data mining," *Lecture Notes in Computer Science,* vol. 3202, pp. 537-539, 2004.

[55] Spider, [Online]. Available: http://www.kyb.tuebingen.mpg.de/bs/people/spider , assessed on 07-Jul-2013.

[56] Plearn, [Online]. Available: http://plearn.berlios.de/, assessed on 07-Jul-2013.

[57] PyML, [Online]. Available: http://pyml.sourceforge.net, assessed on 07-Jul-2013.

[58] I. H. Witten and E. Frank, *Data Mining: Practical machine learning tools and techniques,* Morgan Kaufmann, 2nd edition, 2005.

Chapter 7

Preventive Control Scheme Based on Decision Trees

7.1 Introduction

In this chapter, a decision tree (DT) based systematic approach for cooperative online power system dynamic security assessment (DSA) and preventive control is proposed. This approach adopts a new methodology that trains two contingency oriented DTs on daily basis by the databases generated from power system simulations. Fed with real-time wide area measurements, one DT about measurable variables is employed for online DSA to identify potential security issues and the other DT about controllable variables provides online decision support on preventive control strategies against those issues. Then, a cost effective algorithm is adopted in this proposed approach to optimize the trajectory of preventive control. An importance sampling algorithm on database preparation for efficient DT training for power systems with high penetration of wind power and distributed generation is also proposed in this chapter.

Nowadays, continuously increase of electricity consumption has driven power systems to be operated closer to their secure operating limits. Meanwhile, integration of high level of renewable energy to already burdened power system pushes it to highly stressed and unpredictable conditions. It becomes more challenging to protect a modern power system from insecurity by relying only on localized protection schemes. Hence, a power system should be secured proactively at the system level by advanced system protection schemes for online situational awareness and proactive wide area coordinating control [1]. For instance, an elaborated proactive system protection scheme may integrate both online DSA for identification of potentially insecure conditions and system-level optimization and execution of control strategies for prevention of identified insecure conditions. Phasor measurement units (PMU) can provide high resolution real-time power system measurements synchronized by global positioning system (GPS). Based on PMUs, wide area measurement systems (WAMS) have been built in many countries and would enable the development of aforementioned proactive system protection schemes.

Pattern recognition techniques, such as Artificial Neural Networks (ANN) [2], Support Vector Machine (SVM) [3] and Decision Trees [4]-[17] can be applied in

DSA of power systems. Among them, some DT algorithms [18], have gained increasing attraction because they not only provide the results of security assessment but also reveal the principles learned by DTs for security assessment. Those principles provide useful information required for the remedial actions against recognized insecure conditions. With the aid of WAMS and advanced computing resources, DTs may be integrated into online DSA tools for large interconnected complex power systems. For instance, reference [4] applies DTs in an online DSA method by adaptively updating the database to train DTs on daily basis for foreseen system conditions. In [5], a method for efficient database generation for DT training is introduced to enhance DT accuracy in DSA and decrease the computation burden in DT training. In [6], multiple optimal DTs are proposed to increase the accuracy for the assessment of static voltage security. In addition, DTs can also be used in adaptive protection [7], controlled islanding [8], [9], load shedding [10], loss of synchronization detection [11], quick restoration schemes [12] and energy markets [13].

With the increasing penetration of renewable energy resources and other decentralized generation, more uncertainties will be brought to the operation of transmission systems, since those resources are not as accessible for direct monitoring and control from control centers as conventional central power plants [14]. Thus, a significantly increased number of scenarios need to be covered by DTs to address these uncertainties. However, it also becomes more important to minimize the computation burden with DT based online applications for real-time DSA and the associate sensitivity analysis [15]. Most of the existing works apply DTs mainly for security assessment, whose predictors to be measured in real time are the system variables that are most effective in detecting security problems, e.g. line flows and angle differences. However, the DTs focusing on decision support for preventive control may employ a different set of variables as predictors that can directly be controlled, e.g. generation outputs. Thus it is advisable to build two DTs respectively for DSA and preventive control based on two sets of predictors selected separately.

The DT-based approach proposed in this chapter aims at addressing the aforementioned problems. First, it studies the database preparation for training accurate DTs for power systems with high penetration of wind generation and other DG. Without losing generality, this research focuses on a power system supported by three types of generation: traditional central power plant (CPP) generation, wind power generation and other DG mainly from combined heat and power plants (CHP). An importance sampling technique, considering the random distribution of various generation resources, is developed and applied in the proposed approach to enhance the information contained in the databases for DT training. Second, the approach is

designed to be a systematic integration of cooperative online DSA and preventive control. The approach adopts a new methodology that offline trains two contingency oriented DTs by databases generated from power system simulations. Fed with real-time wide-area measurements, one DT is employed for online DSA to identify potential security issues and the other DT provides system operators with the online decision support on allowed preventive control strategy to guide the operating point from a potentially insecure state to a secure state. Then the optimal control trajectory is searched out by minimizing the total economic cost incurred by generation rescheduling.

The rest of the chapter is organized as follows. Section 7.2 presents the flowchart and stages of the proposed approach. In Section 7.3, database preparation with due considerations to power systems with high penetration of wind power generation and other DG is described. An importance sampling technique is adopted and presented in the approach. Section 7.4 describes in detail the cooperative application of proposed two types of DTs to predict and prevent the potential insecure issues with the least economic cost implication. Section 7.5 gives the concluding remarks of this approach. The performance of this approach will be demonstrated by the operational model of western Danish power system in Chapter 9.

7.2 Flowchart of Systematic Approach

The flowchart of the proposed DT-based systematic approach is shown in Fig. 7.1. The proposed approach is executed in the following four stages:

7.2.1 Stage I: Identification of the Security Boundary

Since wind forecasts are not highly accurate and DG is unpredictable, the power flow pattern in a next period is highly uncertain. However, a security boundary separating secure operating conditions (OCs) from insecure ones at each load level can be estimated and presented in multiple-dimensional space with coordinates of aforementioned stochastic variables, such as CPP generation, CHP generation and wind power generation.

7.2.2 Stage II: Importance Sampling

Considering the intermittency of wind power generation in wind farms and the variation of power generation in CPPs, importance sampling is used to bias a number of samples of OCs towards the security boundary by revising the sampling distribution function.

7.2.3 Stage III: Offline Time-Domain Simulation and DT Training

A large number of T-D simulations for each "*N-1*" contingencies and selected "*N-k*" contingencies are carried out to form a database, from which a series of operating guidelines are obtained by DTs.

7.2.4 Stage IV: Online Optimal Preventive Control

If online measurements violate pre-formulated guidelines, available preventive control schemes can be concluded from DTs and the optimal control trajectory can be provided to system operators.

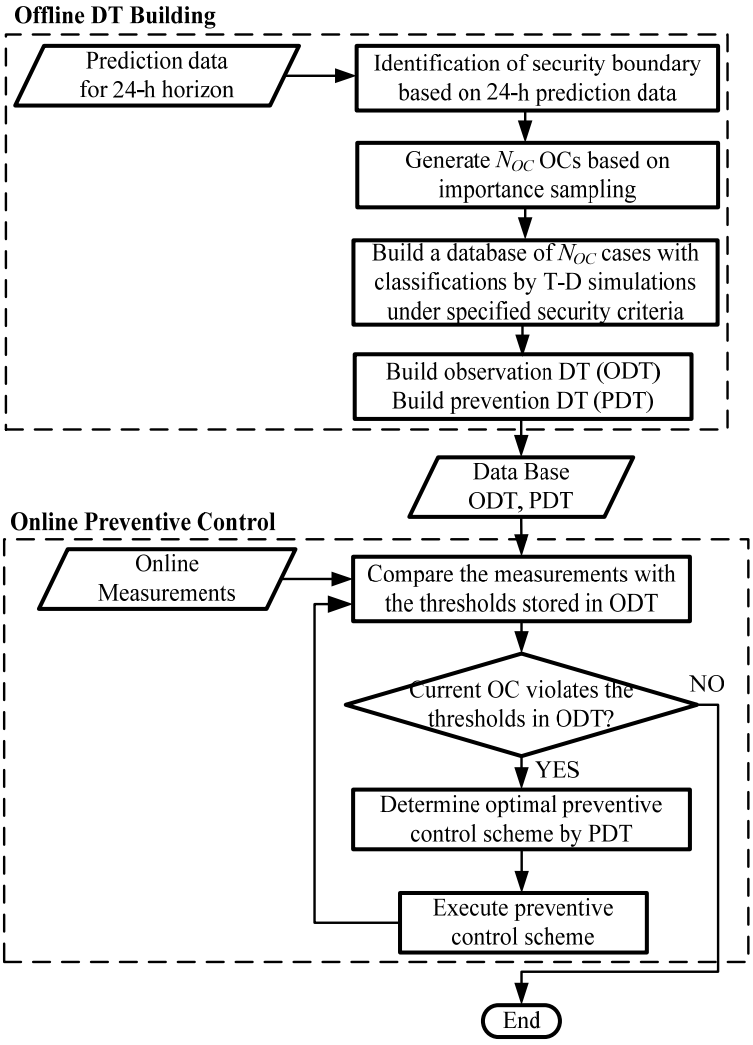

Fig. 7.1 Flowchart of DT-based DSA and preventive control approach.

7.3 Database Preparation Based on Importance Sampling

For a two-class classification problem (Secure or Insecure), the concept of entropy, commonly accepted in the information theory, is used here to evaluate the information content in the database [19], as defined in (7.1).

$$Entropy(\boldsymbol{S}) = -p_S \log_2 p_S - p_I \log_2 p_I \tag{7.1}$$

where $\boldsymbol{S}$ is the training database, p_S, p_I are the proportions of $\boldsymbol{S}$ classified as secure and insecure respectively. Therefore, a general prediction of security boundary is required and good representation of sampling OCs on both sides of the boundary is desirable.

Bisection method is adopted to approximately identify a region that contains the security boundary. Thus, only OCs adjacent to that region are simulated so as to significantly decrease the number of simulations. As illustrated in Fig. 7.2, the security boundary region is searched out by repeatedly bisecting the slot over Predictor Variable *2*. In each iteration, the slot is selected in such a way that one end of the selected slot falls in secure region and the other end in insecure region and the repeated process should eventually converge at the security boundary. Then a security boundary is created by polynomial curve fitting of those points located between a secure case and an insecure case.

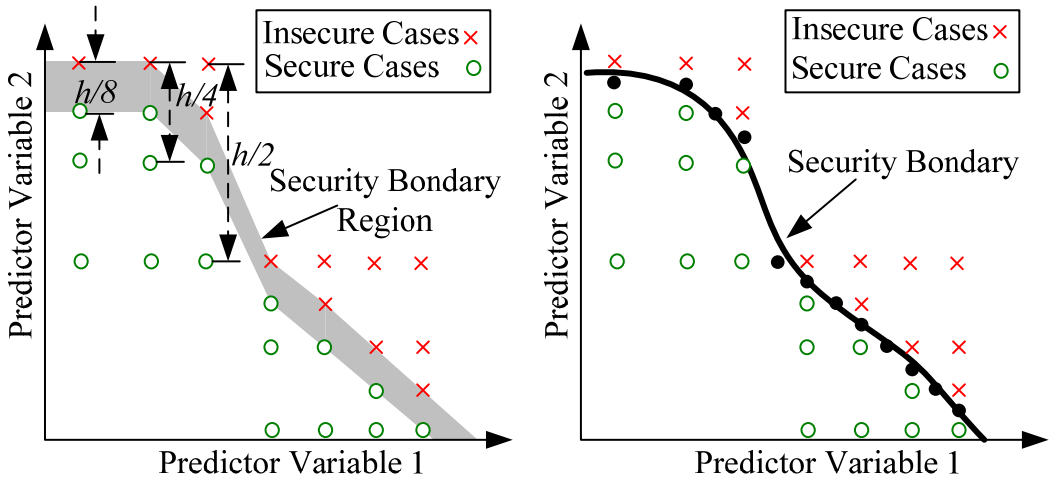

(a) Bisection method (b) Curve fitting of security boundary

Fig. 7.2 Prediction of the security boundary.

Through this approach, the security boundary is traced in a multi-dimensional space of involved influencing factors. For example, CPPs which have relatively more flexible controllability can be used to compensate the uncertainties of wind power generation and other DG. During the search of security boundary in the space of CPP generation, wind generation and DG generation, other fixed important factors such as load and international power exchange should be maintained at their scheduled values.

However, it is important to mention that consideration of all possible generation uncertainties would result in a huge database. Given that the security boundary lies in the rare probability region, a database containing the sampling OCs within this rare probability region conveys more information, as the cases closer to the security boundary affect the process of making splitting rules much more than the cases away from the security boundary. So importance sampling is adopted to select the cases containing more information by revising the sampling distribution function *f(d)* towards the security boundary, so as to reduce the computation cost.

The Gaussian distribution $N(0,\sigma^2)$ with probability function *f(d)* is adopted to sample the OCs, as defined in (7.2),

$$f(d) = \frac{1}{\sigma\sqrt{2\pi}} e^{-\frac{d^2}{2\sigma^2}} \tag{7.2}$$

where *d* is the 2-norm distance from the sampled OC point *x* to the security boundary *y*, as defined in (7.3).

$$d = \left(\sum_{i=1}^{n} |x_i - y_i|^2 \right)^{1/2} \tag{7.3}$$

As shown in Fig. 7.3, the sampling OCs in the space of involved factors subject to Gaussian distribution. The cases close to the security boundary have higher probability to be selected for database than that away from the boundary. So a number of OCs are selected and biased to the interested region adjacent to the security boundary. The parameter σ, the standard deviation of the samplings, controls the degree of convergence to the security boundary.

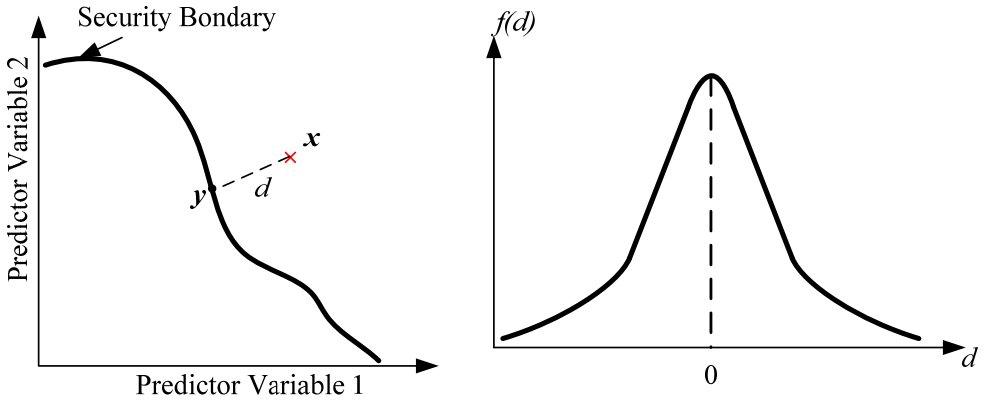

(a) 2-norm distance to the boundary (b) Probability density function

Fig. 7.3 Probability function of sampling OCs.

As illustrated in Fig. 7.4, on a comparison between two sampling methods, the number of cases given by importance sampling is significantly reduced but they still

contain the critical information to differentiate insecure cases from secure ones, assuming that the splitting of databases created by normal sampling (NS) and that created by importance sampling (IS) have the same boundary, i.e. the equally accurate results. However, the DT with IS usually suggests a lower value of accuracy due to two main reasons: *i)*, a number of secure and insecure cases by IS overlap each other in the interested region, which makes clear splits more difficult; *ii)*, a large number of apparent secure or insecure cases from NS outside the interested region, have minor effect on the final splits but are counted in the denominator of the accuracy ratio. A detailed analysis on the accuracies due to NS and IS is given in Appendix B.

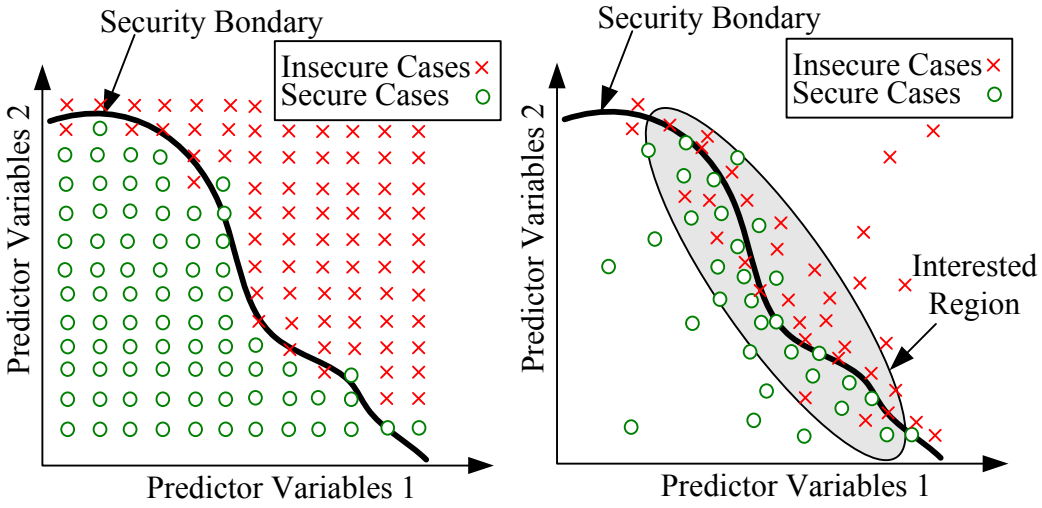

(a) Normal sampling (b) Importance sampling

Fig. 7.4 Selection of operating conditions.

7.4 Preventive Control Scheme

When a power system at a given OC is detected to be vulnerable to a specific credible contingency, the operators are supposed to take preventive actions to ensure its security in post contingency condition. Generation rescheduling which involves shifting generation among centralized generators so as to restore the system from insecure state to secure state is usually adopted by operators.

For each OC among N_{OC} initially obtained OCs from importance sampling, detailed T-D simulations for all the critical contingencies are executed. Specific security criteria such as transient instability, transient voltage dip, insufficient damping on T-D simulation results are examined to determine the security classification for each case. In this research, two DTs are trained for each contingency. One is for observation of insecure condition called as the observation DT (ODT) and the other is for prevention

of insecure conditions called as prevention DT (PDT). The security boundary in the space of measurements is specified by the ODTs, while the PDTs provide the direction of generation shift when the system is identified as an insecure state.

7.4.1 Observation Decision Tree (ODT)

In a database of N_{OC} cases, each case includes a vector of measurements to present an OC before the disturbance which serves as predictors and the results of T-D simulations after the disturbance (Secure or Insecure) which serve as the target for aforementioned predictors. For each OC, synchronized data from PMU measurements, including voltage, current and power are able to provide accurate predictor values. In addition, predictors also can be selected from SCADA system, if the values do not change frequently.

ODT is used to detect the current security state by providing accurate thresholds of security boundary and calculating out the security margins of current OC. Since the ODT is trained from all measurable values as predictors, the data mining algorithm is able to seek out the accurate boundary in the space of dominant observable values. In other words, ODT is the subspace of the most dominant measurements before the disturbance that is able to accurately predict the post-disturbance security condition.

7.4.2 Prevention Decision Tree (PDT)

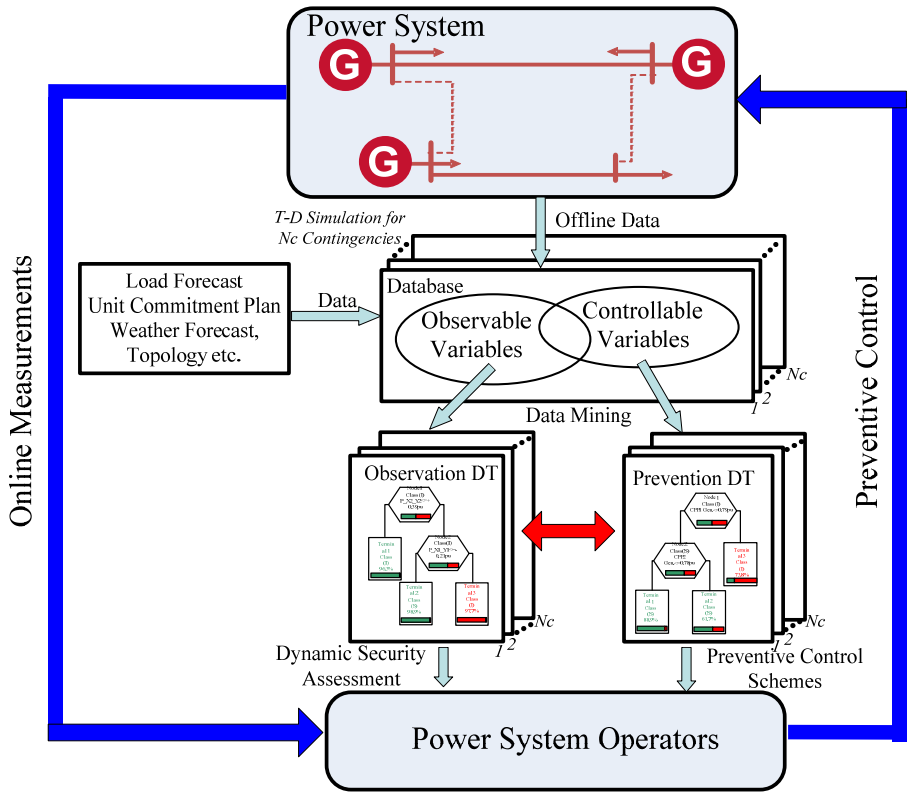

Fig. 7.5 Systematic approach for DSA and preventive control scheme.

PDT is the decision tree which selects only the controllable variables as predictors from measurements, e.g. outputs of generators, power exchange across HVDC links. Although PDT has lower accuracy than ODT due to the fewer number of predicting values, it is capable of searching out the most effective controllable variables among all the measurable control parameters and providing the potential direction of control to draw the system back to a secure state.

As shown in Fig. 7.5, this systematic approach offline trains two paralleled DTs for each critical contingency based on 24-hour horizon system prediction data, such as load forecast, weather forecast, unit commitment-based generation plan, network topology as well as the unavailability of system elements due to scheduled maintenance, etc.. Fed with online measurements, ODT is employed for online DSA to identify the margins of predictors against their thresholds determined from DT training. If any online measurements of predictors violate the thresholds, ODT would provide situational awareness on insecurity if that contingency really happens. At the same time, PDT would provide system operators with preventive control schemes to drive the state to a new OC without insecurity under that contingency. Therefore, the parallel and cooperative utilization of PDT and ODT in the control schemes provides both the situational awareness and the preventive control against critical contingencies.

7.4.3 Control Strategy Based on ODT and PDT

As illustrated in Fig. 7.6, two 2-dimensional (2-D) nomograms in Fig. 7.6 (c) and in Fig. 7.6(d) are adopted to represent the secure operating regions determined by ODT in Fig. 7.6(a) and the PDT in Fig 7.6(b) from the predictors and their thresholds, respectively. The percentages in both DTs are given as an example, in which the percentages of accuracy in the ODT are normally higher than that in PDT. When the current OC "*O*" is in the insecure region shown in Fig. 7.6(c), the direction of preventive control can be easily found in Fig. 7.6(d), i.e. to reduce generation in CPP*2*. Moreover, the variation in generators' outputs will definitely lead to the variation of the power flows in transmission lines, so the trajectory in PDT nomogram has its corresponding projection in ODT nomogram, for example the dashed lines in both Fig. 7.6(c) and Fig. 7.6(d).

Additionally, many constraints on OCs should still apply. For example, in order to maintain the international power exchange invariant, the sum of generation from involved CPP, CHP generation and wind power generation minus network loss and total load consumption must maintain as their scheduled value, as defined by (7.4).

$$\sum_{i=1}^{n} Gr_i + \sum_{j=1}^{p} Dr_j + \sum_{k=1}^{m} Wr_k - Pr_{loss} - Pr_{load} == \sum_{i=1}^{n} Gs_i + \sum_{j=1}^{p} Ds_j + \sum_{k=1}^{m} Ws_k - Ps_{loss} - Ps_{load} \quad (7.4)$$

where n, p and m are the total number of involved CPP generators, CHP generators and wind power plants respectively. Gr, Dr, Wr, Gs, Ds and Ws are real-time values and scheduled values of CPP generation, CHP generation and wind power generation in each generation unit respectively.

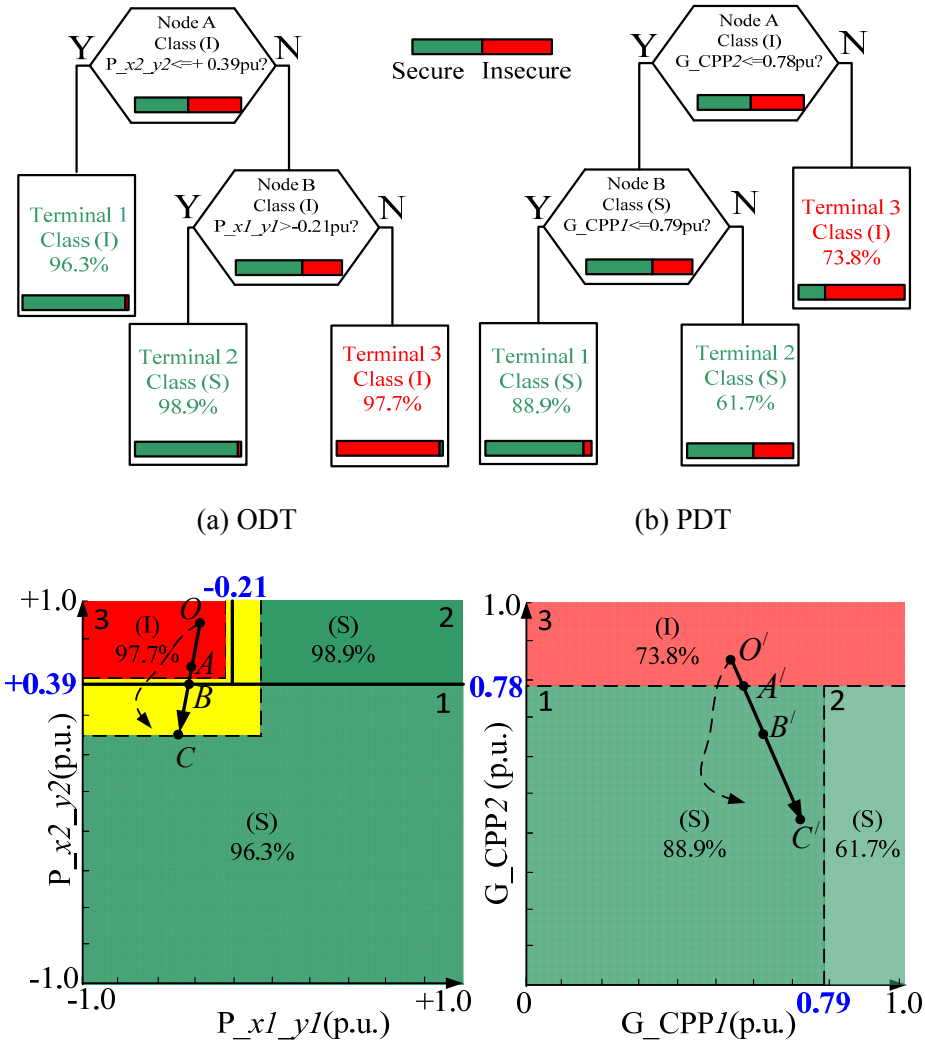

Fig. 7.6 Illustrations of observation DT and prevention DT.

Thus, the process-cum-direction of preventive control can be represented by the trajectory shown in Fig. 7.6(d) by the solid line in PDT nomogram. "*O*" and "*O'*" are the original insecure OC. "*A*" and "*A'*"represent the OC on the threshold of PDT, while "*B*" and "*B'*" represent the OC on the threshold of ODT. The thresholds in ODT are more accurate than the thresholds in PDT, so the regions below "*B*" and "*B'*" can be deemed as secure regions.

The block diagram shown in Fig. 7.7 describes more clearly the detailed procedure of how ODT and PDT work in tandem to implement online DSA and preventive control scheme.

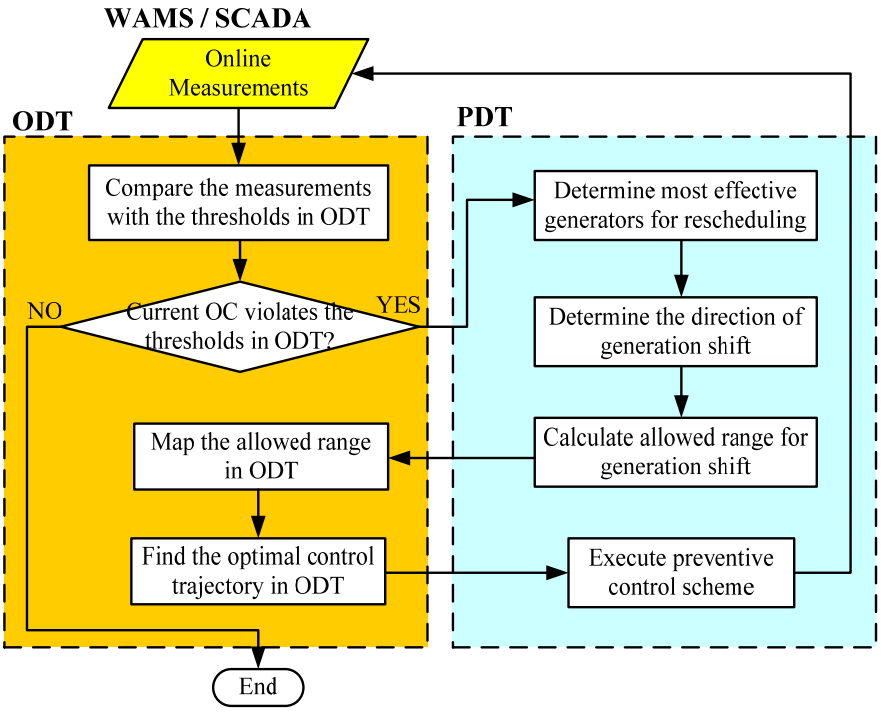

Fig. 7.7 Block diagram of cooperative scheme with ODT and PDT.

7.4.4 Prior Probability Adjustment for Higher Reliability

As mentioned in Chapter 6, prior probability is used to adjust the control guidelines over the tradeoff between dependability and security. By adjusting the ratio of prior probabilities of secure cases π_s and insecure cases π_i from 0.5/0.5 to 0.99/0.01, one can find the security boundary in 2-D ODT nomogram with higher security. Conversely, by adjusting the ratio π_s/π_i from 0.5/0.5 to 0.01/0.99, the security boundary with higher dependability can be found in 2-D ODT nomogram. The patch between these two boundaries is the fuzzy region, shown in yellow in Fig. 7.6(c). The regions below "*C*" and "*C'* " stand for the regions with high security in which the probability of exception (i.e. insecure case) is below 0.01.

Therefore, by monitoring the OC in ODT nomogram, the operators are informed of the exact amount of generation rescheduling that should be adopted.

7.4.5 Optimization of Preventive Control

As mentioned earlier, PDT and ODT are able to provide operators with the allowed range of generation rescheduling. Then the optimal control trajectory is searched out by minimizing the total economic cost due to generation rescheduling, as $f(x,\lambda,\mu)$

defined in (7.5). A security constrained optimal power flow (OPF) problem can be defined as

$$\text{min. } f(x,\lambda,\mu) = c(x,\lambda) + p(x,\mu) \tag{7.5}$$

$$\text{st. } g(x,\lambda,\mu) = 0 \text{ and } h(x,\lambda,\mu) \le 0 \tag{7.6}$$

$$\text{st. } \lambda \in \mathcal{R} \text{ and } \mu \notin \mathcal{R} \tag{7.7}$$

where x represents the variables in power flow, λ and μ are control variables, e.g. generation outputs of CPPs involved in preventive control. $\mathcal{R}$ in (7.7) is a set representing the allowed range of generation rescheduling to maintain international power exchange invariant. Two items on right side of (7.5) are respectively the cost of generation rescheduling and the penalty on violation of scheduled international power exchange, (7.6) gives equality constraints i.e. power flow equations and inequality constraints representing operational constraints, i.e. security criteria.

7.5 Summary

This chapter proposes a importance sampling based methodology to prepare the database efficiently for hourly online OC and presents a DSA method based on contingency-oriented DTs with high accuracy. Then an online systematic preventive control scheme based on cooperative application of parallel DTs, i.e. ODT and PDT, is proposed. Moreover, the optimization of preventive control trajectory with consideration of domestic generation rescheduling cost and international penalty is conducted. The scheme will be demonstrated on the operational model of western Danish power system in the Chapter 9.

The main content of this chapter has also been reported in the author's previous publications in [J1], [C6] and [C11].

References

[1] V. Madani, D. Novosel, S. Horowitz *et al.*, "IEEE PSRC report on global industry experiences with system integrity protection schemes (SIPS)," *IEEE Trans. Power Syst.*, vol. 25, no. 4, pp. 2143-2155, Oct. 2010.

[2] Q. Zhou, J. Davidson, and A. A. Fouad, "Application of artificial neural networks in power system security and vulnearability assessment," *IEEE Trans. Power Syst.*, vol. 9, no. 1, pp. 525-532, Feb. 1994.

[3] S. Kalyani, and K. S. Swarup, "Classification and assessment of power system security using multiclass SVM," *IEEE Trans. Systems, Mans, and Cybernetics,* vol. 41, no. 5, pp. 753-758, Sep. 2011.

[4] K. Sun, S. Likhate, V. Vittal *et al.*, "An online dynamic security assessment scheme using phasor measurement and decision trees," *IEEE Trans. Power Syst.*, vol. 22, no. 4, pp. 1935-1943, Nov. 2007.

[5] V. Krishnan, J. D. McCalley, S. Henry *et al*., "Efficient database generation for decision trees based power system security assessment," *IEEE Trans. Power Syst.*, vol. 26, no. 4, pp. 2319-2327, Nov. 2011.

[6] R. Diao, K. Sun, and V. Vittal *et al*., "Decision tree-based online voltage security assessment using PMU measurements," *IEEE Trans. Power Syst.*, vol. 24, no. 2, pp. 832-839, May 2009.

[7] E. E. Bernabeu, J. S. Thorp, and V. Centeno, "Methodology for a security/dependability adaptive protection scheme based on data mining," *IEEE Trans. Power Del.*, vol. 27, no. 1, pp. 104-111, Jan. 2012.

[8] N. Senroy, G. Heydt, V. Vittal *et al*., "Decision tree assisted controlled islanding," *IEEE Trans. Power Syst.*, vol. 21, no. 4, pp. 1790-1797, Nov. 2006.

[9] R. Diao, V. Vittal, K. Sun, *et al*, "Decision tree assisted controlled islanding for preventing cascading events," *IEEE PES Power Systems Conference & Exposition*, Seattle, WA, USA, Mar. 2009.

[10] E. M. Voumvoulakis, A. E. Gavoyiannis, and N. D. Hatziargyriou, "Decision trees for dynamic security assessment and load shedding scheme," in *Proc. of PES General Meeting*, Montreal, QC, Canada, Jun. 2006.

[11] K. Mei, and S. M. Rovnyak, "Response-based decision trees to trigger one-shot stabilizing control," *IEEE Trans. Power Syst.,* vol. 19, no. 1, pp. 531–537, Feb. 2004.

[12] Y. Hou, C. C. Liu, K. Sun *et al*., "Computation of milestones for decision support during system restoration," *IEEE Trans. Power Syst.*, vol. 26, no. 3, pp. 1399-1409, Aug. 2011.

[13] K. A. Papadogiannis and N. D. Hatziargyriou, "Optimal allocation of primary reserve services in energy markets," *IEEE Trans. Power Syst.*, vol. 19, no. 1, pp. 652-659, Feb. 2004.

[14] I. Genc, R. Diao, and V. Vittal, "Computation of transient stability related security regions and generation rescheduling based on decision trees," in *Proc. of PES General Meeting*, Minneapolis, MN, USA, Jul. 2010.

[15] I. Genc, R. Diao, V. Vittal *et al.*, "Decision tree-based preventive and corrective control applications for dynamic security enhancement in power systems," *IEEE Trans. Power Syst.*, vol. 25, no. 3, pp. 1611-1619, Aug. 2010.

[16] R. Diao, V. Vittal, and N. Logic, "Design of a real-time security assessment tool for situational awareness enhancement in modern power systems," *IEEE Trans. Power Syst.*, vol. 25, no. 2, pp. 957-965, May 2010.

[17] I. Kamwa, S. R. Samantaray, and G. Joos, "Development of rule-based classifier for rapid security assessment of wide-area post disturbance records," *IEEE Trans. Power Syst.*, vol. 24, no. 1, pp. 258-270, Feb. 2009.

[18] L. Breiman, J. Friedman, R. A. Olshen, and C. J. Stone, *Classification and Regression Trees*. Belmont, CA, Wadsworth, 1984.

[19] E. A. Unger, L. Harn, and V. Kumar, "Entropy as a measure of database information," in *Proc. of the 6th Annu. Computer Security Applications Conf.*, pp. 80-87, Tucsion, AZ, USA, Dec. 1990.

Chapter 8

Online Dynamic Security Assessment Based on Random Forest

8.1 Introduction

The blackout of 1965 in Northeast America started a major focus on the security and reliability of interconnected power systems. Later, especially in the year of 2003, several large blackouts occurred in US [1], Italy [2], Southern Sweden and Denmark [3], forcing power system analysts and researchers to attach more and more importance to the issue of power system security assessment.

Power system stability is defined by IEEE/CIGRE Joint Task Force on Stability Terms and Definitions as the ability of an electric power system, for a given initial operating condition (OC), to regain a state of operating equilibrium after being subjected to a physical disturbance, with most system variable bounded so that practically the entire system remains intact. Power system security refers to the degree of risk in its ability to survive imminent disturbance without interruption of customer service, which relates to the robustness of systems to a large disturbance (contingency) with respect to a certain security criterion [4]. More specifically, contingency is the large disturbance which results in the change of system topology by relay operations designed to protect the system by isolating the faulted area or preventing the abnormal condition [5].

Mathematical analysis of the response and new equilibrium is called security assessment. Basically, security assessment is called static security assessment (SSA) if it only evaluates the expected post-disturbance equilibrium steady-state condition, while it is dynamic security assessment (DSA) if it evaluates the transient response of the system after the disturbance.

This chapter surveys the methods of DSA in Section 8.2. Section 8.3 introduces the fundamental knowledge of Random Forest (RF). In Section 8.4, a methodology that uses RF for online DSA is proposed, which is capable of not only predicting the security states of new OC with high accuracy, but also informing the adaptability of the RF model by Outlier Index (OI). Summary of this approach is given in Section 8.5. The performance of the approach will be demonstrated on a 400-bus, 200-line operational model of the western Danish power system in Chapter 9.

8.2 Methods of Dynamic Security Assessment

DSA is defined by IEEE Power & Energy Society (PES), working group on DSA as an evaluation of the ability of a certain power system to withstand a defined set of contingencies and to survive the transition to an acceptable steady-state condition [6].

Most DSA programs focus on two criteria: 1) short-term voltage security 2) rotor angle stability. The criterion of short-term voltage security is to regulate that the transient voltage profile after the disturbance must remain in the acceptable limits to prevent further damage or loss of element. The criterion of rotor angle stability refers to maintain the synchronization of all synchronous generators in transmission power system.

Generally, there are two methods of DSA, i.e. offline DSA and online DSA. Offline DSA performs detailed time-domain (T-D) simulations for all credible contingencies and a variety of OCs, so as to determine the security thresholds of generation and load as well as the limits of power transfer across important system interfaces. These thresholds and limits are then added with a margin and used as security operation ….guidelines for power system operators. Since the simulations are performed offline, there is no severe restriction on computation burden or simulation time, but it is difficult to make sure that the current online OCs do not have significant difference with the simulated OCs. In other word, even though a large number of simulations are conducted for typical OCs and different contingencies, it is impossible to cover all OCs in power system operation.

Online DSA is able to be updated with current OC to supplement offline DSA for higher reliability. It involves rapid screening process to rank and select the most critical contingencies and intelligent filtering of OCs that should be simulated to update the result of offline DSA [7]-[14]. Then only limited numbers of traditional T-D simulations are carried out to explore the rotor angle swing curves and voltage trajectories. Finally, the guidelines of offline DSA are updated dynamically with precise prediction of security in case of credible contingencies. An overview of methods of DSA is provided below.

8.2.1 Detailed T-D Simulations

Detailed T-D simulation is based on the numerical computation of differential algebraic equations (DAE). Differential equations in (8.1) are used to describe the dynamics of the system model and algebraic equations in (8.2) are applied to represent the network topology and network parameters. Numerical integration algorithms, such as Runge-Kutta methods and trapezoidal methods, are used to solve

the set of first-order differential equations. Theoretically, most elements and control mechanisms can be appropriately modeled for T-D simulation, so this approach can simulate the details of the system and it is the fundamental approach commonly applied in DSA. However, it is generally too computationally intensive for online DSA.

$$\dot{x}(t) = f\left(x(t), y(t), t\right), \tag{8.1}$$

$$0 = g\left(x(t), y(t), t\right). \tag{8.2}$$

where $x(t) \in \boldsymbol{R}^n$ and $y(t) \in \boldsymbol{R}^m$. represent state variables and algebraic variables, respectively.

8.2.2 Direct Methods

Direct methods are adopted to replace the T-D simulation by the evaluation of transient energy function (TEF), also named as Lyapunov energy function. The idea of this approach is based on the assumption that surplus electromagnetic energy after the disturbance will be transformed to mechanic energy to accelerate the speed of generators but the total TEF remains invariant. The value of carefully designed TEF V is calculated at the instant of the last switching in the system and compared with a predetermined critical value V_{cr}. If $V<V_{cr}$, the system is predicted to be stable, and if $V>V_{cr}$, the system is predicted to be instable. Hence, this method can quickly predict the rotor-angle stability of the system at the first instant after the disturbance. Nevertheless, currently there are still drawbacks and unsolved problems of this approach. The complexity of TEF is highly dependent on the scale of the power systems. Moreover, although there are several simplified models to represent the power system, such as B-H model [15], N-M model [16] and T-V-A model [17], it is still difficult to construct an appropriate form of TEF to reflect the internal characteristics of the dynamic system. Besides, this approach is only suitable for rotor-angle stability, but helpless for other security issues, e.g. voltage security.

8.2.3 Pattern Recognition Methods

Pattern recognition methods are used to establish the relationship between the system features and the security state or the security margin relative to the security boundary of the system [18]. Generally, a database is necessary for pattern recognition methods which contains the system features (before the disturbance or system collapse) and the real consequence (i.e. secure/insecure, stable/instable). Then machine learning algorithms such as artificial neural networks (ANN) [19]-[21], fuzzy techniques [22]-[24], support vector machine (SVM) [25] and decision tree (DT) [26] are used to train a model to explore the hidden pattern of the relationship. Then the

model can be used to predict the system security and stability before the real consequences. The advantage of this method is that it can reflect the actual operation of power systems with affordable computation burden. The drawback of this approach is that it is difficult to achieve high accurate prediction of system security and stability for industrial application (i.e. 99.97%).

8.2.4 Probabilistic Methods

In probabilistic methods, DSA is viewed as a probabilistic problem rather than a deterministic one. This approach attempts to find out the probabilistic distribution of power system security and stability in terms of disturbance factors such as fault type, fault location, clearing time and operating factors such as load and generation [27]-[30]. The advantage of this approach is that it is able to consider a lot of influencing factors. The obvious drawback is that the computation burden is high, so it is only suitable for offline DSA. However, combined with pattern recognition method, it may be of great value for online DSA.

8.2.5 Real-time or Faster Than Real Time Simulation Methods

Real time simulation is based on a numerical model of power system that can execute the simulation at the same rate as the actual clock. Generally, it involves the techniques of task dispatch and parallel computation on multiple CPUs, such as Real Time Digital Simulator (RTDS) [31], or field-programmable gate-array (FPGA) chips, such as OPAL-RT [32]. In addition, the simulation model and algorithms can be optimized to achieve simulations even faster than real time, but it is still in the research stage [33]. Since the simulation runs in real time, the power system algorithms are calculated quickly enough to continuously produce output conditions that realistically represent conditions in a real network. Besides, real time simulation provides the Hardware-In-Loop (HIL) environment that can interface numerical simulation with physical devices. However, the high cost of full-fledged paralleled computers impedes it to be used in the simulation of large power systems.

8.3 Fundamental Knowledge of Random Forest

Random Forest (RF), also called Ensemble Decision Trees (EDT), was first proposed by Tin Kam Ho *et al.* of Bell Labs in 1995 [34], and further developed by L. Breiman *et al.* in 2001 [35]. It is an ensemble learning method for classification and regression that operated by construct a number of decision trees.

8.3.1 From Decision Tree to Random Forest

As introduced in Chapter 6, decision tree is a decision support model expressed as single binary tree to predict the possible consequences of the target value by a number of "if-then rules". Random Forest, derived from DT, is composed of a multitude of de-correlated DTs such that each node of DTs depends on a sub-vector randomly selected from the full-vector predictors. Bootstrap sampling is also used in RF to assist in better estimating the distribution of the original dataset so as to enhance the accuracy. For each DT in RF, about one thirds of the cases are left out from the bootstrap sampling called out-of-bag (OOB) data which can be used as test set (TS) to give ongoing estimates of the error.

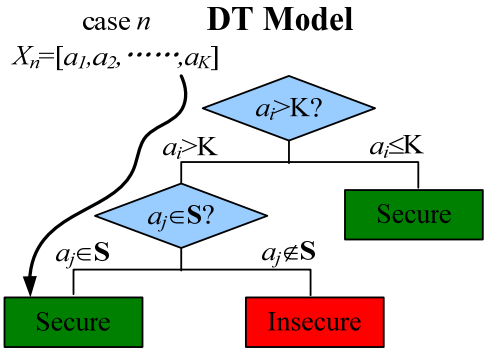

Fig. 8.1. A simple illustrative single DT.

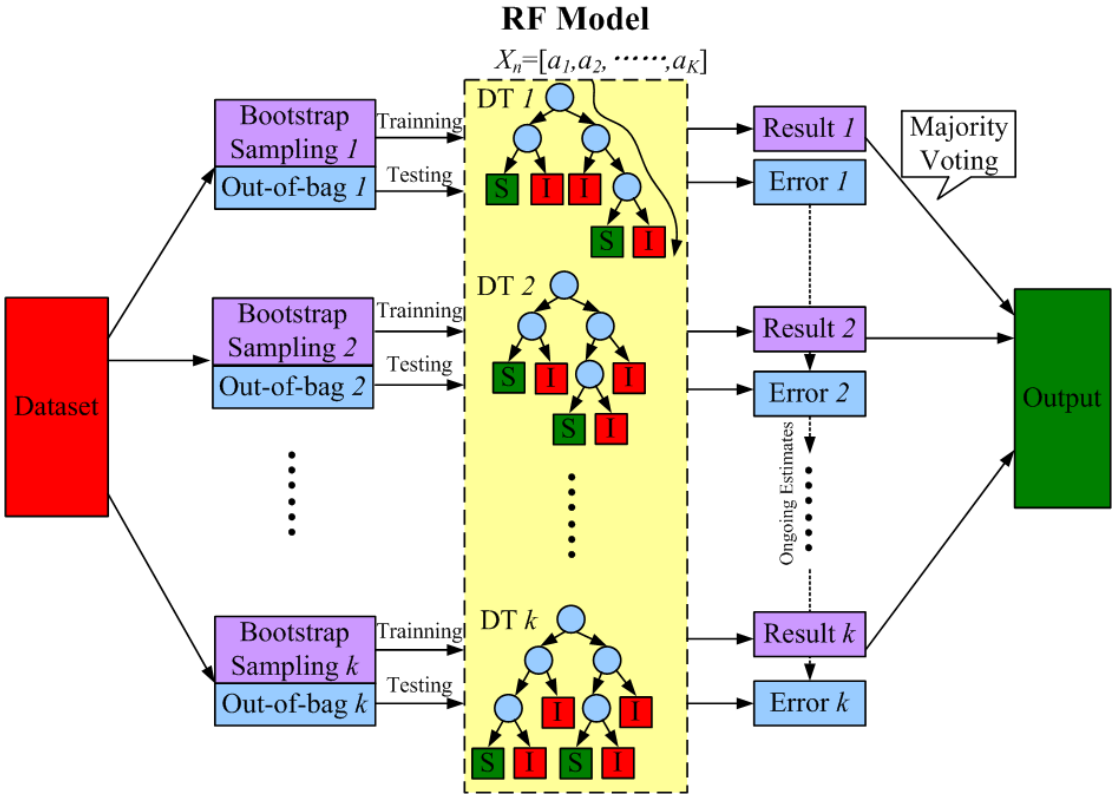

Fig. 8.2. Structure of random forest.

Given a case represented by a set of predictors (i.e. $a_1, a_2, \ldots, a_k$), the output of each DT is obtained by dropping the measurement of the cases downward from the root node to the terminal node of DT. As shown in Fig. 8.1, K is the splitting threshold of the numerical variable a_i, while **S** is a finite set of the categorical variable a_j. Different from DT, the classification output of RF model is the majority voting result (largest fraction) from a large number of DTs. Although each DT is unpruned and over-fitted, the overall RF model can benefit from aggregated-base variance reduction. The structure of RF is shown in Fig. 8.2. Details of RF algorithm can be found in [36].

Assuming we have a database containing N cases, each case is represented by a number of M predictors $x_n=\{a_1,a_2,\ldots,a_M\}$ representing the measurements for a particular operating condition (OC) of case n and a target $C_n = \{S \text{ or } I\}$ stands for the secure or insecure state for case n which is obtained by T-D simulations, the basic idea for RF growing is that for each node in the kth tree ($k \le N_{tree}$, N_{tree} is the number of trees in the RF), the random sub-vector Θ_j is selected, independent of the past random vector $\Theta_1, \Theta_2, \ldots, \Theta_{j-1}$ but with the same distribution; and a tree is grown using the training set $\boldsymbol{X}$ and $\boldsymbol{\Theta}=\{\Theta_1, \Theta_2, \ldots, \Theta_j, \ldots,\}$ resulting in a number of classifiers $h_k(\boldsymbol{X},\boldsymbol{\Theta})$. Therefore, a RF is a classifier consisting of a collection of tree-structured classifiers $C^k_{DT}=\{h_k(\boldsymbol{X},\boldsymbol{\Theta_k}), k = 1, \ldots, N_{tree}\}$ and each tree casts a unit vote for the most popular class at input x_n, defined in (8.3)

$$\hat{C}_{RF}^{N_{tree}}(x_n) = \text{majority voting}\left\{\hat{C}_{DT}^{k}(x_n), k = 1,2,\cdots\cdots, N_{tree}, x_n \in \mathbf{X}\right\} \tag{8.3}$$

where $\hat{C}_{DT}^{k}(x_n)$ is the prediction of the classification of the kth DT in the RF.

8.3.2 Margins

Margin is a measure used to evaluate the confidence of a case or distance to the classification boundary with respect to the RF model. Margin of a case x_n measures the extent to which the average proportion of votes by $\hat{C}_{RF}^{N_{tree}}(x_n)$ for the true class C_n exceeds the average proportion of false votes for any other classes. As defined in (8.4), margin of a case is the proportion of votes for true class minus the maximum proportion of votes of the remaining false classes. Hence, the larger the margin for case x_n implies the higher of confidence of the classification by RF model.

$$\hat{\mathrm{M}}_{\mathrm{RF}}^{\mathrm{N_{tree}}}(x_n, C_n) = \underset{k}{avg}\left(\hat{C}_{DT}^{k}(x_n) = C_n\right) - \max\left(\underset{k}{avg}\left(\hat{C}_{DT}^{k}(x_n) \neq C_n\right)\right) \tag{8.4}$$

Therefore the strength of classifiers in RF can be defined as the average margin of all cases in the dataset, as expressed in (8.5).

$$\mathrm{S}_{\mathrm{RF}}^{\mathrm{N_{tree}}} = \frac{1}{N}\sum_{n=1}^{N} \hat{\mathrm{M}}_{\mathrm{RF}}^{\mathrm{N_{tree}}}(x_n, C_n) \tag{8.5}$$

8.3.3 Variable Importance

Compared with single DT in CART, the ensemble of DTs in RF has the advantage that it gives each variable the chance to appear in the different context with different covariates, so as to better reflect its potentially effect on the response. The importance of variables in RF model is computed to assess the contribution of each variable to grow the RF model and the relevance of each variable over all DTs in the RF.

There are basically two approaches to measure the relative importance of the *m*th variables $VI(a_m)$ in the prediction vector $X_n=\{a_1,a_2,\ldots,a_m,\ldots,a_M\}$. The traditional approach is used by default in CART for a single DT, which is calculated by aggregating the improvement indices, such as the indices expressed in equations (6.5) and (6.6) of splitting variable and the surrogate variables for every node and sort the result downwards. Then, the relative value of variable importance is calculated by scaling these improvement indices such that the largest value is 100% [35].

Although the traditional approach is intrinsic, it is subjected to the over-fitting issues in RF. So the novel approach is used to assess the importance of the *m*th variable $VI(a_m)$, as defined in (8.6):

a) Assume we already know the OOB performance P_0 of a given RF model;

b) Randomly permute all values of variable *m*;

c) Score the data and compute the new OOB performance P_m;

d) Compute the performance drop P_0-P_m;

e) Sort and scale the performance drop.

$$VI(a_m) = P_0 - P_m = \frac{1}{N_{OOB}}\sum_{n=1}^{N_{OOB}}\left\{P_{S_{OOB}}\left(x_n, T_k\left(\mathbf{X},\boldsymbol{\Theta}_k\right)\right) - P_{S_{OOB}}\left(x_n, T_k\left(\mathbf{X}_{\psi_m},\boldsymbol{\Theta}_k\right)\right)\right\} \tag{8.6}$$

where N_{OOB} is the number of cases in OOB and $P_{SOOB}(x_n,T_k)$ is the one-zero function for testing the *n*th case of OOB in RF model, as defined in (8.7)

$$P_{S_{OOB}}\left(x_n, T_k\left(\mathbf{X},\boldsymbol{\Theta}_k\right)\right) = \begin{cases} 1 & \hat{C}_{RF}^{N_{tree}}(x_n) = C_n \\ 0 & \hat{C}_{RF}^{N_{tree}}(x_n) \neq C_n \end{cases} \quad \forall x_n \in S_{OOB,k}. \tag{8.7}$$

where $\boldsymbol{X}$ and $\boldsymbol{X}_{\psi m}$ in (8.6) are predictor vectors of LS before and after permutation of the *m*th variable a_m, as defined in (8.8) and (8.9), respectively

$$\mathbf{X} = \{a_1, \cdots, a_{m-1}, a_m, a_{m+1}, \cdots, a_M\} \tag{8.8}$$

$$\mathbf{X}_{\psi_m} = \{a_1, \cdots, a_{m-1}, \psi(a_m), a_{m+1}, \cdots, a_M\}. \tag{8.9}$$

8.3.4 Proximities and Outliers

Proximity matrix ***Prox*** is introduced by RF to evaluate the Euclidean distance between every two cases in the spaces of observations. The proximity between case *i* and case *j* in the database is the number of times that they occur in the same terminal node of trees, then these counts are normalized by dividing the total number of trees N_{tree}, as defined in (8.10).

$$\mathbf{Prox}(i,j)=\frac{1}{N_{tree}}\sum_{n=1}^{N_{tree}}\left\{C_{i,j}\left(T_k\left(\mathbf{X},\mathbf{\Theta}_k\right)\right)\right\}\in[0,1] \tag{8.10}$$

where $C_{i,j}(T_k)$ is the one-zero function for counting the times that x_i and x_j going to the same terminal node, as defined in (8.11).

$$C_{i,j}\left(T_k\left(\mathbf{X},\mathbf{\Theta}_k\right)\right)=\begin{cases}1 & \text{if } x_i, x_j \text{ in the same terminal node of } T_{\mathrm{k}}\\ 0 & else\end{cases} \tag{8.11}$$

The diagonal elements in the proximity matrix are 1.0 which are self-proximities. Cases that are alike will have proximity close to 1.0; while dissimilar will have proximities close to 0.0.

Outliers are able to be detected as cases having small proximities to all other cases belonging to the same target class. The outlier index (OI) of case *i* is calculated by Average Euclidean Distance (AED) of case *i* to all the cases existed in the database, as defined in (8.12), in which N_k is the number of cases that the classification is the same with case *i*.

$$OI(i)=1\Big/\sum_{k=1}^{N_k}\left(\mathbf{Prox}(i,k)\right)^2,\forall C_k=C_i \tag{8.12}$$

8.4 Random Forest Based Online DSA

The flowchart of the proposed RF-based online DSA is shown in Fig. 8.3. The proposed approach is executed in the following stages.

8.4.1 Stage I: Offline Random Forest Building

The original database is prepared offline by detailed T-D simulations of *Nc*×*Noc* cases for *Nc* critical contingencies and *Noc* OCs based on 24-hour horizon forecasted data of the system, such as load forecast, wind forecast, unit-commitment-based generation plan, network topology as well as the unavailability of system elements

due to scheduled maintenance, etc. Then, the original contingency-oriented RF model is trained based on the prepared database.

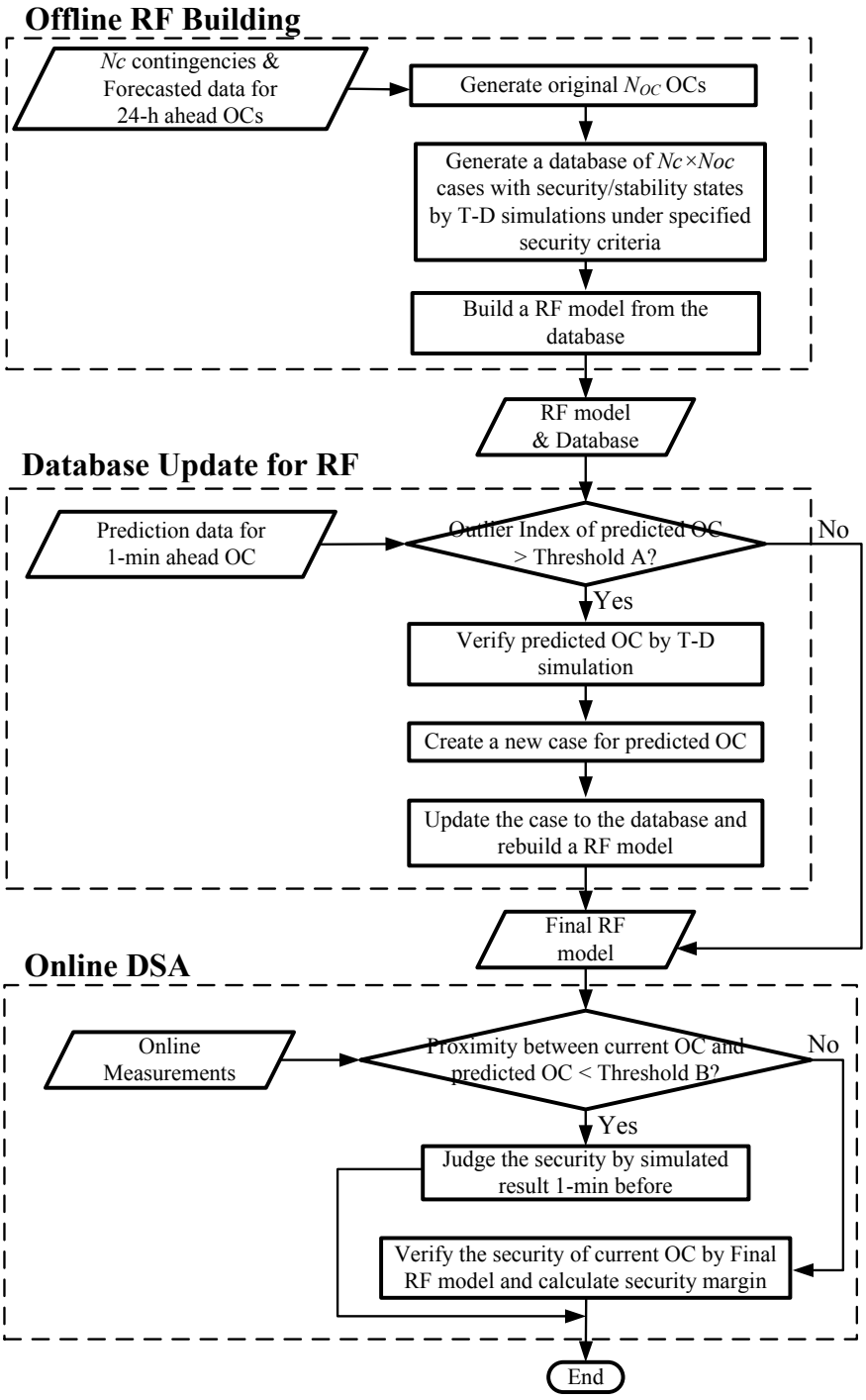

Fig. 8.3 Flowchart of RF-based online DSA.

8.4.2 Stage II: Database Update for Random Forest

System OC of 1 minute ahead can be predicted with much higher accuracy by short-term power flow prediction algorithms, such as short-term load forecast and short-term wind forecast, etc. Then Outlier Index of 1-min ahead OC is calculated

according to (8.12) to evaluate the Average Euclidean Distance of the predicted OC to all the cases already existed in the database. Given a threshold of OI, the predicted OC with OI larger than the specified threshold will be filtered out as unsure case for immediate verification by T-D simulation. Then the original database will be updated by the new case of predicted OC together with the existed cases. Finally, an upgraded RF model will be built straightaway with strengthened information of the updated database.

8.4.3 Stage III: Online Dynamic Security Assessment

Fed by online measurement from WAMS and SCADA system, the proximity between current OC and predicted OC is calculated by (8.10). If the proximity is smaller than the specified proximity threshold, which implies that the current OC matches the predicted OC, then the security of the current OC is decided by detailed T-D simulation conducted 1-min before. If the proximity is larger than the specified proximity threshold, the security of the current OC is judged by final RF model built in Stage II and security margin for current OC is calculated by the equation in (8.4).

8.5 Summary

This chapter gives an overview of dynamic security assessment methods. Among those methodologies, pattern recognition methods combined with probabilistic and statistic concepts are of great value. An approach of online DSA based on RF is proposed which can not only provide a RF model to predict of power system security with high accuracy, but also indicate the degree of dependence of the created model. Based on the calculation of outlier index and proximity, the database can be periodically updated and strengthened with new OCs, and the misclassified cases are filtered out as unsure cases for further verification 1 minute in advance. Performance of the approach will be demonstrated on western Danish power system in Chapter 9.

The main content of this chapter has also been reported in the author's previous publication in [C7].

References

[1] U.S.-Canada Power System Outage Task Force, Final Report on the August 14, 2003 Blackout in the United States and Canada: Causes and Recommendations, Apr. 2004.

[2] UCTE Investigation Committee, Final Report of the Investigation Committee on the 28 September 2003 Blackout in Italy, Apr. 2004.

[3] Elkraft System, Power failure in Eastern Denmark and Southern Sweden on 23 September 2003 Final Report on the Course of Events, Nov. 2003.

[4] P. Kundur, J. Paserba, V. Ajjarapu *et al.*, "Definition and classificaiton of power system stability," *IEEE Trans. Power Syst.*, vol. 19, no. 2, pp. 1387-1401, May 2004.

[5] P. W. Sauer, K. L. Tomsovic, and V. Vittal, "Dynamic security assessment," in *Power System Stability and Control,* 2nd ed, CRC Press, Boca Raton, FL, USA, 1985, ch. 15.

[6] Working group on Dynamic Security Assessment, PES Committee, "Dynamic security assessment practices in North America," *IEEE Trans. Power Syst.*, vol. 3, no. 3, pp. 1310-1321, Aug. 1998.

[7] V. Chadalavada, V. Vittal, G. C. Ejebe *et al.*, "An on-line contingency filtering scheme for dynamic security assessment," *IEEE Trans. Power Syst.*, vol. 12, no. 1, pp. 153-161, Feb. 1997.

[8] M. A. Pai, *Energy Function Analysis for Power System Stability*, Kluwer, Boston, MA, 1989.

[9] A. A. Fouad and V. Vittal, *Power System Transient Stability Analysis Using the Transient Energy Function Method*, Prentice-Hall, Englewood Cliffs, NJ, 1992.

[10] M. Pavella and P. G. Murthy, *Transient Stability of Power Systems: Theory and Practice*, John Wiley, New York, 1993.

[11] E. Vaahedi, Y. Mansour, A. Y. Chang *et al.*, "Enhanced 'second kick' method for on-line dynamic security assessment," *IEEE Trans. Power Syst.*, vol. 11, no. 4, pp. 1976-1982, Nov. 1996.

[12] K. Sun, S. Likhate, V. Vittal *et al.*, "An online dynamic security assessment scheme using phasor measurement and decision trees," *IEEE Trans. Power Syst.*, vol. 22, no. 4, pp. 1935-1943, Nov. 2007.

[13] L. Wehenkel, *Automatic Learning Techniques in Power Systems*, Kluwer Academic Publishers, Boston, MA, 1998.

[14] I. Kamwa, R. Grondin, and L. Loud, "Time varying contingency screening for dynamic security assessment using intelligent-systems techniques," *IEEE Trans. Power Syst.*, vol. 16, no. 3. pp. 526-536, Aug. 2001.

[15] A. R. Bergen and D. J. Hill, "A structured preserving model for power system stability analysis," *IEEE Transaction on Power Apparatus and Systems*, vol. PAS-100, no. 1, pp. 25-35, Jan. 1981.

[16] N. Narasimhamurthi and M. T. Musavi, "A generalized energy function for transient stability analysis of power systems," *IEEE Transaction on Circuits and Systems*, vol. CAS-31, no. 7, pp. 637-645, Jul. 1984.

[17] N. A. Tsolas, A. Arapostathis and P. P. Varaiya, "A structured preserving energy function for power system transient stability analysis," *IEEE Transaction on Circuits and Systems*, vol. CAS-32, no. 10, pp. 1041-1049, Oct. 1985.

[18] C. K. Pang, F. S. Prabhakara, A. H. El-Abiad *et al.*, "Security evaluation in power systems using pattern recognition," *IEEE Transaction on Power Apparatus and Systems*, vol. PAS-93, no. 3, pp. 969-976, Jan. 1974.

[19] CIGRE TF38-06-06, "Artificial neural networks for power systems: a literature survey," *Engineering Intelligent Systems*, vol. 1, no. 3, pp. 133-158, Dec. 1993.

[20] A. D. Papalexopoulos, S. Hao, and T. M. Peng, "An implementation of a neural network based load forecasting model for the EMS," *IEEE Trans. Power Syst.*, vol. 9, no. 4, pp. 1956-1962, Nov. 1994.

[21] Q. Zhou, J. Davidson, and A. A. Fouad, "Application of artificial neural networks in power system security and vulnerability assessment," *IEEE Trans. Power Syst.*, vol. 9, no. 1, pp. 525-532, Feb. 1994.

[22] J. M. G. Alvarez and P. E. Mercado, "Online inference of the dynamic security level of power systems using fuzzy techniques," *IEEE Trans. Power Syst.*, vol. 22, no. 2, pp. 717-726, May 2007.

[23] C. G. Groom, K. W. Chan, R. W. Dunn *et al.*, "Real-time security assessment of electrical power systems," *IEEE Trans. Power Syst.*, vol. 11, no. 2, pp. 1112-1117, May 1996.

[24] I. Kamwa, S. R. Samantaray, and G. Joos, "Development of rule-based classifier for rapid security assessment of wide-area post disturbance records," *IEEE Trans. Power Syst.*, vol. 24, no. 1, pp. 258-270, Feb. 2009.

[25] S. Kalyani, and K. S. Swarup, "Classification and assessment of power system security using multiclass SVM," *IEEE Trans. Systems, Mans, and Cybernetics,* vol. 41, no. 5. pp. 753-758, Sep. 2011.

[26] L. Wehenkel Th. Van Cutsem, and M. Ribbens-Pavella, "An artificial intelligence framework for on-line transient security assessment of power systems," *IEEE Trans. Power Syst.*, vol. 4, no. 2. pp. 789-800, May 1989.

[27] A. D. Patton, "Assessment of the security of operating electric power systems using probability methods," *Procedings of IEEE*, vol. 62, no. 7, pp. 892-901, Jul. 1974.

[28] F. F. Wu and Y. K. Tsai, "Probabilistic dynamic security assessment of power systems: Part I – basic model," *IEEE Transaction on Circuits and Systems*, vol. CAS-30, no. 3, pp. 148-159, Mar. 1983.

[29] F. F. Wu, Y. K. Tsai and Y. X. Yu, "Probabilistic steady-state and dynamic security assessment," *IEEE Trans. Power Syst.*, vol. 3, no. 1, pp. 1-9, Feb. 1989.

[30] E. Chiodo, F. Gagliardi, M. La Scala *et al.*, "Probabilistic on-line transient stability analysis," *IEE Proc. Gener. Trasm. Distrib*, vol. 146, no. 2, pp. 176-180, Mar. 1999.

[31] OPAL-RT Technologies, [Online]. Available: http://www.opal-rt.com/ , assessed on 09-Aug-2013.

[32] RTDS Technologies, [Online]. http://www.rtds.com , assessed on 09-Aug-2013.

[33] M. Matar and R. Iravani, "The reconfigurable-hardware real-time faster than-real-time simulator for the analysis of electromagnetic transients in power systems," *IEEE Trans. Power Del.*, vol. 28, no. 2, pp. 619-627, Apr. 2013.

[34] T. K. Ho, "Random decision forest," in *Proc. of the 3rd Int. Conf. on Document Analysis and Recognition*, Montreal, QC, Canada, pp. 289-282, Aug. 1996

[35] L. Breiman, J. Friedman, R. A. Olshen, and C. J. Stone, *Classification and Regression Trees. Belmont*, CA, Wadsworth, 1984.

[36] L. Breiman, "Random forest," *Mach. Learn.* vol. 45, pp. 5-32, 2001, [Online]. Available: http://www.stat.berkeley.edu/users/breiman/RandomForests , assessed on 09-Aug-2013.

Chapter 9

Case Study of Online DSA and Corresponding Preventive Control in Danish Power System

9.1 Introduction

As mentioned in Chapter 3, Danish power system has a high penetration of onshore wind generation and other DG units, which are mostly integrated to the distribution system, but Danish TSO can not fully access or control these types of DG units. In addition, although the technologies of wind forecast in meteorology have significant progress in recent years, the prediction of wind generation and dispersed generation are not highly accurate, which may result in considerable mismatch between the predicted power flow and the actual power flow patterns in real time (e.g. in the case of large scale wind turbine shut down), so the online DSA and wide-area preventive control scheme in Danish grid is of great importance.

The key aspect of online DSA is the reliability of the prediction. The US electric power system is designed and operated to meet a '3-nines' reliability standard, which means that the electric grid power should be 99.97% reliable [1].

In Chapter 7, a decision tree based systematic approach for cooperative online power system DSA and optimal preventive control is proposed. In Chapter 8, random forest (RF) based approach for online DSA to improve the reliability is proposed. In this chapter, the performance of the proposed approaches is demonstrated on a 400-bus, 200-line operational model of western Danish power system.

The rest of this chapter is organized as follows. Section 9.2 introduces the used tools for the development and the verification of proposed approaches. Section 9.3 presents the criteria of security assessment and the creation process of decision trees. Section 9.4 presents the implementation of preventive control scheme in western Danish power system based on paralleled decision trees. Section 9.5 gives the optimized preventive control trajectory with the lowest economic cost. Section 9.6 evaluates the overall reliability of proposed approach by considering other critical contingencies in western Danish power systems. Section 9.7 demonstrates the implementation of RF based high reliable online DSA followed by the concluding remarks in Section 9.8.

9.2 Analysis Tools

In this research, five tools have been used to develop the proposed approach: *DIgSILENT/PowerFactory* is used to create system OCs and conduct power flow calculations and T-D simulations; *Excel* is interfaced with *DIgSILENT* via *DIgSILENT Programming Language (DPL)* to manage simulations and record the results; *Salford Predictive Miner* including CART and RF sub-packages is used for data mining [2]; *Microsoft Visual C++* is interfaced with Salford Predictive Miner to calculate margins, proximities, outlier indices, etc. of RF. *MATLAB* is used for data collection, database creation, surface fitting.

9.3 Creation of Decision Trees

As mentioned in Section 7, the training of DTs should be based on a database which is built offline by screening N_C "*N-1*" contingencies and "*N-k*" typical contingencies from Danish transmission system operator's (Energinet.dk) historical record and experience on each OC. The "*N-1*" contingencies are the three-phase faults at the terminals of 400/150kV transmission lines with clearing time of 0.12 sec (6 cycles). The database contains not only the predictor values such as active power, reactive power, phase, voltage and current before the disturbances calculated by power flow, but also the target values which are the results of T-D simulation secure (S) or insecure (I) based on criteria as given below:

- Transient stability: The system is considered as transient instable for a given contingency, if the systems transient stability index (TSI) defined by (9.1) is lower than 10%, in which $\Delta\delta_{max}$ is the maximum angle separation of any two rotor angles in degree.

$$TSI = \frac{360 - \Delta\delta_{\max}}{360 + \Delta\delta_{\max}} \times 100\% \tag{9.1}$$

- Short-term voltage security: The system is considered to be insecure if the duration of any bus voltage going out of range from 0.8pu to 1.1pu is longer than 0.5sec.

Other criteria, e.g. frequency drop, reactive power starvation, oscillation damping, etc. can also be included in this approach by simple modification in the programming. However, due to the severity status and special requirement of Danish power system, other specific criteria are not included for examination. Out of all possible contingencies, only a small proportion can result in the insecurity of power system and only those corresponding critical OCs violate the security criteria. Hence, only

those critical contingencies will be selected to generate the contingency-oriented DTs. To demonstrate the proposed approach, the maximum load scenario is selected as the candidate scenario and the contingency selected is short circuit in 400kV *KAS_400_LAG* overhead line close to the substation of *KAS*, as tagged in Fig. 9.1.

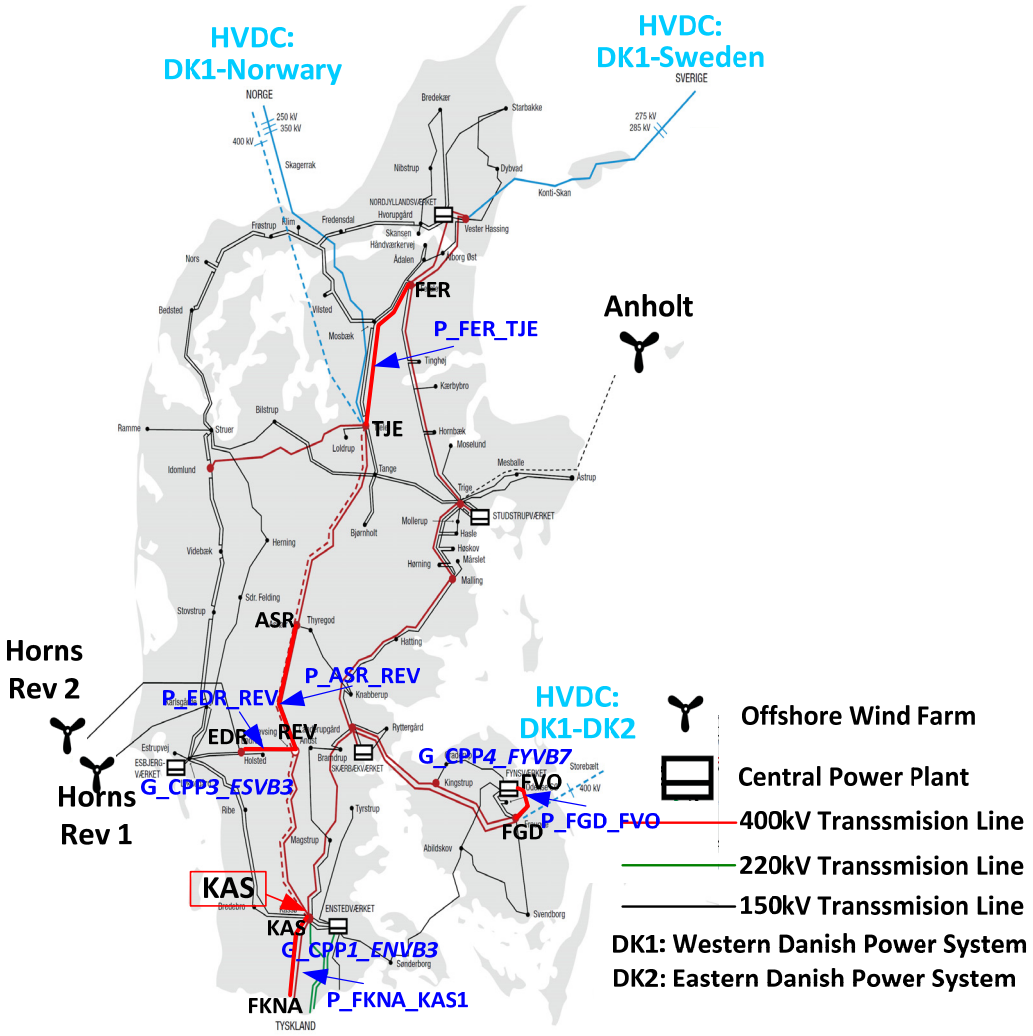

Fig. 9.1 Geographical map of western Danish power system.

Based on bisection search technique programmed by *DIgSILENT/DPL*, the approximate security boundary for contingency near 400kV substation *KAS* under maximum loading scenario is drawn by *MATLAB surface fitting toolbox*, shown in Fig. 9.2, in which the upper side is predicted to be the insecure region and the lower side is predicted to be the secure region.

Then, importance sampling is utilized to bias the sampling towards this security boundary so that the cases closer to the security boundary would have higher probability to be selected for final refined database. Additionally, the number of cases in insecure region and secure region are controlled to be generally the same to maximize the entropy of the database. As shown in Fig. 9.3, given the standard

deviation σ = 0.1, 330 OCs each in secure region (green spots) and insecure region (red spots) for offline study are generated by importance sampling respectively, in which each spot represents an OC for the corresponding percentages of total CPP generation. Moreover, the outputs in each generation units are subjected to random distribution and the outputs of each wind farms are based on the probability distribution density of forecast error with respect to forecasted wind power generation in Danish power system [3]. The process which consider the randomization on output of each generation unit and simultaneously maintain the total generation can assist PDT to automatically find the most effective units for rescheduling.

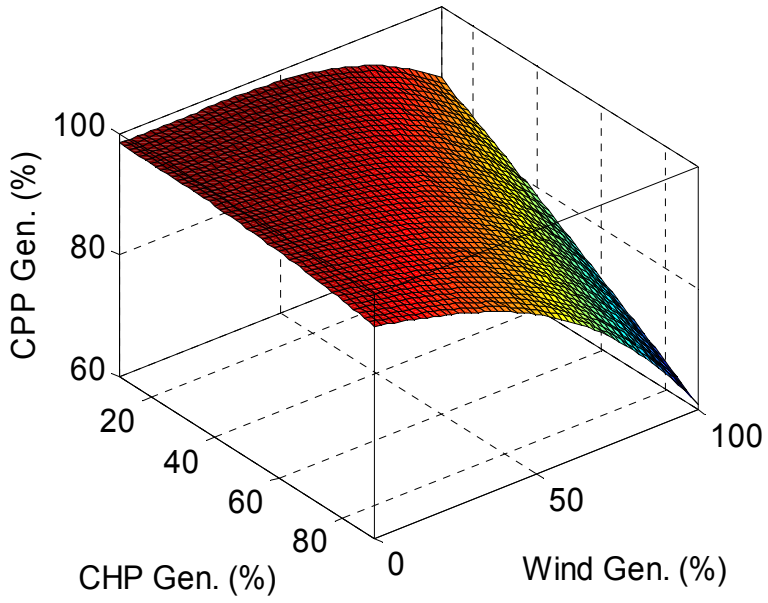

Fig. 9.2 Approximate security boundary.

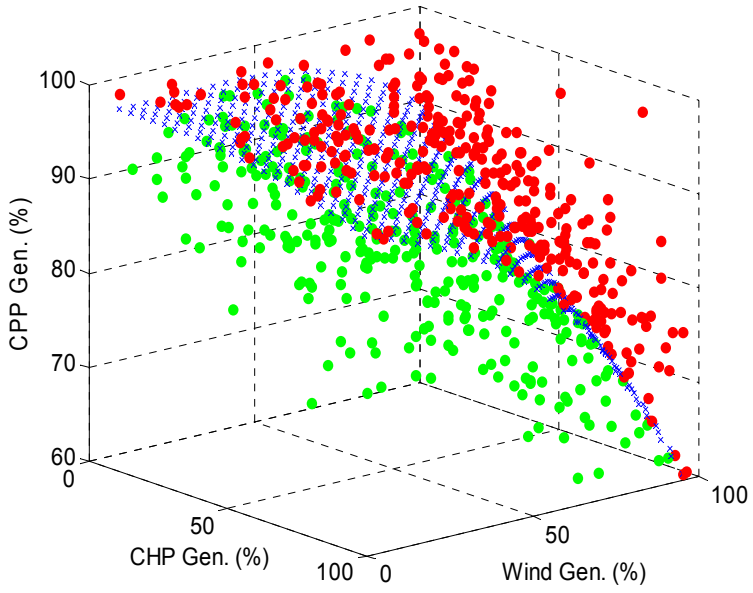

Fig. 9.3. Selected OCs by importance sampling.

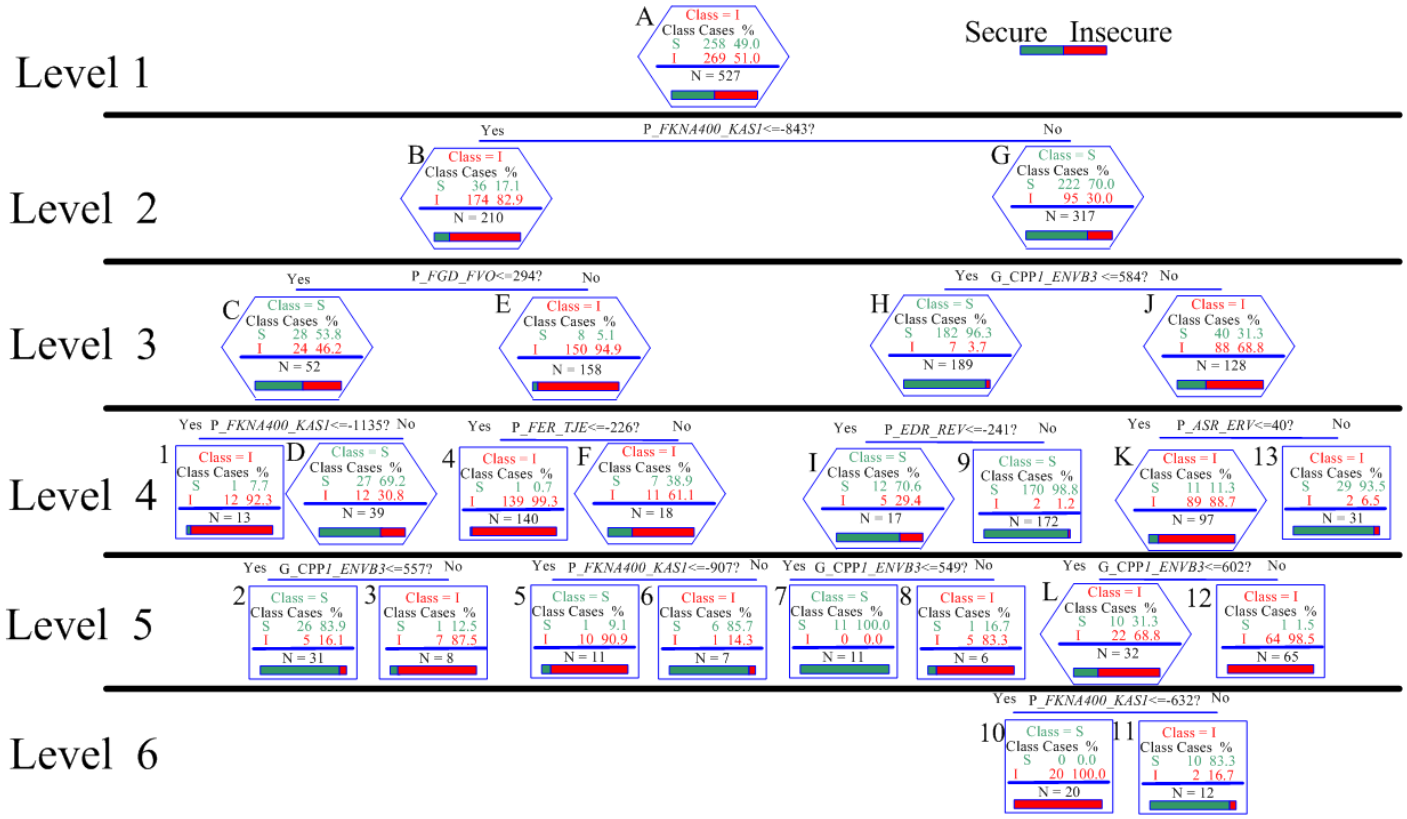

Fig. 9.4 The ODT for contingency near *KAS*.

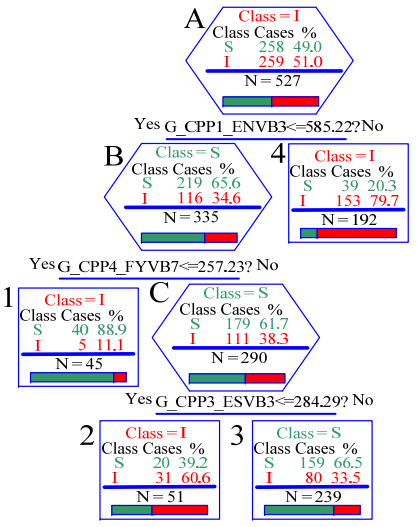

Fig. 9.5 The PDT for contingency near *KAS*.

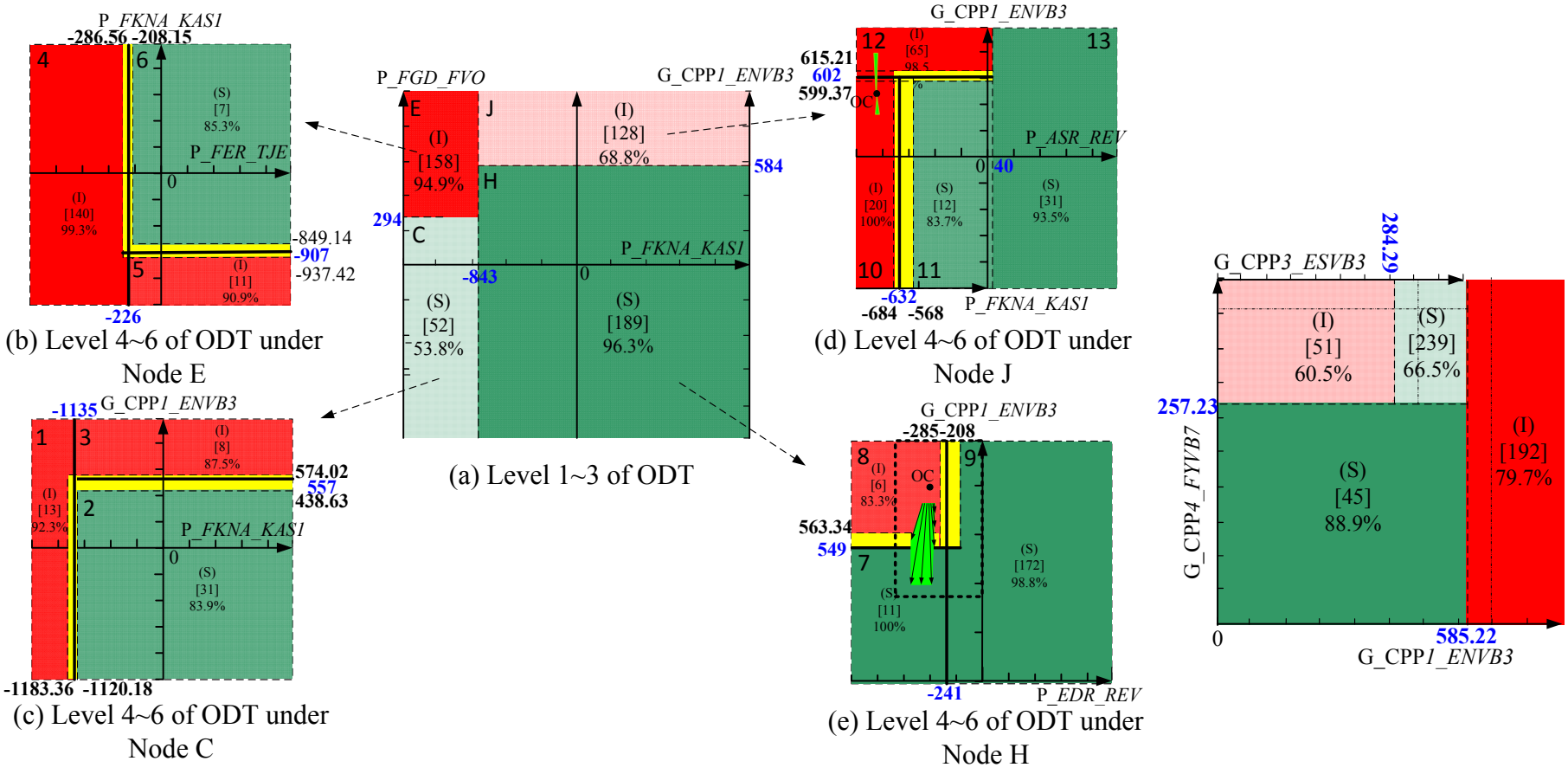

(b) Level 4~6 of ODT under Node E

(a) Level 1~3 of ODT

(d) Level 4~6 of ODT under Node J

(c) Level 4~6 of ODT under Node C

(e) Level 4~6 of ODT under Node H

Fig. 9.6 The 2-D nomogram of ODT .

Fig. 9.7 The 2-D nomogram of PDT.

It is assumed that measurements are available from entire 400kV transmission system including all CPPs' generation outputs (G_CPP*x*). 660 power flow calculations (P_*x*_*y*, Q_*x*_*y*) before the disturbance are conducted to create the predictors of the database and 660 T-D simulations are carried out for the results of security after the disturbance. 80% of the cases are randomly selected as the LS, and the rest 20% of the cases are selected as TS. Finally, a PDT and an ODT are created by CART algorithm in Salford Predictive Miner v6.6 [2], shown in Fig. 9.4 and Fig. 9.5, where "A"~"L" are the serial numbers of inner nodes, "1"~"13" are the serial numbers of terminal nodes.

TABLE 9.1 THE PERFORMANCE OF DECISION TREES AND RANDOM FOREST

Datasets	Insecure (I/S)	Secure (S/I)	Average (%)	Overall (%)
LS of ODT w/o A_*x*_*y* by DT	**257**/12	**252**/6	96.61	96.58
TS of ODT w/o A_*x*_*y* by DT	**73**/4	**51**/5	92.94	93.23
LS of ODT w/ A_*x*_*y* by DT	**255**/14	**256**/2	97.01	96.96
TS of ODT w/ A_*x*_*y* by DT	**76**/1	**52**/4	95.78	96.24
OOB test of ODT w/ A_*x*_*y* by RF	**299**/15	**338**/8	96.61	96.58
TS of ODT w/ A_*x*_*y* by RF	**76**/1	**53**/3	96.67	96.99

It is worth to mention that by considering phase angle differences between any two buses (A_*x*_*y*). The accuracy of DSA is improved. The comparison of accuracy between the measurement vectors with and without A_*x*_*y* shows the superiority of WAMS over SCADA by increasing the accuracy of about 3%, as shown in Table 9.1. However, it is imperative to mention that in a small power system with relative less line loading, the angle differences are relatively small which may result in erroneous judgment if it is not taken carefully during practical implementation. Some other advanced algorithms such as RF can also be used to predict the security with higher accuracy, as shown in Table 9.1. However, the model trained by RF contains a large number of deep-grown DTs, which are difficult to be interpreted for preventive control. The combination of RF and preventive control is currently being pursued. As mentioned in Chapter 7, the values of accuracy seem still lower than the industrial requirement. It is because of the implementation of importance sampling method, which is analyzed in Appendix B. Besides, one can easily adjust prior probability in the process of DT training to find the fuzzy region so as to significantly increase the reliability to achieve '3 nines' reliability standard [1].

In Fig. 9.4, ODT has five critical attributes of transmission lines, i.e. P_*FKNA_KAS1*, P_*FGD_FVO*, P_*FER_TJE*, P_*EDR_REV*, P_*ASR_REV*, and one critical attributes of generator output G_*CPP1_ENVB3*, which have been highlighted in Fig. 9.1. In Fig. 9.5, PDT has three critical attributes from three CPPs, i.e. G_CPP*1_ENVB3*, G_CPP*3_ESVB3*, G_CPP*7_FYVB7*. Most critical attributes selected by ODT for transmission lines belong to one backbone on Jylland Peninsula

and one for the key transmission line on Fyn Island. All the critical attributes selected by PDT are generators in the southern part, close to the selected contingency. P_*FKNA_KAS1* is one of the paralleled key transmission lines connecting German power system.

9.4 Preventive Control Based on Decision Trees

The ODT and PDT in Fig. 9.4 and Fig. 9.5 can be reproduced to 2-D nomograms to depict the space and its regions, as shown in Fig. 9.6 and Fig. 9.7. In each region the percentage of correctness and the serial numbers of the corresponding nodes are indicated. The red regions are insecure regions tagged by (I), while the green regions are secure regions tagged by (S). The thresholds in ODT in Fig. 9.4 are highlighted by solid lines and blue figures in 2-D nomograms in Fig. 9.6. The yellow regions between dashed lines are the fuzzy regions, in which the prior probability of insecure cases is between 0.01 and 0.99. As shown in Table 9.2, the ODT has higher classification accuracy than that of PDT because fewer variables are selected as predictors of PDT. However, the lower accuracy of PDT does not affect the reliability of preventive control because PDT can successfully search out the most effective controllable variables and provide the control directions. As shown in Fig. 9.7, the PDT nomogram is capable of informing the most influential CPPs (*ENVB3*, *FYVB7* and *ESVB3*) that need to be controlled and their control direction, i.e. to reduce generation in *ENVB3* and *FYVB7* and simultaneously to increase generation in *ESVB3*.

TABLE 9.2 THE PERFORMANCE OF ODT AND PDT

Datasets	Insecure (I/S)	Secure (S/I)	Average (%)	Overall (%)
LS of ODT	**257**/12	**252**/6	96.61	96.58
TS of ODT	**73**/4	**51**/5	92.94	93.23
LS of PDT	**184**/85	**199**/59	72.77	72.68
TS of PDT	**53**/24	**32**/24	62.99	63.91

Fig 9.8 shows the annual data of total CPP generation, total CHP generation and total wind generation represented by percentages based on their installed capacities [4]. At 09:00am, February 2nd, 2011, the OC is detected to be in the insecure region, shown by the black point tagged with "OC" in Fig. 9.9.

In order to maintain the constant value of total generation in Denmark, the equation (9.2) must be respected.

$$\text{G\_CPP1}\_ENVB3 + \text{G\_CPP3}\_ESVB3 + \text{G\_CPP4}\_FYVB7 = \text{Const.} \quad (9.2)$$

Other constraints such as PQ-capacity limits of each generator and individual limits of CPP generation rescheduling should also be applied, which are given in Table 9.3.

Hence, for this particular case as defined by (9.2), a surface boundary can be found, within which the total generation is maintained constant, respecting the abovementioned constraints, as shown in Fig. 9.9. The trajectories “A”, “B” and “C” are some of the feasible control directions on the surface which would lead the system to the secure region.

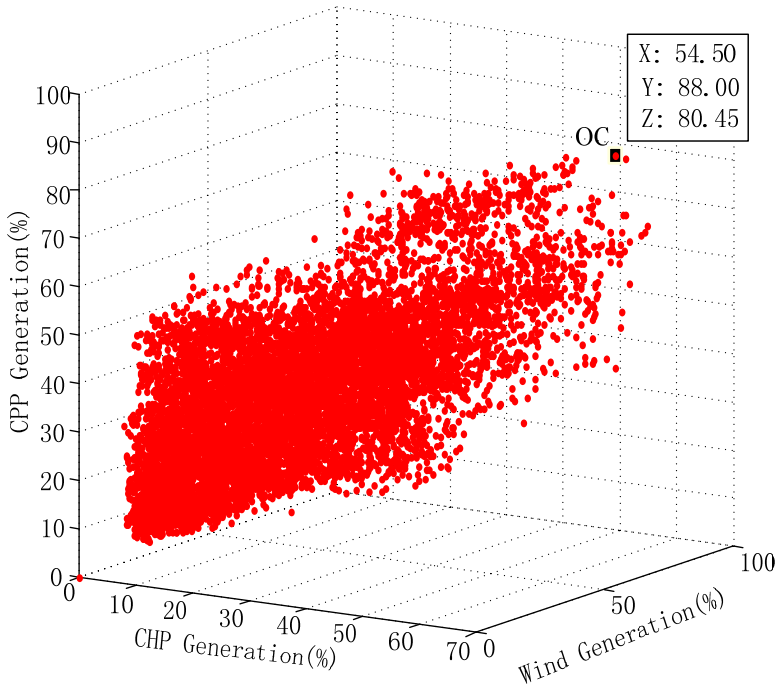

Fig. 9.8 Annual data of generation.

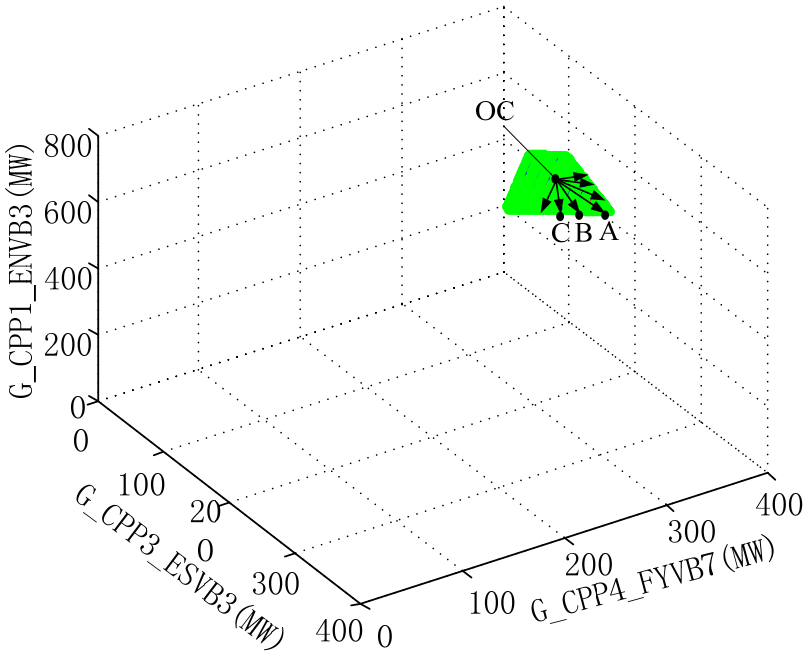

Fig. 9.9 Control constraint surface.

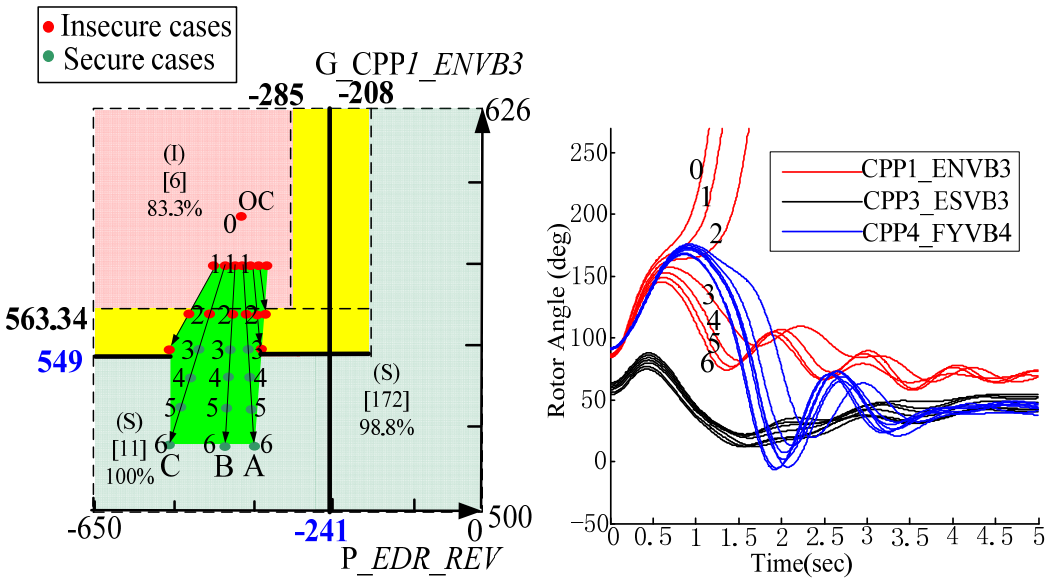

(a) Simulation results on ODT nomogram (b) Rotor angle on Trajectory A

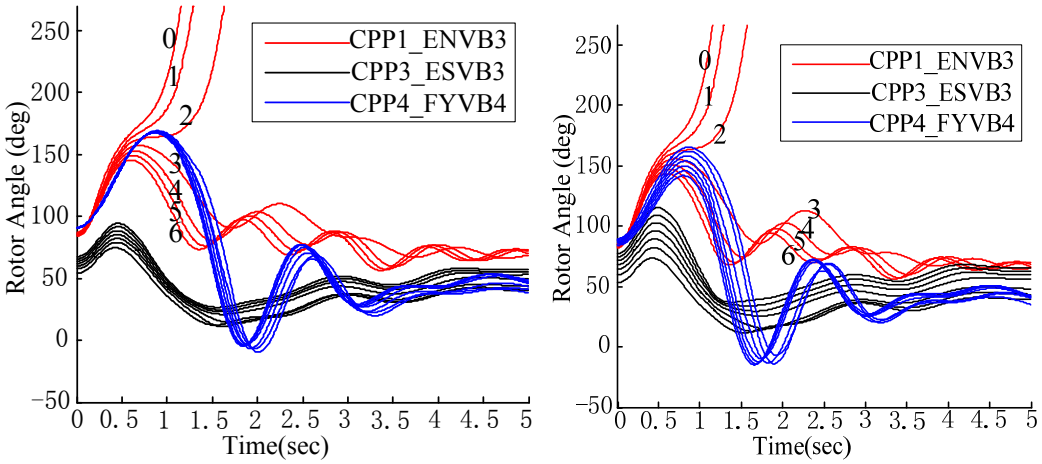

(c) Rotor angle on Trajectory B (d) Rotor angle on Trajectory C

Fig. 9.10 Rotor angles curves of involved generators in Trajectories A~C.

As shown in Fig. 9.9, the surface of generation rescheduling in the 3-D space of involved generators can be reproduced by its corresponding surface in 2-D ODT nomogram, which shows the effect of generation rescheduling with more clarity in the feasible region as shown in Fig. 9.10(a) which is the enlarged version of Fig. 9.6(e). The green spots on the surface represent the secure cases, while the red spots represent the insecure cases. It can be observed that the trajectories “A”, “B” and “C” are the control directions which are able to reliably draw the system to the secure region.

The prediction of DT is followed by its verification through T-D simulations. Only the criterion of transient stability is violated in this case, so Fig. 9.10(b) (c) and (d)

show the rotor angle curves of the involved generators for OCs tagged with "0" to "6" on the control trajectories "A", "B" and "C" respectively, in which the disturbance near *KAS* takes place at 0sec, and lasts for 0.12sec.

The results successfully verified the prediction of power system security as well as the guidelines of preventive control scheme. By rescheduling the generators instructed by this systematic preventive control scheme, the power system insecurity can be averted.

9.5 Optimal Preventive Control Trajectories

According to the actual regulations of Danish power system, (giving considerations to the prices of domestic reserve services and the penalty in cases of international exchange mismatch) further optimization on the trajectory of preventive control is conducted to minimize the total cost incurred by generation rescheduling, as defined in (9.3).

$$\min .C = \min .\left(\sum_{i \in \mathcal{G}} C_i + f\left(\Delta P_{EX}\right) \right) \tag{9.3}$$

a) Cost of reserve services

$$C_i = C_{Fi} + P_{UPi} \cdot \left|\Delta G_{UPi}\right| + P_{DNi} \cdot \left|\Delta G_{DNi}\right|, \forall i \in \mathcal{G} \tag{9.4}$$

$$\Delta G_{UP_i} = \begin{cases} Gr_i - Gs_i & \text{if } Gr_i > Gs_i \\ 0 & \text{else if } Gs_i \le Gr_i \end{cases} \tag{9.5}$$

$$\Delta G_{DNi} = \begin{cases} 0 & \text{if } Gr_i \ge Gs_i \\ Gr_i - Gs_i & \text{else if } Gr_i < Gs_i \end{cases} \tag{9.6}$$

$$\text{Subject to } G_i^{\min} \le Gr_i \le G_i^{\max} \tag{9.7}$$

$$\text{Subject to } 0 \le \Delta G_{UPi} \le \Delta G_{UPi}^{\max} \text{ and } \Delta G_{DNi}^{\min} \le \Delta G_{DNi} \le 0 \tag{9.8}$$

As defined in (9.4)~(9.6), the cost of reserve services is composed of fixed cost C_{Fi} and variable cost depending on the actual quantity of generation rescheduling in effect, either upward ΔG_{UPi} or downward ΔG_{DNi}. In (9.4), $\mathcal{G}$ is the set of CPP generators participating in the preventive control, and P_{UPi} and P_{DNi} are the prices of upward and downward generation rescheduling in CPP i. In (9.5) and (9.6), Gr_i and Gs_i are real-time and scheduled generation of CPP i. The amount of generation rescheduling in each generator should also subject to the P-Q capacity (i.e. G_i^{min} and G_i^{max}) and the

limitations of the maximum available generation reserves in both directions (i.e. ΔG_{UPi}^{max} and ΔG_{DNi}^{max}), as defined in (9.7) and (9.8).

b) Penalty due to mismatch of international power exchange

$$\Delta P_{EX} \approx \sum_{i \in \mathcal{G}} \Delta P_{UPi} + \sum_{i \in \mathcal{G}} \Delta P_{DNi}, \forall i \in \mathcal{G} \tag{9.9}$$

$$f\left(\Delta P_{EX}\right) = \begin{cases} P_{<50} \cdot \Delta P_{EX} & \text{if } \left|\Delta P_{EX}\right| \in (0,50] \\ P_{<100} \cdot \Delta P_{EX} + C_{PEN1} & \text{if } \left|\Delta P_{EX}\right| \in [50,100) \\ P_{\geq 100} \cdot \Delta P_{EX} + C_{PEN2} & \text{if } \left|\Delta P_{EX}\right| \in [100,\infty) \end{cases} \tag{9.10}$$

Assuming that the network loss is invariant during preventive control, the imbalance between generation and load introduced by generation rescheduling in Denmark is compensated by German power system, as defined by (9.9). In (9.10), $P_{<50}$, $P_{<100}$ and $P_{\geq 50}$ are unit prices of international power exchange mismatch below 50MW, between 50MW and 100MW, large than 100MW, respectively. For mismatch between actual and scheduled power exchange larger than 50MW or 100MW, penalties C_{PEN1} or C_{PEN2} are applicable respectively. As given in Table 9.3, the prices of reserve services from participating generators in Denmark and the cost of international power exchange between Denmark and Germany are assumed based on the typical data.

TABLE 9.3 THE PRICES OF RESERVE SERVICES AND INTERNATIONAL POWER EXCHANGE

Price	**CPP*1_ENVB3***	**CPP*3_ESVB3***	**CPP*4_FYVB4***
G_i^{max} (MW)	626	378	372
G_i^{min} (MW)	188	98	110
ΔP_{UPi}^{max} (MW)	+39	+113	+32
ΔP_{DNi}^{max} (MW)	-75	-64	-38
C_{Fi} (DKK)	2230	1940	1880
C_{UPi} (DKK/MW)	535	390	450
C_{DNi} (DKK/MW)	328	208	236
Price	**International Power Exchange with Germany**		
$P_{<50}$ (DKK/MW)	400		
$P_{<100}$ (DKK/MW)	450		
$P_{\geq 100}$ (DKK/MW)	500		
C_{PEN1} (DKK)	100,000		
C_{PEN2} (DKK)	500,000		

Fig. 9.11 shows the cost of preventive control along trajectories A, B and C in Fig. 9.10(a). Trajectory A is to shift generation from CPP*1_ENVB3* to CPP*4_FYVB4*. Trajectories B and C are to shift generation from CPP*1_ENVB3* to CPP*4_FYVB4* and CPP*3_ESVB3*. In this case, the preventive control does not violate the scheduled international power exchange, so it is a linear optimization problem. However, if the preventive control violate the scheduled international power exchange and subject to the international penalty, the case becomes a piecewise linear optimization problem. After the optimization in MATLAB, trajectory A is found to be the most economical

trajectory and the optimal objective OC after generation rescheduling is below the threshold of reliable security boundary between "3" and "4" on trajectory A. The minimum cost is 42,392 Danish Kroners (DKK).

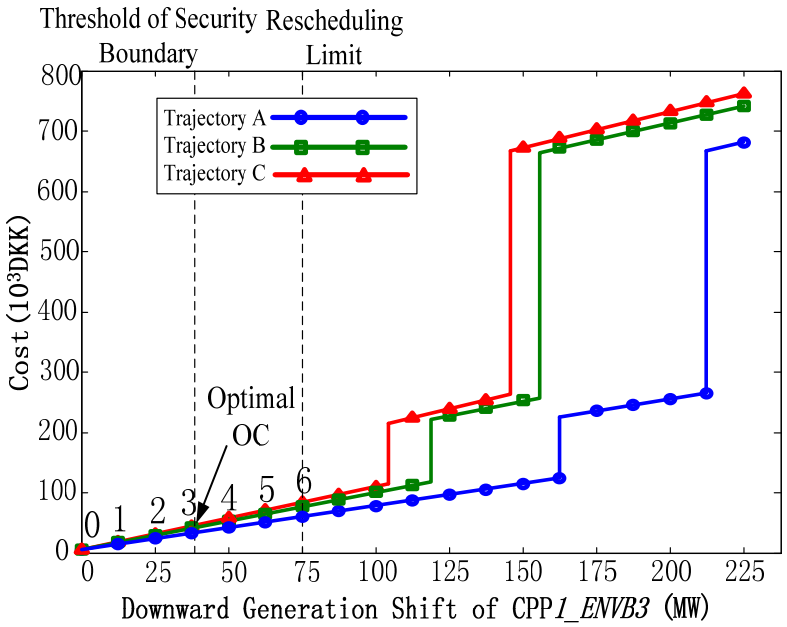

Fig. 9.11 Cost of preventive control along Trajectories A, B and C.

9.6 Overall Evaluation of Other Contingencies

TABLE 9.4 VERIFICATION OF THE MOST CRITICAL CONTINGENCIES

Cont. No.	Fault Event	Switch Event	DT Size	Ove. Accuracy of LS (%)	Ove. Accuracy of TS (%)	Suc. Rate
1	KAS	KAS_400_LAG	13	96.58	93.23	**20**/20
2	KAS	KAS_400_REV	14	97.54	94.66	**19**/20
3	LAG	LAG_400_SVS	18	96.03	93.13	**19**/20
4	LAG	LAG_400_MAL	17	96.39	95.52	**20**/20
5	TRI	FER_400_TRI	n/a	n/a	n/a	n/a
6	TRI	MAL_400_TRI	21	97.87	96.52	**20**/20
7	NVV	NVV_400_VHA	n/a	n/a	n/a	n/a
8	NVV	FER_400_NVV	n/a	n/a	n/a	n/a
Tot.						**98.0%**

To evaluate the overall reliability of this approach, multiple contingency-oriented DTs are created for eight most critical *N-1* contingencies which have been screened out by critical clearing time (CCT) calculations of western Danish power system in [5]. The size, overall accuracies of LS and TS of these DTs are shown in Table 9.4. Among these contingencies, only five events violate the transient stability or short-term voltage security criteria. For each contingency, 20 insecure OCs are randomly generated. 98% of the random generated insecure OCs can be controlled and guided

back to the secure region (across the fuzzy region), if international power exchange is maintained as invariant. The remaining 2% OCs can certainly be controlled by varying the international exchange power with Germany, however at the cost of penalty.

9.7 Online DSA Based on Random Forest

As discussed in Section 9.3, RF can be adopted to improve the accuracy of classification in the application of power system online DSA [7], [8]. Besides, the unsure cases can be filtered out by RF model using Outlier Index (OI) in (8.12) for immediate verification by T-D simulation to improve the accuracy.

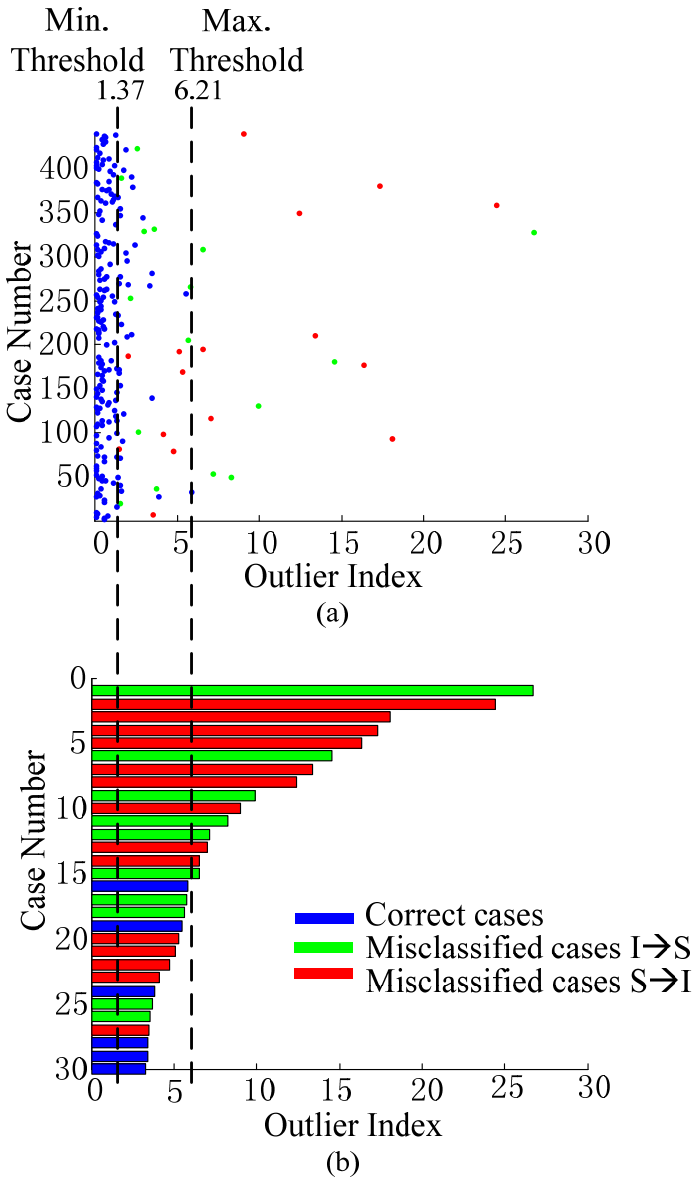

Fig. 9.12 Cases in the test set with respect to their outlier index.

The same 660 cases are used for the training of RF model, which are composed of power flow patterns (including 202 variables of *P_x_y*, *Q_x_y* and *A_x_y)* before the disturbance serving as predictors and 660 T-D simulations of security after the disturbance serving as the target. The RF model contains 500 deep-grown DTs, and 10 out of 202 predictors are randomly selected as the predictors within each node of every DTs. After the training process of RF model, 440 cases are generated to test the created RF model, which are independent from with the 660 cases used to train the RF.

Fig. 9.12(a) shows the 440 cases in the test set with respect their OI, which is then sorted in a descendent order. As shown in Fig. 9.12(b), the misclassified cases are all within the 30 cases with the highest OI. The blue cases are the correct ones, while the green and red cases are the misclassified ones.

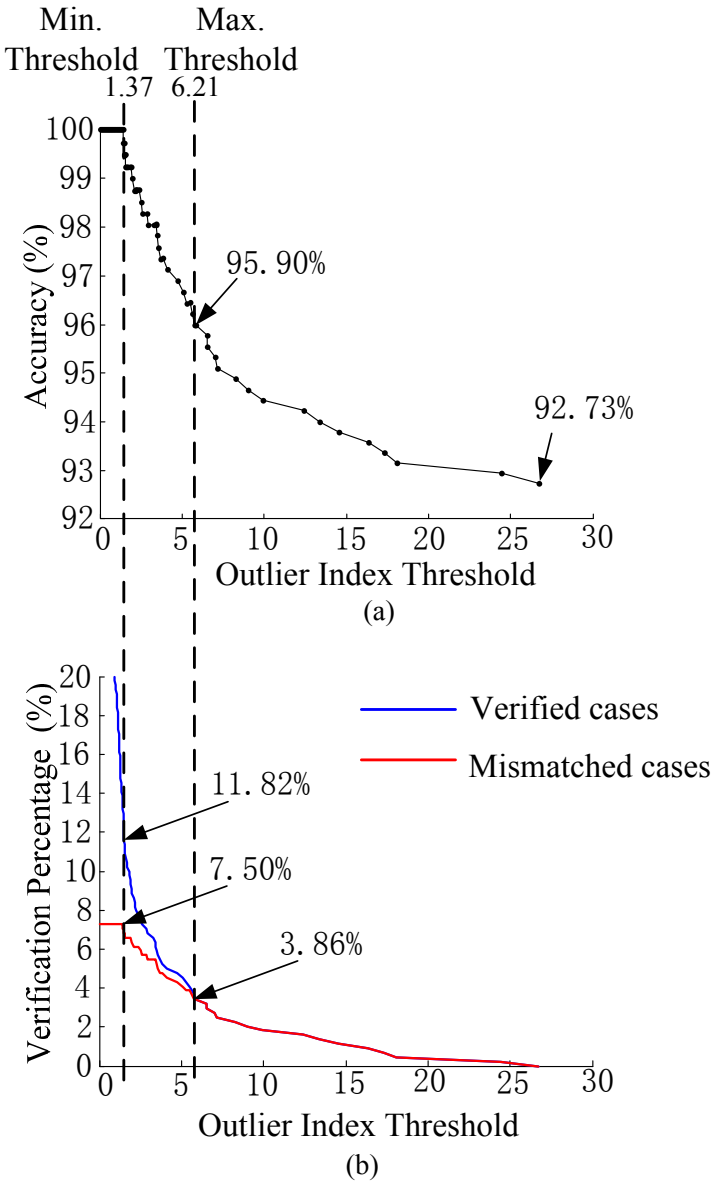

Fig. 9.13 Accuracy and verification percentage with respect to outlier index threshold.

As mentioned in Chapter 8, given a threshold of OI, the predicted OC with OI larger than the specified threshold will be filtered out as unsure case for immediate verification by T-D simulation. As shown in Fig. 9.13(a), the original accuracy of RF model is tested as 92.73%. If the OI threshold is given as 6.21, and all the cases with OI larger then 6.21 are verified by further T-D simulation, the accuracy can be increased to 95.90%. Whilst, if stricter threshold is given (i.e. 1.37), the accuracy can reach to even 100%. Fig 9.13(b) shows the percentage of cases that need for further verification. Only a percentage of 3.86% out of 440 cases are needed to be verified if the threshold is given as 6.21. Nevertheless, a percentage of 11.82% out of 440 cases are needed to be verified if stricter threshold is given as 1.37, and within these cases, a percentage of 7.50% are the mismatched cases.

Afterward, the database can be periodically updated by the new cases together with the existed cases. Finally, a stronger RF model can be created straight away with strengthened information of the updated database. Therefore, the percentage of filtered out cases for verification should be significantly decreased if more cases are added into the database for upgrading the RF model.

9.8 Summary

This chapter presents a DSA method based on contingency-oriented DTs with high accuracy and proposes an online systematic preventive control scheme based on cooperative application of parallel DTs, i.e. ODT and PDT. The scheme was demonstrated on the operational model of western Danish power system. The verified results have shown that the generation rescheduling guided by DTs is able to reliably control and bring the system back to security region hence prevent the possible power system insecurity. The proposed cost effective optimization for preventive control is capable of finding the optimal control trajectory. Additionally, the outlier index of RF model is able to improve the accuracy of online DSA to 100%.

During this control strategy, the cost of generation rescheduling adopted domestically is significantly less compared to the penalty on violating the prescheduled exchange across international tie lines. However, in some specific cases, especially for peak load OCs where local generators might be operating close to their limits, and for large exchange to neighboring countries, curtailment on power exchange across international tie lines becomes inevitable to maintain system security.

The main content of this chapter has also been reported in the author's previous publications in [J1], [C6], [C7] and [C13].

References

[1] Electric Advisory Committee: 'Smart grid: enabler of the new energy economy'. US Department of Energy, Dec. 2008, [Online]. Available: http://energy.gov/sites/prod/files/oeprod/DocumentsandMedia/finalsmart-grid-report.pdf , assessed on 15-Aug-2013.

[2] CART Tree-Structured Non-Parametric Data Analysis, [Online]. Available: http://www.salford-systems.com/en/products/spm, assessed on 15-Aug-2013.

[3] W. Hu, Z. Chen, and B. Bak-Jensen, "Stochastic optimal wind power bidding strategy in short-time electricity market," *International Review of Electrical Engineering*, vol. 7, no. 1. pp. 186-197, Feb. 2012.

[4] Hourly Danish power system data, [Online]. Available: http://www.energinet.dk/EN/El/Engrosmarked/Udtraek-af-markedsdata/Sider/default.aspx , assessed on 15-Aug-2013.

[5] C. Liu, Z. Chen, C. L. Bak *et al.*, "Transient stability assessment of power system with large amount of wind power penetration: the Danish case study," in *Proc. of the 10th International Power and Energy Conf.,* Ho Chi Minh City, Vietnam, Dec. 2012.

[6] I. Kamwa, S. R. Samantaray, and G. Joos, "Catastrophe predictors from ensemble decision-tree learning of wide-area severity indices," *IEEE Trans. Smart Grid*, vol. 1, no. 2, pp. 144-158, Sep. 2010.

[7] I. Kamwa, S. R. Samantaray, and G. Joos, "On the accuracy versus transparency trade-off of data-mining models for fast-response PMU-based catastrophe predictors," *IEEE Trans. Smart Grid*, vol. 3, no. 1, pp. 152-161, Mar. 2012.

PART IV

OTHER APPLICATIONS OF PMU

Chapter 10

Identification of Load Characteristics and the Corresponding Adaptive Corrective Scheme

10.1 Introduction

In the past decades, voltage instability has become a major threat of power system operation. Voltage instability usually takes on the form of drop of power system voltage, which may lead to wide area power system voltage collapse. It is caused by unavailability of reactive power support in some nodes of the network, where the voltage uncontrollably falls [1]. For this reason, more and more TSO have installed WAMS in order to prevent cascading voltage drop by estimating the proximity of voltage collapse point [2]. As mentioned in previous chapters, WAMS is based on widely installed PMUs, which opens a window to observe the dynamic behavior of power system in real time [3], [4]. This technology is attractive, since the high frequency samples of real-time voltage and current, the accurate frames of magnitudes and phasors and the availability of data synchronization by GPS time stamps can offer a better anticipation function by detecting the inception of instability instead of its consequences [5].

There are two defense strategies against voltage instability: preventive and corrective. For preventive aspects, PMUs help to make sure the voltage is in the regulated limits and to optimize the active and reactive power flow [6]. However, for corrective defense, PMU assists to detect the onset of voltage instability to implement the emergency scheme to save the voltage from collapse and avoid wide area blackouts and cascading trips by the following countermeasures:

- Control of generator excitation, e.g. Automatic Voltage Regulator (AVR);
- Control of reactive power compensation, e.g. Static Var Compensator (SVC);
- Blocking of on-load tap changer (OLTC);
- Load Shedding, etc. [7], [8].

Most research concentrates on the steady-state voltage stability problem by continuous load flow calculation [9]-[11]. On the contrary, this research focuses on

corrective voltage control based upon the detection of the onset of voltage collapse triggered by large disturbances rather than by scenarios such as smooth load increase.

In [12] and [13], sensitivity function is used to early detect the voltage collapse. However, the effect of different load characteristics is not considered. In this chapter, the identification of load and power source by PMU is implemented. *P0-V* curve instead of *P-V* curve is proposed to predict the voltage collapse. The adaptive corrective scheme is implemented in cases of large disturbances.

10.2 Theoretical Background

10.2.1 Basic Theory of Voltage Stability

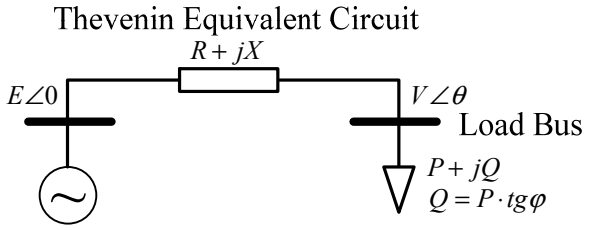

Fig. 10.1 Single-load infinite-bus system.

The analysis of voltage stability usually begins with a simple single-load infinite-bus system, which enables easy analytical derivations and provides insight into the voltage stability problem. As shown in Fig. 10.1, the infinite bus is represented by an ideal voltage source $\overline{E}=E\angle 0$ as well as a series resistance R and reactance X, so the transmission impedance is $\overline{Z}=R+jX$. Alternatively, $\overline{Z}$ can be also considered as the impedance of Thevenin equivalent circuit to represent the external power system as seen from a load bus. For the sake of simplicity, the transmission resistance R is neglected and the voltage of the load bus is denoted as $\overline{V}=V\angle\theta$, so (10.1) can be easily obtained.

$$\overline{V} = \overline{E} - jX\overline{I} \tag{10.1}$$

The complex power absorbed by the load can be represented as (10.2),

$$S = P + jQ = \overline{V}\cdot\overline{I}^{*} = \overline{V}\cdot\frac{\overline{E}^{*} - \overline{V}^{*}}{-jX} = \frac{j}{X}\left(EV\cos\theta + jEV\sin\theta - V^{2}\right) \tag{10.2}$$

which consists of active power P in (10.3) and reactive power Q in (10.4).

$$P = -\frac{EV}{X}\sin\theta \tag{10.3}$$

$$Q = -\frac{V^2}{X} + \frac{EV}{X}\cos\theta \tag{10.4}$$

By eliminate θ from (10.3) and (10.4), a quartic equation about V is obtained as (10.5).

$$V^4 + (2QX - E^2)V^2 + X^2(P^2 + Q^2) = 0 \tag{10.5}$$

which can be simplified to (10.6).

$$\left(\frac{PX}{E^2}\right)^2 + \left[\frac{QX}{E^2} + \left(\frac{V}{E}\right)^2\right]^2 = \left(\frac{V}{E}\right)^2 \tag{10.6}$$

The condition to have at least one solution for (10.6) is denoted in (10.7),

$$(2QX - E^2)^2 - 4X^2(P^2 + Q^2) \geq 0 \tag{10.7}$$

which can also be simplified to (10.8).

$$\left(\frac{PX}{E^2}\right)^2 + \frac{QX}{E^2} \leq \frac{1}{4} \tag{10.8}$$

As shown in Fig. 10.2, the expressions provided in (10.6) and (10.8) can be used to visualize the relationship between P, Q and V as a three dimensional surface, with the normalized coordinates of PX/E^2, QX/E^2 and V/E, respectively. On the P-Q-V surface, the green line represents the maximum deliverable active power with conditions of constant power factor, where $\partial P/\partial V = 0$. By projecting the green line to the P-Q plane, the condition of at least one solution is obtained, as defined in (10.8). A few red lines on the P-Q-V surface represent the conditions of constant load power factor $cos\varphi$, where $tg\varphi = Q/P$ with φ varying from $-\pi/8$ to $\pi/3$. A projection of these red lines onto the P-V plane results in the traditional nose curves (P-V curves), as shown in Fig. 10.3.

As shown in Fig. 10.4, the contour on the P-Q-V surface represents the conditions of constant normalized active power PX/E^2 at the receiving end, where PX/E^2 varies from 0.1 to 1.0 with 0.1 intervals. A projection of these black contours results in the traditional Q-V curves, as shown in Fig. 10.5.

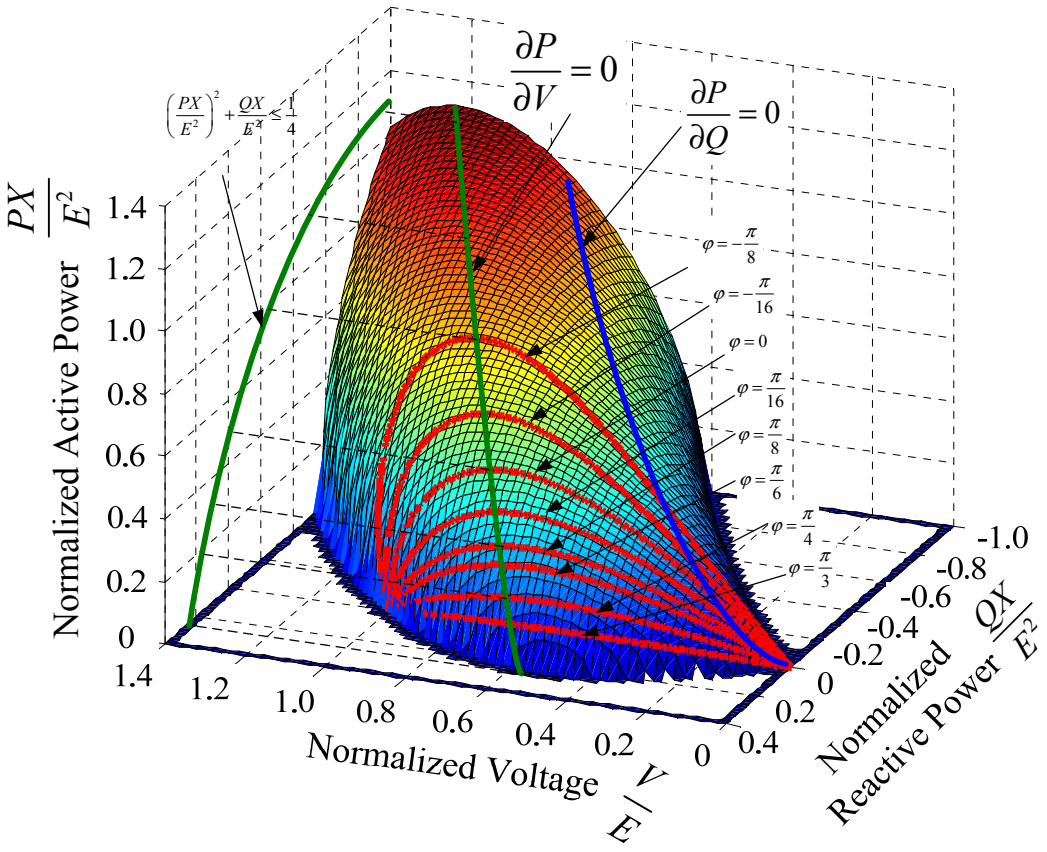

Fig. 10.2 *P-Q-V* surface and the curves of constant power factor.

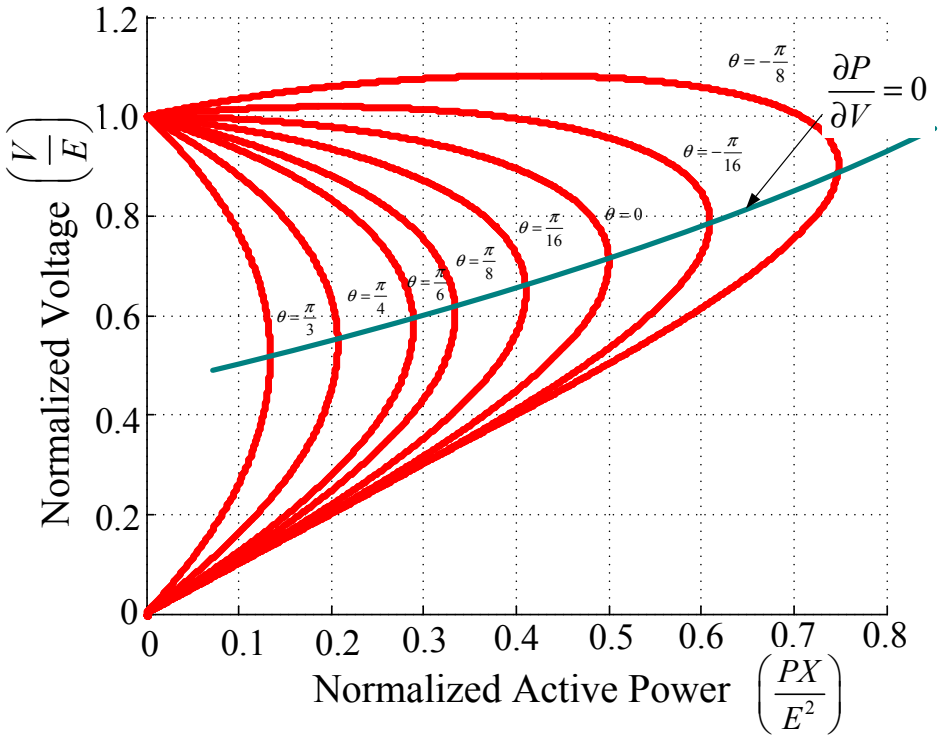

Fig. 10.3 *P-V* curves.

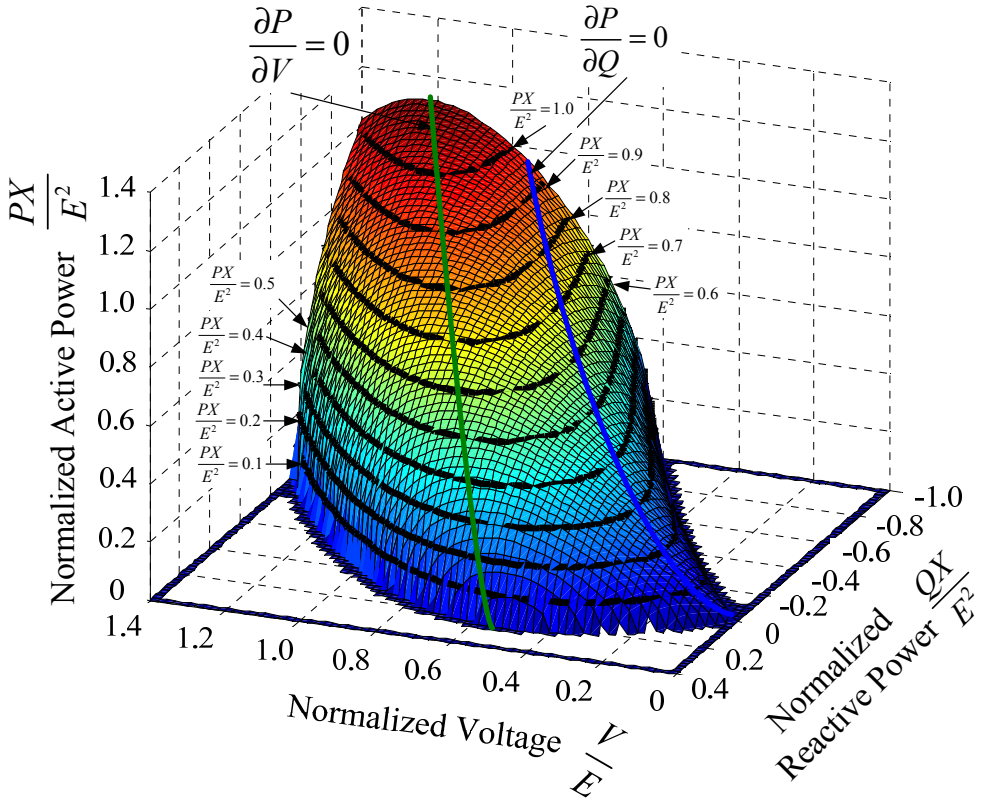

Fig. 10.4 *P-Q-V* surface and the curves of constant active power.

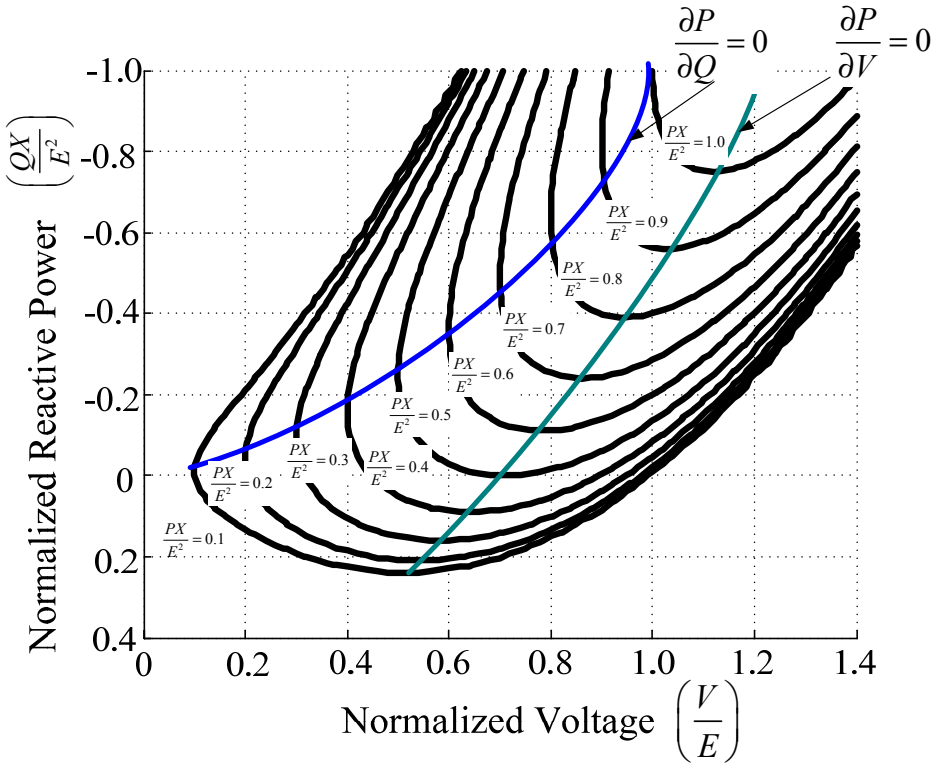

Fig. 10.5 *Q-V* curves.

10.2.2 Identification of Thevenin Equivalent Parameters

In previous section, variables of P, Q and V on the P-Q-V surface are normalized, providing that voltage source E and reactance X of Thevenin equivalent circuit are fixed and the resistance R of the Thevenin equivalent circuit is neglected. However, these assumptions are not accurate for real power systems, where the parameters of Thevenin equivalent circuit are fluctuating. In order to deal with this issue, PMUs with intelligent algorithms can be used to identify the parameters of Thevenin equivalent circuit online, due to its high sampling frequency and high resolution.

WAMS with hierarchical architecture is widely applied in modern power systems. Most of the PMU applications are based on measuring the local electrical variables, and then directly transmitting these electrical variables to the upper level without further processing. In this application, apart from the conventional measuring and transmitting functions, PMU also takes the responsibilities of identifying the parameters of Thevenin equivalent circuit and estimating the load characteristics. The deployment of PMU in this application aims at monitoring the voltage stability of load bus where it is installed, as shown in Fig. 10.6. A PMU having sufficient current channels may measure the current in all of the ingoing lines and outgoing lines of one substation, so the active and reactive power $P+jQ$ in the outgoing lines can be calculated by PMU with high speed [2].

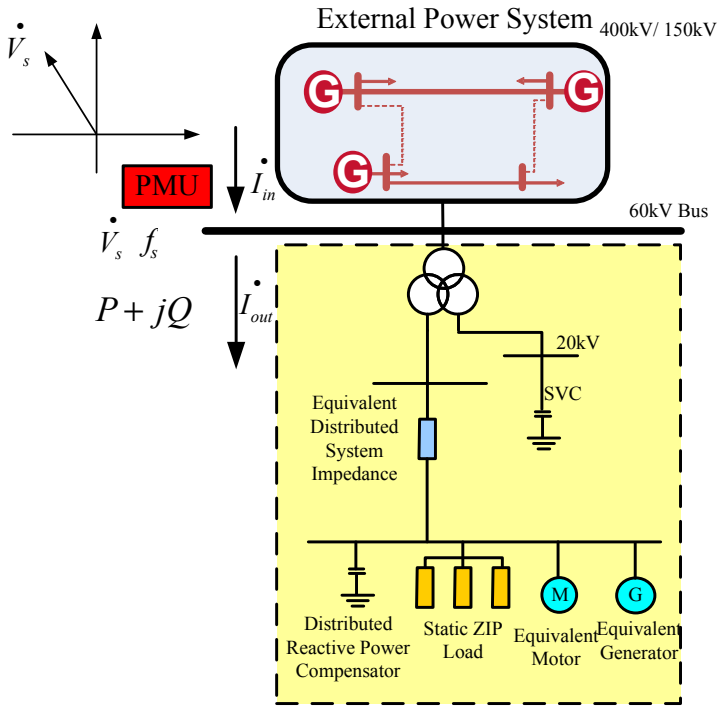

Fig. 10.6 Deployment of PMU in the application of local voltage stability monitoring.

The voltage stability monitoring is based on the simplification of the external power system to a time-dependent single-load infinite-bus equivalent circuit, which is composed of a voltage source $\overline{E}_k$ that supplies local load $P_{L,k}+jQ_{L,k}$ over a branch $\overline{Z}_k = R_k + jX_k$, as shown in Fig. 10.7. All variables are synchronized with time stamp as $t=t_k$.

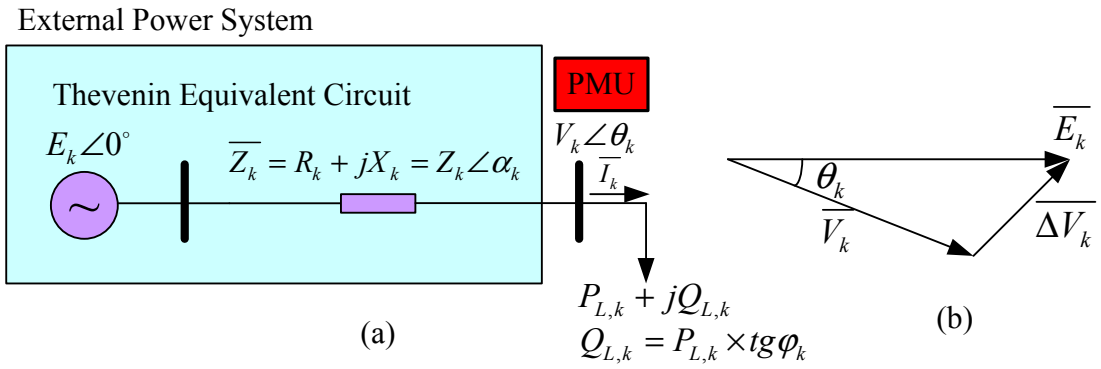

Fig. 10.7 Two-bus equivalent circuit and phasor diagram of voltage.

The phasor of voltage $\overline{V}_k$ and current $\overline{I}_k$ can help to online identify the parameters of Thevenin equivalent circuit ($\overline{E}_k$ and $\overline{Z}_k$) to represent the external power grid in real time. At the time instant $t=t_k$, the voltage of local bus is given as (10.9),

$$\overline{V}_k = \overline{E_k} - \overline{Z}_k\overline{I}_k \tag{10.9}$$

where $\overline{V}_k = V_{Rk} + jV_{Xk}$, $\overline{I}_k = I_{Rk} + jI_{Xk}$ and $\overline{Z}_k = R_k + jX_k$.

The equation in (10.9) can also be written in (10.10)~(10.13) by dividing $\overline{V}_k$, $\overline{I}_k$ and $\overline{Z}_k$ the to real part and imaginary part

$$\mathbf{y}_k = \mathbf{H}_k^T\mathbf{x}_k \tag{10.10}$$

where

$$\mathbf{y}_k = \left[V_{R_k}, V_{I_k}\right]^T \tag{10.11}$$

$$\mathbf{x}_k = \left[E_{R_k}, E_{I_k}, R_k, X_k\right]^T \tag{10.12}$$

$$\mathbf{H}_k^T = \begin{bmatrix} 1 & 0 & -I_{R_k} & I_{I_k} \\ 0 & 1 & -I_{I_k} & -I_{R_k} \end{bmatrix} \tag{10.13}$$

Equation (10.10) is a group of two linear equations with four unknown values, i.e. E_{Rk}, E_{Ik}, R_k and X_k, so multiple samples of $\boldsymbol{y}$ and $\boldsymbol{H}$ in different time instants from PMU should be used to identify these four parameters of Thevenin equivalent circuit in (10.12). Besides, it is assumed that parameters of external grid have no significant variation during the sampling window. Therefore, the unknown vector $\boldsymbol{x}_k$ in time instant $t=t_k$ is determined by the equations, as defined in (10.14),

$$\begin{cases} \hat{\mathbf{x}}_k = \hat{\mathbf{x}}_{k-1} + \mathbf{G}\left[y_k - \mathbf{H}_k^T \hat{\mathbf{x}}_{k-1} \right] \\ \mathbf{G}_k = \mathbf{P}_{k-1}\mathbf{H}_k \left[\lambda \mathbf{I} + \mathbf{H}_k^T \mathbf{P}_{k-1} \mathbf{H}_k \right]^{-1} \\ \mathbf{P}_k = \dfrac{\left[\mathbf{I} - \mathbf{G}\mathbf{H}_k^T \right] \mathbf{P}_{k-1}}{\lambda} \end{cases} \tag{10.14}$$

where λ is the forgetting factor assigning lower weight to old measurements in the sampling window.

10.2.3 Identification of Load Characteristic Parameters

The voltage magnitude V_k, active power P_k and reactive power Q_k, measured and calculated by PMU, can also be used to estimate important parameters in the load side. Although other systems such as SCADA, fault recorder can also identify the load characteristics, PMU/WAMS has advantages over these systems in terms of higher accuracy, since its high sampling speed and synchronization function realize the capture of the dynamic variation of active and reactive power in response to the change of voltage.

Based on practical assumption that the load consumption is dependent on the exponential function of voltage, the load model can be expressed as (10.15),

$$\begin{cases} P = P_0 \left(V / V_0 \right)^{p_u} \\ Q = Q_0 \left(V / V_0 \right)^{q_u} \end{cases} \tag{10.15}$$

where the exponents p_u and q_u are equal to the slope of dP/dV and dQ/dV at nominal voltage $V=V_0$, respectively.

For static load model, the PMU measures a series of voltage and power $\{V_k, P_k, Q_k\}$, $k = 1, 2,\ldots, N$. A number of samples on V_k and P_k can help to identify the parameters of P_0 and p_u, as defined in (10.16), where $\widehat{P_0}$ and $\widehat{p_u}$ are variables to be estimated.

$$P_k = \widehat{P_0} \left(V_k / V_0 \right)^{\widehat{p_u}} \tag{10.16}$$

To increase the accuracy of parameters identification, (10.16) can be simplified to (10.17) by using logarithmic function in both sides.

$$\ln P_k = \ln \widehat{P}_0 + \widehat{p}_u \ln V_k - \widehat{p}_u \ln V_0 \tag{10.17}$$

where V_0 is the nominal voltage of the load bus which can be given as 1.0pu, and P_0 is the active power consumption at the nominal voltage V_0. A series of measurements in the sampling window from $k = 1$ to $k = N$ can be used to estimate the parameters of $\widehat{P_0}$ and $\widehat{p_u}$, based on Least Square Estimation (LSE) method, where the voltage V_k ($k = 1, 2,..., N$) should have a little deviation with respect to the nominal value 1.0pu.

Vector $\hat{\theta}_p^{/}$ to be estimated is defined in (10.18) and vectors of measured value $\overline{P^{/}}$ and $\phi_p^{/}$ are defined in (10.19) and (10.20), respectively.

$$\hat{\theta}_p^{/} = \begin{bmatrix} \hat{P}_0 & \hat{p}_u \end{bmatrix}^T \tag{10.18}$$

$$\overline{P^{/}} = \left[\ln P_1, \ln P_2, \cdots, \ln P_N\right]^T \tag{10.19}$$

$$\phi_p^{/} = \begin{bmatrix} 1 & 1 & \cdots & 1 \\ \ln V_1 & \ln V_2 & \cdots & \ln V_n \end{bmatrix} \tag{10.20}$$

Therefore, $\widehat{P_0}$ and $\widehat{p_u}$ in vector $\hat{\theta}_p^{/}$ can be calculated by LSE, as defined in (10.21).

$$\hat{\theta}_p^{/} = \left(\phi_p^{/T}\phi_p^{/}\right)^{-1}\phi_p^{/T}\overline{P^{/}} \tag{10.21}$$

For the sake of succinctness, only load characteristic of active power is introduced here, for load characteristic of reactive power, the algorithm is the same.

10.2.4 Analysis of Voltage Collapse Point

In Section 10.2.2 and Section 10.2.3, parameters of Thevenin equivalent circuit (i.e. E_k, $\overline{Z_k}$) and major parameters of load characteristics (i.e. p_u, q_u) can be identified by PMU installed in the substations in the load area. In the following sections, a novel approach is proposed to predict the voltage collapse point.

It is worthy to mention here that load characteristic has significant impact on voltage stability. Assuming that power system is working in two identical steady state power flow patterns but with different load characteristics, the ability of enduring the disturbance is entirely different, because they have different nonlinear behaviors after disturbance. In fact, after the disturbance, the dynamic response and the non-linear behaviors of power system are excited. The variation of voltage definitely has impact on power consumption of the load. Conversely, the change of load consumption also has effect on the distribution of power flow. The following analysis is able to mathematically find out the voltage collapse point based on aforementioned parameters identified by PMU. In addition, by generalizing the problem to any load characteristics, the author proposes the *P0-V* curve instead of traditional *P-V* curve to eliminate the interaction impact incurred by the non-linearity of load.

As shown in Fig. 10.7, PMU can accurately identify the parameters, such as $\overline{E_k}$, $\overline{Z_k}$, p_u and q_u, so nonlinear power flow model to represent the relationship between power and voltage is expressed as (10.22).

$$\begin{cases} P_{L,k} - \left[\dfrac{E_k V_k}{Z_k} \cos(\alpha_k + \theta_k) - \dfrac{V_k^2}{Z_k} \cos\alpha_k \right] = 0 \\ Q_{L,k} - \left[\dfrac{E_k V_k}{Z_k} \sin(\alpha_k + \theta_k) - \dfrac{V_k^2}{Z_k} \sin\alpha_k \right] = 0 \end{cases} \tag{10.22}$$

where $P_{L,k}=P_{L0}V_k^{pu}$, $Q_{L,k}=Q_{L0}V_k^{qu}$.

a) Constant Power Load

For constant power load ($p_u=q_u=0$), the power consumption of the load at time instant t_k ($P_{L,k}$ and $Q_{L,k}$) is not dependent on the voltage V_k, as defined in (10.23).

$$\begin{cases} P_{L,k} = P_{L0} \\ Q_{L,k} = Q_{L0} \\ tg\varphi_k = Q_{L,k} / \mathrm{P}_{L,k} \end{cases} \tag{10.23}$$

Critical point of *P0-V* curve ($P_{L0,m}$, $V_{k,cr}$) meets equation defined in (10.24), where $P_{L0,m}$ is maximum power consumption in the nominal voltage V_0, $V_{k,cr}$ is the voltage collapse point, and α_k is the angle of impedance in Thevenin equivalent circuit.

$$-V_{k.cr}^2 \cos\alpha_k + \frac{E_k \sqrt{4V_{k.cr}^2 - E_k^2}}{2} \sin\alpha_k + \frac{E_k^2}{2} \cos\alpha_k - P_{L0,m} Z_k = 0 \tag{10.24}$$

Knowing power factor $cos\varphi_k$ at time $t=t_k$, the critical point ($P_{L0,m}$, $V_{k,cr}$) in (10.24) can be expressed in (10.25).

$$\begin{cases} P_{L0,m} = E_k^2 \cos\varphi_k / \left\{ 2Z_k \left[1 + \cos(\alpha_k - \varphi_k) \right] \right\} \\ V_{k.cr} = E_k / \sqrt{2\left[1 + \cos(\alpha_k - \varphi_k) \right]} \end{cases} \tag{10.25}$$

where E_k, Z_k, α_k are identified by PMU, and angle of power factor φ_k is measured by PMU. Proof of (10.24) and (10.25) can be found in Appendix C.1.

b) Constant Current Load

For constant current load ($p_u=q_u=1$), the power consumption at time instant t_k ($P_{L,k}$ and $Q_{L,k}$) is the linear function of voltage V_k, as defined in (10.26).

$$\begin{cases} P_{L,k} = P_{L0} V_k \\ Q_{L,k} = Q_{L0} V_k \\ tg\varphi_k = Q_{L,k} / \mathrm{P}_{L,k} \end{cases} \tag{10.26}$$

Critical point of *P0-V* curve ($P_{L0,m}$, $V_{k,cr}$) meets the equation defined in (10.27).

$$\begin{cases} \alpha_k + \theta_{cr} \neq n\pi \\ \theta_{cr} = (2m+1)\pi / 2 \end{cases} \tag{10.27}$$

Knowing the power factor $cos\varphi_k$ at time $t=t_k$, the critical point ($P_{L0,m}$, $V_{k,cr}$) in (10.27) can be expressed in (10.28). Proof of (10.27) and (10.28) can be found in Appendix C.2

$$\begin{cases} P_{L0,m} = E_k / \left[Z_k \left(\sin\alpha_k - \cos\alpha_k tg\varphi_k \right) \right] \\ V_{k.cr} = E_k \left(\sin\alpha_k tg\varphi_k + \cos\alpha_k \right) / \left(\cos\alpha_k tg\varphi_k - \sin\alpha_k \right) \end{cases} \tag{10.28}$$

c) Constant Impedance Load

For constant impedance load ($p_u=q_u=2$), the power consumption at time instant t_k ($P_{L,k}$ and $Q_{L,k}$) is the quadratic function of voltage V_k, as defined in (10.29).

$$\begin{cases} P_{L,k} = P_{L0} V_k^2 \\ Q_{L,k} = Q_{L0} V_k^2 \\ tg\varphi_k = Q_{L,k} / \mathrm{P}_{L,k} \end{cases} \tag{10.29}$$

Critical point of *P0-V* curve ($P_{L0,m}$, $V_{k,cr}$) meets the equation defined in (10.30)

$$E_k / \left(Z_k V_{k,cr}^2 \right) = 0 \tag{10.30}$$

Because $E_k>0$ and $Z_k>0$, so the critical voltage point is $V_{k,cr} = \pm\infty$, which proves that the voltage of bus connected with constant impedance load is always stable (will not collapse). Proof of (10.29) and (10.30) can be found in Appendix C.3

c) General Static Load

For general exponential voltage load ($p_u=m$, $q_u=r$) the power consumption at time instant t_k ($P_{L,k}$ and $Q_{L,k}$) is the exponential function of voltage V_k, as defined in (10.31).

$$\begin{cases} P_{L,k} = P_{L0} V_k^m \\ Q_{L,k} = Q_{L0} V_k^r \\ tg\varphi_k = Q_{L,k} / \mathrm{P}_{L,k} \end{cases} \tag{10.31}$$

Critical voltage collapse point ($V_{k,cr}$, θ_{cr}) meets the equation defined in (10.32), where θ_{cr} is the voltage phase angle of load bus. Proof of (10.32) can be found in Appendix C.4.

$$\begin{aligned} F(V_{k,cr},\theta_{cr}) = & \left[\frac{E_k V_{k,cr}}{Z_k} \sin\left(\alpha_k + \theta_{cr}\right) \right] \left[r P_{L0} V_{k,cr}^{r-1} tg\varphi_k + \frac{2V_{k,cr}}{Z_k} \sin\alpha_k - \frac{E_k}{Z_k} \sin\left(\alpha_k + \theta_{cr}\right) \right] \\ & + \left[\frac{E_k V_{k,cr}}{Z_k} \cos\left(\alpha_k + \theta_{cr}\right) \right] \left[m P_{L0} V_{k,cr}^{m-1} + \frac{2V_{k,cr}}{Z_k} \cos\theta_{cr} + \frac{E_k}{Z_k} \cos\left(\alpha_k + \theta_{cr}\right) \right] = 0 \end{aligned} \tag{10.32}$$

The analytical solution of the critical point ($P_{L0,m}$, $V_{k,cr}$) is difficult, however, when V_k, θ_k can be measured by PMU, Thevenin equivalent circuit parameters E_k, Z_k and α_k can be estimated, P_{L0}, Q_{L0}, p_u and q_u can be identified by PMU measurements, so one can judge the voltage stability based on the following theorem:

If $F(V_k, \theta_k) > F(V_{k,cr}, \theta_{cr})$, the system is stable, there is no voltage collapse point.

If $F(V_k, \theta_k) \leq F(V_{k,cr}, \theta_{cr})$, the system is unstable, the voltage will collapse.

However, it is pertinent to mention that this theorem is based on the precondition that the dynamic effect of the load can be neglected.

The expression in (10.32) for constant power load ($p_u=q_u=0$), constant current load ($p_u=q_u=1$) and constant impedance load ($p_u=q_u=2$) can be visualized as three dimensional surfaces in *P0-Q0-V* space, with the scaled coordinates of P_0X, Q_0X and V, as shown in Fig. 10.8, Fig. 10.9 and Fig. 10.10, respectively. In Fig. 10.8 and Fig. 10.9, green lines represent the maximum deliverable normalized power P_0 with respect to the voltage collapse point. Nevertheless, there is no voltage collapse point in Fig. 10.10. A few red lines on the *P0-Q0-V* surface represent the conditions of constant load power factor $cos\varphi$, where $tg\varphi=Q/P$ with φ varying from -π/8 to π/3.

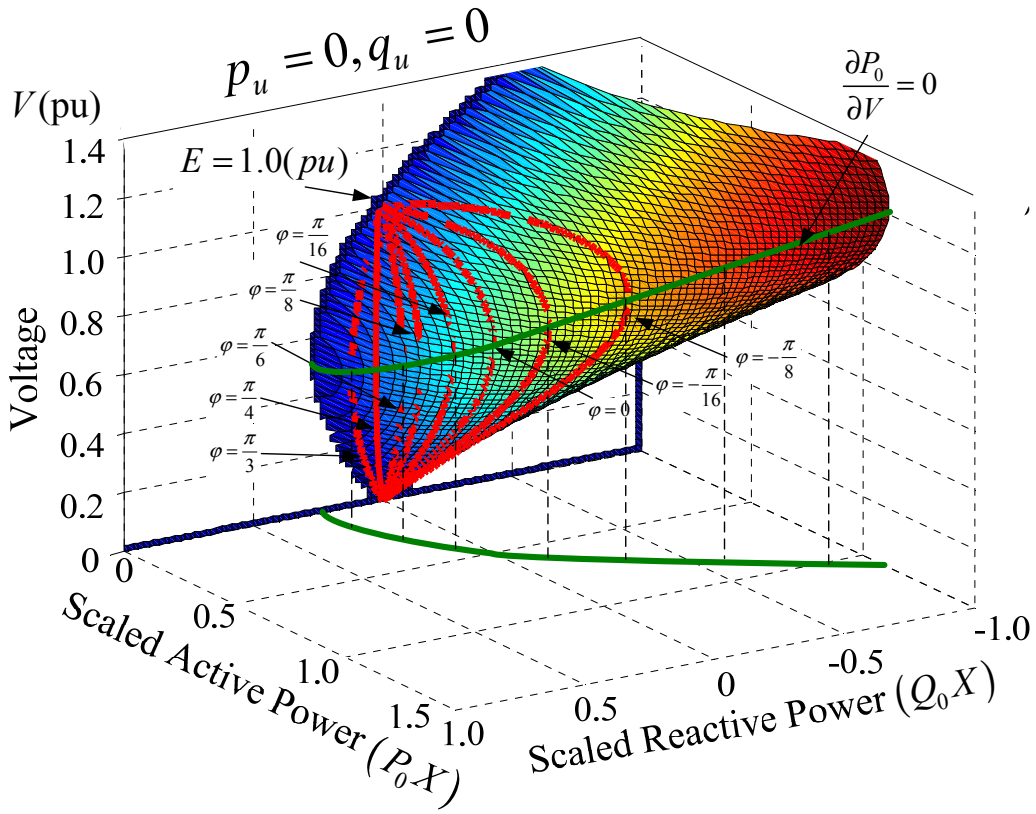

Fig. 10.8 *P0-Q0-V* surface in constant power load.

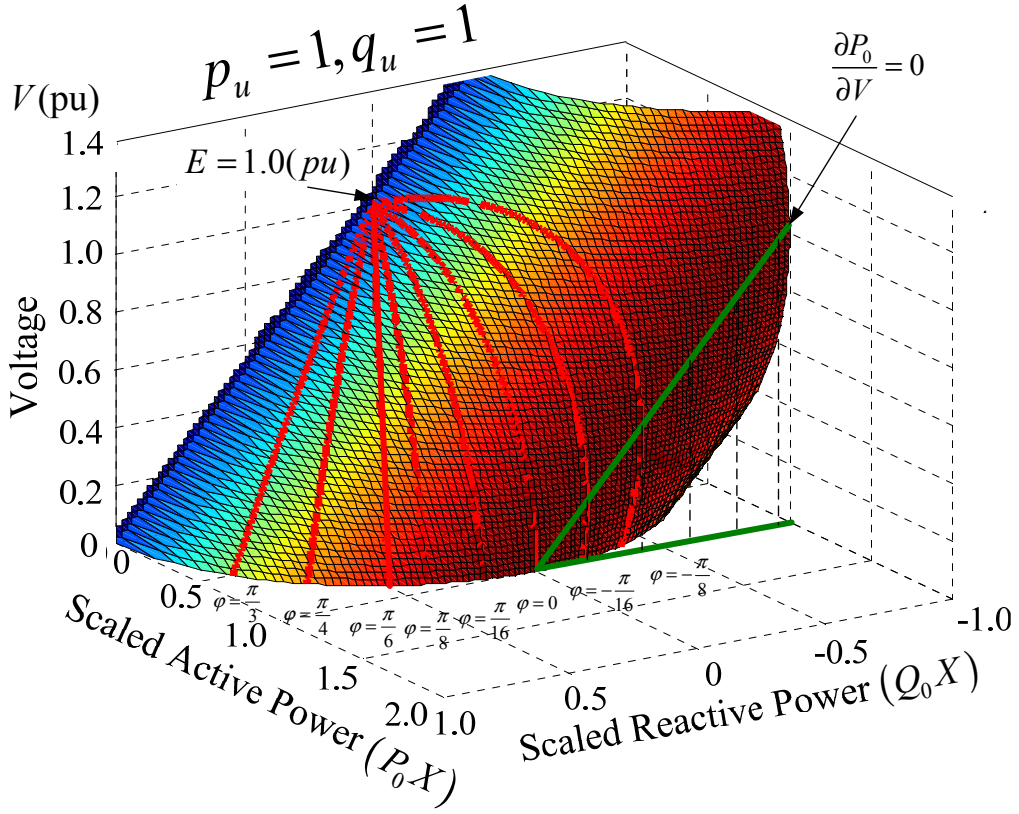

Fig. 10.9 *P0-Q0-V* surface in constant current load.

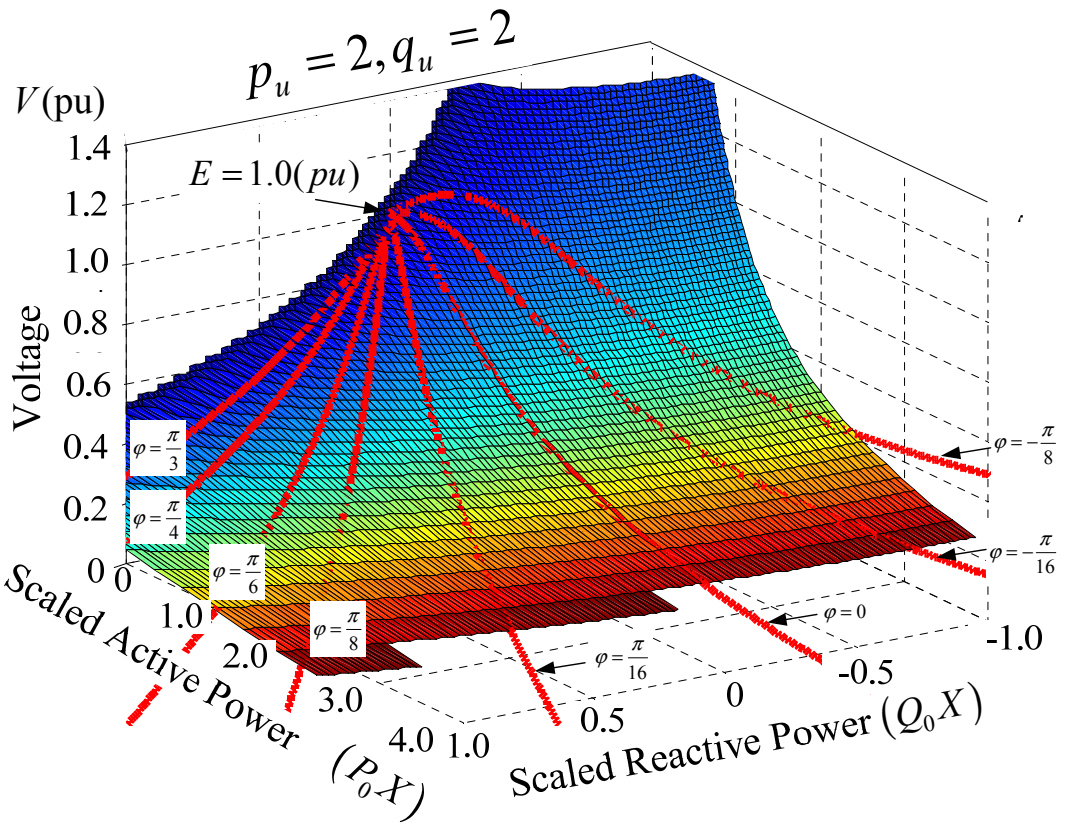

Fig. 10.10 *P0-Q0-V* surface in constant impedance load.

10.2.5 Adaptive Corrective Scheme to Prevent Voltage Collapse

A number of power system blackouts due to voltage collapse derive from single or multiple concurrent disturbances followed by trips of important transmission lines in the scenario that power system is heavily loaded. The regulating mechanisms, such as AVR, SVC and OLTC etc., try to restore the voltage of power system within the required range. However, the voltage restoration further stresses the already overloaded power system, resulting in voltage instability or even voltage collapse. For example, the extremely low voltage would result in motor stalling within a few seconds. These stalled motors would absorb large amount of reactive power and impede fast voltage recovery after short-circuit clearing.

An adaptive corrective scheme is proposed to prevent voltage collapse more intelligently. PMU takes the responsibility of predicting the voltage collapse point based on the identification of system parameters so as to classify the upcoming voltage instability issue to short-time or long-term categories.

a) Short-term Voltage Stability

When the load exponent parameters are less than 1.0 (min. $[p_u, q_u] < 1.0$), it can be predicted to be the short-term voltage stability problem. Control mechanisms of synchronous generators increase their reactive power to restore the voltage after the voltage drop triggered by disturbances. In this situation, the reactive generation reserve of synchronous generators and shunt capacitors take actions promptly after the disturbance. If the excitation current of synchronous generators increases to its over excitation limit (OEL), the voltage will collapse very soon. Therefore, the only solution is to trigger the under voltage load shedding (UVLS) immediately to meet reactive power balance without delay. The load shedding performs the predefined actions.

b) Long-term Voltage Stability

When the load exponent parameters are larger than 1.0 (min. $[p_u, q_u] \geq 1.0$), the voltage will not collapse immediately, so it is classified to long-term voltage stability problem. In this circumstance, the scheme is to block the OLTC if the bus voltage continues to decrease. Then, multi-step load shedding with different time delays is activated to restore the voltage of load bus so as to minimize the total amount of load shedding.

10.3 Test Power Systems

The proposed methodology is implemented in a detailed model of 4-Bus test system. 4-Bus test system is built in *Power System Analysis Toolbox (PSAT)* integrated in MATLAB [13], [14].

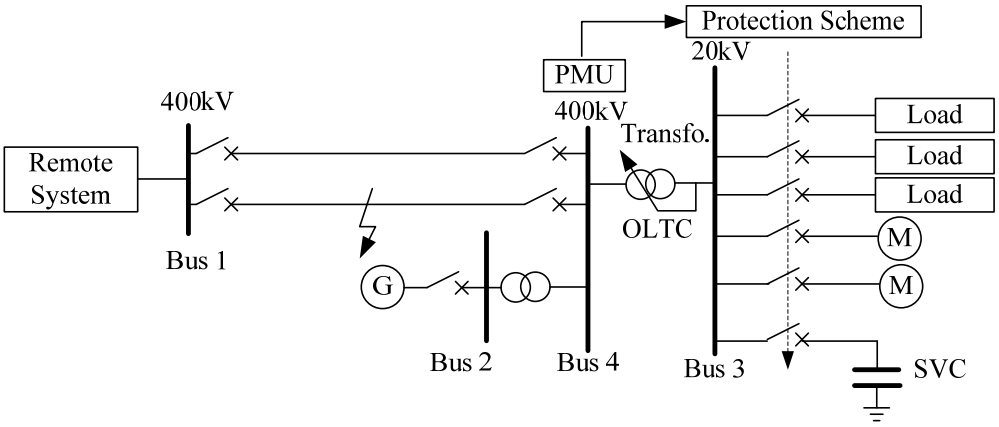

Fig. 10.11 Single-line diagram of 4-Bus test system.

The single-line diagram of the test system is shown in Fig. 10.11. The load at Bus3 is fed though a transformer equipped with OLTC. The remote power system connected to Bus1 provides most of the power though long paralleled double-circuit transmission lines, while the local generator connected to Bus2 supplies the remaining load demand.

The detailed data of the test system is given in Appendix D. OLTC has different delays on its first and subsequent tap changers with 5% dead zone. The generator at Bus2 uses 6-th order model, together with a simple representation of its governor, AVR and OEL. The OEL has an inverse-time characteristic to limit the field current of excitation. The overall base power is 100MVA, and the base voltage is the rated voltage of each voltage level. This model is simple but it is sufficient to analyze main mechanisms of voltage instability issue, both long-term voltage instability and short-term voltage instability [15].

As mentioned before, PMU placed on high voltage load bus (Bus4) can identify the parameters of load and Thevenin equivalent circuit in normal operation states. Therefore, the intelligent unit of PMU can identify the accurate model of both load and power source and update the parameters continuously based on the measurements. During dynamic response after disturbances, it is feasible to assume that load characteristics of aggregated load identified by PMU change slightly. However, this is not the case for parameters in the Thevenin equivalent circuit in the power resource side, since non-linear behavior and associated control mechanisms of generators will definitely change the parameters of power resources. Therefore, PMU only modifies

the parameters of Thevenin circuit in short time-slot after disturbance to model the external part of the power system.

The intelligent unit of PMU implements the adaptive corrective scheme based on the algorithm proposed in Section 10.2. The settings of OLTC and load shedding, such as threshold value and time delay, are usually predefined, but in this approach, they can be online configured by PMU with adaptive schemes. As analyzed before, voltage instability mechanism highly relies on the load characteristics, so the proposed adaptive corrective scheme to prevent voltage instability adopts different corrective schemes in terms of different scenarios.

The disturbance to be analyzed is a 3-phase bolted fault in the middle (50%) of one of paralleled transmission lines between Bus1 and Bus4, followed by tripping of the faulted line.

PMU calculates the voltage collapse point based on different load characteristics. The *P0-V* curves with respect to different load characteristics are shown in Fig. 10.12. Moreover, collapse point can be predicted on the load bus considering the impact of load characteristics. Table 10.1 lists the collapse points in each load model. Fig. 10.13(a)~(c) show the *P0-V* curves in the scenarios of constant power load, constant current load and constant impedance load with respect to different power factors.

TABLE 10.1 VOLTAGE COLLAPSE POINTS WITH RESPECT TO LOAD EXPONENTS

p_u=q_u	0.0	0.5	0.8	1.0	1.2	15	2.0	2.5
$V_{k,cr}$(pu)	0.7071	0.5774	0.4328	0.0116	n/a	n/a	n/a	n/a
P_{m0}(pu)	3.3331	4.3157	4.9275	6.6664	n/a	n/a	n/a	n/a

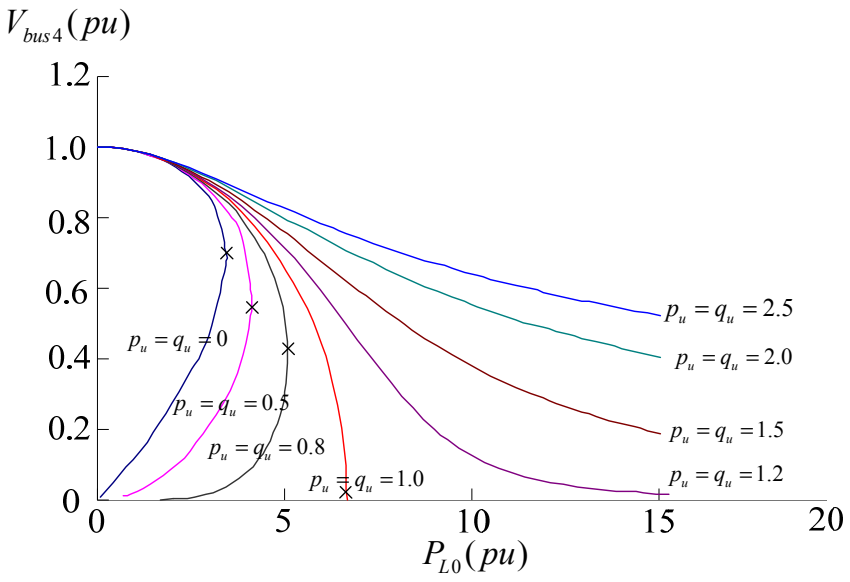

Fig. 10.12 *P0-V* curves in different load exponents.

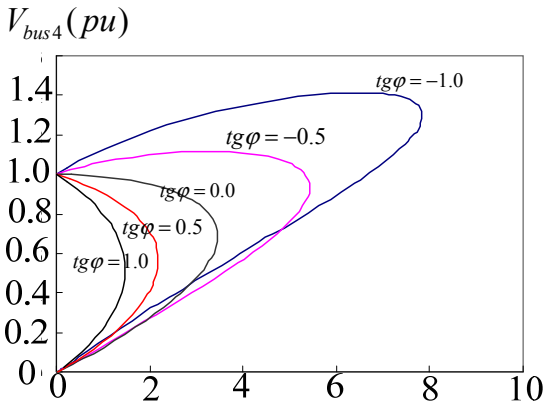

(a) *P0-V* curves with p_u=q_u=*0*.

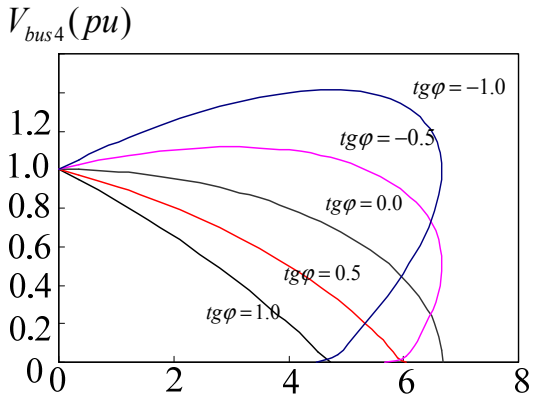

(b) *P0-V* curves with p_u=q_u=*1*.

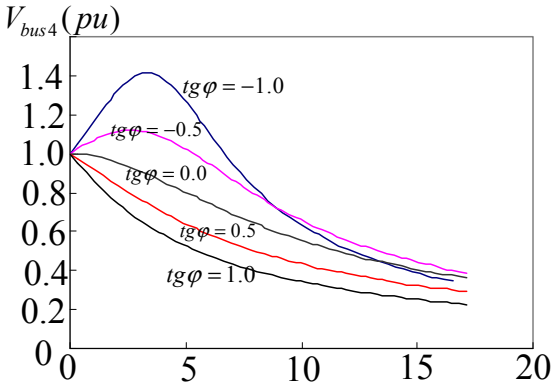

(b) *P0-V* curves with p_u=q_u=*2*.

Fig. 10.13 *P0-V* curves with respect to power factors.

10.4 Simulation Results and Discussion

PMU identifies the load model regularly in normal conditions. Fig. 10.14 and Table 10.2 show the results of load identification of the following two cases: Case A is the case with high load exponents, and Case B is the case with low load exponents. If the power consumption is the same in Case A and Case B in nominal voltage (i.e. 1.0pu), the load absorbs lower power in Case A than that in Case B, if it is subjected to a voltage drop, due to its higher exponents.

TABLE 10.2 RESULT OF LOAD PARAMETER IDENTIFICATION

Load Parameter	P_0	Q_0	p_u	q_u
Case A	16.17	3.27	1.245	1.502
Case B	15.51	3.09	0.802	0.603

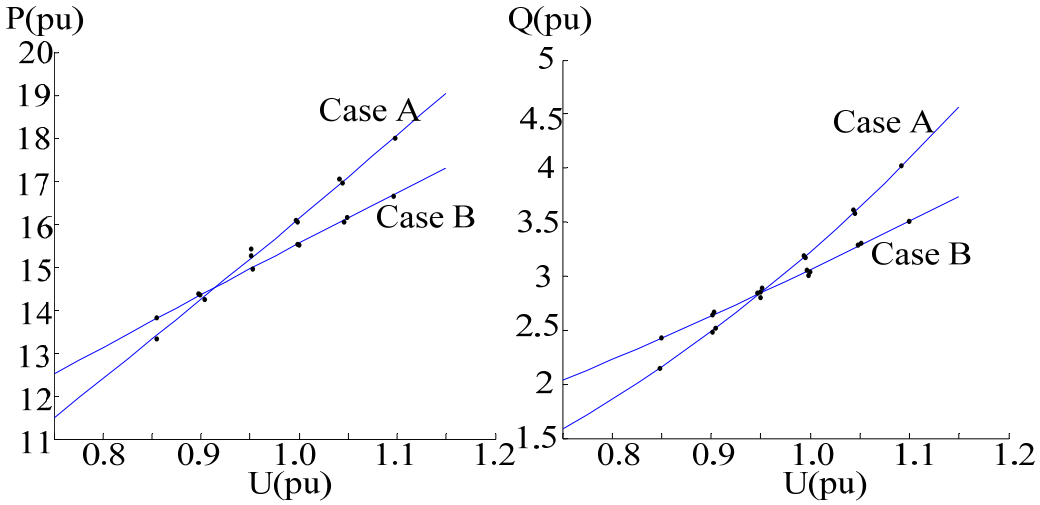

Fig 10.14 Load characteristics in Case A and Case B.

As mentioned in Section 2, if the load exponents represent low values (less than 1.0), the main aim of emergency control strategy is to maintain the power balance in a short-term. The conventional scheme should be implemented since there is not enough time to perform the optimization of control scheme. When the load exponents are higher than 1.0, no voltage collapse point exists, the time scale of voltage instability is identified to be the mid-term or long-term.

Case A: High load exponents

Before the disturbance, remote power system and local generator support the heavy load on Bus3 (P_L=1500MW Q_L=300MVar). The disturbance takes place at t = 1sec. After the disturbance, the power flow transferred to the other transmission line, the control mechanism of local generator increased its output to restore the voltage and tried to maintain the voltage stability. If there was no emergency measure (e.g. OLTC blocking), the voltage at Bus4 will collapse, as shown in Fig. 10.15. The *P-V* trajectory is plotted in Fig. 10.16 to illustrate the evolution of voltage collapse at Bus4.

- The disturbance takes place at t = 1sec.
- Shunt capacitors are automatically connected at t = 1.2sec.
- Oscillations are quickly damped out.
- OEL of generator is activated at t = 32.6sec.
- OLTC of transformer starts to act at t = 19.4sec, trying to restore the voltage of Bus3.
- OLTC arrives at the lowest ratio at t = 120sec.
- Voltage of Bus4 collapses at t=138sec.

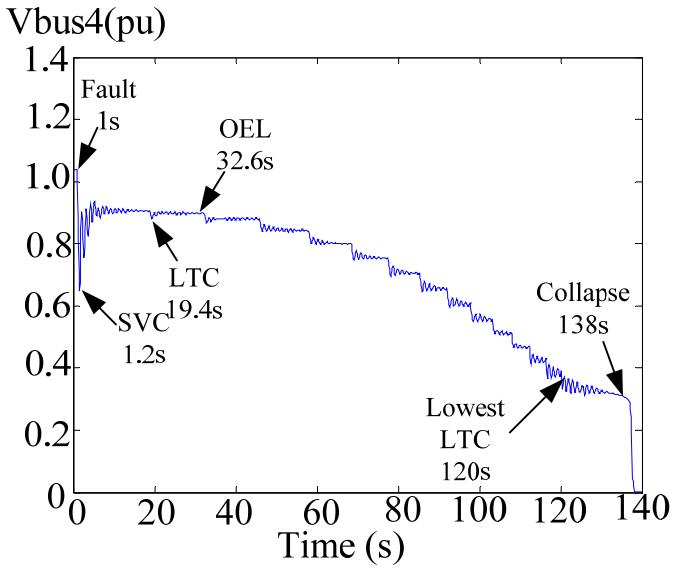

Fig. 10.15 Voltage of Bus 4 in Case A without adaptive corrective scheme.

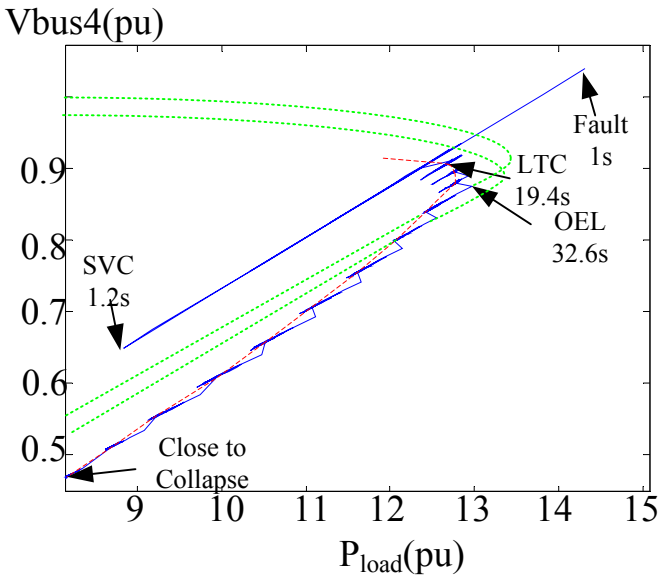

Fig. 10.16 *P-V* trajectory of Bus4 in Case A without adaptive corrective scheme.

If the adaptive corrective scheme is implemented, PMU can predict the voltage trajectory based on the parameters of load and power source. Since the load exponents are higher than 1.0, it is predicted that the voltage will not collapse soon. The countermeasure is OLTC blocking if the bus voltage continues decreasing. If the voltage is still lower than the lower limit, the cascading multi-step load shedding is activated with different time delays. Fig. 10.17 shows the voltage of Bus4. The OLTC blocked at t = 60.2sec, the voltage is stable but still lower than required value (0.9pu), so 2 steps of load shedding (each with 5%) draw the voltage back to normal condition at t = 70sec and t = 90sec respectively.

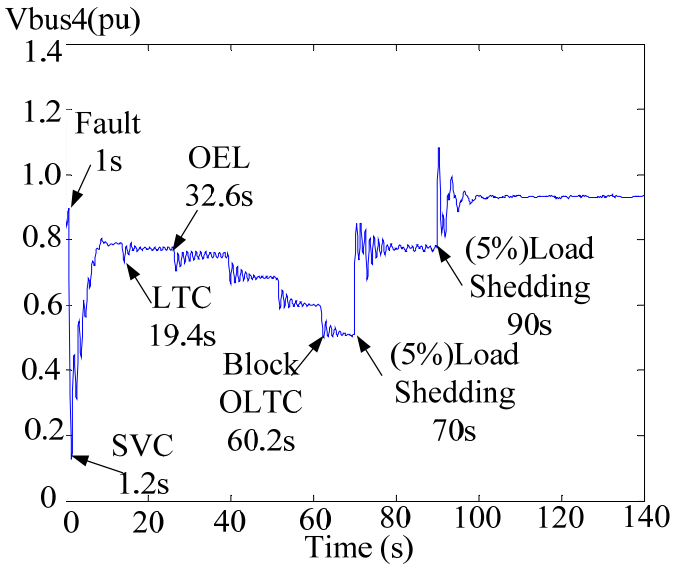

Fig. 10.17 Voltage of Bus4 in Case A with adaptive corrective scheme.

Case B: Low load exponents

The load in Case B is the same with Case A but with low load exponents as 0.802 and 0.603, respectively. The voltage would collapse immediately after the disturbance due to the load imbalance, unless the prearranged 5% load shedding took action at t = 1.2sec. Fig. 10.18 shows the voltage of Bus4 and Fig. 10.19 shows the *P-V* trajectory of Bus4.

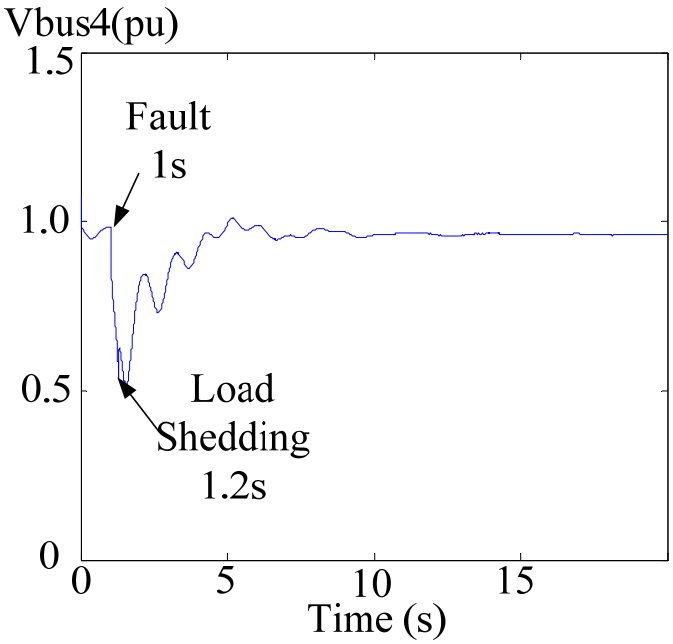

Fig. 10.18 Voltage of Bus 4 in Case B with adaptive corrective scheme.

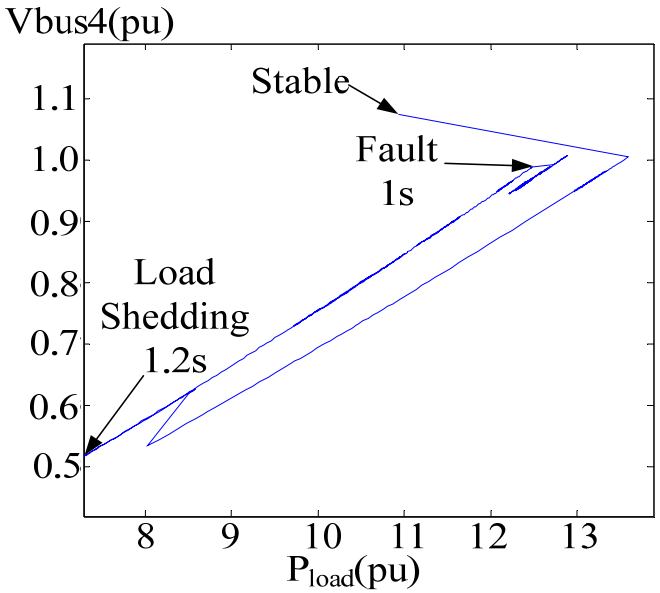

Fig. 10.19 *P-V* trajectory of Bus 4 in Case B with corrective scheme.

10.5 Summary

This chapter analyzes the principles of voltage stability problem and explores the relationship between voltage collapse points and the load characteristics. An adaptive voltage corrective scheme based on the identification of load characteristic and power source parameters using PMU measurements is proposed. The proposed methodology can predict and classify the long-term and short-term voltage instability and minimize the amount of load shedding in the circumstance of mid-term or long-term voltage instability. The test is demonstrated on a 4-Bus small-scale power system. However, more detailed verification will be carried out on western Danish power system in the future.

References

[1] C. W. Taylor, *Power System Voltage Stability*. New York: McGraw-Hill, 1994.

[2] B. Milosevic and M. Begovic, "Voltage-stability protection and control using a wide-area network of phasor measurements," *IEEE Trans. Power Syst*, vol. 18, no. 1, pp. 121-127, Feb. 2003.

[3] A. G. Phadke, "Synchronized phasor measurements in power systems," *IEEE Comput. Appl. in Power*, vol. 6, no. 2, pp. 10-15, Apr. 1993.

[4] R. K. Mai, Z. Y. He, L. Fu *et al.*, "Dynamic phasor and frequency estimator for phasor measurement units," *IET Trans. Gener., Transm. and Distrib.*, vol. 4, no. 1, pp. 73-83, Jan. 2010.

[5] M. Zima, M. Larsson, P. Korba *et al.*, "Design aspects for wide-area monitoring and control systems," *Proc. of the IEEE*, vol. 93, no. 5, pp. 980-996, May 2005.

[6] V. Ajjarapu, *Computational Techniques for Voltage Stability Assessment and Control.* New York: Springer, 2006.

[7] Th. Van Cutsem, "Voltage instability: phenomena, countermeasures, and analysis methods," *Proc of the IEEE*, vol. 88, no. 2, pp. 208-227, Feb. 2000.

[8] C. Rehtanz and J. Bertsch, "Wide area measurement and protection system for emergency voltage stability control," in *Proc. of PES Winter Meeting*, New York, NY, USA, Jan. 2002.

[9] K. Vu, M. Begovic, D. Novosel *et al.*, "Use of local measurements to estimate voltage-stability margin," *IEEE Trans. Power Syst.*, vol. 14, no. 3, pp. 1029-1035, Aug. 1999.

[10] I. Smon, G. Verbic and F. Gubina, "Local voltage-stability index using Tellegen's theorem," *IEEE Trans on Power Syst.*, vol. 21, no. 3, pp. 1267-1275, Aug. 2006.

[11] M. Glavic and Th. Van Cutsem, "Wide-area detection of voltage instability from synchronized phasor measurements. Part I: principle," *IEEE Trans. Power Syst.*, vol. 24, no. 3, pp. 1408-1416, Aug. 2009.

[12] M. Glavic and Th. Van Cutsem, "Wide-area detection of voltage instability from synchronized phasor measurements. Part II: simulation results," *IEEE Trans. Power Syst.*, vol. 24, no. 3, pp. 1417-1425, Aug. 2009.

[13] *Power System Analysis Toolbox User Manual*, University of Castilla-La Mancha, Ciudad Real, Spain.

[14] F. Milano, *Power System Modelling and Scripting*, Springer, London, Aug. 2010.

[15] Th. Van Cutsem and C. Vournas, *Voltage Stability of Electric Power Systems*, Norwell, MA, USA: Kluwer Academic Publisher, 1998.

PART V

CONCLUSIONS AND PERSPECTIVES

Chapter 11

Conclusions and Future Work

11.1 Conclusions

The main objective of this research is to develop adaptive and intelligent control and protection schemes based on WAMS to ensure the secure operation of western Danish power system. This dissertation has assessed the structural and dynamic vulnerability of western Danish power system with large scale wind power generation and other dispersed generation, addressed various technical issues in the wide-area control and protection of the transmission power system in western Denmark under the help of WAMS/PMU, such as dynamic security assessment, preventive control and corrective control schemes.

Since the invention of PMU in the 1990s, the installation of PMUs has increased considerably all over the world and applications of WAMS have undergone a rapid expansion. Danish power system is also paying effort to the development of WAMS, and many PMUs have been commissioned in recent years. However, the full utilization of these PMUs has extraordinary significance for Danish power system. More specifically, the WAMS in Danish power system should not only be used in power system monitoring as the current application but also in the system-level control and protection to maintain the secure operation of power system, to improve the system stability, to reduce the risk of blackouts, etc. as future applications.

Many advanced WAMPAC techniques have been developed worldwide so far, but they should be based on the fully understanding of the vulnerable areas and thoroughly evaluation of power systems characteristics. In terms of the characteristics of current Danish power system and the challenges of future Danish power system, the vulnerability of Danish power system has been assessed based on two aspects: structural vulnerability and dynamic vulnerability.

For the aspect of structural vulnerability, several vulnerability indices have been evaluated to assess the impact of DG on power systems. The assessment shows that DG units are able to shorten the electrical distance between power sources and power loads, alleviate long-distance large-capacity transmission, improve the reliability of power system after contingencies, and increase transmission efficiency.

For the aspect of dynamic vulnerability, CCT is computed by the screening of a number of contingencies in various OCs in western Danish power system. It has been concluded that the transient stability is highly dependent on the power flow patterns. The outputs of CPPs are the most dominant factor of transient stability. Besides, under the same load of CPP, the less load consumption and the higher wind power generation are generally harmful to the transient stability of western Danish power system.

It has been observed that the critical contingencies identified by both aspects of vulnerability assessment are different due to different evaluation criteria. In Chapter 4, structural vulnerability assessment is to evaluate the ability of a network in transmitting the electric power from the power sources nodes to the load consumption nodes from statistical point of view, which is related to the steady-state operation of the power grid, so power flow calculation is sufficient for the study of structural vulnerability assessment. Whilst, dynamic vulnerability assessment in Chapter 5, mainly focuses on the transient stability considering the dynamic behavior of power system, so T-D simulation is necessary for the study of dynamic vulnerability assessment. Especially, the recognized critical contingencies by dynamic vulnerability assessment can also provide the reference (credible contingency set) for the study of online DSA in Chapter 9.

Since power system is a non-linear dynamic system and integrated with a large number of renewable energy generation units, the dynamic behavior of such a complex system after the disturbance is complicated. In addition, a huge number of OCs together with a lot of credible contingencies bring more challenges to the DSA of power systems, especially considering the generation from a large number of wind farms and DG units. Therefore, data mining is a suitable solution to this complex issue. Superior to other data mining techniques, DT and its associated algorithms have been adopted for western Danish power system, because they can not only provide the results of DSA with high accuracy but also reveal the principles learned by DTs for preventive control scheme.

Then, importance sampling method has been adopted to prepare the database of data mining in order to reduce the computation burden of online DSA. A cooperative strategy based on the application of paralleled DTs has been used in preventive control to draw the operating point to the secure region in the case of the insecure operation of power system. Later on, the optimization of preventive control trajectory with consideration of domestic generation rescheduling cost and international penalty has been carried out for western Danish power system. According to the verification by a set of critical contingencies, 98% of the random generated extreme insecure OCs

can be controlled and guided back to the secure region without violation of international power exchange. If the practical data from industry can be obtained and considered, the result will indicate much higher reliability rate than 98%.

Furthermore, RF has been implemented for the online DSA of western Danish power system, which is capable of not only predicting the security of power system with higher accuracy, but also telling the adaptability of the created RF model in terms of outlier index. The utilization of outlier index has successfully filtered out the unsure cases and improved the accuracy of online DSA to 100%.

Other applications of PMU have also been proposed. The PMU has been used to identify the load characteristics and parameters of the Thevenin equivalent circuit of external grid. Since the load characteristic has close relationship with the voltage collapse pioint, *P0-V* curve instead of *P-V* curve has been proposed to predict the voltage collapse. Then online adaptive corrective scheme based on different load characteristics has been used to successfully minimize the load shedding for preventing the mid-term and long-term voltage instability.

As concluded above, this PhD dissertation has addressed some of the major issues regarding wide-area control and protection of Danish transmission power system. Issues with online DSA, preventive control, corrective control have been covered. Simulation results have showed that these proposed methodologies are able to successfully address these issues.

11.2 Future Work

Although many aspects regarding adaptive and intelligent control and protection of power systems based on WAMS have been covered by this dissertation, several other issues are interesting for future investigation. Some of the issues that are deemed valuable are listed as follows:

1. This research concentrates on the issues of transient stability and voltage stability due to the severity status and the requirement of Danish power system. Other stability issues, such as frequency stability and small signal stability have not been included in this research, but some of the approaches can deal with these stability issues by simple modification in the programming.

2. The issues of bit error and communication delay of WAMS have not considered and the observability redundancy has not been taken into account in this research. For the future research, the issue of missing data and the backup

strategy for the malfunction of PMU or the malfunction of communication channels should be explored.

3. In the online DSA of Danish power system, wind farm outputs are based on the probability distribution density of forecast error with respect to the forecasted wind power generation level of whole Danish power system. However, in the future research, the wind farm outputs should be associated with their geographical information, and the portfolio effect of wind speed to power system stability should be investigated.

4. The model of dynamic elements in Danish power system is of crucial importance because the effectiveness of online DSA and preventive control scheme is dependent on the accuracy of power system model. Some dynamic models are not accurate (e.g. HVDC model), the dynamic support from HVDC control, especially VSC-HVDC links connecting Norway and Netherlands for future Danish power system can be investigated.

5. The wind farms are modeled according to current Danish grid codes (discussed in Chapter 5). The impact of wind farms' dynamic control (e.g. LVRT and virtual inertia) on system security can be considered and evaluated for the future research.

6. In Chapter 9, the reliability of online DSA and preventive control scheme for Danish power system are of great significance for industrial application. However, due to the limited time and the lack of real operational data from industry, the reliability of the proposed approach still stays in the estimated values. After further cooperation with Danish TSO, the author is confident that the proposed approach can be used for Danish TSO one day. However, there will be a lot of work regarding field-test and verification, as well as the visualization and man-machine interface of the proposed approach.

7. In Chapter 10, the research of corrective scheme based on load characteristics identification, the dynamic load, such as induction motors, has not been considered. An adaptive load shedding scheme also considering dynamic characteristics of load will be developed in the near future.

APPENDICES

Appendix A –Map of Danish Power System in 2010

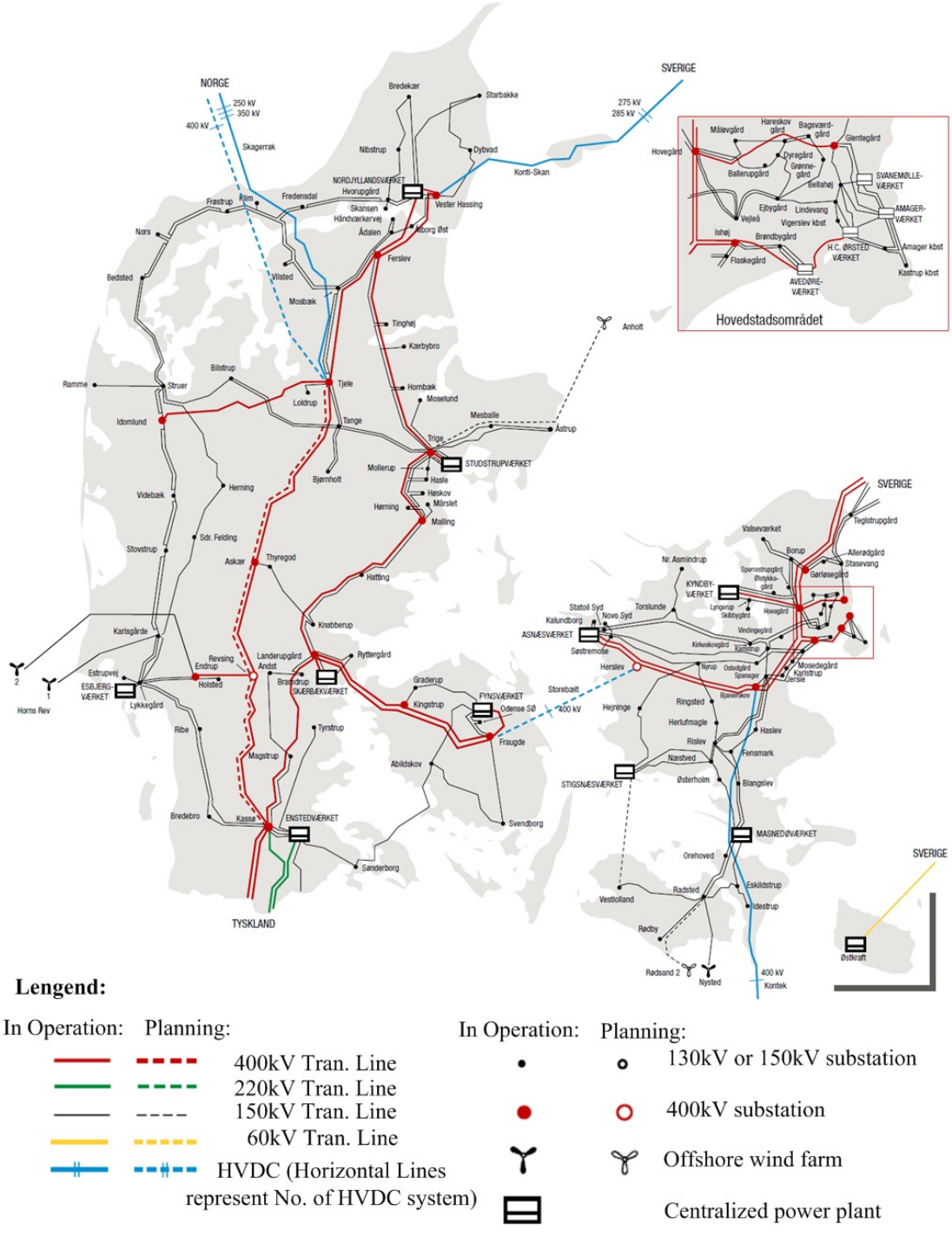

Fig. A.1 Geographical map of Danish transmission system in 2011.

Reference: Dansk elforsyning 2009, statistik, pp. 9. danskenergi, 2009, [Online]. Available: http://www.danskenergi.dk/~/media/Energi_i_tal/Dansk_Elforsyning_Statistik_2009.pdf.ashx assessed on 21-Sep-2013.

Appendix B – Analysis of Accuracy of Decision Trees

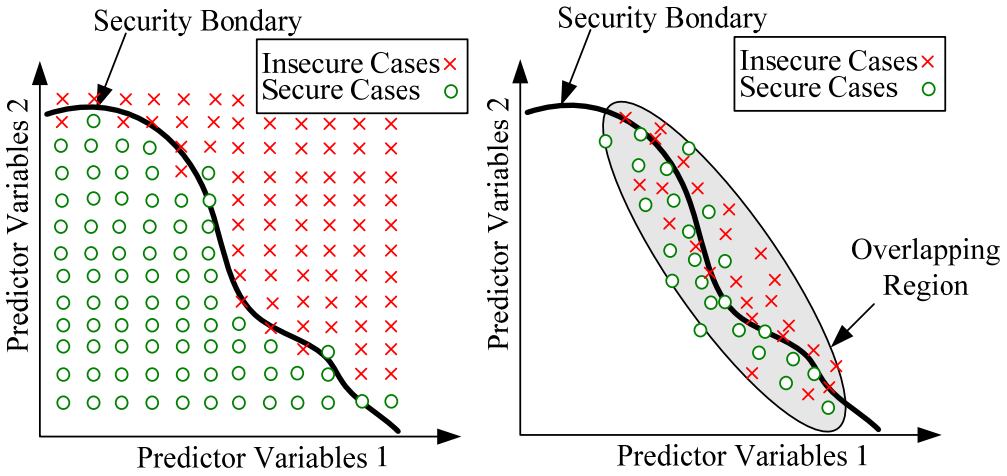

(a) Conventional sampling (b) Importance sampling

Fig. B.1 Selection of operating conditions.

Assuming that all cases by importance sampling are within the overlapping region, as shown in Fig B.1., the accuracy percentages calculated by different sampling methods are expressed by equations in Table B.1, where m_I and m_N are the numbers of misclassified cases by importance sampling (IS) and normal sampling (NS) respectively; N_1 and N_2 are the numbers of cases sampled inside the overlapping region and outside the overlapping region, respectively; δ is the rare-event probability that OCs locates in the overlapping region, which is from the statistical data of industry. Normally, $m_I > m_N$, $N_1 < N_2$, and $\delta << 1$, so the accuracy percentage with database prepared by IS indicates lower values, as shown in (B.1).

$$1-\frac{m_I}{N_1} < 1-\frac{m_N}{N_1+N_2} < 1-\frac{\delta m_N}{\delta N_1+(1-\delta)N_2} \tag{B.1}$$

TABLE B.1 EXPRESSIONS OF ACCURACY

Sampling methods	Accuracy (%)
Internal test with N_1 samples by IS	$(1-m_I/N_1)*100$
Internal test with N_1+N_2 samples by NS	$[1-m_N/(N_1+N_2)]*100$
Industrial data	$\{1-\delta m_N/[\delta N_1+(1-\delta)N_2]\}*100$

Appendix C – Proof of Equations of *P0-V* Curve

The proof of equations to represent *P0-V* curve is based on Bifurcation Theory, most commonly applied to mathematical study of dynamic systems. A bifurcation occurs when a small variation in parameter values of a system causes a sudden structural or topological change in the qualitative behavior of the dynamic system. A power system is also a dynamic non-linear physical system which can be represented by a group of differential equations and algebraic equations, as defined in (C.1)

$$\begin{cases} \dot{\mathbf{x}} = f(\mathbf{x}, \mathbf{y}, \mu) \\ \mathbf{0} = g(\mathbf{x}, \mathbf{y}, \mu) \end{cases} \tag{C.1}$$

where $\mathbf{x}$ is the vector of state variables, $\mathbf{y}$ is the vector of output variables, μ is the control parameter. When the non-linear system is in equilibrium state, the system can be defined as equations in (C.2),

$$\begin{cases} 0 = f(x_0, y_0, \mu_0) \\ 0 = g(x_0, y_0, \mu_0) \end{cases} \tag{C.2}$$

where ($\mathbf{x}_0$, $\mathbf{y}_0$, μ_0) is the equilibrium state. Assuming the input parameter is static, $d\mu=0$, non-linear system can be linearized by Jacobian Matrix at ($\mathbf{x}_0$, $\mathbf{y}_0$, μ_0), as expressed in (C.3).

$$\begin{cases} \dfrac{dx}{dt} = \dfrac{\partial f(x_0, y_0, \mu_0)}{\partial x} dx + \dfrac{\partial f(x_0, y_0, \mu_0)}{\partial y} dy \\ 0 = \dfrac{\partial g(x_0, y_0, \mu_0)}{\partial x} dx + \dfrac{\partial g(x_0, y_0, \mu_0)}{\partial y} dy \end{cases} \tag{C.3}$$

(C.3) can be transformed to (C.4),

$$\frac{dx}{dt} = \left[J_1 - J_2 J_3^{-1} J_4 \right] dx \tag{C.4}$$

where $J_1 = \dfrac{\partial f(x_0, y_0, \mu_0)}{\partial x}$ $J_2 = \dfrac{\partial f(x_0, y_0, \mu_0)}{\partial y}$ $J_3 = \dfrac{\partial g(x_0, y_0, \mu_0)}{\partial y}$ $J_4 = \dfrac{\partial g(x_0, y_0, \mu_0)}{\partial x}$

From (C.4), it is easy to find out that when $|J_1 - J_4^{-1} J_3| = 0$, there is no solution for the next step of x, the system approaches to the static bifurcation point, which is shwon in (C.5).

$$\left| J_1 - J_2 J_4^{-1} J_3 \right| = 0 \Rightarrow \left| J_4 \right| \neq 0, \text{ and } \left| J_1 J_4 - J_2 J_3 \right| = 0 \tag{C.4}$$

As shown in Fig. C.1, for a 2-bus single load power system, power flow equation is defined in (C.5).

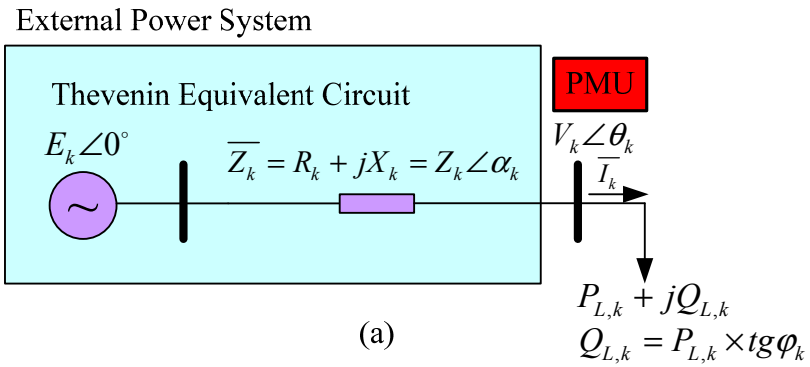

Fig. C.1. Two-bus power system.

$$\begin{cases} P_{L,k} - \left[\dfrac{E_k V_k}{Z_k}\cos(\alpha_k+\theta_k) - \dfrac{V_k^2}{Z_k}\cos\alpha_k\right] = 0 \\ Q_{L,k} - \left[\dfrac{E_k V_k}{Z_k}\sin(\alpha_k+\theta_k) - \dfrac{V_k^2}{Z_k}\sin\alpha_k\right] = 0 \end{cases} \tag{C.5}$$

Appendix C.1 Constant Power Load

For constant power load, when (p_u=q_u =0).

$$\begin{cases} P_{L,k} = P_{L0} \\ Q_{L,k} = Q_{L0} \\ tg\varphi_k = Q_{L,k}/\mathrm{P}_{L,k} \end{cases} \tag{C.6}$$

Then, (C.7) is obtained by substituting (C.6) into (C.5).

$$\begin{cases} F(V_k,\theta_k,Q_{L0}) = Q_{L0} - \left[\dfrac{E_k V_k}{Z_k}\sin(\alpha_k+\theta_k) - \dfrac{V_k^2}{Z_k}\sin\alpha_k\right] = 0 \\ G(V_k,\theta_k,P_{L0}) = P_{L0} - \left[\dfrac{E_k V_k}{Z_k}\cos(\alpha_k+\theta_k) - \dfrac{V_k^2}{Z_k}\cos\alpha_k\right] = 0 \end{cases} \tag{C.7}$$

In (C.7), V_k and θ_k are state variables, and P_{L0} and Q_{L0} are considered as control parameters, so Jacobian Matrix of (C.7) is expressed by the following equations (C.8)-(C.11)

$$J_1 = \frac{\partial F}{\partial V_k} = -\frac{E_k}{Z_k}\sin(\alpha_k+\theta_k) + \frac{2V_k}{Z_k}\sin\alpha_k \tag{C.8}$$

$$J_2 = \frac{\partial F}{\partial \theta_k} = -\frac{E_k V_k}{Z_k}\cos(\alpha_k+\theta_k) \tag{C.9}$$

$$J_3 = \frac{\partial G}{\partial V_k} = -\frac{E_k}{Z_k}\cos(\alpha_k+\theta_k) + \frac{2V_k}{Z_k}\cos\alpha_k \tag{C.10}$$

$$J_4 = \frac{\partial G}{\partial \theta_k} = \frac{E_k V_k}{Z_k}\sin(\alpha_k+\theta_k) \tag{C.11}$$

Based on the bifurcation theory, the collapse point ($P_{L0,m}$, $V_{k,cr}$) must satisfy the equation in (C.4).

a) $|J_4| \neq 0$, so that $\alpha_k + \theta_{cr} \neq n\pi$.

b) $|J_1 J_4 - J_2 J_3| = 0$, one can obtain the equation in (C.12) and (C.13)

$$\cos\theta_{cr} = \frac{E_k}{2V_{k,cr}} \tag{C.12}$$

$$\sin\theta_{cr} = -\sqrt{1-\left(\frac{E_k}{2V_{k,cr}}\right)^2} \tag{C.13}$$

Substituting (C.12) and (C.13) to (C.7), the power flow equations can be transformed to (C.14).

$$\begin{cases} -V_{k.cr}^2 \sin\alpha_k - \dfrac{E_k\sqrt{4V_{k.cr}^2 - E_k^2}}{2}\cos\alpha_k + \dfrac{E_k^2}{2}\sin\alpha_k - Q_{L0,m}Z_k = 0 \\ -V_{k.cr}^2 \cos\alpha_k + \dfrac{E_k\sqrt{4V_{k.cr}^2 - E_k^2}}{2}\sin\alpha_k + \dfrac{E_k^2}{2}\cos\alpha_k - P_{L0,m}Z_k = 0 \end{cases} \tag{C.14}$$

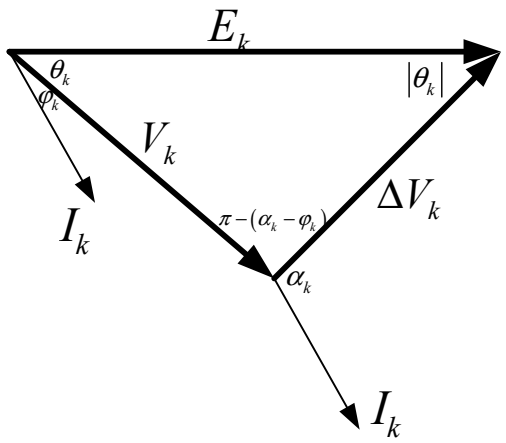

Fig. C.2. Phasor vector diagram of 2-bus power system in critical point.

Assuming the power factor angle φ_k at time $t=t_k$ is measured and calculated by PMU according to $\varphi_k = arcctg(Q_k/P_k)$, the collapse point ($P_{L0,m}$, $V_{k,cr}$) in (C.14) can be expressed (C.15). Please note that (C.15) can also be calculated by Law of Cosines, according to Fig. C.2, where $V_k = \Delta V_k$.

$$\begin{cases} P_{L0,m} = E_k^2 \cos\varphi_k \Big/ \left\{2Z_k\left[1+\cos\left(\alpha_k-\varphi_k\right)\right]\right\} \\ V_{k.cr} = E_k \Big/ \sqrt{2\left[1+\cos\left(\alpha_k-\varphi_k\right)\right]} \end{cases} \tag{C.15}$$

Appendix C.2 Constant Current Load

For constant power load, when (p_u=q_u =*1*).

$$\begin{cases} P_{L,k} = P_{L0} V_k \\ Q_{L,k} = Q_{L0} V_k \\ tg\varphi_k = Q_{L,k} / \mathrm{P}_{L,k} \end{cases} \tag{C.16}$$

Then, (C.17) is obtained by substituting (C.16) into (C.5).

$$\begin{cases} F(V_k, \theta_k, Q_{L0}) = Q_{L0} - \left[\dfrac{E_k}{Z_k} \sin(\alpha_k + \theta_k) - \dfrac{V_k}{Z_k} \sin\alpha_k \right] = 0 \\ G(V_k, \theta_k, P_{L0}) = P_{L0} - \left[\dfrac{E_k}{Z_k} \cos(\alpha_k + \theta_k) - \dfrac{V_k}{Z_k} \cos\alpha_k \right] = 0 \end{cases} \tag{C.17}$$

In (C.17), V_k and θ_k are state variables, and P_{L0} and Q_{L0} are considered as control parameters, so Jacobian Matrix of (C.17) is expressed by the following equations (C.18)-(C.21)

$$J_1 = \frac{\partial F}{\partial V_k} = \frac{\sin\alpha_k}{Z_k} \tag{C.18}$$

$$J_2 = \frac{\partial F}{\partial \theta_k} = -\frac{E_k}{Z_k} \cos(\alpha_k + \theta_k) \tag{C.19}$$

$$J_3 = \frac{\partial G}{\partial V_k} = \frac{\cos\alpha_k}{Z_k} \tag{C.20}$$

$$J_4 = \frac{\partial G}{\partial \theta_k} = \frac{E_k}{Z_k} \sin(\alpha_k + \theta_k) \tag{C.21}$$

Based on the bifurcation theory, the collapse point ($P_{L0,m}$, $V_{k,cr}$) must satisfy the equation in (C.4).

a) $|J_4| \neq 0$, so that $\alpha_k + \theta_{cr} \neq n\pi$.

b) $|J_1 J_4 - J_2 J_3| = 0$, one can obtain the equation in (C.22)

$$\left[\frac{\sin\alpha_k}{Z_k} \right] \left[\frac{E_k}{Z_k} \sin(\alpha_k + \theta_{cr}) \right] - \left[-\frac{E_k}{Z_k} \cos(\alpha_k + \theta_{cr}) \right] \left[\frac{\cos\alpha_k}{Z_k} \right] = 0 \tag{C.22}$$

(C.22) can be simplified to (C.23)

$$E_k \cos\theta_{cr} = 0 \tag{C.23}$$

where $\theta_{cr} = -\pi/2$. Assuming the power factor angle φ_k at time $t=t_k$ is measured and calculated by PMU according to $\varphi_k = arcctg(Q_k/P_k)$, the collapse point ($P_{L0,m}$, $V_{k,cr}$) in (C.23) can be expressed (C.24).

$$\begin{cases} P_{L0,m} = E_k / \left[Z_k (\sin\alpha_k - \cos\alpha_k tg\varphi_k) \right] \\ V_{k.cr} = E_k (\sin\alpha_k tg\varphi_k + \cos\alpha_k) / (\cos\alpha_k tg\varphi_k - \sin\alpha_k) \end{cases} \tag{C.24}$$

Appendix C.3 Constant Impedance Load

For constant power load, when (p_u=q_u =*2*).

$$\begin{cases} P_{L,k} = P_{L0}V_k^2 \\ Q_{L,k} = Q_{L0}V_k^2 \\ tg\varphi_k = Q_{L,k}/\mathrm{P}_{L,k} \end{cases} \tag{C.25}$$

Then, (C.26) is obtained by substituting (C.25) into (C.5).

$$\begin{cases} F(V_k,\theta_k,Q_{L0}) = Q_{L0} - \left[\dfrac{E_k}{Z_kV_k}\sin(\alpha_k+\theta_k) - \dfrac{1}{Z_k}\sin\alpha_k\right] = 0 \\ G(V_k,\theta_k,P_{L0}) = P_{L0} - \left[\dfrac{E_k}{Z_kV_k}\cos(\alpha_k+\theta_k) - \dfrac{1}{Z_k}\cos\alpha_k\right] = 0 \end{cases} \tag{C.26}$$

In (C.17), V_k and θ_k are state variables, and P_{L0} and Q_{L0} are considered as control parameters, so Jacobian Matrix of (C.26) is expressed by the following equations (C.27)-(C.30)

$$J_1 = \frac{\partial F}{\partial V_k} = \frac{E_k}{Z_kV_k^2}\sin(\alpha_k+\theta_k) \tag{C.27}$$

$$J_2 = \frac{\partial F}{\partial \theta_k} = -\frac{E_k}{Z_kV_k}\cos(\alpha_k+\theta_k) \tag{C.28}$$

$$J_3 = \frac{\partial G}{\partial V_k} = \frac{E_k}{Z_kV_k^2}\cos(\alpha_k+\theta_k) \tag{C.29}$$

$$J_4 = \frac{\partial G}{\partial \theta_k} = \frac{E_k}{Z_kV_k}\sin(\alpha_k+\theta_k) \tag{C.30}$$

Based on the bifurcation theory, the collapse point ($P_{L0,m}$, $V_{k,cr}$) must satisfy the equation in (C.4).

a) $|J_4| \neq 0$, so that $\alpha_k + \theta_{cr} \neq n\pi$.

b) $|J_1J_4 - J_2J_3| = 0$, one can obtain the equation in (C.31)

$$\frac{E_k}{Z_kV_k^2}\frac{E_k}{Z_kV_k}\left[\sin^2(\alpha_k+\theta_k) + \cos^2(\alpha_k+\theta_k)\right] = 0 \tag{C.31}$$

The collapse point must meet (C.32)

$$E_k^2 / \left(Z_k^2V_{k,cr}^3\right) = 0 \tag{C.32}$$

where E_k>*0* and Z_k>*0*, so the critical voltage point is $V_{k,cr}$ = ±∞.

Appendix C.4 General Static Load

For general static load, when (p_u=*m*, q_u =*r*).

$$\begin{cases} P_{L,k} = P_{L0} V_k^m \\ Q_{L,k} = Q_{L0} V_k^r \\ tg\varphi_k = Q_{L,k} / \mathrm{P}_{L,k} \end{cases} \tag{C.33}$$

Then, (C.34) is obtained by substituting (C.33) into (C.5).

$$\begin{cases} F(V_k, \theta_k, Q_{L0}) = Q_{L0} - \left[\dfrac{E_k V_k^{1-r}}{Z_k} \sin(\alpha_k + \theta_k) - \dfrac{V_k^{2-r}}{Z_k} \sin\alpha_k \right] = 0 \\ G(V_k, \theta_k, P_{L0}) = P_{L0} - \left[\dfrac{E_k V_k^{1-m}}{Z_k} \cos(\alpha_k + \theta_k) - \dfrac{V_k^{2-m}}{Z_k} \cos\alpha_k \right] = 0 \end{cases} \tag{C.34}$$

In (C.34), V_k and θ_k are state variables, and P_{L0} and Q_{L0} are considered as control parameters, so Jacobian Matrix of (C.34) is expressed by the following equations (C.35)-(C.38)

$$J_1 = \frac{\partial F}{\partial V_k} = \frac{(2-r)V_{k,cr}^{1-r}}{Z_k} \sin\alpha_k - \frac{E_k(1-r)V_{k,cr}^{-r}}{Z_k} \sin(\alpha_k + \theta_{cr}) \tag{C.35}$$

$$J_2 = \frac{\partial F}{\partial \theta_k} = -\frac{E_k V_{k,cr}^{1-r}}{Z_k} \cos(\alpha_k + \theta_{cr}) \tag{C.36}$$

$$J_3 = \frac{\partial G}{\partial V_k} = \frac{(2-m)V_{k,cr}^{1-m}}{Z_k} \cos\alpha_k - \frac{E_k(1-m)V_{k,cr}^{-m}}{Z_k} \cos(\alpha_k + \theta_{cr}) \tag{C.37}$$

$$J_4 = \frac{\partial G}{\partial \theta_k} = \frac{E_k V_{k,cr}^{1-m}}{Z_k} \sin(\alpha_k + \theta_{cr}) \tag{C.38}$$

Based on the bifurcation theory, the collapse point ($P_{L0,m}$, $V_{k,cr}$) can be expressed in (C.39).

$$\begin{aligned} F(V_{k,cr}, \theta_{cr}) = V_{k,cr} \left[(2-r)\sin\alpha_k \sin(\alpha_k + \theta_{cr}) + (2-m)\cos\alpha_k \cos(\alpha_k + \theta_{cr}) \right] \\ -E_k \left[1 - r\sin^2(\alpha_k + \theta_{cr}) - m\cos^2(\alpha_k + \theta_{cr}) \right] = 0 \end{aligned} \tag{C.39}$$

where $\alpha_k + \theta_{cr} \neq n\pi$. Finally, critical voltage point ($V_{k,cr}$, θ_{cr}) is expressed as (C.40),

$$V_{k,cr} = \frac{E_k \left[1 - r\sin^2\left(\dfrac{\alpha_k + \varphi_k}{2} \right) - m\cos^2\left(\dfrac{\alpha_k + \varphi_k}{2} \right) \right]}{(2-r)\sin\alpha_k \sin\left(\dfrac{\alpha_k + \varphi_k}{2} \right) + (2-m)\cos\alpha_k \cos\left(\dfrac{\alpha_k + \varphi_k}{2} \right)} \tag{C.40}$$

where $\alpha_k + \theta_{cr} \neq n\pi$ and $\theta_{cr} = \dfrac{\varphi_k - \alpha_k}{2}$.

Appendix D – Data of 4-Bus Test Power System

TABLE D.1 PARAMETERS OF 4-BUS TEST SYSTEM

System structure parameters (in pu. on 100MVA base)	
Reactance bus1-bus4 X_{14} (pu)	0.035
Reactance bus2-bus4 X_{24} (pu)	0.016
Reactance bus3-bus4 X_{34} (pu)	0.004
Generator parameters (in pu on 500MVA base)	
Generator step-up transformer ratio n	1.04
d-axis reactance X_d (pu), $X_d^{/}$ (pu), $X_d^{//}$ (pu)	2.1, 0.4, 0.204
q-axis reactance X_q (pu), $X_q^{/}$ (pu), $X_q^{//}$ (pu)	2.1, 0.5, 0.3
d-axis time constant $T_{d0}^{/}$ (s), $T_{d0}^{//}$ (s)	8, 0.04
q-axis time constant $T_{q0}^{/}$ (s), $T_{q0}^{//}$ (s)	1.8, 0.03
Inertia H (s)	3.5
Damping G (pu)	4
AVR parameters	
Regulator Gain G	50
Time Constant of Field Circuit T_f	0.7
Maximum Regulator Voltage V_{fdmax}	3
Minimum Regulator Voltage V_{fdmin}	0
OEL parameters	
Integrator time constant T_0	5
Maximum field current i_{fdmin}	0.825
OLTC parameters	
Maximum tap ratio r_{max}	1.1
Minimum tap ratio r_{min}	0.8
Tap ratio step $\triangle r$	0.02
Dead zone $d\%$	5%
Inverse time constant T_i	0.01

Practical Testing and Performance Analysis of Phasor Measurement Unit Using Real Time Digital Simulator (RTDS)

Chengxi Liu, Zakir Hussain Rather[#], Nathen Stearn[§], Zhe Chen*, Claus Leth Bak*, Paul Thøgersen[#]*

* Department of Energy Technology, Aalborg University
Pontoppidanstraede 101, Aalborg, Denmark-9220.

Innovation center kk-electronic a/s
Pontoppidanstraede 101, Aalborg, Denmark-9220

§ ALSTOM GRID,Substation Automation Solutions, St Leonards Avenue, Stafford, ST17 4LX, United Kingdom.

ABSTRACT

Wide Area Measurement Systems (WAMS) and Wide Area Monitoring, Protection and Control Systems (WAMPACS) have evolved rapidly over the last two decades [1]. This fast emerging technology enables real time synchronized monitoring of power systems. Presently, WAMS are mainly used for real time visualisation and post event analysis of power systems. It is expected however, that through integration with traditional Supervisory Control and Data Acquisition (SCADA) systems, closed loop control applications will be possible. Phasor Measurement Units (PMUs) are fundamental components of WAMS. Large WAMS may support PMUs from multiple manufacturers and therefore it is important that there is a way of standardising the measurement performance of these devices. Currently the IEEE Standard C37.118 is used to quantify the measurement performance of PMUs.

While standard specifications are also available for the testing of PMUs [2] there is a lack of specialised test equipment for performing such testing efficiently [3].

In this paper, RTDS based steady state and dynamic testing of the ALSTOM MiCOM P847 PMU using hardware in the loop is demonstrated. A correction algorithm supported by promising results is also proposed to realize highly precise phasor measurements. Further a comparative study based on features of PMUs from different major manufacturers is presented. The selection of optimal parameters, such as phasor format and filter length is also discussed for various applications.

Index Terms— IEEE C37.118, Phasor Measurement Unit, Total Vector Error, Wide Area Monitoring, Protection and Control.

1. INTRODUCTION

Since the beginning of PMU development which was initiated by Dr. Arun G. Phadke and Dr. James S. Thorp at Virginia Tech in 1988, the WAMS and WAMPACS have gained acceptance widely and developed rapidly around the world. Following several power system blackouts caused by system instability especially in 2003, WAMS and WAMPAC technologies have been pushed to the front of power system research. The PMU is capable of sampling voltage and current signals, processing these signals and transmitting them to a Phasor Data Concentrator (PDC). The sampling clock of the PMU is synchronized to the Universal Time Coordinated (UTC) signal to enable synchronized phase angle measurement from the instantaneous values of voltage and current.

WAMS help to monitor power system dynamics in real time, identify system stability related weakness and design and implement wide area control and protection schemes. A variety of online and offline applications such as voltage stability assessment [4], power system oscillation damping [5], online dynamic security assessment [6], system integrity protection schemes (SIPS) [7] and dynamic state estimation [8] have been achieved by using WAMS and WAMPAC technologies.

In contrast to standalone devices in a power system, the performance of WAMS is affected by the compatibility and consistency of PMUs. Some power system operators have been developing their WAMS in multiple stages over multiple time spans, so it is very possible that their final WAMS consists of PMUs with various algorithms and from various vendors. There is also a trend today that more and more Intelligent Electronic Devices (IED) such as digital fault recorders, revenue meters, power quality recorders, event recorders and measurements products are integrated with PMU functionality. As the compatibility and consistency among PMUs becomes more of an issue; the standard for PMU testing and performance analysis becomes more important for the development of WAMS and WAMPACS [7].

IEEE Standard C37.118-2005 “IEEE Standard for Synchrophasors for Power Systems” [10] was published in 2006 to replace IEEE Standard 1344-1995 [11], which

This work was supported mainly by ALSTOM GRID(UK) and in parts by kk-electronic a/s and Danske Strategiske Forskningscentre (DSF 09-067255).
Authors can be reached at cli@et.aau.dk or zahus@kk-electronic.com

mainly defined the message format interchanged between PMU devices and PDC

Although the accuracy of PMU measurements is high, there is a need for improvement, particularly under dynamic system conditions, for satisfactory operation of WAMPACS.

There have been ongoing activities for PMU testing and calibration. In [12], a comparative test was conducted among four PMUs from different manufacturers by Virginia Tech at both nominal and off-nominal frequencies. They have concluded that these PMUs responded differently in most of the situations, particularly in special conditions like off-nominal frequency. In [13], the author presented the progress of PMU testing and calibration in US and Brazil. In [14], a test setup for steady state testing of the PMU with Doble F6150 amplifier is developed. In [15], standardised testing of PMUs is proposed by Bonneville Power Administration (BPA), composed of steady-states tests, step tests, structured signal tests and noise, latency and environmental tests.

In this research work, a comparative study based on features of PMUs from various major manufacturers is discussed followed by a performance evaluation of the Alstom MiCOM P847 PMU using RTDS. Based on these tests a correction algorithm is also presented to realize high precision WAMS.

2. COMPARISON OF PMU

Since the development of PMUs various market players have evolved mainly due to rapid development of WAMS technology. However because of different design techniques and algorithms used by different PMU manufacturers, PMUs from different vendors do not show identical characteristics. WAMS which involve different no. of PMUs depending on the size of the targeted area and network topology, demand identical characteristics from all involved PMUs. Most WAMS projects are implemented in stages over a period of years, so it is likely that PMUs from different manufacturers will be installed in the same WAMS. Due to a lack of absolute standards and the requirement for innovation the possibility of different behaviors from PMUs from different manufacturers is to be expected.

We have made a comparative analysis of PMUs from major PMU manufacturers to highlight the differences in features provided by their devices. This comparative analysis is tabulated in the Appendix. It can be observed that features like frequency resolution, phasor resolution etc. are different for PMUs from different manufacturers. The difference in this characteristic behavior from these PMUs is bound to affect the accuracy of WAMS. The purpose of this comparative analysis is to reinforce the need for standards which can ensure the identical or close to identical measurement characteristics from all PMUs irrespective of the manufacturer.

3. RTDS BASED PMU TEST SETUP

The hardware in loop setup based on RTDS has been used to carry out the testing and performance analysis of the PMU. The architecture of the test set up is shown in Fig. 1 where the RTDS is the main source of power system signal generation (voltage and current) and these signals are fed to the PMU. Measured signals from the PMU are communicated to a Phasor Data Concentrator (PDC) through the Ethernet based TCP (Transmission Control Protocol) mode of communication. The PMU used in this experimental setup is a MiCOM P847 PMU from ALSTOM which is synchronized to the Global Positioning System (GPS) through a GPS receiver and antenna. The main features of the MiCOM P847 PMU are given in Table-I. Output signals with the desired parameters are generated from the RTDS using a Giga-Transceiver Analog Output (GTAO) interface.

Table I: Main features of the PMU used in the test setup

Model	P847-B
Voltage Inputs	3 (1 x 3-phase set or 3 x individual)
Current Inputs	4 x 3-phase set, or 12 individual
Relay Outputs	8
Digital Inputs	16
Redundant Ethernet	Yes

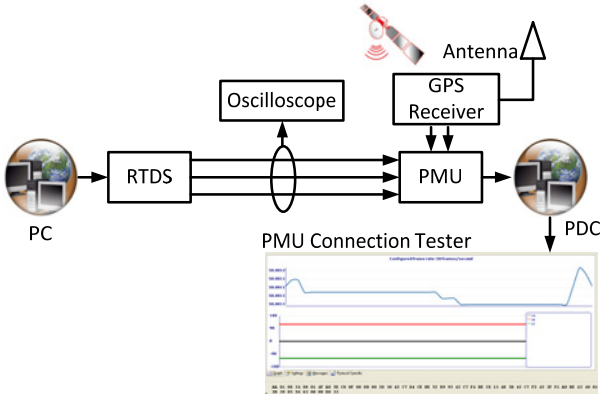

Fig. 1 Architecture of RTDS based Test Set up

Fig. 2 shows the pictorial view of the hardware setup with two rack based RTDS showing different connection details. From the GTAO card fixed in rack-1 of the RTDS, voltage and current signals are sent to the P847 PMU. The PMU is also connected to a PDC through serial port communication for configuration and data verification of Ethernet based communication. The Personal Computer (PC) is used to run and operate the RTDS software. The Oscilloscope is used to measure the input signal to the PMU.

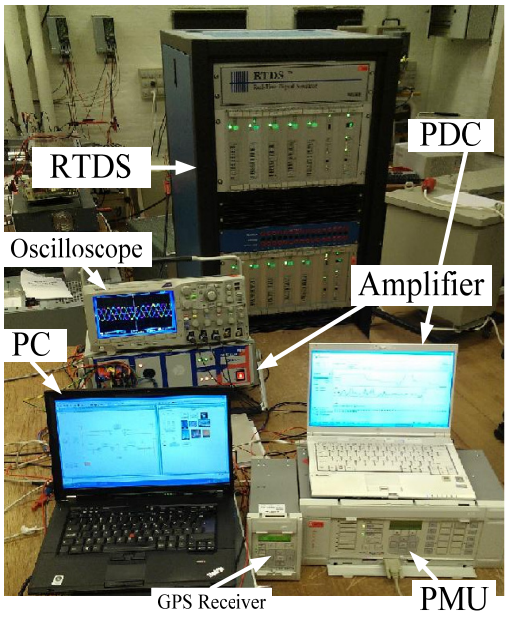

Fig.2 Hardware setup of the RTDS based PMU testing platform.

3. STEADY STATE TESTING

The steady state testing is the fundamental part of PMU performance estimation. For the steady state testing, steady state power system signals (voltage and current) are fed to the PMU from the RTDS via the GTAO card. In our experimental setup the following tests were performed to assess the impact of changing different parameters on the measurement performance of the PMU.

3.1 Effect of frequency on magnitude measurement

A voltage signal of 99.905 Volts at variable frequency was generated from the RTDS and supplied to the PMU. The corresponding measurement recorded by the PDC is plotted in Fig.3. It can be observed that for frequencies below the nominal value (50Hz) the measured voltage is below the actual value of input signal and with the increase in signal frequency from 45Hz to 50Hz the error in voltage magnitude decreases until it reaches a minimum at the nominal value. Further increases in frequency beyond the nominal value again increases the error in the measured value, however now the measured value is higher than the input signal value. Fig. 4 shows the effect of system frequency on the magnitude error confirming the least error at nominal frequency.

It can be concluded that the value of the magnitude error increases with the increase in variation of the signal frequency from the nominal value.

In order to realize high precision reliable WAMS, each PMU measurement can be corrected using a correction

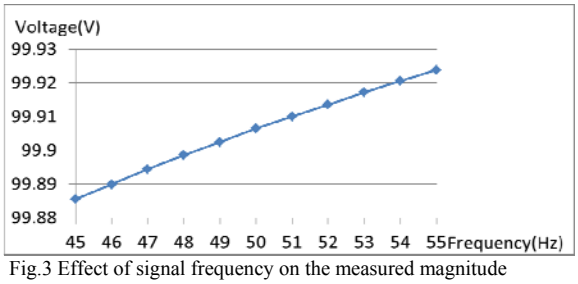

Fig.3 Effect of signal frequency on the measured magnitude of 99.905V input signal.

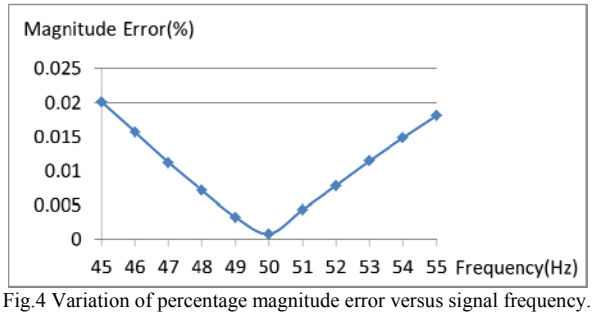

Fig.4 Variation of percentage magnitude error versus signal frequency.

signal based on appropriate test results for that specific PMU. For example in the case of this particular PMU, the percentage of magnitude error on different operating frequencies can be used to obtain the corrected value from the actual measured one.

3.2 Effect of signal frequency on phase and frequency Measurement.

Due to the PMU filter length and other design parameters, PMUs are relatively more precise at nominal frequency. The power system frequency however, often differs from the nominal value due to small perturbations in the system, both from the load as well as from the generation side. Moreover during disturbances in the power system, when higher measurement accuracy is of utmost need, measurements from PMU show an error depending on the offset from nominal frequency. In order to assess the effect of the signal frequency on the phase and frequency measurement error, two separate tests were performed on the ALSTOM MiCOM P847 PMU. Fig 5 and Fig 6 shows the phase error and frequency error at different signal frequencies. In order to achieve the smallest degree of measurement error, a correction factor for all measured variables could be implemented in the PDC. Therefore, in a similar way, tests showing the impact of different parameters on the measurement of PMUs could be performed through a reliable testing platform which eventually could be used to formulate a correction algorithm to process the measured data from different PMUs.

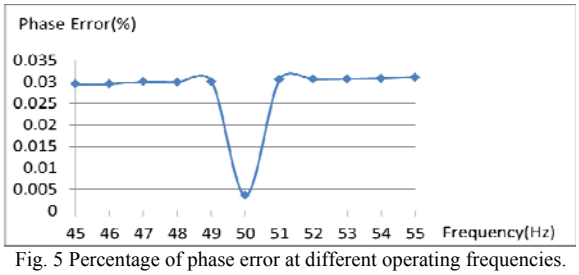

Fig. 5 Percentage of phase error at different operating frequencies.

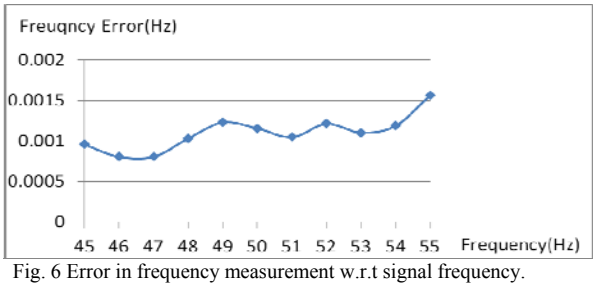

Fig. 6 Error in frequency measurement w.r.t signal frequency.

3.3 Total Vector Error

In order to assess PMU performance, the IEEE C37 118-2005 standard for synchrophasors has defined a performance index known as Total Vector Error (TVE). If a signal represented in the phasor domain $f = x_r^n + jx_i^n$, where x_r^n and x_i^n are real and imaginary components of a signal being sent to the PMU, then for the measured value of $g = x_r + jx_i$ corresponding to signal 'f', the TVE is defined as given by (1).

$$TVE = \sqrt{\frac{(x_r^n - x_r)^2 + (x_i^n - x_i)^2}{x_r^2 + x_i^2}} \qquad (1)$$

The value of the TVE under various conditions should be under 1% as given in Table II. In our experimental study the effect of the signal frequency on the TVE was observed as shown in Fig.7.

Since TVE involves aggregated error in the magnitude and phase of the measured signal, the TVE is expected to vary, similar to the variation of the magnitude and phase value of a particular signal. For this particular PMU, the maximum

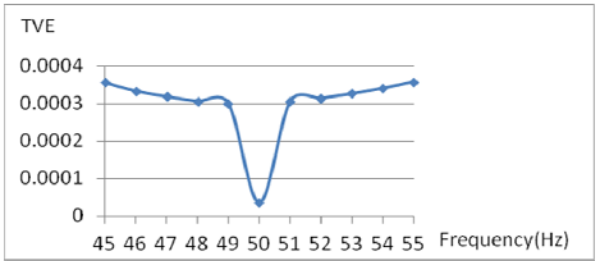

Fig. 7. Effect of Signal frequency on TVE.

TVE is 0.035% at the off nominal frequencies of 45Hz and 55Hz, however the minimum TVE is at nominal frequency as expected from the magnitude and phasor plots described earlier.

Table II. IEEE Std C37.118 – Compliance Requirements

Influence Quantity	Reference condition	Range Influence quantity with respect to reference and maximum allowable TVE in percent(%) for each compliance level			
		Level 0		Level 1	
		Range	TVE (%)	Range	TVE (%)
Signal Frequency	$F_{nominal}$	+/- 0.5Hz	1	+/- .5Hz	1
Signal Magnitude	100% rated	80% to 120% rated	1	10% to 120% rated	1
Phase angle	0 radians	+/- pi radians	1	+/- pi radians	1
Harmonic distortion	<0.2% (THD)	1% any harmonic up to 50th	1	10% any harmonic up to 50th	1
Out-of-band interfering signal at frequency f_i where mod(f_i-f_o)> F_s/2, F_s=Phasor reporting rate, f_o=$F_{nominal}$	<0.2% of input signal magnitude	1% of input signal magnitude	1	10% of input signal magnitude	1

3.4 Realization of Least Erroneous WAMS

As demonstrated in section 3.1-3.3 the error in measurements from PMUs varies with variation of signal parameters. The least error is observed at nominal values of parameters for which PMUs are designed. Since WAMS generally comprise of PMUs from different manufacturers or different models from the same manufacturer, the error in measurement will vary accordingly. Notwithstanding the difference in characteristics, even WAMS having identical PMUs will exhibit errors in measurements depending on the values of signal parameters like frequency. From our experimental study, it was observed that the behaviour of measurement errors with the variation in signal parameter is identical irrespective of the value of measured quantity. For example, the variation of voltage magnitude error at a particular frequency is almost same irrespective of the value of voltage magnitude. Therefore based on the test characteristics obtained from the PMU, a correction algorithm can be formulated and implemented in the PDC to minimize the net error of the measurements received. It is important to mention here that this proposed correction algorithm will be different for each PMU depending on its characteristic curves obtained from testing before its installation in the power system.

To demonstrate the proposed correction algorithm we have applied the correction factors for magnitude error obtained from the magnitude error characteristics for the voltage signal of 99.905V shown in Fig. 4. This correction factor was then applied to another signal of 89.919V and the measured data from the PMU was processed in the PDC using the correction algorithm. Actual measured and PDC corrected measurement data is plotted in Fig.8. Relative errors of actual PMU measurement and PDC corrected data is plotted in Fig. 9. The impact of the correction algorithm is clear as the relative error has reduced by around 83% at the maximum offset of 45Hz and 55Hz.

This correction algorithm can be extended to every measured variable like current, frequency and rate of change of frequency (ROCOF) to realize the minimum possible measurement error which shall help the effective implementation of WAMPACS in an online control application. It is pertinent to mention here that the correction algorithm shall be applicable for both steady state and dynamic conditions because of the fact that correction factor depends on the signal parameter instead of state of the system. Implementation of the correction algorithm will also allow flexibility in having PMUs with different characteristics from different manufacturers as the correction algorithm will take care of the error of each PMU separately.

It is worth to mention here that currently the main potential applications of WAMS include real-time measurement of power system states, power system operation & control, real time monitoring of power system dynamics and fault detection/event recording, however for real time protection, WAMS would be preferred for secondary defence instead of fast primary protection mainly due to relatively slow sampling rate of measurement by PMU which is one sample per cycle.

Further the error introduced in measurement by PMUs is relatively insignificant compared to the errors introduced by instrument transformers. The error introduced by current transformer (CT) can be as high as 5 % for ratio error and 60 minutes for phase error, similarly the allowed error limit for voltage by voltage transformer (VT) is as high as 3% for ratio error and 40 minutes for phase displacement [16-17]. However in case of PMU, the allowed TVE which includes both magnitude and phasor error is maximum of 1 % and as shown above in section 3.3, TVE for ALSTOM MiCOM P847 is 0.035%. The proposed least erroneous method is expected to reduce TVE to the extent where error introduced by PMU can be neglected compared to the errors introduced by instrument transformers.

It is also pertinent to mention that the burden provided by PMU is also low compared to traditional measuring devices where burden can be as high as 25 volt-amperes (VA), however in case of PMU corresponding value is relatively very low, 0.66VA for ALSTOM MiCOM P847.

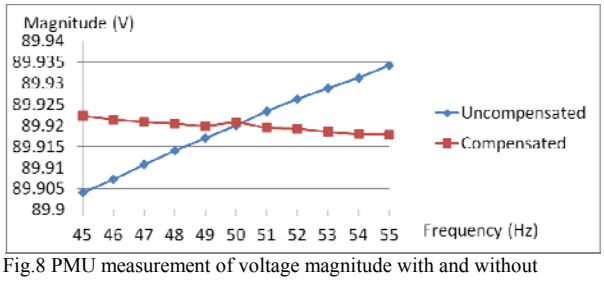

Fig.8 PMU measurement of voltage magnitude with and without correction factor.

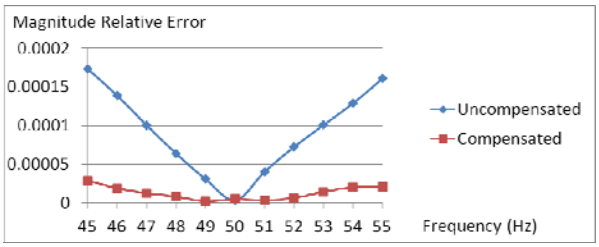

Fig. 9 Magnitude relative error with and without correction factor.

4. DYNAMIC TESTING

Although the performance of PMUs under dynamic conditions has improved since the introduction of PMUs in real power system applications, there is a need for further improvements in the dynamic performance of PMUs. WAMPACS can be used to improve the performance, control, protection, stability and hence reliability of power systems provided the WAMS is highly precise and reliable during steady state as well as dynamic conditions. For the verification of the satisfactory performance of PMUs during dynamic conditions, dynamic tests are performed.

Using the RTDS, dynamic response tests for step changes in magnitude, phase and frequency have been performed. Since the dynamic response depends on many factors like the measurement filter, measurement window and the decimation of the output data, the effect of the filter implementation is also investigated.

A step change of 10% was introduced in the voltage signal from RTDS to PMU and the response in the measured value was recorded from the PDC as shown in Fig. 10. It can be observed the response is over damped, however close to critical damping, therefore a very small overshoot can be seen in the magnitude step response. The ALSTOM MiCOM P847 PMU is provided with three filter lengths, 5 cycles, 7 cycles and 13 cycles. The affects of all three filter lengths were observed and as expected, for higher filter lengths the response time is higher. Response times of 0.11s, 0.18s and 0.2 s were noted for filter lengths of 5 cycles, 7 cycles and 13 cycles respectively.

The response to step changes in the phase value and frequency yields similar results as shown in Fig. 11 and Fig. 12 respectively. A step change of 75% in phase and 0.5Hz in frequency was performed and the response was recorded.

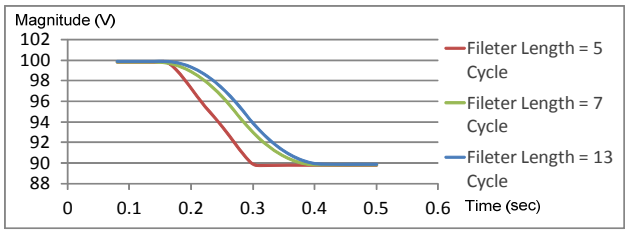

Fig. 10 Response to step change in voltage magnitude.

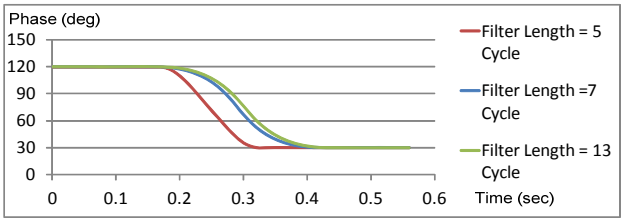

Fig. 11 PMU response to step change in phase.

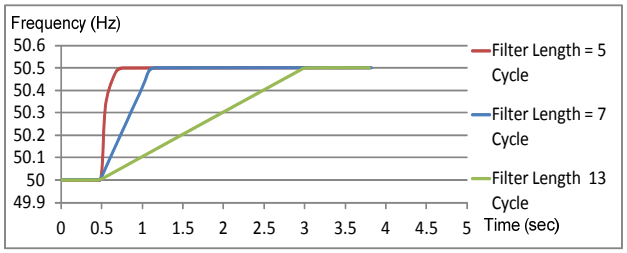

Fig. 12 PMU response to step change in frequency.

APPENDIX

Manufacture	**Alstom**[18]	**ABB**[19]	**Siemens**[20]	**Satang**[21]	**SEL**[22]	**Arbiter** [23]	**CEPRI**[24]
Product Name/ Model	**P847B**	**RES 521**	**SIMEAS R-PMU VCDAU**	**CCS-200/1A1**	**SEL 421**	**1123A**	**PAC-2000**
Input Channels(AI[1])	3 Voltage 12 Current	12 Voltage 6 Current	4 Voltage 4 Current	18 Voltage 18 Current	12 Voltage 6 Current	12 Voltage 6 Current	48 Voltage or Current
Input Channels (DI[2])	8	8	16	44	8	8	16
AD[3] Sampling Frequency (Samples/Cycle)	48	20	192	96	20	20	96
Reporting Rate (frame/sec)	10/25/50Hz(50Hz) 10/12/15/20/30/60Hz (60Hz)	once per 1/2/4 cycle	10/25/50 sec (50Hz) 10/12/15/20/30/60 sec (60Hz)	25/50/100Hz (50Hz)	once per 1/2/4 cycle	once per 1/2/4 cycle	25/50/100/sec(50Hz)
Outputs	V, I, P, Q, f, Phasor	V, I, P, Q, f, Phasor	V, I, P, Q, f, Phasor	V, I, P, Q, f, Phasor	V, I, P, Q, f, Phasor	V, I, P, Q, f, Phasor	V, I, P, Q, f, Phasor
Resolution of Volt. and Curr.	±1%	±0.5%	±0.25% Volt. /±0.5% Curr.	±0.2%	±1%	±0.5%	±0.1%
Resolution of Phasor	0.5deg	0.1deg	-	0.1deg	0.1deg	0.1deg	0.1deg
Resolution of Freq.	0.025Hz	0.005Hz	-	0.001Hz	0.005Hz	0.005Hz	0.001Hz
Resolution of Sync. Time	±1us	±0.5us	±5us	±1us	±1us	±1us	±100ns
Min. GPS Satellites	4	3	-	3	3	3	1
A/D Resolution	16 bit	12 bit	-	14/16 bit	12 bit	12 bit	16 bit
Max. PMU Storage	No storage.	No storage	1GByte	For 2 weeks	No storage	No storage	For 2 weeks
Over Freq. Trig.	Yes	Yes	Yes	Yes	Yes	Yes	Yes
Differential Freq.	Yes	Yes	Yes	Yes	Yes	Yes	Yes
Over Curr. Over Volt.	Yes	Yes	Yes	Yes	Yes	Yes	Yes
Over Zero-Sequence	Yes	No	No	Yes	No	No	Yes
Over Neg-Sequence	Yes	No	Yes	Yes	No	No	Yes
Max. Offset Power Angle	Yes	No	Yes	Yes	No	No	Yes
Manual/Remote Trigger	Yes	Yes	Yes	Yes	Yes	Yes	Yes
Real-time Monitor	Yes	Yes	Yes	Yes	Yes	Yes	Yes
Real-time Record	Yes	Yes	Yes	Yes	Yes	Yes	Yes
Waveform Record	Yes	Yes	Yes	Yes	Yes	Yes	Yes
Harmonic Analysis	No	Yes	No	No	Yes	Yes	Yes

1. Analog input(AI), 2.Digital input(DI), 3. Analog to Digital(AD)

The effect of the filter length on the phase and frequency step change response is similar to that of the magnitude response. Lower filter lengths improve the response time at the cost of steady state accuracy and vice versa. Therefore the choice of filter length will be mainly decided by the WAMS application. For control applications a lower filter length with a fast response is preferred and for state estimation, a longer filter length with a slower response. Nevertheless for a multipurpose application an optimal value of filter length can be chosen.

5. CONCLUSION

The application of a RTDS for PMU testing including both steady state and dynamic tests was demonstrated in this paper.

The need for universal well defined standards was reinforced through a comparative analysis of PMUs available from different manufacturers.

A correction algorithm to realize a WAMS with the highest possible accuracy was proposed and supported by promising results from a RTDS and PMU based experimental setup. This proposed correction algorithm will ensure that the least erroneous measurement can be implemented in real time WAMS and WAMPAC applications.

7. REFERENCES

[1] A. G. Phake, "Synchronized phasor measurements in power systems," IEEE Comput. Appl. Power, vol.6, no. 2, pp. 10-15, Apr. 1993.

[2] North American Synchron Phasor Initiatibe (NASPI), Performance and Standards Task Team (PSTT), "PMU System Testing and Calibration Guide", 5 November 2007.

[3] Y. Hu "Progresses in PMU testing and calibration", Electric Utility Deregulation and Restructuring and Power Technologies, 2008. DRPT 2008. Third International Conference on, pp 150-155, 6-9 April 2008

[4] C. Liu, Z. Chen, C. L. Bak, Z.. Liu., "Adaptive voltage stability protection based on load identification using Phasor Measurement Units," Advanced Power System Automation and Protection (APAP), 2011 International Conference on , vol.2, no., pp.1246-1251, 16-20 Oct. 2011

[5] J.A. de la O Serna, and K.E. Martin, "Improving phasor measurements under power system oscillations," IEEE Transactions on Power Systems, vol. 18, pp. 160–166, Feb. 2003.

[6] J. Yan, C. C. Liu, and U. Vaidya, "PMU-based monitoring of rotor angle dynamics," IEEE Transactions on Power Systems, vol.26, no.4, pp.2125-2133, Nov. 2011.

[7] V. Madani, D. Novosel, S. Horowitz, M. Adamiak, J. Amantegui, D. Karlsson, S. Imai, A. Apostolov, "IEEE PSRC Report on Global Industry Experiences With System Integrity Protection Schemes (SIPS)," IEEE Transactions on Power Delivery, vol.25, no.4, pp.2143-2155, Oct. 2010.

[8] R. K. Mai, Z. Y. He, L. Fu, W. He, Z. Q. Bo, "Dynamic phasor and frequency estimator for phasor measurement units," IET Transaction on Generation, Transmission & Distribution, vol.4, no.1, pp.73-83, January 2010.

[9] K. E. Martin, G. Benmouyal, and M. G. Adamiak, et. al. "IEEE Standard for Synchrophasor for Power Systems," IEEE Trans. Power Delivery, vol. 13, pp. 73-77, Jan. 1998.

[10] IEEE Std 1344-1995(2001), Power System Relaying Committee of the IEEE Power Engineering Society, IEEE Standard for Synchrophasors for Power Systems[S].

[11] IEEE Std C37.118-2005, Power System Relaying Committee of the IEEE Power Engineering Society, IEEE Standard for Synchrophasors for Power Systems[S].

[12] J. Depablos, V. Centano, A. G. Phadke, M. Ingram, "Comparative testing of synchronized phasor measurement units", IEEE Power Engineering Society General Meeting, 2004, June 2004, pp 948-954 Vol 1.

[13] Y. Hu; D. Novosel, "Progresses in PMU testing and calibration," Electric Utility Deregulation and Restructuring and Power Technologies, 2008. Third International Conference on DRPT 2008., vol., no., pp.150-155, 6-9 April 2008.

[14] K. Narendra, Z. Zhang; J. Lane, B. Lackey, E. Khan, "Calibration and testing of TESLA Phasor Measurement Unit (PMU) using doble F6150 test instrument," Bulk Power System Dynamics and Control - VII. Revitalizing Operational Reliability, 2007 iREP Symposium, vol., no., pp.1-13, 19-24 Aug. 2007.

[15] K. Martin, T. Faris, J. Hauer, "Standardized testing of phasor measurement units" Fault and Disturbance Analysis Conference 2006, Georgia Tech, Atlanta, GA.

[16] IEC 60044-1 standard, edition 1.2, 2003.

[17] IEC 60044-2 standard, edition 1.2,2003.

[18] MICOM ALSTOM P847B&C PMU Technical Manual. [Online] Available: http://www.alstom.com

[19] ABB RES 521 PMU Technical Manual [Online] Available: http://www.abb.com

[20] SIMEAS R–PMU Technical Manual. [Online]. Available: http://www.siemens.com

[21] Sifang CSS-200/1 Distributed PMU Techinical Manual [Online] Available: http://www.sf-auto.com/Pages/index.aspx

[22] SEL 421 PMU Technical Manual [Online] Available: http://www.selinc.com/SEL-421/

[23] Arbiter 1133A PMU Technical Manual [Online] Available: http://www.arbiter.com

[24] China Electric Power Research Institute PAC-200 PMU Technical Manual [Online] Available: http://www.epri.sgcc.com.cn/en/

A Communication-less Overcurrent Protection for Distribution System with Distributed Generation Integrated

Chengxi Liu, Zhe Chen, Zhou Liu
Department of Energy Technology, Aalborg University
Pontoppidanstraede 101, Aalborg East, DK-9220, Denmark
cli@et.aau.dk, zch@et.aau.dk, zli@et.aau.dk

***Abstract*—The increasing penetration of distributed generation (DG) in distribution systems has resulted in a challenge for the conventional protection methods, due to the bi-directional power flow and the variation of fault current contribution. Moreover, the operation of distribution system in islanded mode is still an issue due to the difference between the short circuit current in islanded mode and grid-connected mode. This paper proposed a novel adaptive protection method, measuring only the local information rather than using the communication, to adapt the protection settings to the states, such as the change of operation mode (grid-connected or islanded), the change of network topology (radial or meshed) as well as the disconnection of some DG. The directional overcurrent relays (DOCR) is adopted in the distributed system to shorten the tripping time in order to maintain the DG's connection. The relay settings are calculated offline and modified online according to the state detection, including the islanding detection, the power flow detection and the fault section detection. This protection method is verified by simulating a distribution system of Denmark in DIgSILENT PowerFactory.**

Keywords- ***Adaptive protection, communication-less directional overcurrent relay, distributed generation, DIgSILENT PowerFactory.***

I. INTRODUCTION

Nowadays, various types of small generation sources, better known as distributed generation (DG), are connected to the distribution power systems. Due to the CO2 reduction goals, many of the small units integrated in the distribution systems are renewable energy sources, such as wind turbines, photovoltaic panels, and small scale hydro plants. Also, high efficient non-renewable energy resources, such as small Combined Heat and Power (CHP) plants have been implemented. In Denmark, about 40% of the total generation capacity is based on distributed generation units, which are connected to the electrical distribution systems from 400V to 60kV.

A large scale integration of DG units would play significant roles as power sources in modern power systems, which makes the protection of the power system more complicated. One of the major challenges is the bi-directional power flow in such electrical distribution system and the need for short time tripping. When there is a fault in the distribution system, not only the transmission system but also the DG units contribute to the fault current. Some DG units have low voltage ride through (LVRT) ability, remaining connected to the power system only for a short time. However, the conventional 3-sectional definite time over-current protection would be too slow to clear the fault [1]. Hence, the protection relays are necessary to achieve features of both directional sensitive and short tripping time. The time directional overcurrent relay is suitable for these requirements.

The other challenge is the variation of the short circuit current. On one hand, due to the change of the power system topology, such as losing some DGs and meshing the distributed feeder, the short circuit current would vary significantly. So the settings of the relays and the coordination of them should be adapted to the variation accordingly. On the other hand, the higher DG penetration makes it possible to operate the distribution system in an islanded mode, in which the distribution system works as a microgrid which is electrically isolated from the transmission system. When a distribution system is islanded, the fault current is lower than the fault current when the distribution system is connected to the transmission system.

In [2], a single setting for islanded mode is used for relays, but it is likely to island the system frequently. In [3], the author presents the principle of adaptive protection in distribution network, using digital relay and advanced communication. Whereas, when the fault current is low, this protection would lose coordination. Some researchers focus on using storage units to increase the short-circuit power to make the fault detection possible [4,5]. In [6], a high-speed communication-based protection method is proposed to cooperate with energy storage units to achieve fast, selective and reliable operation. However, implementing a communication between the relays is expensive and unreliable.

A protection method based on local information is proposed in [7], which uses current traveling wave to identify the faulted feeder, but it is not suitable for small scale

This work was supported by the Danske Strategiske Forskningscentre under DSF 09-067255.

distribution system. In [8], a simple adaptive protection for overcurrent relays without communication is invented as well. However, all the relays assume that the current they have measured is the actual fault current, but this may not be accurate, because the downstream DG also contributes to the fault current.

This paper proposes a novel adaptive protection method, in which the trip characteristic is based on offline analysis and online selection. For normal operation states, this method is able to adapt to the state changes, such as change of operation mode (grid-connected or islanded) and changing of the topology (radial or meshed). For abnormal operation states, such as some DGs are lost after a fault, this method can also detect the faulted section based on auto-reclosure time detection and then adapt to the new state. All the detections of the system state use only the local information.

II. TEST DISTRIBUTION SYSTEM

Fig.1 shows the one-line model of the test distribution system, which is originally from a part of a distribution system owned by Himmerlands Elforsyning (HEF), in Aalborg, Denmark. The test system consists of 6 loads and 7 buses (from Bus1 to Bus7). 'R12' stands for the relay, and the following 2 numbers represent the beginning bus and the end bus of its protection zone. The system is integrated with five gas turbine generators (GTG) and one variable speed wind turbine generator (WTG). The WTG is a 2MW doubly fed induction generator (DFIG) with power electronic converters. The data for the WTG are given in Table I. The GTG are 3.3MVA with governor and excitation control, given in Table II.

The distributed generation has the ability to support all the local loads. The distribution system is able to be meshed by Line67 to achieve higher reliability. R67 and R76 are normally open circuit breakers (CB). The line data and load data for this test distribution system is given in Table III.

TABLE I. DATA OF WIND TURBINE GENERATORS

Parameters	**Value**
Rated power (MW)	2
Stator rated voltage (kV)	0.69
Stator resistance (p.u.)	0.0108
Stator reactance (p.u.)	0.0121
Magnetic reactance (p.u.)	3.362
Rotor resistance (p.u)	0.004.
Rotor reactance (p.u.)	0.05
Crowbar resistance (p.u.)	0.5
Crowbar reactance (p.u.)	0.1
Generator inertia (kgm2)	255.105
Rotor inertia (kgm2)	6.1×106
Drive train stiffness (Nms/rad)	8.3×107
Drive train damping (Nm/rad)	1.4×106
Nominal turbine speed (rpm)	18
Rotor radius (m)	50
Max. current for crowbar insertion (kA)	5

TABLE II. DATA OF GAS TURBINE GENERATORS

Parameters	**Value**
Rated power (MW)	2
Rated voltage (kV)	3.3
Stator resistance and reactance(p.u.)	0.0108, 0.0121
d-axis reactance X_d, $X_d^{/}$ $X_d^{//}$ (p.u.)	1.5, 0.256, 0.168
q-axis reactance X_q, $X_q^{//}$ (p.u.)	0.75, 0.184
d-axis time constant $T_{d0}^{/}$, $T_{d0}^{//}$ (sec)	0.53, 0.03
q-axis time constant $T_{q0}^{//}$ (sec)	0.03
Inertia time constant (sec)	0.54

TABLE III. LINE DATA AND LOAD DATA

Line	**Resistance(Ohm)**		**Reactance(Ohm)**
Line12	0.6720		0.3160
Line23	0.9560		0.4485
Line34	2.4370		1.1420
Line45	0.6730		0.4530
Line56	0.6730		0.4530
Line17	0.6280		0.7020
Line67	0.6730		0.4530
Load	**P_L(MW)**	**Q_L(MVar)**	**$S_L$max(MVA)**
Load1	0.4523	0.2003	1.0000
Load2	0.7124	0.3115	2.0000
Load3	1.1131	0.0501	2.0000
Load4	1.1131	0.0501	3.0000
Load5	1.1131	0.0501	3.0000
Load6	7.6471	1.1607	10.0000

III. PROPOSED METHODOLOGY

A. Fault Current Analysis

The fault current depends on the short circuit power. The transmission system generally has higher short circuit power compared to distribution system integrated with DG. The maximum short circuit current of three-phase short circuit faults at the end of each line for grid-connected and islanded mode are shown in Fig.2. One can notice that there should be a significant difference in the protection settings of the forward relays (R12, R23, R34, R45, R56 and R17) for these two modes.

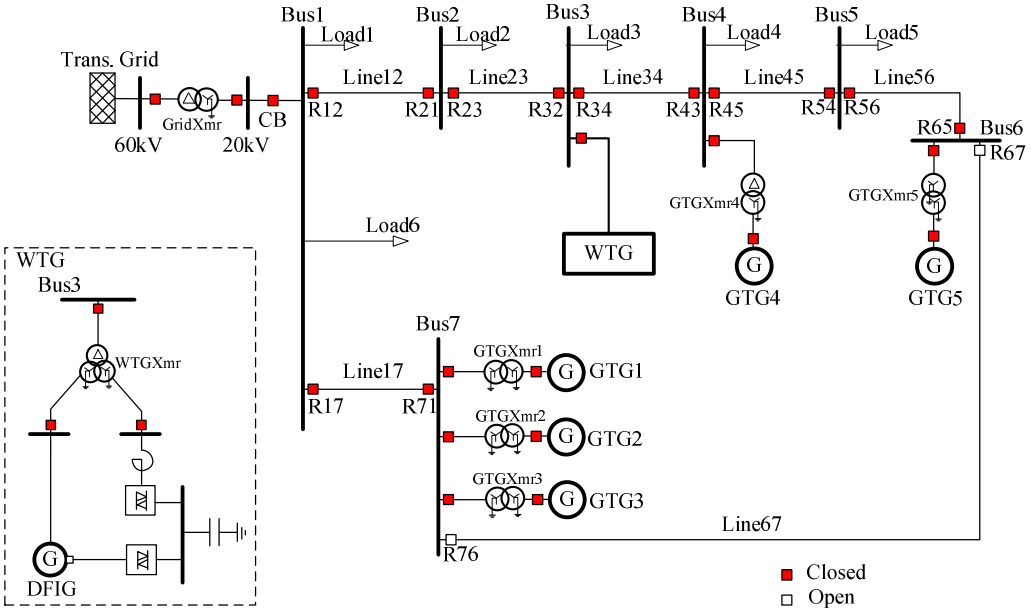

Figure 1. Test Distribution System

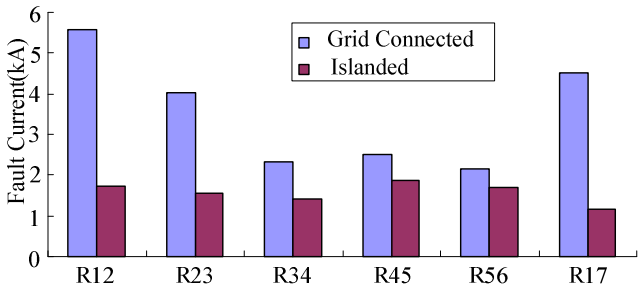

Figure 2. Maximum 3-ph fault current.

On the other hand, the short circuit power can also be reduced when losing some of the DG. The maximum short circuit current of three-phase short circuit faults at the beginning of each line for normal condition and a condition when GTG5 is disconnected are shown in Fig.3. One can notice that there should be a variation in the protection settings of the backward relays (R21, R32 and R43) for these two conditions.

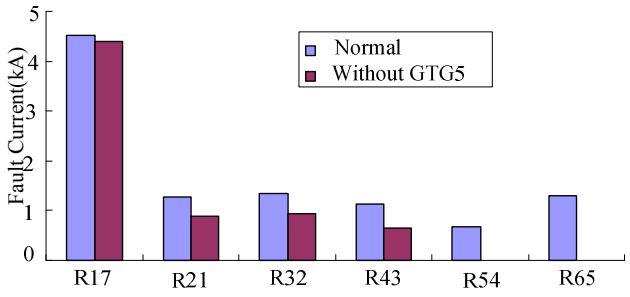

Figure 3. Maximum 3-ph fault current.

Furthermore, when the system is meshed by closing the circuit breakers of Line67, all the power sources could contribute the short circuit power from two directions. So meshing the distribution system changes the short circuit current seen by most of the relays, no matter grid-connected mode or islanded mode. Fig.4 and Fig.5 compare the maximum short circuit current in radial and meshed topology for grid-connected mode and islanded mode, respectively.

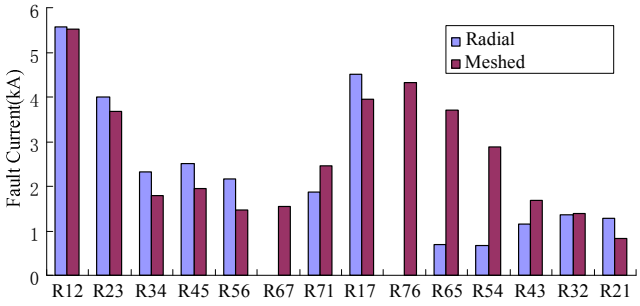

Figure 4. Maximum 3-ph fault current in grid-connected mode

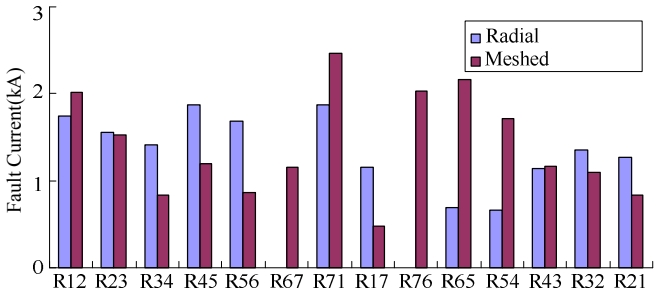

Figure 5. Maximum 3-ph fault current in islanded mode

B. Time Directional Overcurrent Protection (DOCR)

The time DOCR consists of two parts, instantaneous part and inverse-time part, shown in Fig.6. For higher fault current, the relay pick time is fixed to the instantaneous one, similar to Zone I overcurrent protection. For lower fault current, the operating time is inversely changed with the current. So, higher current will operate the relay faster than lower ones. The advantage over definite time relays is that much shorter tripping times can be achieved without any risk to protection selection process, as illustrated in Fig.7.

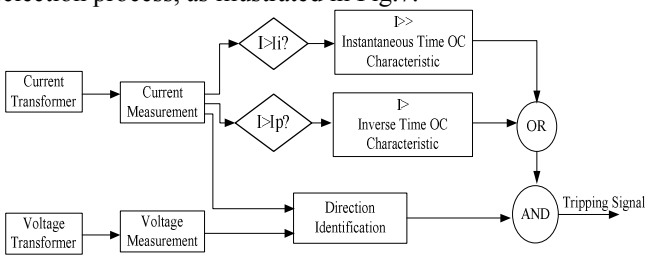

Figure 6. Block diagram of directional overcurrent relay

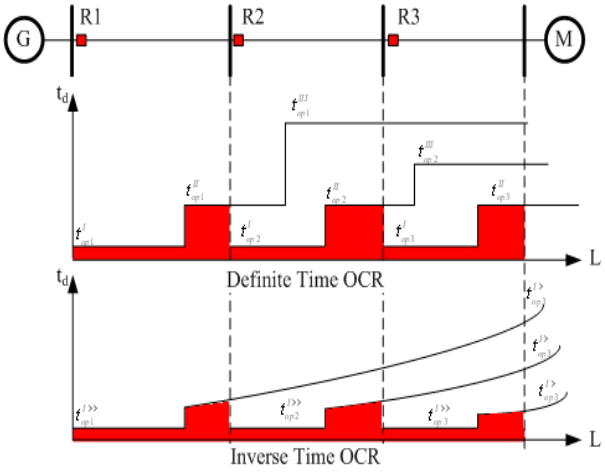

Figure 7. The pickup time of definite time OCR and the inverse time OCR.

The operating time of inverse-time OCR is based on IEC 255-3 (Normal Inverse) overcurrent characteristic, given by (1)

$$t = \frac{0.14 \times T_p}{\left(I / I_p\right)^{0.02} - 1} (\text{sec}) \qquad (1)$$

where Ip, I and Tp are pick up current, fault current and time dial setting of the relay, respectively. Ip is set to 1.5 times the maximum load current. The instantaneous pick up time Tins is set as 50ms, the instantaneous pick up current Ii is set to 1.2 times the maximum short circuit current at the end of the protection zone to assure the selectivity.

The time dialing setting of each relay is designed in such a way that the upstream relay provides a backup function for its downstream relays. The backup function is based on the difference of the inverse-time characteristic. R1 is the backup relay for R2 and R3, so the shortest pickup time Tinv of inverse DOCR should be high than R2 and R3. The figure shown in Fig.8 is the protection coordination for the simple system shown in Fig.7. The coordination relationship is given by (2).

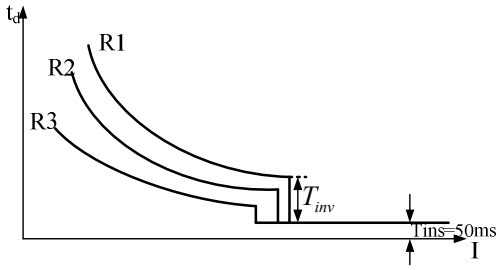

Figure 8. The characteristic of time overcurrent relay.

$$T_{inv}(R1) > T_{inv}(R2) > T_{inv}(R3) \qquad (2)$$

C. Protection Coordination of Different States

As mentioned earlier, one of the major advantages of high DG penetrated distribution system is the possibility of operating it in the islanded mode, which may be due to a fault in transmission system or any other disturbances. Although currently almost all utilities require DG to shut down once a distribution system is islanded, implementation of islanding operation of DG is one of the promising task for future consideration [9].

Let us consider the protection coordination of four normal operation states of the distribution system.

Normal State 1: The distribution system is grid-connected with radial topology (CB=Closed, R67=R76=Open). The forward and backward relays should coordinate with its downstream relays respectively. For example, R45 should be the backup protection of R56. In case of R56 dose not trip instantaneously, R45 should trip after a delay time, thus $T_{inv}(R45) > T_{inv}(R56)$. The protection coordination should follow (3) and (4).

$$T_{inv}(R12) > T_{inv}(R23) > T_{inv}(R34) > T_{inv}(R45) > T_{inv}(R56) \qquad (3)$$

$$T_{inv}(R65) > T_{inv}(R54) > T_{inv}(R43) > T_{inv}(R32) > T_{inv}(R21) \qquad (4)$$

Normal State 2: The distribution system is grid-connected with meshed topology (CB=Closed, R67=R76=Closed). Since the distribution system is a loop network, the protection coordination should follow (5) and (6).

$$T_{inv}(R12) > T_{inv}(R23) > T_{inv}(R34) > T_{inv}(R45) > T_{inv}(R56) > T_{inv}(R67) > T_{inv}(R71) \qquad (5)$$

$$T_{inv}(R17) > T_{inv}(R76) > T_{inv}(R65) > T_{inv}(R54) > T_{inv}(R43) > T_{inv}(R32) > T_{inv}(R21) \qquad (6)$$

Normal State 3: The distribution system is islanded with radial topology (CB=Open, R67=R76=Open). The protection coordination should follow (7) and (8).

$$T_{inv}(R71) > T_{inv}(R12) > T_{inv}(R23) > T_{inv}(R34) > T_{inv}(R45) > T_{inv}(R56) \qquad (7)$$

$$T_{inv}(R65) > T_{inv}(R54) > T_{inv}(R43) > T_{inv}(R32) > T_{inv}(R21) > T_{inv}(R17) \qquad (8)$$

Normal State 4: The distribution system is islanded with meshed topology (CB=Open, R67=R76=Closed). Considering the power flow direction, the protection coordination should follow (9) and (10).

$$T_{inv}(R71) > T_{inv}(R12) > T_{inv}(R23) > T_{inv}(R34) > T_{inv}(R45) > T_{inv}(R56) > T_{inv}(R67) \qquad (9)$$

$$T_{inv}(R76) > T_{inv}(R65) > T_{inv}(R54) > T_{inv}(R43) > T_{inv}(R32) > T_{inv}(R21) > T_{inv}(R17) \qquad (10)$$

D. *Normal Operation State Detection*

Adaptive protection is "an online activity that modifies the preferred protective response by means of externally generated signals or control action" [10]. Therefore this protection method should be able to detect the operation state and then modify the protection settings according to the operation state. All the protection settings are calculated offline and activated online.

The states flow for the states detection is shown in Fig.9. The relays measure the voltage and frequency to detect that the distribution system is connected to transmission system or islanded, as presented in [11,12]. A lot of other islanding detection technologies can also be used. Fig.10 shows the voltage and frequency variation when changing from grid-connected states to islanded states at t = 1sec.

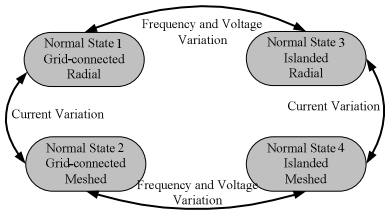

Figure 9. State flow of distribution system.

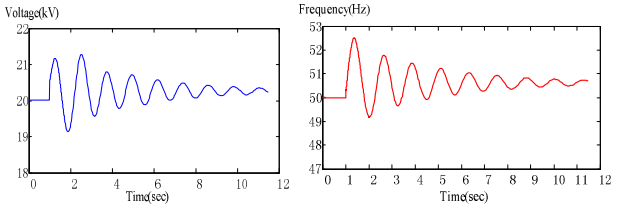

Figure 10. Voltage and frequency variation when the system is islanded.

When changing the system topology, i.e. meshing the feeders, the power flow changes evidently. Thus all the relays would measure a step change in their current due to the distribution system changing from radial topology to meshed topology. Fig.11 shows the current in each transmission line when the distribution system become meshed at t=1sec.

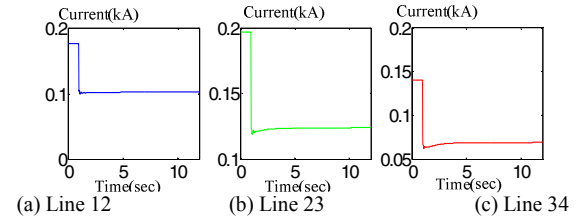

(a) Line 12 (b) Line 23 (c) Line 34

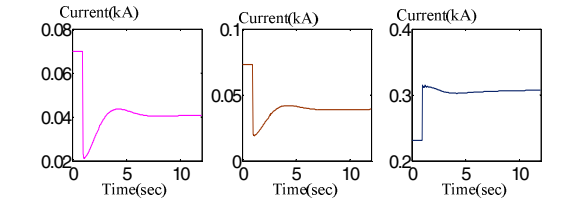

(d) Line 45 (e) Line 56 (f) Line 67

Figure 11. Current variation when the system is meshed.

E. *Abnormal Operation State Detection*

As presented earlier, if some generators are lost after a fault, relays may not see the same amount of fault current as compared to the normal operation states. The adaptive relays detect the faulted section by using fault section detection algorithm and select the right characteristics accordingly.

The fault section detection algorithm is based on the auto-reclosure time detection. For example, if there is a 3 phase fault in the beginning of Line45 in Normal State 1, as shown in Fig.12, the forward relays R12, R23, R34 and R45 see the fault current. R45 should be tripped by its time over current protection. As most of the faults are temporary faults, a three-phase auto-reclosure should be set to restore the system. If we set the auto-reclosure time differently, the upstream relays could accurately identify which relay has tripped. After successfully identifying the faulted section, the upstream forward relays R23 and R34 would know which distributed generation has lost, and update the new protection settings to their adjacent backward relays R21 and R32.

However, not all the fault will lead to losing distributed generation. We assume that the distribution system can not be split and operate as 2 isolated areas. For example, when the R65 detects there would be islanded due to a fault in the distribution system rather than intentional islanding, GTG5 would be tripped immediately after the islanding. Now we consider the following 4 abnormal states.

Abnormal State 1: The distribution system is grid-connected with radial topology. Line45 has tripped, shown in Fig.12. GTG5 will be disconnected to avoid the splitting operation. No matter whether the fault is unrecoverable fault or temporary fault restored by auto-reclosure, GTG5 would be disconnected and the R21, R32 and R43 should change their protection settings.

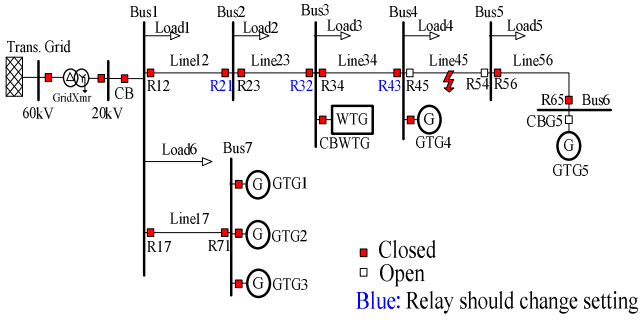

Figure 12. The distribution system in Abnormal State 1.

Abnormal State 2: The distribution system is grid-connected with meshed topology, Line45 has tripped, shown in Fig.13. All the DG can be connected, because there is no splitting area. If the fault is temporary fault and restored by auto-reclosure, the distribution system would recover to meshed topology. No protection settings would be changed. Whereas, if the fault is unrecoverable fault, the distribution system changes to radial topology with 2 feeders, all the protection settings and their coordination should be changed.

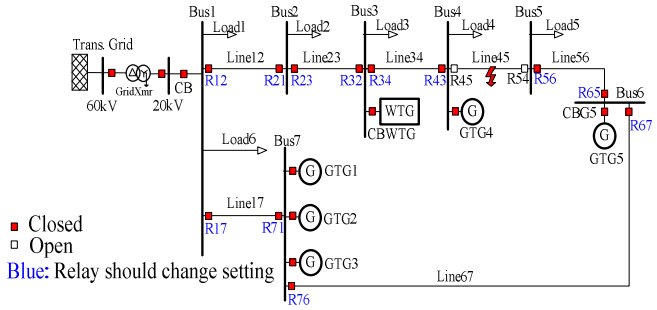

Figure 13. The distribution system in Abnormal State 2.

Abnormal State 3: The distribution system is islanded with radial topology, Line45 has tripped, shown in Fig.14. It is similar to Abnormal State 1, except for R17 should also change its setting to adapt to the disconnection of GTG5.

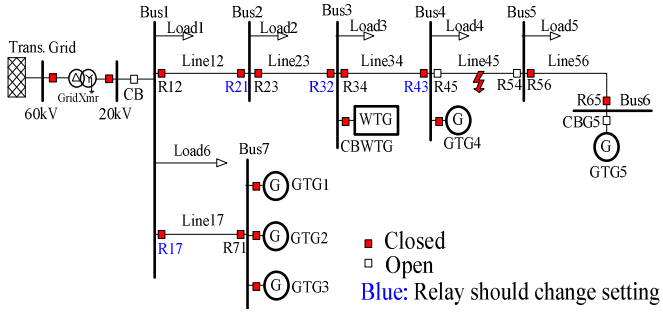

Figure 14. The distribution system in Abnormal State 3.

Abnormal State 4: The distribution system is islanded with meshed topology, Line45 has tripped, shown in Fig.15. The adaptive protection scheme is the same as Abnormal State 2. The relay shown in blue are the ones should be modified.

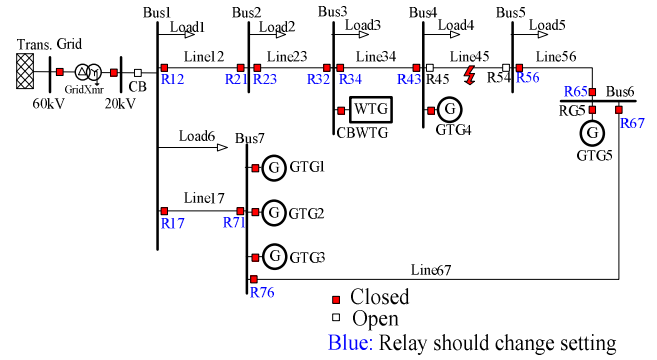

Figure 15. The distribution system in Abnormal State 4.

IV. Design of the Overcurrent Protection

Although the islanding operation is a promising way of improving the reliability in the future, currently, Danish grid code requires the islanding operation up to 25MW is avoided [9,13]. So, in this paper, only Normal State 1 and 2 are designed and tested. The time dial settings, pickup current and instantaneous pickup current in Normal State 1 and 2 are listed in Table IV and Table V. The time-distance diagrams are shown in Fig.16 and Fig17, in which the pickup time for each relay is dependent on the location of fault in the lines.

TABLE IV. Time Overcurrent Settings in Normal State 1

Relay	Ip(A)	Tp	Ii(A)	Relay	Ip(A)	Tp	Ii(A)
R12	440	0.1669	5532	R21	350	0.0243	1075
R23	350	0.1275	4210	R32	350	0.0427	1140
R34	260	0.0848	2646	R43	260	0.0629	900
R45	130	0.0649	2465	R54	130	0.0862	488
R56	130	0.0208	2208	R65	130	0.1073	500
R67	-	-	-	R76	-	-	-
R71	390	0.1232	1426	R17	350	0.0183	4746

TABLE V. Time Overcurrent Settings in Normal State 2

Relay	Ip(A)	Tp	Ii(A)	Relay	Ip(A)	Tp	Ii(A)
R12	260	0.2808	4900	R21	200	0.0090	694
R23	170	0.2403	3310	R32	200	0.0390	1194
R34	90	0.1964	1746	R43	200	0.0739	1521
R45	60	0.1696	1597	R54	60	0.1911	2388
R56	60	0.1111	1228	R65	90	0.2358	3100
R67	140	0.0474	1220	R76	180	0.2462	3760
R71	480	0.0100	1918	R17	180	0.2922	3806

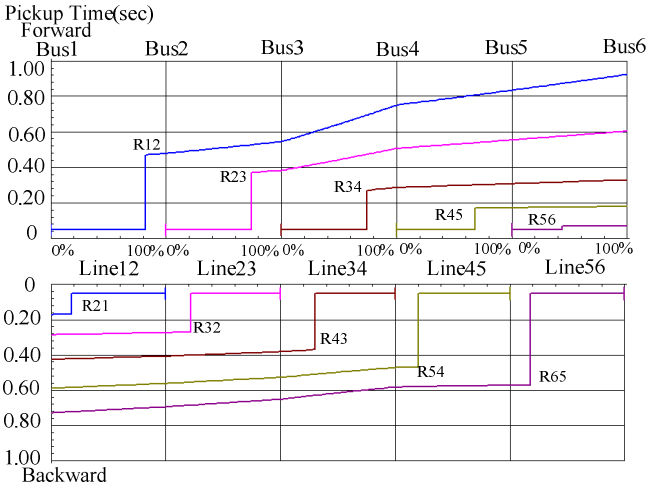

Figure 16. The time-distance of protection settings in Normal State 1.

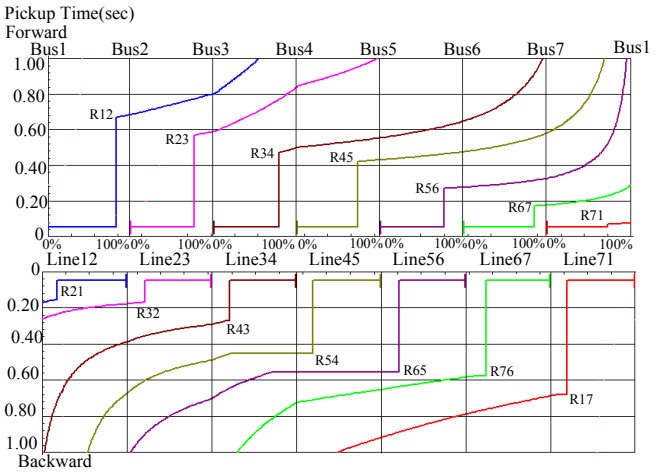

Figure 17. The time-distance of protection settings in Normal State 2.

V. SIMULATION RESULTS

In the simulation, we assume the relay takes 10ms to close its trip contacts and the circuit breaker takes 60ms to clear the fault, the instantaneous pickup time is 50ms to detect the fault. So the minimum tripping time is 120ms after a fault.

The wind turbine generator should satisfy the Danish grid code demands for fault right through below 100kV, as shown in Fig.18.

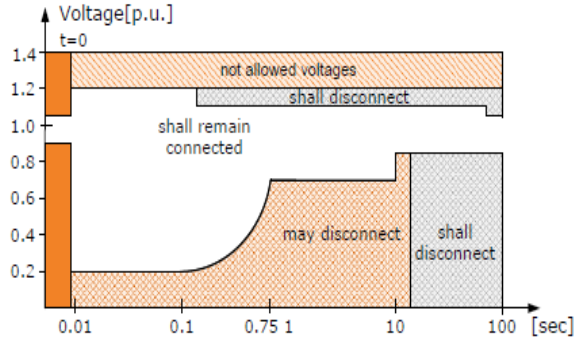

Figure 18. The Danish grid code for low voltage ride through at below 100kV[9].

A. *Adaptive Protection Settings in Normal States*

Scenario A is the grid-connected mode with radial topology, a three phase short circuit with 0.05 Ω fault resistance takes place in the middle (50%) of Line34 at t=1sec.

The protection setting is shown as Table IV. Fig.19 shows the actual states of the circuit breakers. CB34 and CB43 trip at t=1.12secc to clear the fault, 120ms after the fault. The wind turbine generator should still connect to the distribution system because of the LVRT ability.

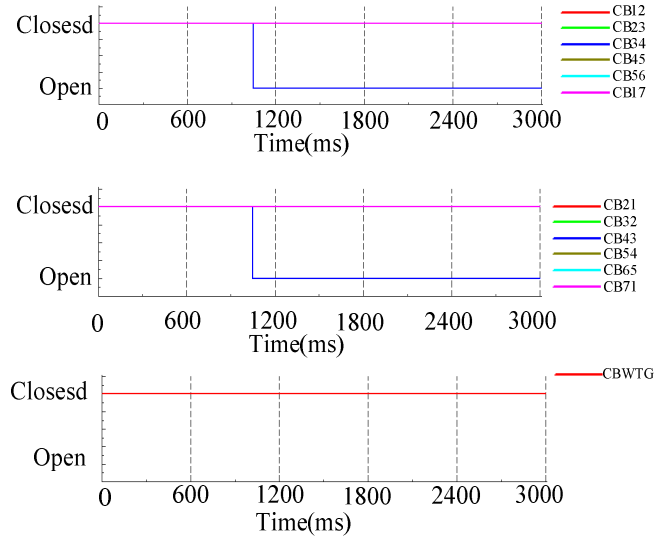

Figure 19. The states of CB in Scenario A with protection settings in Table IV.

Scenario B is the grid-connected mode with meshed topology, a three phase short circuit with 0.05 Ω fault resistance takes place in the middle (50%) of Line34 at t=1sec.

If the protection settings do not change, shown in Table V, the CB 34 would trip at t=1.291sec. It is too slow because the WTG would be disconnected at t=1.262sec, shown in Fig.20.

As discussed in Section III, the relays have the ability to detect the islanding and select the protection settings, shown in Table IV. Fig.21 shows the actual states of the circuit breakers. One can see that after modifying the relay settings to the meshed mode. The circuit breakers clear the fault in time and the wind turbine generator still connects to the distribution system.

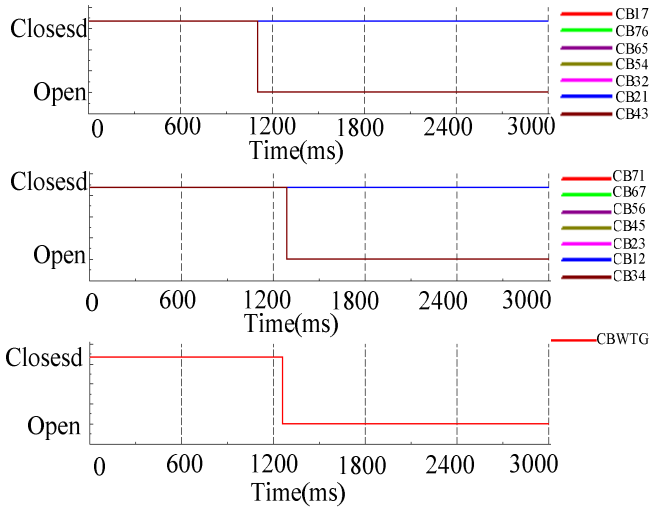

Figure 20. The states of CB in Scenario B with protection settings in Table IV.

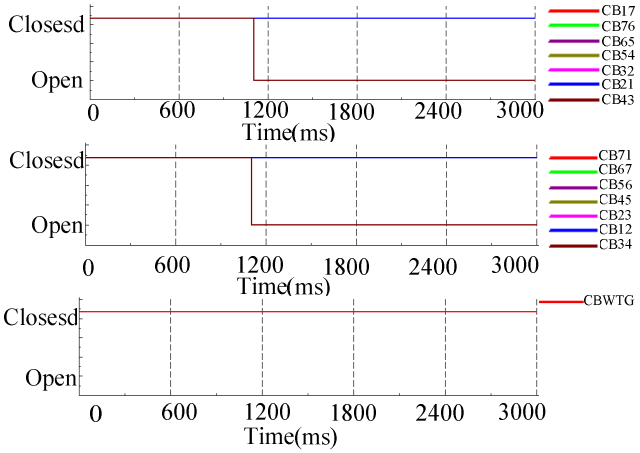

Figure 21. The states of CB in Scenario B with protection settings in Table V.

B. *Fault Section Detection for Abnormal States*

As mentioned earlier, the fault section detection can be easily achieved by setting different auto-reclosure time delay, as shown in Table VI.

TABLE VI. TIME OVERCURRENT SETTINGS IN NORMAL STATE 2

Relay	Reclosure Time (ms)	Relay	Reclosure Time (ms)
R12	500	R21	500
R23	1000	R32	1000
R34	1500	R43	1500
R45	2000	R54	2000

Relay	Reclosure Time (ms)	Relay	Reclosure Time (ms)
R56	2500	R65	2500
R67	3000	R76	3000
R71	3500	R17	3500

Scenario C is the grid-connected mode with radial topology, a unrecoverable three phase short circuit with 5 Ω fault resistance takes place at the end of Line34 (90%).

As shown in Fig.22, R12 and R23 can measure the fault current and detect that the fault clears at t=1.458sec. Then, at t=3.028sec, 1570ms after the fault clearing time, the fault current occurs again, since the fault is permanent fault. Based on the different reclosure time delay shown in Table VI, R12 and R23 are able to detect that R34 has tripped. So, R12 and R23 can detect GTG4 and GTG5 have been lost and should modify the protection settings.

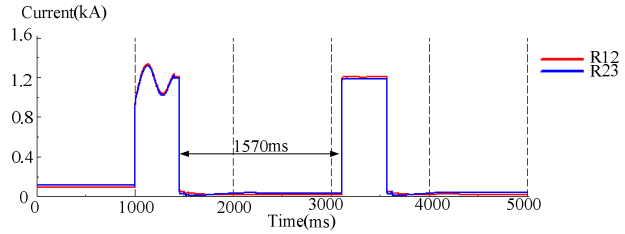

Figure 22. The current measured by R12 and R23 in Scenario C.

Scenario D is the grid-connected mode with radial topology, a unrecoverable three phase short circuit with 5 Ω fault resistance takes place at the beginning of Line45 (10%).

As shown in Fig.23, R12 and R23 can measure the fault current and detect that the fault clears at t=1.219sec. Then, at t=3.289sec, 2070ms after the fault clearing time, the fault current occurs again. By looking for the reclosure time delay shown in Table VI, R12 and R23 are able to detect that R45 has tripped. So, R12 and R23 can detect that GTG5 has been lost and should modify the protection settings.

Based on this methodology, all the relays are able to detect the fault section and modify their proper protection settings only using local information. Thus, the adaptive protection scheme can be achieved without communication.

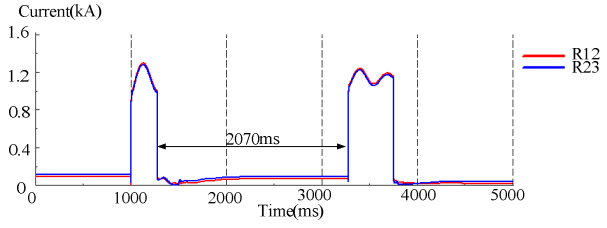

Figure 23. The current measured by R12 and R23 in Scenario D.

VI. Conclusion

An accurate adaptive protection can be achieved only using the local information. This methodology is able to detect not only the normal states (grid-connected or islanded, radial or meshed) but also the abnormal states (losing some DG) based on the reclosure time delay detection. Then, all the relays modify their protection settings to adapt to the new states. The simulation results based on DIgSILENT ProwerFactory show that this protection scheme is effective for distribution system integrated with DG.

Although this paper only considered the symmetrical fault, for the unsymmetrical fault, this methodology can also be useful, if the grounding of the neutral point can be assured.

References

[1] P. M. Anderson, “Power System Protection”, IEEE Press, 1999.

[2] H. Nikkhajoei and R. Lasseter, “Microgrid protection,” in Proc. IEEE Power Eng. Soc. Gen. Meet., Tampa, FL, Jun. 24-28, 2007, pp. 1-6.

[3] A. Oudalov and A. Fidigatti, “Adaptive network protection in microgrid,” [Online]. Available: http://wwww.microgrid.eu/documents/519.pdf

[4] N. Jayawarna, N. Jenkins, M. Barnes, M. Lorentzou, S. Pathanassiou and N. Hatziargyriou, “Safty analysis of a microgrid,” in Proc. Int. Conf. Future Power Syst., Amsterdam, The Netherlands, Nov. 16-18, 2005, pp. 1-7.

[5] M. Pedrasa and T. Spooner, “A survey of techniques used to control microgrid generation and storage during island operation,” in Proc. Australian Univ. Power Eng. Conf. (AUPEC), Melbourne, Australia, Dec. 10–13, 2006, pp. 1–6.

[6] H. J. Laaksonen, "Protection principles for future microgrids," IEEE Trans. Power Electronics, vol. 25, pp. 2910-2918, Dec. 2010.

[7] S. Shi, B. Jiang, X. Dong and Z. Bo, "Protection of microgrid," Developments in Power System Protection (DPSP 2010). Managing the Change, 10th IET Int. Conf. Managing the Developments in Power System Protection, Manchester, UK, 2010.

[8] P. Mahat, Z. Chen, B. Bak-Jensen and C. L. Bak, “A simple adaptive overcurrent protection of distribution system with distributed generation,” IEEE Trans. Smart Grid, vol. 2, pp. 428-437, Sep. 2011.

[9] IEEE Standard for Interconnecting Distributed Resources into Electric Power Systems, IEEE Standard 1547TM, Jun. 2003.

[10] G. D. Rockefeller, C. L. Wagner, J. R. Linders, K. L. Hicks and D. T. Rizy, “Adaptive transmission relaying concepts for improved performance,” IEEE Trans. Power Del., vol. 3, no. 4, pp. 1446–1458, Oct. 1988.

[11] P. Mahat, Z. Chen, and B. Bak-Jensen, “A hybrid islanding detection technique using average rate of voltage change and real power shift,” IEEE Trans. Power Del., vol. 24, no. 2, pp. 764–771, 2008.

[12] P. Mahat, Z. Chen, and B. Bak-Jensen, “Control and operation of distributed generation in distribution systems,” Electr. Power Syst. Res., vol. 81, no. 2, pp. 495–502, Feb. 2011.

[13] K. Christensen, et. al., “Technical Regulation for Thermal Power Station Units of 1.5 MW and higher,” Energinet.dk, Fredericia, Denmark, Regulation for grid connection TF 3.2.3, 2008.

International Journal of Smart Grid and Clean Energy

Multi agent system based adaptive protection for dispersed generation integrated distribution systems

Chengxi Liu[a*], Zakir Hussain Rather[a,b], Zhe Chen[a], Claus Leth Bak[a]

[a] *Department of Energy Technology, Aalborg University, 9220 Aalborg Denmark*
[b] *Innovation Center, kk-electronic, a/s, 9220 Aalborg Denmark*

Abstract

The increasing penetration of dispersed generation (DG) brings challenges to conventional protection approaches of distribution system, mainly due to bi-directional power flow and variable fault current contribution from different generation technology-based DG units. Moreover, the trend of allowing islanded operation of distribution systems necessitates the adoption of adaptive protection methods for distribution systems. In order to improve the reliability and selectivity of protection for such kind of distribution systems, a coordinative adaptive protection based on multi agent system (MAS) is proposed. The adaptive protection intelligently adopts suitable settings for the variation of fault current from diversified DG units. Furthermore, the structure of mobile MAS with additional flexibility is capable of adapting the changes of system topology in a short period, e.g. radial/meshed, grid-connected/islanded. The protection method is tested on a simplified distribution system model of Denmark in DIgSILENT/PowerFactory.

Keywords: Adaptive protection, dispersed generation, distribution protection, multi agent system

1. Introduction

Due to scarcity of fossil fuel reserves and the energy policy of CO_2 emission reduction, various types of renewable energy (RE) are being integrated into power systems at tremendous pace. Because of the decentralized characteristics of these natural resources, significant part of these RE-based generating units is connected to distribution systems. In Denmark, currently more than 40% of today's installed capacity is from DG units, which are mostly connected to grid at the distribution level (60/20/10/0.4 kV). Large scale RE-based and other DG units would play significant roles as power resources in the modernized power systems, which make the protection of power systems more complicated than that of traditional systems.

At distribution voltage level, one of the major challenges is the variability and uncertainty of short circuit current from these flexible DG resources. The operating conditions of renewable generation are highly unpredictable. Moreover, low voltage ride through (LVRT) capability mandates DG units' connectivity to the network only for a short period. Therefore, the protection settings of distribution system are of crucial importance, because it should be able to not only isolate the faulted part of the system in a short time to prevent large scale tripping of DG units, but also immediately adapt to the new scenarios to achieve high reliability and selectivity [1].

The other challenge is the change of network topology, such as disconnecting some DG units and meshing the distribution feeders. In future, the increasing penetration of DG is expected to support all loads in the distribution system and hence be possible for islanded operation. Compared with grid connected mode, the fault current seen by protection relays in islanded mode is relatively much less.

Adaptive protection is defined as "an online activity that modifies the preferred protection settings in response to changes in system condition or requirements in a timely manner by means of external generated signals or control actions" [2]. Many researchers have proposed both communication-based adaptive protection methods [3]-[8] and communication-less adaptive protection methods [9]-[14] for DG

* Manuscript received July 17, 2013; revised July 30, 2013.
Corresponding author Tel.: +45 2252 8660; Fax: +45 9815 1411. *E-mail address*: cli@et.aau.dk.

integrated distribution systems. In this paper, multi agent system (MAS) is proposed for adaptive protection schemes to deal with these variable scenarios after analyzing the impact of DG units on protection coordination. The mobile structure of MAS with more flexibility is capable of adapting the variation of renewable generation and the changes of system topologies in a short time, so as to correctly protect the system from multiple instantaneous faults.

2. Test Distribution System

Fig. 1 shows the single-line model of the test distribution system, which is a part of distribution system owned by Danish Distribution System Operator (DSO), Himmerland Elforsyning (HEF) in Aalborg, Denmark. The test system consists of 6 loads (numbered from Load1 to Load6) and 7 buses (numbered from Bus1 to Bus7). Relays are represented by symbols "R*ij*", where numbers *i* and *j* represent the beginning bus and the ending bus of its protection zone, respectively. Five Gas Turbine Generators (GTGs) and one variable speed wind turbine generator (WTG) are connected to the system. The WTG is a detailed model of 2 MW doubly-fed induction generator (DFIG) based wind turbine with power electronic converters and other control models, e.g. aerodynamic model, mechanical model, etc.. The GTGs are 3.3 MVA with governor and excitation control. The penetration level of DG units is sufficient to support all local loads across the distribution network in islanded operation mode. Meanwhile, the distribution system is capable of forming a ring type topology by Line 67 equipped with circuit breakers (CBs) to support the important load, (i.e. Load 5). R67 and R76 control normally open CBs. The data of WTG, GTGs, distribution lines and loads are given in [13].

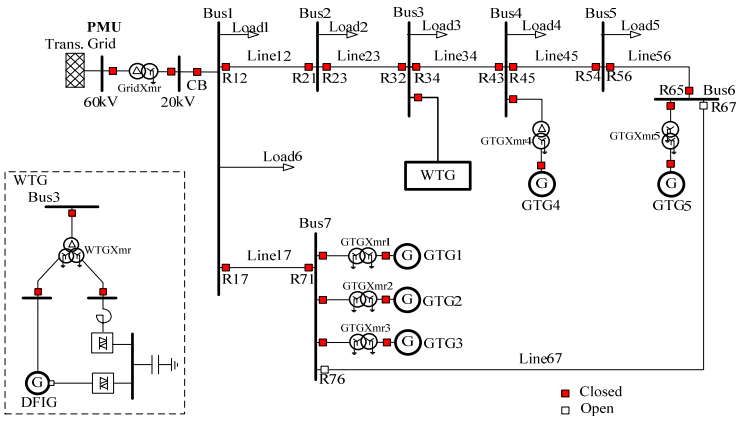

Fig. 1. Test distribution system.

3. Proposed Methodology

3.1. Fault Current Analysis

Future distribution systems trend to have ability to be operated in islanded mode for higher reliability. Compared with the grid-connected mode, in which the transmission system provides significant part of the short-circuit power, the short-circuit current in islanded mode is significantly less. The maximum 3-phase bolted fault current at the end of each protection zone for grid connected mode and islanded mode are shown in Fig. 2. The difference of short-circuit current only has impacts on the protection settings of forward relays in distribution feeders, (i.e. R12, R23, R34, R45, R56 and R17).

The short circuit current reduces when some of the DG units are disconnected. Fig. 3 compares the maximum short circuit current of 3-phase faults at the beginning of each protection zone when some of DG units are disconnected. The difference of short-circuit current only have impacts on the protection settings of the backward relays in the distribution feeders, (i.e. R17, R21, R32, R43, R54 and R65).

Furthermore, in order to support important load (i.e. Load 5) in the end of distribution feeder, the

network can be meshed by closing the normally open CBs of Line 67. In these cases, all power resources can contribute the short circuit power from two directions. Therefore, meshing of the network changes the short circuit current seen by most of the forward and backward relays, irrespective of grid-connected mode or islanded mode, as shown in Fig. 4 and Fig. 5, respectively.

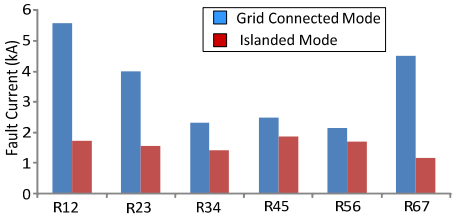

Fig. 2. Max. 3-ph fault current of radial topology.

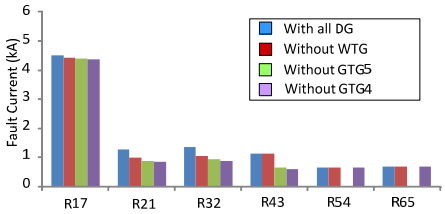

Fig. 3. Max. 3-ph fault current with/without DG integrated.

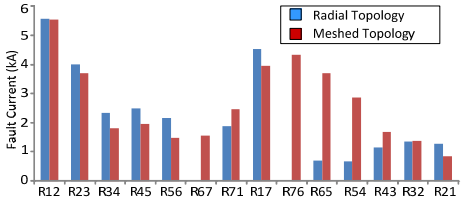

Fig. 4. Max. 3-ph fault current in grid connected mode.

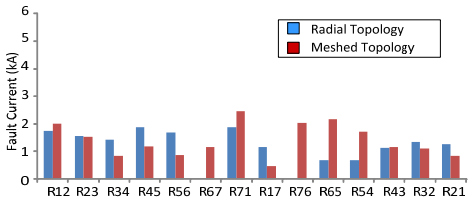

Fig. 5. Max. 3-ph fault current in islanded mode.

3.2. Inverse-time Directional Over Current Relay (DOCR) Protection

Inverse-time directional overccurent relay (DOCR) protection is adopted in the distribution system, which consists of two parts, instantaneous part and inverse-time part. For higher fault current (I>>), the relay pick-up time is fixed to t_{ins}. While for lower fault current (I>), the operation time is inversely changed with the fault current. Compared with traditional definite time DOCR, inverse-time DOCR has much shorter tripping time to reduce the risk of large scale DG disconnections. In this study, the operating time-current curve of inverse-time DOCR follows Normal Inverse Curve in IEC 60255-3 [15], given in (1)

$$t = \frac{0.14 T_p}{\left(I / I_p\right)^{0.02} - 1} (\text{sec}) \tag{1}$$

where I, I_p and T_p are fault current, pick-up current, and time dial settings. The instantaneous pick-up current I_{ins} is set as 1.05 times of the max short circuit current at the end of protection zones. Therefore, I_p, T_p, I_{inc} are the three configurable setting values for an adaptive DOCR to fit for current operating mode.

3.3. Architecture of Multi Agent System

Multi Agent System (MAS), also known as “self-organization system” is defined as a computerized system composed of many intelligent agents cooperatively adapting to the environment. Each autonomous agent can freely participate in or leave a group to cooperate with other agents with the help of communication [16]. The proposed MAS based adaptive protection scheme adopts three-level hierarchical architecture, which is built up with centralized control level, cooperation society level and distributed agent level, as shown in Fig. 6. These agents are geographically distributed in a number of intelligent electronic devices (IEDs), which have basic functions, such as computation, I/O interface, communications features, and decision making capability.

MAS in the distribution network consist of Relay Agents Society (RAS), DG Agents Society (DGAS) as well as Equipment Agents Society (EAS). Agents in the MAS can communicate with each other not only within the same agent society, but also between different agent societies.

Each relay is regarded as one relay agent (RA), which searches for relevant information from the communication bus and interacts with other agents. With the help of MAS, RAs not only fulfill the primary protection and back up protection with better performance than conventional methods, but also

detect events, such as CB failures, CB mal-operations and DG connection status, etc..

Every DG unit is considered as a DG agent (DGA). In MAS environment, DG units not only communicate with the local RA to provide the message of connection status, but also transmit important information, such as status and power generation, to DGAS.

The equipment agent (EA) includes CB agents, current transformer (CT) agents, voltage transformer (VT) agents, etc. These agents can send local important information, such as mal-function, mis-operation, alarm signals etc. to local RAs, and also can communicate with other EAs in the EAS to provide back up and coordination function.

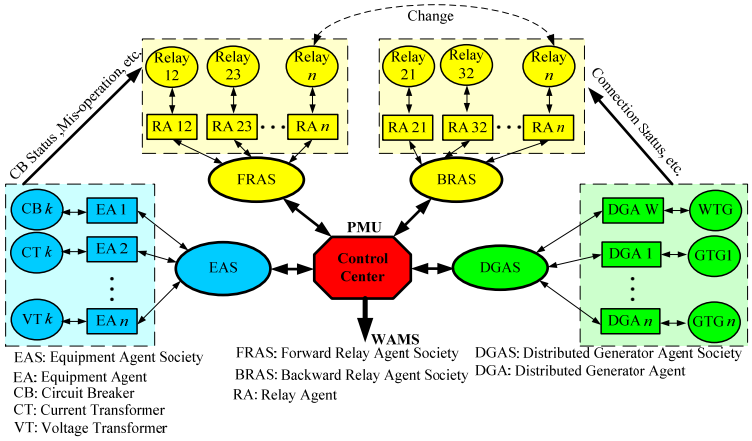

Fig. 6. Architecture of MAS based adaptive protection system.

3.4. Mobile Multi Agent System

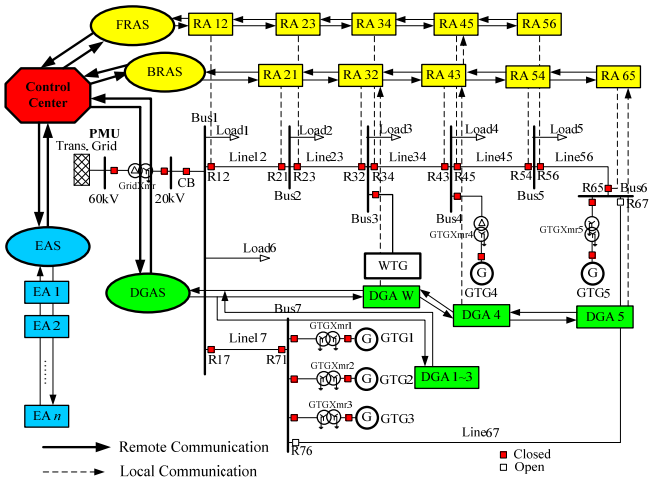

Fig. 7. Structure of MAS in the test distribution system.

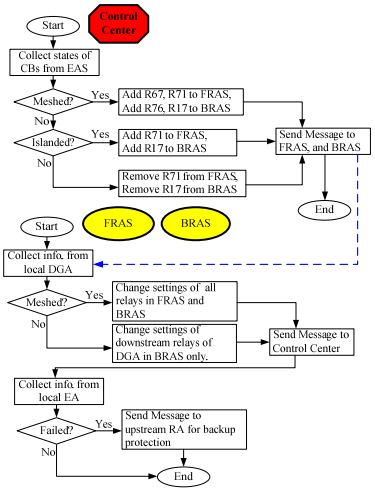

Fig. 8. Block diagram of mobile MAS.

Fig. 7 shows MAS in the test distribution system. Based on geographical distribution of agents in the distribution system, the communication can be divided into local communication and remote communication. Mobile MAS is adopted in this approach. As shown in Fig. 8, intelligent electric devices e.g. PMU, located in the substation of transmission system, can serve as the control center of the distribution system. The control center collects the states of CBs from EAS to detect the topology of the network, then to correctly change the classification of relays in Forward Relay Agent Society (FRAS) and Backward Relay Agent Society (BRAS). The protection settings of relays are calculated and stored offline in RAs. Then RAs receive the requests to adopt correct settings to adapt to current operating states. The protection settings must coordinate with each other in the same society, as shown in Table 1, in

which "⇨" means the back-up relationship between protection relays, e.g. "R12⇨R23" means R12 is the back up protection for R23. The adoption of mobile MAS aims at reducing the communication delay for transmitting the request of setting adjustment.

Table 1. Coordination of FRAS and BRAS with respect to different topologies

Topology	Coordination of FRAS	Coordination of BRAS
Radial Grid-connected	R12⇨R23⇨R34⇨R45⇨R56	R65⇨R54⇨R43⇨R32⇨R21
Radial Islanded	R71⇨R12⇨R23⇨R34⇨R45⇨R56	R65⇨R54⇨R43⇨R32⇨R21⇨R17
Meshed Grid-connected	R12⇨R23⇨R34⇨R45⇨R56⇨R67⇨R71	R17⇨R76⇨R65⇨R54⇨R43⇨R32⇨R21
Meshed Islanded	R12⇨R23⇨R34⇨R45⇨R56⇨R67⇨R71	R17⇨R76⇨R65⇨R54⇨R43⇨R32⇨R21

4. Case Study

According to Danish grid code, WTG should withstand faults for at least 100ms without disconnection [17]. In this case study, it is assumed that the instantaneous pick-up time T_{ins} is 10ms to detect the fault and relays take another 10ms to close its trip contacts. CBs take 60ms to clear the fault. So the minimum tripping time is 80ms after short-circuit. The communication is simulated by DIgSILENT Simulation Language (DSL) in the DIgSILENT. An Ethernet LAN communication network with ring topology is considered in the distribution system, so that communication delay between any adjacent agents can be assumed to be the typical value of 3.707ms [8]. The connection status of DG units will definitely decide the protection settings of its downstream relays and the request signal is transmitted along the feeders in the distribution network. Table 2 shows communication delay of transmitting the new settings throughout the network after the change of DG connection status.

The change of connection status of GTG5 is demonstrated in this study. The instantaneous pick-up current I_{ins}, reverse-time pick-up current I_p, time dial setting T_p of all relays with GTG5 connected and disconnected are listed in Table 3. Accordingly, the time-overcurrent plot of forward relays and backward relays are shown in Fig. 9 and Fig. 10. The time over-current curves of the BRAS in the Fig. 9 (b) and Fig. 10 (b) cross each other but they do not lack of selectivity, owing to the in-feed current from WTG, GTG4 and GTG5 along the distribution feeder.

Table 2. Communication delay for transmitting new protection settings throughout the network.

DG connection states (network topology)	Msg. of protection settings communicate in FRAS of MAS	Delay (ms)	Msg. of Protection Settings communicate in BRAS of MAS	Delay (ms)
WTG disconnected (meshed)	R34,R45,R56,R67,R71,R12,R23	11.121	R32,R21,R17,R76,R65,R54,R43	11.121
GTG4 disconnected (meshed)	R45,R56,R67,R71,R12,R23,R34	11.121	R43,R32,R21,R17,R76,R65,R54	11.121
GTG5 disconnected (meshed)	R56,R67,R71,R12,R23,R34,R45	11.121	R32,R21,R17,R76,R65,R54, R43	11.121
WTG disconnected (radial, islanded)	R34,R45,R56	7.414	R32,R21,R17	7.414
GTG4 disconnected (radial, islanded)	R45,R56	3.707	R43,R32,R21,R17	11.121
GTG5 disconnected (radial, islanded)	n/a	n/a	R65,R54,R43,R32,R21,R17	11.121
WTG disconnected (radial, grid-connected)	R34,R45,R56	7.414	R32,R21	3.707
GTG4 disconnected (radial, grid-connected)	R45,R56	3.707	R43,R32,R21	7.414
GTG5 disconnected (radial, grid-connected)	n/a	n/a	R65,R54,R43,R32,R21	11.121

Table 3. Time overcurrent settings with and without GTG5.

Protection Settings of Grid-connected & Radial w GTG5								Protection Settings of Grid-connected & Radial w/o GTG5							
Relay	I_p(A)	T_p(sec)	I_{ins}(A)	Relay	I_p(A)	T_p(sec)	I_{ins}(A)	Relay	I_p(A)	T_p(sec)	I_{ins}(A)	Relay	I_p(A)	T_p(sec)	I_{ins}(A)
R12	440	0.1669	5532	**R21**	350	0.0243	1075	**R12**	440	0.1669	5532	**R21**	210	0.0356	945
R23	350	0.1275	4210	**R32**	350	0.0427	1140	**R23**	350	0.1275	4210	**R32**	210	0.0615	987
R34	260	0.0848	2646	**R43**	260	0.0629	900	**R34**	260	0.0848	2646	**R43**	130	0.0986	682
R45	130	0.0649	2465	**R54**	130	0.0862	488	**R45**	130	0.0649	2465	**R54**	-	-	-
R56	130	0.0208	2208	**R65**	130	0.1073	500	**R56**	130	0.0208	2208	**R65**	-	-	-
R71	390	0.1232	1426	**R17**	390	0.0183	4746	**R71**	390	0.1232	1426	**R17**	390	0.0183	4606

The operating state is the grid-connected mode with radial topology. The extreme scenario is two 3-ph faults with resistance of 0.05Ω close to the end (90%) of Line43 and Line56, taking place at the same

time *t=1000 ms*. The protection settings are restored for adaptive adjustment for DG disconnection, as listed in Table 3. Fig. 11 shows actual states of CBs for conventional pilot protection, in which WTG is tripped at *t=1262 ms*. However, with the help of MAS-based adaptive protection, WTG still remains connected to the network, due to quick change of protection settings to adapt to the new operating states with the help of MAS, as shown in Fig. 12. The sequences of events in the case of conventional pilot protection and MAS-based adaptive protection are compared in Table 4 and the signals transmitted in both of communication-based protections are shown in Fig.13 and Fig. 14.

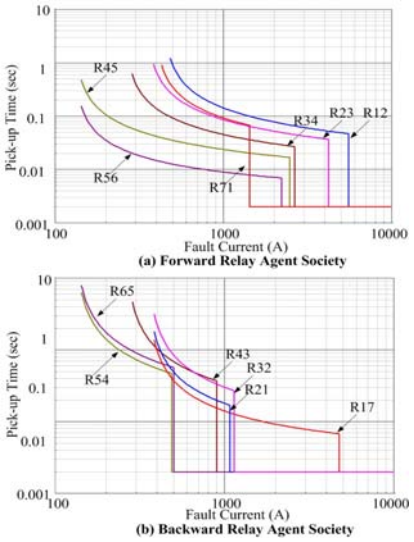

Fig. 9. Time-overcurrent plot with GTG5 connected.

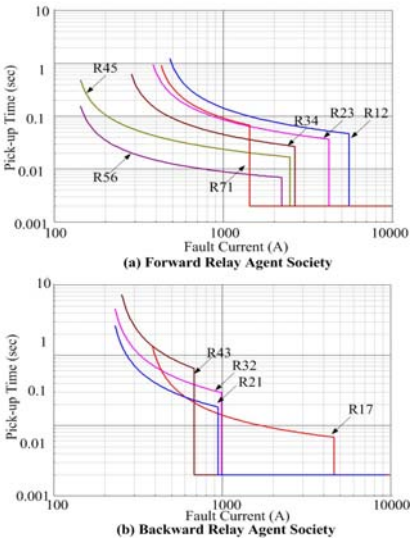

Fig. 10. Time-overcurrent plot with GTG5 disconnected.

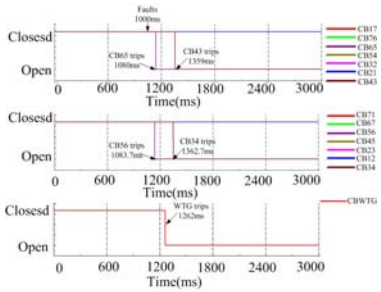

Fig. 11. States of CBs in conventional pilot protection.

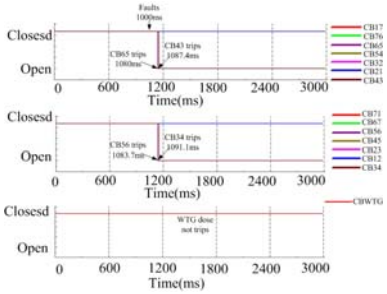

Fig. 12. States of CBs in MAS-based adaptive protection.

Table 4. Sequence of events of the conventional pilot protection and MAS-based adaptive protection

Conventional pilot protection	Time (ms)	MAS-based adaptive protection	Time (ms)
3-ph short circuit fault at Line34 and Line56	1000	3-ph short circuit fault at Line34 and Line56	1000
R65 is picked up by instantaneous DOCR	1010	R65 is picked up by instantaneous DOCR	1010
R65 sends tripping signal to R56	1010	R65 sends tripping signal to R56, and requests for adjusting protection setting in BRAS	1010
R56 receives the tripping signal from R65	1013.7	R56 receives the tripping signal from R65	1013.7
CB65 trips, GTG5 trips	1080	R54 receives the request for adjust settings	1013.7
CB56 trips	1083.7	R43 receives the request for adjust settings	1017.4
WTG trips	**1262**	R43 is picked up by instantaneous DOCR	1027.4
R34 is picked up by reverse-time DOCR	1289	R43 sends tripping signal to R34	1027.4
R34 sends tripping signal to R43	1289	R34 receives the tripping signal from R43	1031.1
R43 receives the tripping signal from R34	1292.7	CB65 trips, GTG5 trips	1080
CB34 trips	1359	CB56 trips	1083.7
CB43 trips	1362.7	CB43 trips	1087.4
		CB34 trips	1091.1

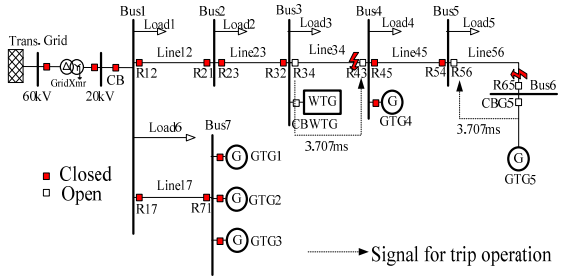

Fig. 13. Signals in conventional pilot protection.

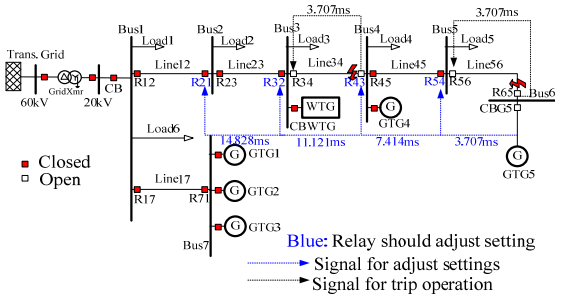

Fig. 14. Signals in MAS-based adaptive protection.

5. Conclusion

A coordinative adaptive protection based on MAS is proposed, which adapts itself for multiple variations, i.e. operating states of DG units, network topology, in DG integrated distribution system. The cooperative nature of proposed MAS based protection scheme adjusts settings of protection equipments to fits for current states at high speed. The proposed protection scheme has been applied to a real distributions system and the results have demonstrated the effectiveness of MAS based protection scheme.

Acknowledgements

The authors would like to acknowledge financial support from the project "Development of a Secure, Economic and Environmentally-friendly Modern Power Systems" (*DSF 09-067255*).

References

[1] P. M. Anderson, *Power System Protection*, McGraw-Hill, 1999.
[2] G. D. Rockefeller, C. L. Wagner, J. R. Linder, K. L. Hicks and D. T. Rizy, "Adaptive transmission relaying concepts for improved performance," *IEEE Trans. on Power Delivery*, vol. 3, no. 4, pp. 1446–1458, Oct. 1988.
[3] H. Wan, K. K. Li and K. P. Wong, "An adaptive multiagent approach to protect relay coordination with distributed generators in industrial power distribution system," *IEEE Trans. on Ind. Appl.*, vol. 46, no. 5, pp. 2118–2124, Sept./Oct. 2010.
[4] D. P. Buse and Q. H. Wu, "Mobile agents for remote control of distributed systems," *IEEE Trans. on Ind. Electron..*, vol. 51, no. 6, pp. 1142–1149, Dec. 2004.
[5] I. S. Baxevanos and D. P. Labridis, "Implementing multiagent systems technology for power distribution network control and protection management," *IEEE Trans. on Power Delivery.*, vol. 22, no. 1, pp. 433–443, Jan. 2007.
[6] S. J. Park and J. T. Lim, "Modeling and control of agent-based power protection systems using supervisors" *IEE Proc. in Control Theory Appl..*, vol. 153, no. 1, pp. 92–98, Jan. 2006.
[7] S. Shi, B. Jiang, X. Dong, and Z. Bo, "Protection of microgrid," *Proc. in 10th IET Conf. on Developments in Power System Protection,* Manchester, UK, Apr. 2010.
[8] M. Wei and Z. Chen, "Distribution system protection with communication technologies," *Proc. in IECON*, Glendale, AZ, USA, Nov. 2010.
[9] Z. Bo, "Adaptive noncommunication protection for power lines BO scheme 1 – the delayed operation approach," *IEEE Trans. on Power Delivery.*, vol. 17, no. 1, pp. 85–91, Jan. 2002.
[10] Z. Bo, "Adaptive noncommunication protection for power lines BO scheme 2 – the instant operation approach," *IEEE Trans. on Power Delivery.*, vol. 17, no. 1, pp. 92–96, Jan. 2002.
[11] Z. Bo, "Adaptive noncommunication protection for power lines BO scheme 3 – the accelerated approach," *IEEE Trans. on Power Delivery.*, vol. 17, no. 1, pp. 97–104, Jan. 2002.
[12] Z. Bo, X. Dong, B. Caunce and R. Millar, "Adaptive noncommunication protection of double-circuit line system," *IEEE Trans. on Power Delivery.*, vol. 18, no. 1, pp. 43–49, Jan. 2003.
[13] P. Mahat, Z. Chen, B. B. Jensen and C. L. Bak, "A simple adaptive overcurrent protection of distribution system with distributed generation," *IEEE Trans. on Smart Grid*, vol. 2, no. 3, pp. 428–437, Sept. 2011.
[14] C. Liu, Z. Chen and Z. Liu, "A communication-less overcurrent protection for distribution system with distributed generation integrated," *Proc. in Power Electronics for Distributed Generation System,* Aalborg, Denmark, Jun. 2012.
[15] *IEC 60255-3*, Electrical Relays - Single Input Energizing Quantity Measuring Relays with Dependent or Independent Time.
[16] M. Wooldridge, *An Introduction of Multi Agent Systems*, John Wiley & Sons, 2002.
[17] *IEEE Standard for Interconnceting Distributed Resources into Electric Power Systems*, IEEE Standard 1547TM, Jun, 2013.